

**Regulation of chromatin positioning in *Arabidopsis*
*thaliana***

Dissertation

der Mathematisch-Naturwissenschaftlichen Fakultät

der Eberhard Karls Universität Tübingen

zur Erlangung des Grades eines

Doktors der Naturwissenschaften

(Dr. rer. nat.)

vorgelegt von

Bi Xiuli

(毕秀丽)

aus

Shandong Juye, China

Tübingen

2020

Tag der mündlichen Qualifikation: 02.09.2020

Dekan:

1. Berichterstatter:
2. Berichterstatter:

Prof. Dr. Thomas Lahaye

Prof. Dr. Ulrike Zentgraf

Table of contents

1. Introduction..... 1

1.1 Storage of hereditary material into nucleus..... 1

1.2 The methodology for exploring 3D chromatin organization 2

1.2.1 Visualizing chromatin regions of interest 3

 1.2.1.1 FISH and its variants3

 1.2.1.2 Live-cell imaging.....4

1.2.2 Inferring 3D chromatin organization 5

 1.2.2.1 Chromosome Conformation Capture: one to one.....6

 1.2.2.2 Circular Chromosome Conformation Capture: one to all6

 1.2.2.3 Chromosome Conformation Capture Carbon Copy: many to many6

 1.2.2.4 Genome-wide Chromosome Conformation Capture: all to all.....7

 1.2.2.5 Derivative C-technologies with reduced complexity9

1.3 The genome in a 3D nucleus 10

1.3.1 Global and local levels of chromatin organization 10

 1.3.1.1 Chromosome territories (CTs).....10

 1.3.1.2 Chromosome compartments12

 1.3.1.3 Chasing TADs in plants.....14

 1.3.1.4 Chromatin loops15

1.3.2 Chromatin positioning in the nuclear space 16

 1.3.2.1 Tethering chromatin in and around nucleolus17

 1.3.2.2 Chromatin positioning at the NP18

1.4 Aim of the thesis..... 27

2. Materials and Methods.....28

2.1 Materials..... 28

2.1.1 Plants 28

2.1.2 Bacterial strains 29

2.1.3 Media and antibiotics 29

2.1.4 Vectors 30

2.1.5 *Agrobacterium tumefaciens* contain plasmid-DNA..... 30

2.1.6 Enzymes and antibodies	31
2.1.7 Chemicals, beads and solutions.....	31
2.1.8 Oligonucleotides	31
2.2 Methods	31
2.2.1 Plant growth	31
2.2.1.1 Growth conditions and treatments.....	31
2.2.1.2 Seed surface sterilization.....	32
2.2.2 Microbe cultivation	32
2.2.2.1 Growth of <i>Escherichia coli</i>	32
2.2.2.2 Growth of <i>Agrobacteria</i>	32
2.2.3 Plant methods	32
2.2.3.1 Stable transformation of <i>Arabidopsis thaliana</i>	32
2.2.3.2 Genotyping analysis of T-DNA insertion lines	33
2.2.3.3 Generation of tagging lines	33
2.2.3.4 Crossing of <i>Arabidopsis</i>	34
2.2.4 Molecular biology	34
2.2.4.1 Isolation of plasmid from <i>E. coli</i>	34
2.2.4.2 Isolation of genomic DNA from plant material	34
2.2.4.3 Standard PCR	35
2.2.4.4 DNA agarose gel electrophoresis	35
2.2.4.5 Sequencing	35
2.2.4.6 Quantitative fluorescent real time PCR.....	35
2.2.4.7 Digestion of plasmid with restriction endonuclease.....	36
2.2.4.8 Preparation and calibration of Serapure Beads	36
2.2.4.9 Purification of DNA fragments	36
2.2.4.10 Gibson Assembly [®]	36
2.2.4.11 Construction of plasmid	37
2.2.4.12 Preparation and transformation of chemically competent <i>E. coli</i> DH5 α cells	39
2.2.4.13 Preparation and transformation of electrical competent cells of <i>Agrobacteria</i>	40
2.2.4.14 Western blot analysis.....	40
2.2.4.15 RE-ChIP sequence library preparation.....	41

2.2.4.16 FISH	43
2.2.5 Immunohistostaining.....	46
2.2.6 Microscopy and image processing.....	46
2.2.7 Statistical analysis.....	47
3. Results	48
3.1 Identification and characterization of chromatin anchoring at the NP in <i>Arabidopsis</i>	48
3.1.1 Non-random chromatin distribution at the NP revealed by RE-ChIP.....	48
3.1.2 Chromatin positioning at the NP shows similar patterns in various tissues	52
3.1.3 Chromatin positioned at the NP was enriched with repressed domains	56
3.1.4 Positioning of TEs at the NP correlates with different silencing pathways.....	57
3.2 Plant lamin-like proteins are required for specific chromatin positioning at the NP.....	60
3.2.1 Compare genomic loci positioning at the NP with FISH.....	60
3.2.2 Plant lamin-like proteins are required for selectively tethering chromatin at the NP.....	63
3.2.3 Knocking out of <i>KAKU4</i> has no influence on specific chromatin positioning at the NP	65
3.2.4 Specific chromatin positioning at the NP is not affected in <i>neap</i> mutants	67
3.2.5 Knockout <i>CRWN1</i> , <i>CRWN4</i> or <i>KAKU4</i> locus decreases the size of nuclei.....	68
3.3 Role of H3K9me in specific chromatin positioning at the NP	70
3.4 Role of non-CG methylation in specific chromatin positioning at the NP	71
3.4.1 Non-CG methylation contributes to specific chromatin positioning at the NP	71
3.4.2 CG methylation has no effect on chromatin positioning at the NP.....	74
3.5 <i>crwn</i> mutants lose specific chromatin positioning at a chromosomal scale	75
3.6 Exploration of CRWN1-chromatin interactions	78
3.6.1 A native <i>CRWN1</i> tagging construct can fully rescue <i>crwn1</i> phenotypes.....	78
3.6.2 CRWN1 directly interacts with chromatin at the NP.....	83
3.7 Characterization of <i>crwn1</i> mutants under different treatments.....	85
3.7.1 Morphological response of <i>crwn1</i> to hydrogen oxide.....	86
3.7.2 Morphological response of <i>crwn1</i> to salt stress	87
3.7.3 Morphological response of <i>crwn1</i> to inorganic nitrogen	89
3.7.4 Morphological response of <i>crwn1</i> to zeocin treatment.....	90
3.8 Generating functional <i>CRWN2</i> and <i>CRWN4</i> tagging lines	91

3.9 Loss of <i>CRWNs</i> increased root hair density in <i>Arabidopsis thaliana</i>	96
4. Discussion	100
4.1 Specific perinuclear positioning of repressed chromatin regions revealed by RE-ChIP .	100
4.2 Specific chromatin positioning at the NP requires plant lamin proteins	103
4.3 Roles of heterochromatin marks on specific chromatin positioning at the NP	109
4.4 Do CRWN1-chromatin interactions have any biological relevance?	111
5. Summary.....	113
6. Zusammenfassung	114
7. References.....	116
8. Appendix.....	132
9. Acknowledgements	142
10. Curriculum vitae.....	144

List of figures

Figure 1. Plant nuclear chromatin organization and key elements involved in nuclear dynamics.
..... 26

Figure 2. Experiment workflow of RE-ChIP-seq with transgenic *Arabidopsis* plants expressing NUP1:GFP. 43

Figure 3. Procedure of 2C nuclei collection for FISH. 45

Figure 4. Identification of chromatin regions localized at the NP by NUP1:GFP RE-ChIP...... 50

Figure 5. Comparison between RE-ChIP and regular ChIP...... 51

Figure 6. NUP1 and CENH3 display complementary patterns at the NP...... 52

Figure 7. NUP1:GFP RE-ChIP-seq signals in various tissues. 54

Figure 8. Comparison of NUP1-enriched chromatin segments in different tissues...... 55

Figure 9. Comparison of NUP1-enriched genes in the two replicates...... 55

Figure 10. Enrichment of heterochromatin and silenced genes at the NP. 56

Figure 11. Comparison of DNA methylation over TEs. 59

Figure 12. Design of probes targeting chromatin regions. 61

Figure 13. Probing chromatin localization with FISH. 62

Figure 14. Analyses of FISH signals in *Arabidopsis* mutants of lamin-like gene. 64

Figure 15. Analyses of FISH signals in *kaku4* mutant...... 66

Figure 16. Analyses of FISH signals in *neap* mutants. 67

Figure 17. Characterization of nuclear morphology of *Arabidopsis* 2C nuclei. 69

Figure 18. Characterization of nuclear morphology of *Arabidopsis* 8C nuclei. 70

Figure 19. Analyses of FISH signals at in *svh4/5/6*. 71

Figure 20. Analyses of FISH signals in *Arabidopsis* mutants losing non-CG methylation...... 73

Figure 21. Analyses of FISH signals in *Arabidopsis* mutants losing CG methylation. 74

Figure 22. Design and labeling of dual-color FISH probes covering a 10 Mb region in chromosome 1 according to NUP1 RE-ChIP-seq signals. 75

Figure 23. Approximation of chromosome painting data. 76

Figure 24. Deficiency of *crwn* mutants in specific chromatin positioning at the NP revealed by chromosome painting...... 77

Figure 25. Predication of structural motifs from the CRWN1 sequence...... 79

Figure 26. A native <i>CRWN1</i> tagging construct can rescue the nuclear phenotype of <i>crwn1</i>	81
Figure 27. <i>CRWN1</i> gene model and genotyping of <i>CRWN1</i> tagging line.	82
Figure 28. Distance distribution of probed genomic regions to the NP in the 2C nuclei of <i>CRWN1</i> tagging lines.	82
Figure 29. Distribution of <i>CRWN1</i> :2HA at the NP.	83
Figure 30. Expression of <i>CRWN1</i> :2HA in <i>crwn1</i> leaves.	83
Figure 31. Chromatin regions targeting green FISH probes are enriched by <i>CRWN1</i> :2HA ChIP.	84
Figure 32. Comparison of NP-chromatin interaction patterns revealed from different ChIP methods.	85
Figure 33. Phenotypes of WT, <i>crwn1</i> and <i>kaku4</i> seedlings under H ₂ O ₂ stress.	87
Figure 34. Sensitivity of WT, <i>crwn1</i> and <i>kaku4</i> seedlings to NaCl.	88
Figure 35. Sensitivity of WT, <i>crwn1</i> and <i>kaku4</i> seedlings to NO ₃ ⁻ or NH ₄ ⁺	89
Figure 36. Phenotypes of WT, <i>crwn1</i> and <i>kaku4</i> seedlings under zeocin treatments.	91
Figure 37. Blast Hits on <i>CRWN1</i> protein sequence with the other three <i>CRWN</i> proteins.	92
Figure 38. Predication of structural motifs from the <i>CRWN4</i> sequence.	93
Figure 39. A native <i>CRWN4</i> tagging construct can rescue the nuclear phenotype of <i>crwn4</i>	93
Figure 40. <i>CRWN4</i> gene model and genotyping of <i>CRWN4</i> tagging lines.	94
Figure 41. Expression of <i>CRWN4</i> :2HA in <i>crwn4</i> leaves.	94
Figure 42. Predication of structural motifs from the <i>CRWN2</i> sequence.	95
Figure 43. A native <i>CRWN2</i> tagging construct can rescue the whole-plant phenotype of <i>crwn1/2</i>	95
Figure 44. <i>CRWN2</i> gene model and genotyping of <i>CRWN2</i> tagging lines.	96
Figure 45. Expression of <i>CRWN2</i> :2HA in <i>crwn1/2</i> leaves.	96
Figure 46. Morphology of root hairs of <i>crwn</i> mutants.	98
Figure 47. Comparison of cell length of root cells in <i>crwn</i> mutants.	99
Figure 48. Representative confocal images showing localizations of FISH signal in 2C nuclei of WT and <i>crwn1</i> plants.	105
Figure 49. Representative confocal images of chromosome painting.	106
Figure 50. Distribution of distances of probed genomic regions to the NP in <i>crwn</i> mutants.	107

List of tables

Table 1. <i>Arabidopsis</i> mutants used in this study	28
Table 2. The tagging lines used in the study.....	29
Table 3. Bacterial strains used in this study	29
Table 4. Media used in this study	29
Table 5. Antibiotics used in this study	30
Table 6. Vectors used in this study	30
Table 7. Plasmids in <i>Agrobacteria</i> used in this study.....	30
Table 8. Antibodies used in this study.....	31
Table 9. Oligonucleotides used in this study.....	132
Table 10. Reads of ChIP-seq and NUP1:GFP RE-ChIP	135
Table 11. Reads of NUP1:GFP RE-ChIP in various tissues	136
Table 12. FISH BACs paired loci to compare ~300 kb genomic regions.....	137
Table 13. FISH BACs for chromatin painting	138

Abbreviations

m^6A	Adenine-6-methylation
AGI24	AGAMOUS-LIKE 24
<i>APOLO</i>	<i>AUXIN REGULATED PROMOTER LOOP</i>
At	<i>Arabidopsis thaliana</i>
BAC	Bacterial artificial chromosome
BAF	Barrier-to-autointegration factor
Bzip18	Basic-leucine zipper domain transcription factor
bp	base pair
<i>CAB</i>	<i>CHLOROPHYLL A/B BINDING</i>
<i>C. elegans</i>	<i>Caenorhabditis elegans</i>
ChIP	Chromatin immunoprecipitation
CRWN	CRWODED NUCLEI
ChIA-PET	Chromatin interaction analysis by paired-end tag sequencing
cLADs	Constitutive lamina-associated domains
CMT2	CHROMOMETHYLASE 2
CT	Chromosome territories
DamID	DNA adenine methyltransferase identification
ddH ₂ O	Autoclaved milli-Q water
DNA	Deoxyribonucleic acid
DNMT1	DNA cytosine-5 methyltransferase 1
DRM2	DOMAINS REARRANGED METHYLASE 2
DSB	DNA double-strand breaks
<i>E. Coil</i>	<i>Escherichia coli</i>
EDTA	Ethylenediaminetetraacetic acid
ESCs	Embryonic stem cells
FACS	Fluorescence-activated cell sorting
FISH	Fluorescence <i>in situ</i> hybridization
fLADs	Facultative lamina-associated domains

GAM	Genome Architecture Mapping
GFP	Green fluorescent protein
H ₂ O ₂	Hydrogen oxide
<i>HBB</i>	mammalian β -globin gene
H3K9me	Histone H3 lysine 9 methylation
H3K9me2	Histone H3 lysine 9 di-methylation
H3K9me3	Histone H3 lysine 9 tri-methylation
H3K27me3	Histone H3 lysine 27 tri-methylation
HiPMap	High-throughput position mapping platform
Hi-C	Genome-wide Chromosome Conformation Capture
HP1 α	Heterochromatin protein 1 alpha
HRP	Horseradish Peroxidase
IHI	Interactive Heterochromatin Island
INM	Inner nuclear membrane
KASH proteins	Klarsicht/ANC-1/Syne homology domain proteins
Kb	Kilobases
KEE	KNOT Engaged Element
LADs	Lamina-associated domains
LINC	Linker of nucleoskeleton and cytoskeleton
LBR	Lamin B receptor
LB medium	Luria-Bertani Broth medium
Mb	Megabases
MET1	Methyltransferase 1
N	Nitrogen
NADs	Nucleolus-associated domains
NASC	Nottingham Arabidopsis Stock Center
NE	Nuclear envelope
NETs	NE transmembrane proteins
NEAPs	Nuclear envelope-associated proteins
NH ₄ ⁺	Ammonium

NL	Nuclear lamina
NLSs	Nuclear localization signals
NMCPs	Nuclear matrix constituent proteins
NO ₃ ⁻	Nitrate
NORs	Nucleolus-organizing regions
NP	Nuclear periphery
NPC	Nuclear pore complex
NTL9	NAC WITH TRANSMEMBRANE MOTIFI-LIKE9
NUP	Nucleoporin
ONM	Outer nuclear membrane
(f)PALM	(fluorescence) Photoactivation Localization Microscopy
<i>PID</i>	<i>PINOID</i>
PLAC-seq	Proximity Ligation Assisted Chromatin Immunoprecipitation sequencing
PLADs	Plant lamin-associated domains
Pol I	RNA Polymerase I
POW1	PWWP INTWERACTION OF POLYCOMBS 1
PRC2	Polycomb Repressive Complex 2
PRs	Pericentromeric Regions
PVDF	Polyvinylidene difluoride
qPCR	Quantitative polymerase chain reaction
RdDM	RNA-directed DNA methylation
RE	Restriction enzyme
RE-ChIP-seq	Restriction enzyme mediated chromatin immunoprecipitation sequence
RNA	Ribonucleic acid
ROS	Reactive oxygen species
rRNA	Ribosomal RNA
RT	Room temperature
SDS	Sodium dodecyl sulfate
SDS-PAGE	Sodium dodecyl sulfate polyacrylamide gel electrophoresis
SEP4	SEPALLATA 4

SOC1	SUPPRESSOR OF OVEREXPRESSION OF CONSTANS 1
SPRITE	Split-Pool Recognition of Interaction by Tag Extension
SSIM	Saturated Structured Illumination Microscopy
STED	Stimulated Emission Depletion
STORM	Stochastic Optical Reconstruction Microscopy
SUN	Sad1/UNC84
SUVH4	SU(VAR)3-9 HOMOLOG 4
SVP	SHORT VEGETATIVE PHASE
TADs	Topologically associated domains
TE	Transposable element
<i>TFL1</i>	<i>TERMINAL FLOWER1</i>
TFs	Transcription factors
TTS	Transcription termination site
TST	Transcription start site
WIPs	WPP domain-interacting proteins
WITs	WPP domain-interacting tail-anchored proteins
WT	Wild-type
YEP medium	Yeast Extract Peptone medium
1/2 MS medium	1/2 Murashige-Skoog Medium
3C	Chromatin Conformation Capture
3D	Three-dimensional
4C	Circular Chromosome Conformation Capture
5C	Chromosome Conformation Capture Carbon Copy

1. Introduction

1.1 Storage of hereditary material into nucleus

The presence of a nucleus is the key feature that defines the difference between a eukaryotic and prokaryotic cell. The nucleus has two major functions: providing a separate space to store the hereditary material—deoxyribonucleic acid (DNA); and serving as one of the principal sites for a number of cell activities, such as DNA replication, transcription, repair and ribonucleic acid (RNA) processing. Therefore, the nucleus could be considered as the essence of the cell.

The nucleus is one of the most readily detectable organelles. It was first described at the beginning of the 19th century. From 1829 to 1832, Robert Brown observed nuclei in plant cells (Pederson 2011). In the following ten years, the interest of investigating this organelle continuously increased, resulting in the discovery of chromatin by Walther Flemming in 1878. Thereby, chromatin was defined as a fraction inside the nucleus, which can be stained by aniline dyes. Flemming not only discovered chromatin but also for the first time, observed the formation of stained bodies just before cell division (Flemming 1965). In 1885, Carl Rabl proposed that chromosomes were organized into distinct nuclear regions. Later in 1909, Theodor Boveri introduced the term chromosome territories after observing that the interphase chromosomes occupy specifically distinct regions within a nucleus under microscopy (Cremer and Cremer 2006a; Cremer and Cremer 2006b). After observing the behaviour of chromosomes during mitosis and meiosis, they were proposed as the carriers of genetic information in Boveri-Sutton chromosome theory by Edmond Wilson in 1925 (Cremer and Cremer 2006a; Cremer and Cremer 2006b).

The fate of chromatin has been fascinating to biologists. During mitosis, chromosomes are clearly visible as X-like structures under the microscope (reviewed in (Antonin and Neumann 2016)). However, during interphase, which is the majority of the cell cycle, chromatin is not condensed into chromosomes, such property of chromatin makes it difficult to observe directly under the microscope. Studies performed in the 20th century culminated in the discovery of the DNA as the genetic carrier and how the genetic information is encoded in its linear sequence was revealed (reviewed in (Benham and Mielke 2005)). After that, researchers realized that how the genome works — when and which genomic loci would be transcribed along with various cellular processes is essential for all living things. Proteins in

charge of different cell processes, such as cell cycle facilitation, DNA transcription, replication and repair, must be able to access to certain regions of the genome without disrupting its integrity. In addition, different cell processes happen at different times and recruit diverse genes in different cell types under different environmental conditions, the organization of chromatin should be dynamic. The research topic on DNA packaging within nuclei was transferred to delve into how chromatin is structurally and physically organized inside the three-dimensional (3D) nuclear space.

1.2 The methodology for exploring 3D chromatin organization

Over the past two decades, our understanding of chromatin organization within the 3D nuclear space has been tremendously advanced because of the rapid development of techniques (reviewed in (Ramani et al., 2016; Dekker et al., 2017; Doğan and Liu 2018; Fraser et al., 2015)). Two kinds of technologies have been extensively applied: microscopy-based imaging techniques and Chromatin Conformation Capture (3C) combined with high throughput sequencing. Direct visualization and quantification of physical distances between genomic loci and their location, and movement in single cells can be achieved with imaging tools. On the other hand, the 3C and its derivatives make it possible to acquire an average of genome-wide chromatin conformation from a cell population. Therefore, microscopy-based imaging technologies and the 3C family methods provide complementary views of 3D genome organization, in spite of the several contradictions in certain regions. For example, results achieved by the 3C-based technique (Chromosome Conformation Capture Carbon Copy) and the imaging-based method (fluorescence *in situ* hybridization (FISH)) were reported to be discordant in PRC1 mutant embryonic stem cells (ESCs) (Williamson et al., 2014). Illustration for this difference is that the cell-to-cell and time-dependent variations in chromatin folding leading to a rather wide distribution of the spatial distance between two loci in a cell population. 3C-based methods detect only events where the two loci are in close spatial proximity, that is, events present in only a fraction of cell populations; while imaging-based methods such as FISH can determine the spatial distance between the loci in any cell, and when a relatively small number of cells are analyzed, it might detect cells that are not overlapped with the part which detected by 3C-based methods.

1.2.1 Visualizing chromatin regions of interest

1.2.1.1 FISH and its variants

Traditional FISH and its variants are based on the hybridization of sequence-specific complementary probes to their targets of interest after a denaturation step. The fluorescently labeled genomic regions can then be detected and visualized by using a fluorescence microscope. Sensitivity and resolution are the limiting factors in FISH experiment designing. Sensitivity depends on the light-gathering ability of the particular microscope, which in turn determines the size of a probe that can be detected (in general, the larger probes could produce the stronger signals that can be easily detected by the microscope). Then the probe size will influence the resolution, which refers to the capacity to distinguish between two loci along the length of a chromosome (Huber et al., 2018; Fraser et al., 2015). For example, probes of ~40 kilobases (kb) in size could not be used to detect two loci that are within 100 kb in linear distance, while probes of ~10 kb could (Fraser et al., 2015; Yu and Ren 2017). Additionally, resolution is also dependent on the limit of a physical distance that a microscope can resolve. For instance, a light microscope cannot resolve objects that are separated by less than ~200-300 nm (Lakadamyali and Cosma 2015). As the compaction state of metaphase chromosomes is thousands of times more than interphase chromosomes, which in turn are at least ten times more than the naked DNA. The obtained resolution for metaphase chromosomes, interphase chromosomes and oligonucleotide arrays is megabases (Mb), submegabases, and kb, respectively (Speicher and Carter 2005; Fraser et al., 2015). Thus, such difference in compaction states of metaphase chromosomes, interphase chromosomes and the naked DNA have to be considered when performing FISH experiments.

Different variations of FISH have been applied to directly visualize and measure the physical distance between DNA segments, the nuclear location of DNA segments within a nucleus, and the localization of a DNA segment in relation to the rest of the chromosome, e.g., inside or outside of a CT (reviewed in (Fraser et al., 2015)). In the conventional FISH (two-dimensional (2D)-FISH), cells are fixed in methanol acetic acid in order to flatten the nuclei and thus allow 2D microscopy to acquire images; whereas 3D-FISH refers to FISH pipelines using 3D-preserved cells or nuclei in combination with 3D-microscopy and image reconstruction (Walter et al., 2006; Giorgetti and Heard 2016).

In general, FISH assays could be used to detect limited numbers of genomic loci at a time. Recently, Shachar and colleagues developed a high-throughput position mapping platform

(HIPMap), which is a fully automated FISH-based imaging method for high-throughput, quantitative mapping of spatial location of multiple loci in the mammalian cell nucleus (Shachar et al., 2015). The development of automated imaging analysis techniques such as HIPMap is still on calling to visualize chromatin architecture with high accuracy and high-throughput in diverse conditions.

1.2.1.2 Live-cell imaging

Apart from FISH assays, which are dealing with fixed materials, several more advanced fluorescent labeling techniques have been applied to provide dynamics of chromatin with minimum perturbation to chromatin itself. When employing these techniques, one can either label chromatin-associated proteins such as core histone proteins or the DNA itself. Chromatin associated proteins can be tagged with fluorescent proteins, and this is the easiest way to visualize chromatin, especially in living cells. For example, the core histone-H2B fused with green fluorescent protein (GFP) was employed to track the spatial heterogeneity of the global chromatin organization in individual nuclei (Talwar et al., 2013). However, potential artifacts, such as the altered function and the re-localization of tagged proteins, caused by the overexpression of fusion proteins, might occur. Furthermore, this strategy has no capacity to reveal structural details of chromatin regions of interest due to the lack of sequence-specific labeling.

Live-cell imaging of DNA has long been carried out with a fluorescent operator-repressor system, which enriches fluorescent proteins at a specific genomic region. In the two commonly used systems, Lac operator or Tet operator repeats are incorporated into genomic regions of interest, and they are subsequently visualized upon recognition by fluorescently labeled Lac repressor or Tet repressor, respectively (Gonzalez-Sandoval et al., 2015; Prendergast et al., 2016).

A recent exciting development in labeling specific genomic loci is the application of modified transcription activator-like effectors (TALEs) or CRISPR/dCas9 (deactivated Cas9 without endonuclease activity) fused with fluorescent proteins (Hsu et al., 2014; Lakadamyali and Cosma 2015; Ren et al., 2017; Ma et al., 2016). While studies have evidenced that TALEs are efficient in labeling repetitive sequences (Ren et al., 2017; Fujimoto et al., 2016), CRISPR/dCas9 is feasible for labeling non-repetitive sequences (Ma et al., 2016). In the CRISPR/dCas9 labelling system, a single fluorescent CRISPR/dCas9 protein is guided by a ~20 nucleotides RNA sequence to the locus of interest, which is technically challenging to

observe. This difficulty has been mitigated recently by a novel design, which incorporates tandem tags fused with the CRISPR/dCas9 protein, serving as binding sites of multiple copies of fluorescent proteins (Hong et al., 2018).

Besides visualizing one or several genomic loci at one time, chromatin domains specifically localized in a particular nuclear sub-compartment such as the nuclear periphery (NP) were tracked with the application of an assay that builds upon the Dam (DNA adenine methyltransferase) identification technology (Kind et al., 2013). In this assay, by expressing GFP-tagged ^{m6}A (adenine-6-methylation)-tracer proteins, DNA segments that have direct contact with the nuclear lamina would be adenine methylated and could be visualized with the help of fluorescence microscopy.

In the last decade, several super-resolution microscopy techniques have been developed to overcome the diffraction limit, achieving the resolution of light microscopy to length scales as small as 10-20 nm. These super-resolution approaches include Saturated Structured Illumination Microscopy (SSIM), Stimulated Emission Depletion (STED), Stochastic Optical Reconstruction Microscopy (STORM), and (fluorescence) Photoactivation Localization Microscopy (PALM/fPALM) (reviewed in (Lakadamyali and Cosma 2015)).

1.2.2 Inferring 3D chromatin organization

In addition to methods allowing direct visualizing chromatin regions of interest, the employment of novel molecular and genome-wide technologies has also greatly advanced our knowledge concerning 3D chromatin organization. In contrast to microscopy-based imaging tools used at the single-cell level, high throughput molecular techniques are mostly employed to capture an average of chromatin conformation amongst millions of cells. Essentially, the vast majority of these molecular tools are derivatives of the 3C technique, which we named as “C techniques” collectively. In these methods, chromatin contacts preserved by chemical fixative can be converted into chimeric DNA *via* chromatin fragmentation and re-ligation. Subsequently, the abundance of these ligation products can be assessed using quantitative polymerase chain reaction (qPCR), DNA microarrays or direct DNA sequencing (Simonis et al., 2009; Dostie et al., 2006; Dekker et al., 2002; Lieberman-Aiden et al., 2009). Recently, massively-parallel sequencing technologies have been coupled with the C technologies, creating useful tools that could map genome-wide chromatin contacts (Fang et al., 2016; Fullwood et al., 2009; Hughes et al., 2014; Mumbach et al., 2016; Dryden et al., 2014; Han et al., 2018).

1.2.2.1 Chromosome Conformation Capture: one to one

The Chromosome Conformation Capture (3C) method was the first technique to quantify contact frequency between two preselected loci in yeast (Dekker et al., 2002). It was demonstrated that the interaction frequency of two genomic loci is not solely determined by their physical distance along the genome. The first step in 3C method is cross-linking native chromatin *in vivo* using formaldehyde. Hence, genomic regions in spatial proximity are covalently linked. After isolation of nuclei, which contain cross-linked chromatin, the chromatin is fragmented through restriction enzyme (RE) digestion. Then the chromatin fragments in very close proximity are ligated (known as proximity ligation). After reversing cross-links by heat treatment in the presence of Proteinase K, the frequency of proximity ligation events between genomic segments of interest is determined by qPCR. The resolution of 3C technology varies from several kb to several hundred kb and is dependent on the RE used for fragmenting chromatin (Fraser et al., 2015). Despite the low-throughput feature of 3C, it is still widely applied to detect long-range chromatin interactions owing to its ease of use.

1.2.2.2 Circular Chromosome Conformation Capture: one to all

The Circular Chromosome Conformation Capture (4C) method enables genome-wide identification of all genomic regions that interact with a selected region, which is referred to as the viewpoint (Splinter et al., 2012; Simonis et al., 2009). Different from 3C, one more time RE digestion and ligation are employed after the removal of crosslinking. With the primers designed to target this viewpoint, all the ligation outputs that including this viewpoint sequence can be amplified and subsequently quantified by high-throughput sequencing. A resolution of several kb with a few million sequencing reads could be acquired by 4C technique (Yu and Ren 2017).

1.2.2.3 Chromosome Conformation Capture Carbon Copy: many to many

The Chromosome Conformation Capture Carbon Copy (5C) method is a high-throughput version of 3C containing a ligation-mediated amplification module. It was developed to survey interaction frequencies among a pool of preselected chromatin regions (Dostie et al., 2006). In 5C, a range of primers are designed at the restriction sites of selected genomic segments. These primers are pooled with a 3C library to “copy” a large number of different ligation products in the 3C library, resulting in a 5C library. This 5C library is proliferated with the universal tails contained in the 5C primers and quantified by high-throughput

sequencing (Ferraiuolo et al., 2012). The 5C technology can detect interactions for only the regions covered by the primer library, but interactions among hundreds of thousands of genomic loci can be investigated simultaneously.

1.2.2.4 Genome-wide Chromosome Conformation Capture: all to all

Genome-wide Chromosome Conformation Capture (Hi-C) allows for an unbiased survey of all potential contacts across the genome using high-throughput sequencing (Belton et al., 2012; Lieberman-Aiden et al., 2009). The information of global chromatin interactions produced *via* the Hi-C technology provides a comprehensive view of the 3D genome. In contrast to 3C, there are three main modifications. Firstly, overhangs generated by RE digestion are refilled with nucleotides, one of which is biotinylated. Secondly, ligated fragments are sheared by sonication. Thirdly, fragments with biotin at their ligation junctions are affinity purified by the streptavidin-coated beads. The biotin incorporated at the un-ligated ends of the linear fragments could be removed with the exonuclease activity of T4 DNA polymerase, making sequencing more efficient (Belton et al., 2012).

To improve the resolution and efficiency of proximity ligations and reduce the background noise, researchers have invented several variants of Hi-C (Hsieh et al., 2015; Rao et al., 2015; Beagrie et al., 2017; Nagano et al., 2015). In the original Hi-C assays, fragmentation of chromatin is generally carried out by RE digestion. Therefore, the resolution of genome architecture assessed by conventional Hi-C is restricted to the density of the RE sites on the linear genome. Instead of RE, DNase I or micrococcal nuclease can be applied in Hi-C with DNase I digestion (DNase Hi-C) or Hi-C with micrococcal nuclease digestion (Micro-C) (Hsieh et al., 2015; Ma et al., 2015). In addition, proximity ligation is the critical step of Hi-C. Non-specific ligation of the cross-linked DNA in diluted solution resulting from the chance of inter-molecular collisions is one of the main sources of bias (technical noise). Researchers invented Hi-C with *in situ* ligation (*in situ* Hi-C), in which the conventional Hi-C procedure was modified in such a way that proximity ligation was done within nuclei (Rao et al., 2014; Nagano et al., 2013; Nagano et al., 2015).

It should be noted that Hi-C and other C technologies capture contacts and estimate an average of interaction frequencies in a cell population. On the demanding of the goal to detect chromatin contacts in a single cell, single-cell Hi-C was established (Nagano et al., 2013). In this protocol, individual nuclei are manually isolated under the microscope after *in situ* proximity ligation, followed by the construction of sequencing libraries of Hi-C DNA

obtained from individual nuclei. Application of single-cell Hi-C allows one to infer chromatin interactions at a single-cell scale and uncover cell-to-cell variations, as well as to reveal dynamics of chromatin organization during cell differentiation and proliferation (Nagano et al., 2013; Stevens et al., 2017; Nagano et al., 2017; Du et al., 2017).

Most recently, a method termed as Genome Architecture Mapping (GAM) that does not require any chromatin digestion or ligation steps was invented (Finn and Misteli 2017; Beagrie et al., 2017). In the GAM technique, fixed cells embedded in sucrose and frozen are cryosectioned into a series of thin nuclear profiles, and the single nuclear profiles are harvested by laser microdissection. Subsequently, the DNA contained in each nuclear profile is isolated, amplified and sequenced. Genomic regions that are closer to each other in 3D nuclear space will be preferentially found in the same nuclear profile. GAM can detect clustering of multiple genomic regions, because GAM selects physical proximal genomic regions *via* producing a thin section of the nuclei. By contrast, because of the nature of proximity ligation, C-technologies can only determine pairwise interactions. By applying GAM, researchers have already revealed that interacting regions identified previously by other C-technologies containing clusters of enhancers (“super-enhancers”) and active genes (Beagrie et al., 2017).

Another newly developed method, which is also proximity-ligation-independent, is Split-Pool Recognition of Interaction by Tag Extension (SPRITE) (Quinodoz et al., 2018). In the SPRITE assay, crosslinks between DNA, RNA, and protein are formed in cells, followed by nuclei isolation and chromatin fragmentation. Then interacting molecules within a single complex are barcoded using split-and-pool approach, in which the DNA is split into 96 wells, tagged and then pooled together. This split-and-pool approach is repeated iteratively to generate unique barcodes. Finally, interactions between different genomic regions are identified by sequencing and matching reads containing the same barcode to find the so-called SPRITE clusters. Since SPRITE does not rely on proximity ligation, which is similar like GAM technique, it could be used to identify simultaneous contacts between three or more genomic segments within individual cells. Moreover, compared with GAM, SPRITE has the capacity to map both RNA and DNA interactions simultaneously (Quinodoz et al., 2018; Koch 2018).

1.2.2.5 Derivative C-technologies with reduced complexity

As we all know that Hi-C reveals all possible interactions in the whole genome, extremely large data sets and rigorous computational analysis methods are needed to thoroughly map 3D chromatin organization. By combining capture of targeted chromatin regions with C-technologies, researchers designed several strategies to reduce the complexity of chromatin interaction networks in sequencing libraries.

To identify all the possible interactions associated with preselected genomic regions such as promoters or enhancers, Capture Hi-C (Capture-C) was designed (Dryden et al., 2014). In Capture-C, a library of Hi-C is subject to do targeted capture by hybridizing to pools of DNA or RNA oligos (baits) to enrich all ligation junctions with at least one end of the bait end, leading to a preselected pool of the Hi-C library. This preselected Hi-C library is sequenced and analyzed to identify spatial contacts concerning these regions.

Besides, chromatin interaction analysis by pair-end tag sequencing (ChIA-PET) is a method which combines chromatin immunoprecipitation (ChIP), proximity ligation and sequencing, identifying interactions from a subclass of chromatin regions associated with a specific protein (Fullwood et al., 2009). In ChIA-PET, crosslinked chromatin is sonicated and then immunoprecipitated with antibodies against the protein of interest. Tethered DNA fragments in each of the chromatin-protein complexes are ligated with biotinylated DNA linkers, which enable the purification of ligation products. Then, the ligation products are amplified and sequenced (Fullwood et al., 2010). Therefore, in principle, a deeper sequencing depth of a subset of genomic regions can be achieved by the ChIA-PET method compared to that obtained by Hi-C method, offering us opportunities to reveal more structural details of these regions. ChIA-PET has been successfully used to probe interaction networks associated with RNA polymerase II (Pol II), CCCTC-binding factor, and the estrogen receptor on a genome-wide scale (summarized in (Fraser et al., 2015)). Most recently, researchers developed another two approaches: Proximity Ligation Assisted Chromatin Immunoprecipitation sequencing (PLAC-seq) and Hi-C Chromatin Immunoprecipitation (HiChIP), which are similar to ChIA-PET that are used to enrich long-range chromatin contacts associated with a protein of interest (Fang et al., 2016; Mumbach et al., 2016). Unlike ChIA-PET, in which proximity ligation is performed after ChIP, in PLAC-seq and HiChIP, proximity ligation is carried out in the nucleus prior to chromatin shearing.

1.3 The genome in a 3D nucleus

1.3.1 Global and local levels of chromatin organization

Overwhelming studies have proven that eukaryotic genomes are organized in hierarchical levels in the interphase nucleus (Gibcus and Dekker 2013; Doğan and Liu 2018; Dong et al., 2018). The first level of packaging is wrapping of the double-strand DNA helix around a histone octamer to form nucleosomes, which is similar in all organisms and effectively shortens the length of DNA by 7-fold (Heslop-Harrison and Schwarzacher 2011; Fraser et al., 2015). A nucleosome is composed of a histone octamer with 147 base pairs (bp) of DNA and serves as the basal structural unit of chromatin. The histone octamer itself is composed of two copies each of H2A, H2B, H3 and H4. The histone 1 binds to the linker DNA between two adjacent nucleosomes, generating a 11 nm “beads-on-string” chromatin fiber (Happel and Doenecke 2009). The next scale of genome organization is the formation of Topologically associated domains (TADs), which in general have a size range of tens to hundreds of kb. At a chromosomal scale, large blocks of euchromatin and heterochromatin tend to separate from one another, forming A and B compartments, respectively (Lieberman-Aiden et al., 2009). At the largest scale, different chromosomes occupy distinct volumes in a nucleus, forming chromosome territories (Sexton and Cavalli 2015; Yu and Ren 2017).

1.3.1.1 Chromosome territories (CTs)

The concept that each chromosome occupies a particular nuclear space in the interphase nucleus was first proposed by Carl Rabl in 1885, and was developed by Theodor Boveri who termed these distinct nuclear spaces occupied by chromosomes as CTs for the first time (Schubert and Shaw 2011). The existence of CTs was validated in 1980s in human cells when specific chromosomes were visualized by chromosome painting (FISH with whole-chromosome-specific DNA probes) (Manuelidis and Borden 1988). However, the high content of dispersed repetitive regions within plant genomes made chromosome painting challenging in plants. The first visualization of plant CTs was carried out by using interspecific hybrid lines, which carry one or more pairs of alien chromosomes (Schwarzacher et al., 1989). In this alternative approach, a probe that labeled the whole chromosome sequence of the alien species was used to show the presence of the alien chromosomes. The disadvantage of this approach was that the behaviour of an alien chromosome might not be as the same as that in the original species. Plant CTs were first visualized in *Arabidopsis* using chromosome paints that were chromosome-specific mixed bacterial artificial chromosome

(BAC) FISH probes (Lysak et al., 2001). Although it has not been clearly understood what controls the formation of CTs in the interphase nucleus, studies have suggested that several factors might be involved, e.g., DNA content, distribution of heterochromatin and repetitive regions, and interactions between chromatin and the nuclear envelope (NE) (Schubert and Shaw 2011).

Depending on species and cell type, plant chromosomes can adopt diverse configurations (Doğan and Liu 2018; Rodriguez-Granados et al., 2016; Tiang et al., 2012). The most famous and probably most widespread type of chromosome organization is the Rabl configuration. In the Rabl conformation, chromosomes fold back at their centromere, so that centromeres and telomeres are located at opposite poles of the nucleus. It is suggested that the formation of this configuration is linked to how chromosomes are orientated in the preceding anaphase, which is a time period when chromosomes are separated during mitosis. Chromosomes in plant species with large genomes such as wheat, oats, barley and rye, often adopt a Rabl conformation in all the interphase cell nuclei across various plant tissues (Cowan et al., 2001; Rosa and Shaw 2013). While in rice, Rabl chromosome configuration is observed in xylem vessel cell nuclei (Prieto et al., 2004). On the other side, it has been shown by recent Hi-C data that the chromosome organization in the rice leaf tissues (cells within which are mainly mesophyll cells) does not adopt a Rabl configuration (Liu et al., 2017). Nevertheless, interphase chromosomes in other non-plant systems such as *Drosophila*, *Sacharomyces pombe* and *Sacharomyces cerevisiae*, adopt the Rabl organization; whereas nuclei of generally somatic mammalian cells with very large genomes do not show the Rabl configuration (Schubert and Shaw 2011). Thereby, genome size is unlikely the determinant for the formation of the Rabl configuration (Santos and Shaw 2004).

Another well-known chromosome configuration is the Bouquet configuration, although this configuration is generally only found (or at least described) during meiosis (Cowan et al., 2001). In meiotic cells of maize, wheat and rice, telomeres are clustered at a specific spot beneath the NE while the remain of the chromosomes disperses throughout the nucleoplasm. An early study has indicated that the paring and recombination of homologous chromosomes are impaired in mutants that disrupt the Bouquet configuration (Tomita and Cooper 2006). It has been proposed that the clustering of telomeres in the Bouquet configuration promotes chromosomal pairing, which is crucial for the association of homologous chromosomes during meiosis (Cowan et al., 2001; Tomita and Cooper 2006).

Interestingly, *Arabidopsis* interphase chromosomes adopt neither the Rabl nor the Bouquet configuration, but display an overall Rosette configuration (Fransz et al., 2002; Tiang et al., 2012). In the Rosette configuration, the centromeres of all individual chromosomes and their flanking pericentromeric heterochromatin are highly condensed to generate distinct, dense bodies called chromocenters, which are localized at the NP. Euchromatin loops in Mb-size emanate from chromocenters, and thus resulting in a rosette-like structure of *Arabidopsis* CTs (Fransz et al., 2002). Intriguingly, telomeres are generally located in proximity to each other in all the three types of chromosome configurations – as in the Rosette configuration telomeres were found to cluster around the nucleolus (Fransz et al., 2002; Tiang et al., 2012).

Different types of chromosome configurations can be found in the same plant species, for example, rice chromosomes adopt the Rabl and the non-Rabl configuration in xylem vessel cells and mesophyll cells, respectively; and chromosomes exhibit the Bouquet configuration during meiotic cells. This suggests a possible correlation between chromosome configuration and cell identity. Even for the same cell type, chromosome configurations have been demonstrated to be dynamic (van Holde and Zlatanova 1995; Rodriguez-Granados et al., 2016; Wang et al., 2015a). For instance, the developmental program of etiolated seedlings shifts from skotomorphogenesis to photomorphogenesis upon light perception. This transition leads to the formation of highly condensed heterochromatin and the establishment of chromocenters (Bourbousse et al., 2015). Another sample is that chromocenters are decondensed under heat shock treatment in *Arabidopsis* (Pecinka et al., 2010; Wang et al., 2015b). Furthermore, in rice leaves, the induction of centromere polarization (which is a feature of Rabl configuration) in some interphase nuclei by 5-azacytidine (a DNA hypomethylation drug) treatment indicates that the methylation state of the chromosome can determine the overall CT configuration (Santos et al., 2011). Therefore, the dynamics of chromosome configuration might help plants to adapt to ever-changing environmental conditions.

1.3.1.2 Chromosome compartments

The exhibition of a plaid pattern after transforming the Hi-C contact matrix to the Pearson correlation matrix suggests the presence of two chromatin compartments within CTs (Lieberman-Aiden et al., 2009). Chromatin contacts within the same compartment are enriched, while chromatin contacts between different compartments are depleted. With principal component analysis of the Hi-C data, each chromosome can be segregated into A or B compartments, according to the first component. The A Compartments are associated with

active chromatin (euchromatin) marks such as a high density of genes, strong transcription activities, and enrichment of Histone H3 lysine 36 tri-methylation and DNase I hypersensitive sites (Lieberman-Aiden et al., 2009). By contrast, chromatin regions within B compartments display heterochromatin features such as a low gene density and repressive epigenetic modifications. It was reported that the localization of B compartments was highly correlated with late replicating and lamina-associated chromatin domains (Ryba et al., 2010). The spatial segregation of A/B compartments in nuclei has been confirmed with multiplexed FISH at single-cell level (Wang et al., 2016). Until now, all Hi-C maps have followed this binary classification of chromatin regions (reviewed recently in (Yu and Ren 2017)).

Similar to animals, chromatin compartmentalization in *Arabidopsis* and many crop species is mostly in line with the overall distribution pattern of euchromatin and heterochromatin (Grob et al., 2014; Dong et al., 2017; Liu et al., 2017; Wang et al., 2018a; Grob et al., 2013). Moreover, it has been shown that the annotated plant A/B compartments can be further divided into several sub-compartments, and every individual sub-compartment associates with a specific pattern of euchromatic/heterochromatic modifications (Dong et al., 2017). Furthermore, similar to that in animals, the annotation of A/B compartment in *Arabidopsis* shows a strong correlation to the DNA replication timing (Ryba et al., 2010; Concia et al., 2018).

Both intra- and inter-chromosomal interactions are part of the 3D genome organization (reviewed in (Maass et al., 2019)). In the genome of *Arabidopsis*, multiple genomic loci, which are far apart along the linear genome, form Interactive Heterochromatin Island (IHI) or KNOT Engaged Element (KEE), in which small patches of heterochromatin are dispersed in much bigger euchromatic regions (Feng et al., 2014b; Grob et al., 2014). These IHIs/KEEs are marked with histone 3 lysine 9 di-methylation (H3K9me2) modifications and appear to be enriched with transposable element (TE)-like repeat regions (Feng et al., 2014b; Grob et al., 2014). Even though the chromatin state of these IHIs/KEEs display similarities as that of pericentromeric regions (PRs), there are no enriched interactions between them. It has been revealed by Hi-C data that IHIs/KEEs frequently interact with telomeric and subtelomeric regions, and regions on distal euchromatic arms (Feng et al., 2014b). It remains unclear how these interactions are established, as some other regions that displayed similar epigenomic features do not behave like IHIs/KEEs. Removing most DNA methylation or H3K9me2 modification results in almost no alteration in interactions between IHIs/KEEs, implying that

DNA methylation and H3K9me2 are not directly involved in establishing IHIs/KEEs contacts (Feng et al., 2014b). Because there is no influence on local gene expression when the clustering of IHIs/KEEs is attenuated, it is proposed that the formation of strong chromatin contacts among IHIs/KEEs does not impose transcriptional regulation (Zhu et al., 2017). Most recently, a study suggested a biological role of this type of 3D genome organization in defending against invasive elements (e.g., transposons) by correlating the transgene silencing with the induction of ectopic IHIs/KEEs originated from transgene integration sites (Grob and Grossniklaus 2018). Overall, more efforts are required to understand the biological functions and molecular fundamentals of these regions.

1.3.1.3 Chasing TADs in plants

In the exploration of Hi-C maps, self-associating chromatin domains are detected and are referred to as TADs, which is one of the most predominant features of chromosome configuration (reviewed in (Yu and Ren 2017)). Each TAD is a relatively isolated local packing unit, such that long-range interactions between loci within one TAD are generally preferred over those between different TADs. In consequence, the formation of TADs enables long-range chromatin contacts with space constraints, granting target specificity of *cis*-acting elements. By using Hi-C, 3D FISH, and super-resolution microscopy to individual cells, Szabo and colleagues demonstrated that TADs were not just a reflection of statistical frequencies of chromatin interactions, but they were true structural units in the nucleus (Szabo et al., 2018). With a number of studies to explore how TADs are formed, it has been summarized that two major independent mechanisms are involved. The first one is CTCF (CCCTC-binding factor)-cohesin-dependent, in which loop-extrusion is conducted by cohesins and is stopped by CTCF proteins. The second one is independent of CTCF and cohesin proteins, and it is correlated to the spatial chromatin compartmentalization, which is in accordance with epigenomic landscape and transcriptional activity (Schwarzer et al., 2017; Dekker et al., 2013; Doğan and Liu 2018).

Surprisingly, although TADs have been observed in the genome of animals, they could be hardly found in the chromosome arms of the *Arabidopsis* genome (Feng et al., 2014b; Grob et al., 2014; Wang et al., 2015a). The absence of conventional insulators such as CTCF proteins in plants might be one reason for not observing TADs in *Arabidopsis*. Another reason for this might be technical. Because the input materials for *Arabidopsis* Hi-C are non-homogeneous, unsynchronized nuclei from cells with different types, endopolyploidy levels and cycle stages,

TADs in one specific type of nuclei could be masked (Doğan and Liu 2018). However, thousands of TAD-boundary-like and insulator-like regions have been characterized in *Arabidopsis* with the presence of highly expressed genes and accessible chromatin regions, while TAD interior-like regions have a tendency of inactive gene transcription (Feng et al., 2014b; Wang et al., 2015a).

Apart from *Arabidopsis*, Hi-C maps revealed that TADs are widespread structures in many crop species, such as rice, foxtail millet, sorghum, tomato, cotton and maize (Dong et al., 2017; Wang et al., 2017; Liu et al., 2017; Wang et al., 2018a). Similar to those in animals, TAD borders in plants also have enrichment of active genes and open chromatin with euchromatic histone modifications (Dong et al., 2017; Liu et al., 2017). TADs distribution patterns are conserved in mammalian genomes, but this is not the case for plant genomes with TADs (Rudan et al., 2015; Dong et al., 2017; Dixon et al., 2012). One possible explanation for missing the conservation of TAD pattern in plant species is the lack of CTCF protein, which appears to be associated with conserved TAD boundaries in mammals (Dong et al., 2017). The genome size of a plant species might be another factor that determines whether or not a given plant genome displays TADs (Doğan and Liu 2018). For all the plant species showing TADs, rice has the smallest genome size (~ 430 Mb), which is almost three times of the genome of *Arabidopsis thaliana* (Doğan and Liu 2018). Especially, TADs identified from Hi-C maps in rice are featured with depletion of protein-coding genes and enrichment of DNA methylation (Liu et al., 2017). As gene density of a plant species is negatively correlated with its genome size, it has been speculated that plants with larger genome size are more likely to form TADs (Doğan and Liu 2018).

1.3.1.4 Chromatin loops

The contact frequency of two distant chromatin loci caused by random collision on the basis of the polymeric nature of chromatin fiber is very low. Nevertheless, the real contact frequency of certain chromatin loci is higher than expected, resulting from chromatin fiber bending (chromatin loop). By chromatin looping, a gene's regulatory element can be brought into close spatial proximity. The first case study illustrating the involvement of chromatin looping in gene transcriptional regulation was about the beta (β)-globin locus in yeast (Carter et al., 2002; Tolhuis et al., 2002). Following that, a huge number of studies have demonstrated that chromatin looping has a great influence on gene transcription in animals (reviewed in (Kadauke and Blobel 2009; Bonev and Cavalli 2016)).

In plants, it also has been shown that different types of chromatin loops are involved in diverse developmental processes (summarized in (Rodriguez-Granados et al., 2016)). Generally, chromatin loops in the plant kingdom can be classified into two types: gene looping and enhancer-promoter looping. Gene looping is also called 5'-3' looping, which is a type of intra-chromosomal loop that connects the 5' end and transcription termination site (TTS) of a gene. Besides, many chromatin loops between 5' end of a gene and the corresponding gene body were also found in *Arabidopsis* according to the analysis of a high-resolution Hi-C map (Liu et al., 2016). Another kind of chromatin loop allows physical contact between enhancers and promoters. Although genes with such kind of looping structures are more actively transcribed than those without in *Arabidopsis*, we could not derive a causal relationship between chromatin loops and active transcription. Recent works have suggested that long non-coding RNAs, transcription factors (TFs) were involved in the regulation of this type of chromatin loops (Rodriguez-Granados et al., 2016). A study revealed that a conserved regulatory pathway of floral meristem determination was controlled by MADS TF-mediated chromatin loops. In this example, a chromatin loop between the transcription start site (TSS) and the 3'-distal region of the *TERMINAL FLOWER1 (TFL1)* gene was disrupted by the binding of MADS box TFs such as SUPPRESSOR OF OVEREXPRESSION OF CONSTANS 1 (SOC1), SHORT VEGETATIVE PHASE (SVP), AGAMOUS-LIKE 24 (AGL24), and SEPALLATA 4 (SEP4), leading to the reduced expression of the *TFL1* (Liu et al., 2013). In another example, it was reported that the expression of *PINOID (PID)*, an auxin-inducible gene, was repressed in the absence of auxin. Along with its repression state, the *PID* locus interacts with the *AUXIN REGULATED PROMOTER LOOP (APOLO)* locus, establishing a chromatin loop (repressive loop) that can be disrupted by auxin. After opening this chromatin loop, Pol II starts to transcribe both *PID* and *APOLO*. As a negative feedback mechanism, non-coding *APOLO* transcripts produced by Pol II trigger the re-establishment of the repressive loop to down-regulate the expression of *PID* gene (Ariel et al., 2014).

1.3.2 Chromatin positioning in the nuclear space

Apart from chromatin packing and organization, an increasing number of studies have proven the import function of the spatial localization of chromatin regions on gene transcriptional control (reviewed in (van Steensel and Belmont 2017; Doğan and Liu 2018; Buchwalter et al., 2019)).

1.3.2.1 Tethering chromatin in and around nucleolus

As the largest compartment of the nucleus, the nucleolus has been widely known for its role in controlling the expression of ribosomal RNA (rRNA) genes. Nucleoli also have special functions on the 3D genome organization in the nuclear space by acting as an anchoring site for certain chromatin regions, such as rRNA genes (Németh and Langst 2011). Some of these rRNA genes, for example, 45S rRNA genes, are arranged into tandem repeats and then array at nucleolus-organizing regions (NORs) (Németh and Langst 2011). The mammalian nucleolus is consisting of three functional and structural regions: fibrillar center, dense fibrillar component, and granular component. Active rRNA genes are located within the fibrillar center and are mainly transcribed by RNA polymerase I (Pol I), whereas inactive genes are located outside of the fibrillar center (Németh et al., 2010). Plant nucleoli are also strongly connected with rRNA genes (Pontvianne et al., 2016; Pontvianne et al., 2013; Durut et al., 2014). It has been shown that *Arabidopsis* active rRNA genes are localized within the nucleolus, while inactive rRNA genes are excluded (Pontvianne et al., 2013). However, this specific localization could be altered with changes in epigenetic states of the rRNA genes. Furthermore, Durut and colleagues suggested that the altered expression of some rRNA genes was determined by the active or repressed state of the NORs (Durut et al., 2014). Together, these results suggest that the spatial localization of rRNA genes with respect to nucleoli is corresponding to their transcriptional status. Moreover, it has been reported that the physical association between telomeres and nucleoli in *Arabidopsis* is required to maintain telomere (Armstrong et al., 2001; Pontvianne et al., 2016; Fransz et al., 2002).

Other than rRNA genes, genomic loci associated with nucleoli were identified by genome-wide approaches in mammals. These chromatin regions are referred to as nucleolus-associated domains (NADs) and show enrichment of A/T-rich sequences, low gene density and repressed transcriptional activity (van Koningsbruggen et al., 2010; Németh et al., 2010). Recently, plant NADs in *Arabidopsis* are discovered and characterized (Pontvianne et al., 2016). The authors isolated intact nucleoli from *Arabidopsis* seedlings using a modified fluorescence-activated cell sorting (FACS) method and analyzed the associated DNA. As expected, rRNA genes and telomeric regions were enriched. Besides that, plant NADs were also found to be enriched with TEs and inactive protein-coding genes. These findings imply the involvement of plant nucleoli in transcriptional regulation of not only rRNA genes but also other genomic loci.

1.3.2.2 Chromatin positioning at the NP

The NP has been known for a long time serving as a physical barrier, which separates the nucleus from the cytoplasm. In interphase nuclei of eukaryotic cells, genomic DNA exhibits non-random distribution patterns at the NP. In metazoans, it is well known that the NP provides a docking site for chromatin and plays important roles in genome organization and transcriptional regulation (Buchwalter et al., 2019; Meier et al., 2017).

Contacting chromatin with nuclear pore complexes

The NE is perforated with nuclear pore complexes (NPCs), which function as transport channels for molecules between nucleus and cytoplasm. This highly conserved structure is constructed with multiple copies of ~30 different nucleoporins (NUPs) (Buchwalter et al., 2019). These NUPs can be divided into two classes according to their functions. NUPs in the first class mainly serve as the structural framework of NPCs and do not participate in nuclear transport directly. NUPs in the second class are directly involved in the selective nuclear transport because of their unstructured domains that are rich in phenylalanine and glycine (FG repeats). In 2010, a proteomic study in *Arabidopsis* revealed the complete molecular structure of plant NPCs (Tamura et al., 2010). Most of the plant NUPs are well conserved, even though several NUPs presented in vertebrates have been replaced by plant-specific proteins. For instance, NUP136/NUP1, which contains FG repeats, is only found in plants, and it is thought to be the functional analog of metazoan NUP153 (Tamura et al., 2010; Tamura and Hara-Nishimura 2011).

Although it is assumed that the primary function of NPCs is controlling nucleocytoplasmic transport, an increasing number of studies in animals indicate that NPCs are involved in regulating chromatin organization and gene expression. In 1985, Blobel proposed a “gene gating” hypothesis, in which interactions between active genes and NPCs might promote the export of their mRNAs (Blobel 1985). An early study in yeast supported this hypothesis by demonstrating that some NUPs associated with active genes and these genes were more preferentially localized at the NPCs upon activation (Casolari et al., 2004). Later studies in yeast and *Drosophila* cells also demonstrated that tethering genes to the NPCs facilitated the activation of genes in response to stimuli (Hou and Corces 2010; Taddei et al., 2006; Brickner and Walter 2004). However, a genome-wide analysis in human HeLa cells argued against the “gene gating” model (Brown et al., 2008). It was reported in this study that NPC protein NUP93 predominantly associated at the NPC with chromatin domains with enrichment of

repressive histone marks (Brown et al., 2008). Another arguing evidence against this model is NUP170b, a yeast NPC protein, interacts with chromatin loci and serves as a transcription repressor (Van de Vosse et al., 2013).

Compared with that in animals, functions of plant NUPs regarding spatial chromatin organization and gene regulation have been rarely investigated. In a recent report by Smith et al., these authors tested the putative function of two *Arabidopsis* nucleoporins (SEH1 and NUP50a) in this regard by using the Lac Operator/Lac Repressor system (Smith et al., 2015). Tethering a reporter gene to SEH1 turned out to increase its expression, while anchoring it to NUP50a appeared to have a repressive effect (Smith et al., 2015). These results suggested that plants had the “gene gating” mechanisms, while not all the plant nucleoporins have this function.

Linking chromatin with the linker of nucleoskeleton and cytoskeleton

The linker of nucleoskeleton and cytoskeleton (LINC) complexes, another direct connection between the nucleoplasm and cytoplasm, was first discovered in *Drosophila* and *Caenorhabditis elegans* (*C. elegans*) by screening mutants showing defects in nuclear positioning and/or nuclear migration (Meier et al., 2017). The LINC complex is mainly composed of Sad1/UNC84 (SUN) homology domain proteins in the inner nuclear membrane (INM) and Klarsicht/ANC-1/Syne homology (KASH) domain proteins in the outer nuclear membrane (ONM) (hereafter referred as SUN and KASH proteins) (Meier 2016). There are transmembrane domains in both types of proteins. The KASH domain of KASH proteins is projected into the space between the ONM and INM of the nucleus, where it interacts with the SUN domain of SUN proteins (Chang et al., 2015). This kind of interactions make KASH proteins could not diffuse into the contiguous endoplasmic reticulum (Chang et al., 2015). KASH proteins stretch into cytoplasm, making LINC complexes can interact with different cytoskeleton elements and signaling molecules (Chang et al., 2015). Conversely, SUN proteins are localized in the INM, allowing LINC complexes to contact lamin proteins, chromatin-binding proteins, and other nuclear proteins (Chang et al., 2015). Therefore, the LINC complex is a two-membrane adhesive assembly, which makes it possible to transmit mechanical force across the NE (Chang et al., 2015). Interactions between the cytoplasmic extension of KASH proteins and different cytoskeleton filaments and/or factors enable LINC complexes possess diverse functions, such as nuclear movement, maintaining the centrosome-nucleus connection, nuclear morphology regulation, signal transduction, and moving

chromosomes within the nucleus during meiosis (reviewed in (Burke and Roux 2009; Starr and Fridolfsson 2010)).

Recently, researchers have identified plant LINC complexes and their involvements in nuclear migration in pollen tubes and male fertility, as well as in nuclear positioning in the root hair cells, guard cells, and leaf epidermal cells (reviewed in (Meier et al., 2017)). The phylogenetic relationship of different components of plant LINC complex has been analyzed in a very recent study (Poulet et al., 2017b). This study shows that some KASH proteins are conserved across land plants, while other KASH proteins are angiosperm-specific (Poulet et al., 2017b). Compared to the evolution complexity of the KASH proteins, SUN proteins are much more conserved, with conservation in land plants for C-terminal SUN proteins and conservation throughout the plant kingdom for mid-SUN proteins (Poulet et al., 2017b).

The role of plant LINC complexes in determining the nuclear morphology was also found in plants (Zhou et al., 2015). Potential redundancy among gene families of WPP domain-interacting proteins (WIPs), WPP domain-interacting tail-anchored proteins (WITs), and SUN proteins in regulating nuclear morphology was proposed (Zhou et al., 2015). It was found that WIT2, but not WIT1, was crucial for nuclear morphology, and that SUN1 played a more important role in this process than SUN2. The observed nuclear morphology changes in the *wit* and *sun* mutants are independent of CRWODED NUCLEI1 (CRWN1), although nuclei in *crwn1* mutant become spherical, suggesting that plant nuclear morphology is determined both by cytoplasmic forces transferred to the NE and by nucleoplasmic filaments formed beneath the NE (Zhou et al., 2015).

In attempting to assess the regulatory roles of plant LINC complexes in chromatin architecture, Poulet and colleagues have developed a 3D imaging method to probe the nuclear morphology and chromatin organization in interphase nuclei of *Arabidopsis* mutants of LINC components (Poulet et al., 2017a). It was found that perinuclear localization of chromocenters in WT plants was altered in LINC mutants, and the compaction levels of chromocenters were changed (Poulet et al., 2017a). Interestingly, the authors also found alleviation of transcriptional repression in heterochromatic repeat sequences in several LINC mutants, implying that the *Arabidopsis* NP plays roles in regulating chromatin condensation and gene expression (Poulet et al., 2017a).

Anchoring chromatin to the nuclear lamina

The genome is enclosed within the nucleus by the NE. In metazoans, there is a layer of meshwork underlies the NE, which is called the nuclear lamina (NL). The interaction network of chromatin-NL is a prominent feature of the NP in most cell lines (reviewed in (van Steensel and Belmont 2017)). The NL is composed of lamins and lamin-associated transmembrane proteins, which corporately maintain mechanical properties of the nuclear architecture (Dechat et al., 2008). There are four main lamins in mammalian cells, which can be divided into two types: A-type lamins including lamin A and lamin C, and B-type lamins including lamin B1 and B2. At least one B-type lamins is present in every cell type, while A-type lamins are absent in ESCs, and the expression of type-A lamins is low in pluripotent cells and increases upon cell differentiation (Pombo and Dillon 2015; Buchwalter et al., 2019). Nuclear lamins are necessary for maintaining nuclear shape. Cells with loss-of-function of lamins generally exhibit misshapen nuclei (Pombo and Dillon 2015). A modified DNA adenine methyltransferase identification (DamID) technology with the fusion of lamin A, B1 or B2 to Dam has been applied to identify chromatin regions localized at the NL in *D. melanogaster*, *C. elegans*, and mammalian cells (van Steensel and Belmont 2017). The identified NL-associated chromatin regions, named lamina-associated domains (LADs), vary in size (0.1-10 Mb) and are strongly enriched with genomic and epigenomic features indicative of repressed chromatin (van Steensel and Belmont 2017; Buchwalter et al., 2019). There are two types of LADs in various mammalian cell types: constitutive lamina-associated domains (cLADs) and facultative lamina-associated domains (fLADs). The sizes and positions of cLADs are conserved across different cell lines and even between different mammalian species, whereas fLADs are not (Meuleman et al., 2013).

LADs cover up to one-third of the mammalian genome. In spite of having low gene densities, they still contain thousands of genes, most of which are not expressed or expressed at very low levels (van Steensel and Belmont 2017). This suggests that chromatin-NL interactions at the NP are linked to regulation of gene expression. A growing number of studies have investigated the effect of chromatin-NP interactions on gene expression (Pombo and Dillon 2015; Buchwalter et al., 2019). For example, anchoring a reporter gene to the INM downregulates its expression (Reddy et al., 2008). Similarly, reporter genes inserted within LADs showed reduced expression levels compared to reporter genes residing in nucleoplasm (Akhtar et al., 2013). In addition, deleting the *Drosophila* B-type lamin, lamDm₀, causes

detachment of tissue-specific gene clusters from NL and selective transcriptional up-regulation of these genes (Shevelyov et al., 2009). Moreover, it was shown that repositioning genomic regions to the NP in human cells did not always result in gene silencing (Finlan et al., 2008). This result suggests that perinuclear localization alone is not sufficient for gene silencing.

Furthermore, great efforts have also been put to understand the molecular mechanisms of the formation of chromatin-NL interactions. The identification of proteins that promote tethering LADs toward the NL has made remarkable progress. Lamin proteins and many lamin-binding proteins together constitute the NL (reviewed in (Wilson and Foisner 2010)). Among them, lamin proteins are obvious candidates required for the formation of the chromatin-NL network at the NP, as they interact with both DNA and chromatin in vitro (Gruenbaum and Foisner 2015). In *Drosophila*, the depletion of the B-type lamin resulted in detachment of genes tethered at the NP (Shevelyov et al., 2009). However, elimination of all lamins in mouse ESCs has no significant influence on the establishment of genome-wide LADs at the NP, reflecting from the determination of genomic interactions with emerin (an INM marker) (Amendola and van Steensel 2015). Genetic studies provide a possible explanation that lamin A/C and lamin B receptor (LBR) play redundant roles in establishing chromatin-NL interactions. A study supported this speculation by showing that heterochromatin was localized in the nuclear interior when both LBR and lamin A/C were knocked out in post-mitotic cells (Solovei et al., 2013). Besides, ectopic expression of LBR in retinal cells, which express neither lamin A/C nor LBR, causes the nuclear interior-localized heterochromatin to relocate toward the NP (van Steensel and Belmont 2017). In addition to LBR, numerous other NE transmembrane proteins (NETs) are docked at the INM. Overexpression or depletion of some NETs, such as emerin, can also alter chromatin positioning with respect to the NP (Amendola and van Steensel 2015).

Except for the lamina network, chromatin state in these LADs might also have an impact on forming chromatin-NL interactions. It has been reported in several studies that histone H3 lysine 9 methylation (H3K9me) plays prominent roles in this process. According to genome-wide studies, the heterochromatic mark, histone H3 lysine 9 di-methylation (H3K9me₂), tends to be enriched in LADs (Kind et al., 2013). Inactivation of G9A, the primary enzyme responsible for depositing H3K9me₂ to chromatin, leads to a reduction of LAD-NL contacts, indicating the partial role of H3K9me₂ in facilitating NL-chromatin interactions (Kind et al.,

2013). In accordance with these reports, H3K9me2 and histone H3 lysine 9 tri-methylation (H3K9me3) have been shown to participate in positioning β -globin locus to the NP (Bian et al., 2013). Knockdown of Suv39H1 and Suv39H2, the two H3K9me3 methyltransferases, results in partial detaching endogenous mammalian β -globin gene (*HBB*), and inhibition of G9A leads to incomplete detachment of endogenous locus from the NP (Bian et al., 2013). Only depleting all the three H3K9me methyltransferases, Suv39H1, Suv39H2 and G9A, completely detaches the endogenous *HBB* locus and most of an adjacent \sim 1 Mb LAD from the NP (Bian et al., 2013). These results indicate that these three enzymes play redundant roles in promoting associations of NL with chromatin. Similarly, in *C. elegans*, the peripheral anchoring of transgene repeats and native chromosomal arms requires H3K9me, as eliminating this histone mark leads to the loss of attachment of chromatin from the NP (Towbin et al., 2012).

In *C. elegans*, CEC-4, a chromodomain-containing protein, was reported to link the H3K9me to the NL. CEC-4 was found to be associated with the NE and to interact with mono, di, and tri-methylated H3K9 through its chromodomain. Therefore, it was suggested that CEC-4 could tether heterochromatin to the NL through recognizing methylated H3K9. In addition, decreasing genome-wide chromatin-NL contacts in *cec-4* was similar with that in the *met-2 set-25* double mutants (Gonzalez-Sandoval et al., 2015). In mammals, a protein named PRR14 was found to play similar roles as the *C. elegans* CEC-4 in tethering LADs to the NP (Poleshko et al., 2013). The PRR14 protein possesses two functional domains that are critical for anchoring heterochromatin to the NL. One of the two domains can target NL, and the other one can bind to heterochromatin protein 1 alpha (HP1 α), which is known to bind to H3K9me2 or H3K9me3. PRR14-HP1 α interactions make PRR14 load onto chromosomes immediately after mitosis, whereas later in interphase, Lamin A/C is required for localizing PRR14 at the NL (Poleshko et al., 2013).

Moreover, it has been reported that knockdown of EZH2, a methyltransferase responsible for depositing histone H3 lysine 27 tri-methylation (H3K27me3), results in a reduction of peripheral association of an exogenous LAD fragment (Harr et al., 2015). This report implies that H3K27me3 might also be involved in LADs formation. A study showed that the barrier-to-autointegration factor (BAF), which interacts with LEM-domain containing proteins that are part of the NL, can associate with chromatin at the NP (Kind and van Steensel 2014). BAF associates with the same genomic regions as Lamin B1, Lamin B2 and Lamin A, while

no detectable alterations in LAD-NL interactions were found when knockdown of BAF, suggesting that BAF does not help to tether LADs to the NL during interphase (van Steensel and Belmont 2017). Overall, the lamina network, repressive histone mark H3K9me and bridging proteins are required for specific positioning of LADs at the NP in metazoans.

Plant genomes do not encode proteins with sequence similarity to the animal lamins. However, a complex protein meshwork attached to the INM has been observed in several plant species, indicating the presence of plant lamina (Ciska and Moreno Diaz de la Espina 2014). To date, three plant-specific protein families, localized preferentially at the INM have been proposed as functional lamin analogs. CRWNs are considered as the first group of candidates for plant lamin analogs and are present throughout land plants (reviewed in (Groves et al., 2018)). CRWN proteins with long coiled-coil domains belong to the nuclear matrix constituent proteins (NMCPs) (Meier et al., 2017). In *Arabidopsis*, *CRWN1-4* genes encode four CRWN proteins, which are essential for viability as the quadruple *crwn* mutant could not be isolated (Wang et al., 2013). Among the four CRWN proteins, CRWN1 and CRWN4 are located at the INM, while CRWN2 and CRWN3 are mainly localized in the nucleoplasm (Sakamoto and Takagi 2013; Wang et al., 2013). The nuclei of plants with mutation at *CRWN1* or *CRWN4*, not *CRWN2* or *CRWN3*, exhibit reduced size and increased sphericity (Sakamoto and Takagi 2013; Dittmer et al., 2007; Wang et al., 2013). However, combining *CRWN2* or *CRWN4* mutation with *CRWN1* mutation results in a greater nuclear size reduction (Sakamoto and Takagi 2013; Wang et al., 2013). In *Arabidopsis*, the KAKU4 protein, which shows specific localization at the INM, is considered as the second class of plant lamin candidates (Goto et al., 2014). The KAKU4 protein has a predicted nuclear localization signal (NLS), but no typical transmembrane domains (Goto et al., 2014). An evolution analysis of NE proteins in unicellular algae and multicellular plants revealed that there was only one KAKU4 homolog in every species except for *Glycine max* and *Brassica rapa* (Poulet et al., 2017b). It was observed that *kaku4* mutant plants have spherical and smaller nuclei, which is similar to those of *crwn1* and *crwn4* mutants. At the NP, KAKU4 can physically interact with CRWN1 and its homolog CRWN4. Furthermore, KAKU4 and CRWN1 can deform the NE independently of each other in a dose-dependent manner. Recently, a novel family of plant nuclear envelope-associated proteins (NEAPs) in *Arabidopsis* have been suggested as the third class of plant lamin candidates (Pawar et al., 2016). There are four NEAPs (NEAP1-4) in *Arabidopsis*, with NEAP4 being a truncated form of NEAP3. *Arabidopsis* NEAP1-3 are anchored at the INM and interact with each other to form homomers and heteromers. Besides, NEAP proteins also

interact with members in the LINC complex. The *neap1*, *neap3* and *neap1neap3* mutants show increased nuclear volume in pavement cells and decreased number of chromocenters in both pavement and guard cells. In addition, both pavement and guard cells in *neap3* single mutant exhibit a reduced relative heterochromatin fraction. Together, these results suggest that NEAPs have functions on maintaining nuclear morphology and organization (Pawar et al., 2016).

Aside from being structural proteins that control plant nuclear size and morphology, a number of studies in *Arabidopsis* have suggested that plant lamins play roles in regulating chromatin organization and gene expression at the NP (summarized in (Meier et al., 2016; Groves et al., 2018; Meier et al., 2017)). Firstly, altered chromatin organization has been observed in some plant lamin mutants. Variability in chromocenters number and size in *crwn* nuclei suggests that CRWN proteins are required for maintaining the integrity of chromocenters and the compaction of heterochromatin (Wang et al., 2013; Poulet et al., 2017a). Changes in nuclear organization and reduced heterochromatin fraction have been found in the *neap1 neap3* plants (Pawar et al., 2016). Secondly, it has been reported that some plant lamins can interact with transcription regulators. Interactions between CRWN1 and NAC WITH TRANSMEMBRANE MOTIF1-LIKE9 (NTL9), a NAC transcription factor, were reported recently (Guo et al., 2017). CRWN1 has also been shown to interact with PWWP INTWERACTION OF POLYCOMBS 1 (POW1), which in turn binds to Polycomb Repressive Complex 2 (PRC2) that is responsible for the establishment of H3K27me3 (Mikulski et al., 2019). NEAPs were found to interact with a basic-leucine zipper domain transcription factor (bZIP18). Transient co-expression of bZIP18 and NEAPs leads to the detachment of NEAPs from the NP (Pawar et al., 2016). Thirdly, in a very recent study, the transcriptome data of different *crwn* mutants demonstrated that single knockout of *CRWN1*, *CRWN2* or *CRWN4* gives rise to widespread alterations in their transcript levels, in spite of no whole-plant phenotypes (Choi et al., 2019). Knockout of *CRWN2* in *crwn1* mutant exacerbates the transcriptional alterations in *crwn1*, whereas knockout *CRWN1* in *crwn4* mutant alleviates the transcriptional changes in *crwn4*. The results of the study suggest that CRWN1 and CRWN2, which are close paralogs in the same clade, play overlapping functions, while CRWN1 and CRWN4, which are categorized into two different clades, partially exhibit antagonistic functions.

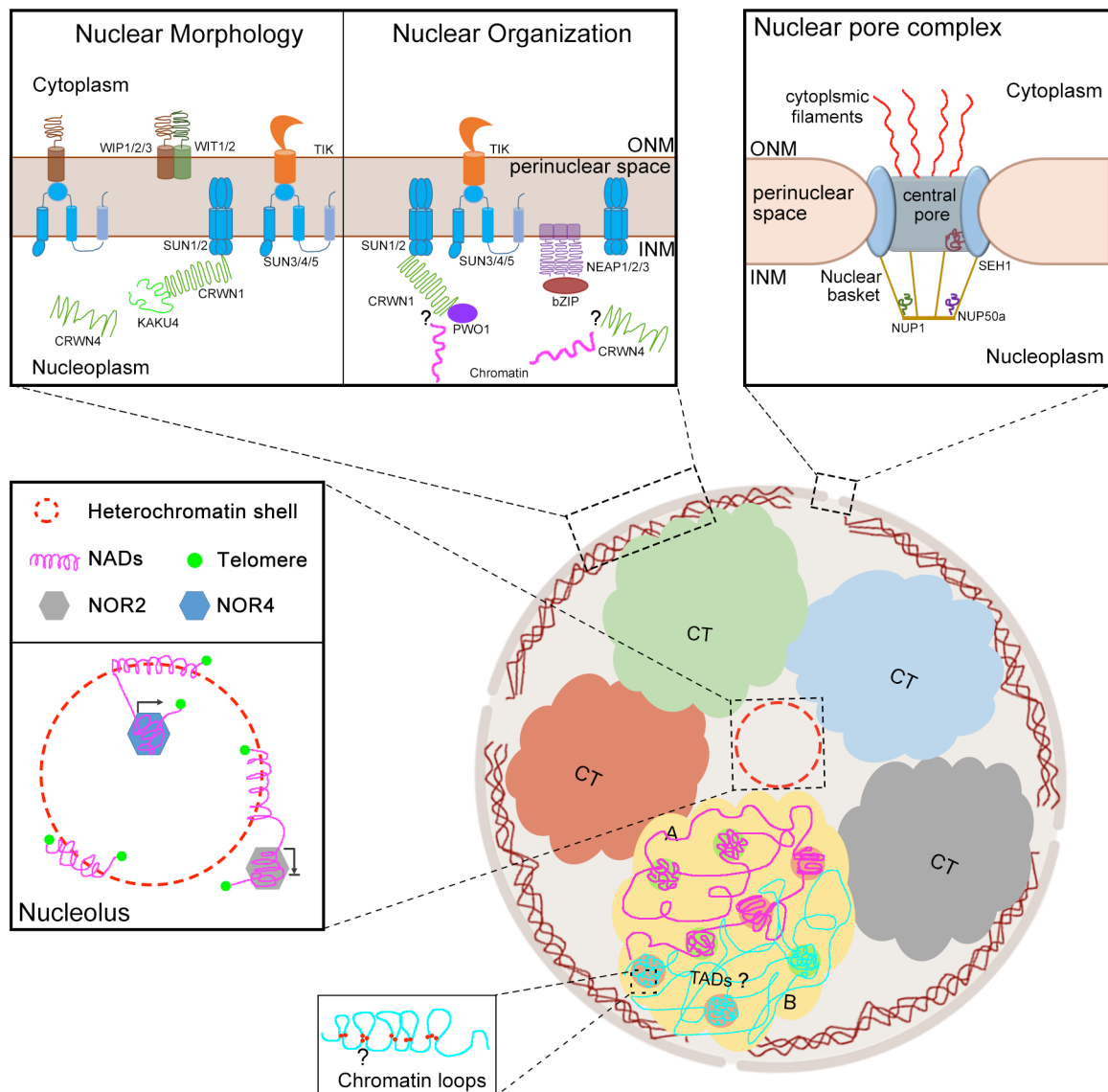


Figure 1. Plant nuclear chromatin organization and key elements involved in nuclear dynamics.

Individual chromosomes at interphase are organized into discrete CTs. CTs can be further partitioned to distinct active (A) and repressive (B) compartments. Chromatin regions, in plants with large genome size, organized into the same TAD exhibit increased interactions, whereas their interactions with adjacent regions outside of the TAD are rather depleted. Except for *Arabidopsis thaliana* and *Arabidopsis lyrata*, TADs are manifested in other examined plant species (question mark). Only a limited number of plant chromatin loops that connect regulatory elements to their target loci have been reported (summarized in (Liu and Weigel 2015)), and the molecular mechanisms of how these plant chromatin loops are formed have not been understood well (question mark). As shown in the middle left box, the nucleolus is surrounded by a heterochromatin shell (red dashes), in which, a dense chromatin meshwork called NADs (purple lines) is included. *Arabidopsis* telomeres (green circles), which are regions of repetitive nucleotide sequences at ends of individual chromosomes, are localized around and within the nucleolus. In *Arabidopsis*, some rRNA genes on chromosome 2 and chromosome 4 are arranged into nucleolus-organizing region 2 (NOR2) and NOR4, respectively. These two NORs occupy alternative subnuclear localization with respect to nucleolus depending on their activity state, in which NOR2 is localized outside of nucleolus and exhibits very low transcriptional activity; while NOR4 is localized within the nucleolus and is actively transcribed. In the top left box, NE-associated proteins that are involved in nuclear dynamics are shown.

In the top right box highlights several components of NPC, which were suggested to be involved in regulating nuclear shape and gene expression.

1.4 Aim of the thesis

Overwhelming LADs studies in animals make us reason whether chromatin positioning at the NP in plants is also non-random. However, little is known about the global NP-chromatin interaction patterns in plants (Armstrong et al., 2001; Fransz et al., 2002). Although plant lamin candidates have been discovered since more than 10 years ago, their relationship with perinuclear chromatin remains unclear (reviewed in (Groves et al., 2018; Meier et al., 2017)). This thesis represents our efforts in understanding the roles of plant lamins in mediating perinuclear chromatin anchoring. The first part of this thesis focuses on the identification and characterization of chromatin regions localized at the NP. By conducting a Restriction Enzyme Mediated Chromatin Immunoprecipitation (RE-ChIP) assay, we provide a genome-wide landscape of the NP-chromatin interactions. The second part of this thesis work focuses on verifying whether heterochromatin-related factors and plant lamin candidates are involved in forming specific perinuclear chromatin anchoring patterns. By conducting dual-color FISH experiments on *Arabidopsis thaliana* 2C nuclei, we demonstrate that plant lamin candidates and non-CG DNA methylation are required for specifically positioning chromatin at the NP. Further, chromosome painting experiments reveal a global alleviation of spatial chromatin positioning patterns in the nuclei of *crwn1* and *crwn4* mutants. Moreover, our ChIP assays reveal that CRWN1 interacts with chromatin directly at the NP.

2. Materials and Methods

2.1 Materials

2.1.1 Plants

All *Arabidopsis thaliana* transfer (T)-DNA insertion lines were ordered from the Nottingham Arabidopsis Stock Center (NASC, UK) or received from other labs. T-DNA lines were in Columbia-0 (Col-0) background and were established as homozygous lines. All the higher-order mutants were generated by crossing different T-DNA lines, with exceptions that *drm1-2 drm2-2* was ordered from NASC and *suvh4 suvh5 suvh6* was received from F. Berger's lab (Gregor Mendel Institute). The T-DNA lines and their derived higher-order lines are summarized in Table 1. The tagging lines generated and used are summarized in Table 2.

Table 1. *Arabidopsis* mutants used in this study

AGI	Gene	Mutant (type)	Stock	Reference
AT3G10650	<i>NUP1</i>	<i>nup136-1 (nup136)</i>	SALK_104728	(Alonso et al., 2003)
AT1G67230	<i>CRWN1</i>	<i>crwn1-1 (crwn1)</i>	SALK_025347	(Alonso et al., 2003)
AT1G13220	<i>CRWN2</i>	<i>crwn2-1 (crwn2)</i>	SALK_076653	(Alonso et al., 2003)
AT1G68790	<i>CRWN3</i>	<i>crwn3-1 (crwn3)</i>	SALK_099283	(Alonso et al., 2003)
AT5G65770	<i>CRWN4</i>	<i>crwn4-1 (crwn4)</i>	SALK_079296	(Alonso et al., 2003)
AT4G31430	<i>KAKU4</i>	<i>kaku4-2 (kaku4)</i>	SALK_076754	(Alonso et al., 2003)
AT3G05830	<i>NEAP1</i>	<i>neap1-1 (neap1)</i>	SAIL_846_B07	McElver et al. 2001
AT1G09470	<i>NEAP3</i>	<i>neap3-1 (neap3)</i>	GABI_221C05	GABI-Kat project
AT4G19020	<i>CMT2</i>	<i>cmt2-3 (cmt2)</i>	SALK_012874	(Alonso et al., 2003)
AT1G69770	<i>CMT3</i>	<i>cmt3-11 (cmt3)</i>	SALK_148381	(Alonso et al., 2003)
AT5G49160	<i>MET1</i>	<i>met1-3 (met1)</i>		(Saze et al., 2003)
AT1G67230 AT5G65770	<i>CRWN1</i> <i>CRWN4</i>	<i>crwn1-1 crwn4-1</i> <i>(crwn1/4)</i>	SALK_025347 SALK_079296	
AT1G67230 AT1G13220	<i>CRWN1</i> <i>CRWN2</i>	<i>crwn1-1 crwn2-1</i> <i>(crwn1/2)</i>	SALK_025347 SALK_076653	
AT5G13960 AT2G35160 AT2G22740	<i>SUVH4</i> <i>SUVH5</i> <i>SUVH6</i>	<i>suvh4 suvh5 suvh6</i> <i>(suvh4/5/6)</i>	SALK_041474 GABI_263C05 SAIL_1244_F04	
AT4G19020 AT1G69770	<i>CMT2</i> <i>CMT3</i>	<i>cmt2-3 cmt3-11</i> <i>(cmt2/3)</i>	SALK_012874 SALK_148381	
AT5G15380 AT5G14620	<i>DRM1</i> <i>DRM2</i>	<i>drm1-2 drm2-2</i> <i>(drm1/2)</i>	SALK_031705 SALK_150863	

AT4G19020 AT5G15380 AT5G14620	<i>CMT2</i> <i>DRM1</i> <i>DRM2</i>	<i>cmt2-3 drm1-2 drm2-2</i> (<i>cmt2 drm1/2</i>)	SALK_012874 SALK_031705 SALK_150863	
AT1G69770 AT5G15380 AT5G14620	<i>CMT3</i> , <i>DRM1</i> , <i>DRM2</i>	<i>cmt3-11 drm1-2 drm2-2</i> (<i>cmt3 drm1/2</i>)	SALK_148381 SALK_031705 SALK_150863	

Table 2. The tagging lines used in the study

<i>pNUP1::NUP1:GFP nup136-1</i>
<i>p35S::CENH3:mcherry pNUP1::NUP1:GFP nup136-1</i>
<i>pCRWN1::CRWN1:2HA crwn1</i>
<i>pCRWN4::CRWN4:2HA crwn4</i>
<i>pCRWN2::CRWN2:2HA crwn1/crwn2</i>

2.1.2 Bacterial strains

Table 3. Bacterial strains used in this study

Species	Strain
<i>Escherichia coli</i>	DH5 α
<i>Escherichia coli</i>	DB 1.3
<i>Agrobacterium tumefaciens</i>	ASE
<i>Agrobacterium tumefaciens</i>	GV3101

2.1.3 Media and antibiotics

The media used in this study were sterilized by autoclaving for 20 minutes (min) at 121°C and are listed in Table 4. All buffers were prepared based on (Molecular cloning, 3rd edition, Sambrook and Russell). Antibiotics were added to the sterilized medium to achieve final concentrations as listed as summarized in Table 5.

Table 4. Media used in this study

Media	Ingredients (1 liter)	Species
Luria-Bertani broth (LB) medium (with or without Agar)	10 g Tryptone, 5 g Yeast extract, 5 g NaCl, pH 7.0	<i>Escherichia coil</i>
Yeast Extract Peptone (YEP) medium	10 g Peptone, 10 g Yeast extract, 5 g NaCl, pH 7.5	<i>Agrobacterium tumefaciens</i>
1/2 Murashige-Skoog Medium (1/2 MS)	2.2 g MS (Duchefa), 10 g sucrose, 3 g Phytigel, pH 5.7	<i>Arabidopsis thaliana</i>

Table 5. Antibiotics used in this study

Antibiotics	Stock concentration (mg/ml)	Solvent	Working concentration (µg/ml)
Kanamycin	50	Water	50
Spectinomycin	100	Water	100
Gentamycin	25	Water	25
Rifampicin	50	Water	50
Tetracyclin	5	Ethanol (70%, v/v)	5
Chloramphenicol	25	Ethanol (70%, v/v)	25

2.1.4 Vectors

Table 6. Vectors used in this study

Vector	Characteristics	Reference
pFK 206	pSa ori, ori, PNOS, TNOS, TE9, T3 promoter, PT7, Plac, lac operator, attB1, attB2, Spec ^r , chlor ^r , Basta ^r . Gateway-compatible pGREEN-IIS binary destination vector	(Karlsson et al., 2015)
pFK 210	P35S, tE9, PA _t 2S3, T _M AS, ori, pSa ori, attB1, attB2, Spec ^r , chlor ^r , Basta ^r . Gateway-compatible pGREEN-IIS binary destination vector including a 35S promoter.	(Karlsson et al., 2015)
pSoup	Helper plasmid	

2.1.5 *Agrobacterium tumefaciens* contain plasmid-DNA

To generate stable *Arabidopsis* tagging lines, we constructed plasmids and transfer them into *Agrobacterium tumefaciens* (*Agrobacteria*) by electroporation, respectively. All the plasmids generated in this study are summarized in Table 7.

Table 7. Plasmids in *Agrobacteria* used in this study

Plasmids	Vectors	Strains of <i>Agrobacteria</i>	Antibiotic resistance	Plant selection marker
<i>pNUP1::NUP1:GFP</i>	pFK206	ASE	Spec ^r , kan ^r , Tetra ^r , chlor ^r	Basta
<i>p35S::CENH3:mcherry</i>	pFK210	ASE	Spec ^r , kan ^r , Tetra ^r , chlor ^r	Basta
<i>pCRWN1::CRWN1:2HA</i>	pFK206	ASE	Spec ^r , kan ^r , Tetra ^r , chlor ^r	At2S3:mCherry
<i>pCRWN4::CRWN4:2HA</i>	pFK206	ASE	Spec ^r , kan ^r , Tetra ^r , chlor ^r	At2S3:mCherry
<i>pCRWN4::CRWN4:2HA</i>	pFK206	GV3101	Spec ^r , gent ^r , Tetra ^r , Rif ^r	At2S3:mCherry
<i>pCRWN2::CRWN2:2HA</i>	pFK206	ASE	Spec ^r , kan ^r , Tetra ^r , chlor ^r	At2S3:mCherry
<i>pCRWN2::CRWN2:2HA</i>	pFK206	GV3101	Spec ^r , gent ^r , Tetra ^r , Rif ^r	At2S3:mCherry

2.1.6 Enzymes and antibodies

Restriction enzymes, ligase and DNA modification enzymes were purchased from Thermo Fisher Scientific and New England BioLabs. Antibodies were purchased from the companies Sigma Aldrich, Invitrogen, Abcam, Santa Cruz and are listed in Table 8.

Table 8. Antibodies used in this study

Experiments		Antibody	Host	Dilution	Company
RE-ChIP		α -GFP	rabbit	2.5 μ g/sample	Abcam
	control	IgG	rabbit	2.5 μ g/sample	Santa Cruz
Western blot		α -HA HRP conjugate	rabbit	1:5000	Santa Cruz
Immunohis- tostaining		α -HA Alexa Fluor 647 conjugate	mouse	1:500	ThermoFisher Scientific
FISH	Primary antibodies	α -digoxin	mouse	1:500	Sigma Aldrich
		α -dinitrophenyl	rabbit	1:500	Sigma Aldrich
	Secondary antibodies	α -mouse Alexa Fluor 488	goat	1:150	Invitrogen
		α -rabbit Alexa Fluor 546	goat	1:150	Invitrogen

2.1.7 Chemicals, beads and solutions

All chemicals used in this study are laboratory grade. They were purchased from Sigma-Aldrich, Carl Roth, Merck, Qiagen, Invitrogen, Duchefa, Fluka, except for specially noted ones. Protein A/G magnetic protein beads were purchased from Thermo Fisher Scientific. AMPure® XP beads were purchased from Beckman Coulter. All buffers and solutions were prepared, if not stated specially, otherwise, with milli-Q water. Sterilization was conducted by autoclaving or filter sterilization upon requirements.

2.1.8 Oligonucleotides

The oligonucleotides used in this study were synthesized by Eurofins MWG Operon. The sequences of these oligonucleotides are listed in Appendix Table 9.

2.2 Methods

2.2.1 Plant growth

2.2.1.1 Growth conditions and treatments

Arabidopsis seeds were sown on steam-sterilized GS90-soil (Gebr. Patzer GmbH) mixed with vermiculite or after surface-sterilization with 70% ethanol (v/v) on sterile 1/2 MS media

plates. After stratification of the seeds at 4 °C in the dark for 2 days, the plants were grown in long-day (16 light/8h dark) environmental chambers or greenhouse under standard conditions (150 μ mol/cm²s light, 40-60% humidity, 22 °C).

To examine the effect of H₂O₂, sodium chloride (NaCl), Ammonium (NH₄⁺), together with Nitrate (NO₃⁻), and zeocin treatments on *Arabidopsis* plant growth. After measurement of root length of five-day-old seedlings which were grown vertically on 1/2 MS media plates, these seedlings were transferred to new media plates supplied with or without one of these chemicals, and continued to vertically grow for another five days. The root length of these seedlings under normal conditions or treatments was measured again.

2.2.1.2 Seed surface sterilization

Sterilization of *Arabidopsis* seeds was conducted by 70% (v/v) ethanol. Seeds were placed into Eppendorf tubes and immersed in 70% (v/v) ethanol. The Eppendorf tubes were laid down on a shaker for ~15 min (100 rpm). After incubation, the seeds were rinsed with autoclaved milli-Q (ddH₂O) water for 3 times and then placed on 1/2 MS square plates (120 mm x 120 mm). The density is ~25 seeds/line, 4 lines/plate.

2.2.2 Microbe cultivation

2.2.2.1 Growth of *Escherichia coli*

Escherichia coli (*E. coli*) strains were cultivated overnight either on LB plates in 37 °C incubator or in liquid LB medium in 37 °C shaker at 180 rpm. Appropriate antibiotics were added into the medium according to the resistance cassettes of each strain.

2.2.2.2 Growth of *Agrobacteria*

Agrobacteria strains were cultivated either on LB plates in 28 °C incubator or liquid LB medium in 28 °C shaker at 180 rpm. Appropriate antibiotics were added into the media on the basis of the resistance cassettes carried by strains of *Agrobacteria* and the containing plasmids.

2.2.3 Plant methods

2.2.3.1 Stable transformation of *Arabidopsis thaliana*

The stable transformed of *Arabidopsis* plants were generated according to the floral dip-method (Clough and Bent 1998). A small volume of pre-culture was prepared from a glycerol stock or a fresh plate. Pre-culture was inoculated into 50-200 ml YEP medium with appropriate antibiotics selection and grown at 28 °C for about a day. The *Agrobacteria* cells

were pelleted at 3000 g for 10 min at room temperature (RT). After removing the supernatant, the bacterial cells were resuspended in fresh 5% sucrose (w/v) solution at a density of ~0.6 (OD600). After adding 0.02% (v/v) Silwet L-77, young *Arabidopsis* inflorescences were dipped into the bacterial suspension for 30 seconds (sec). Laid the plants sideways in a tray and covered the tray with a transparent cover. After 2-day incubation, the plants were transferred into the normal growth conditions. Seeds from dipped plants were then screened for resistance against phosphinothricin (Basta) or based on mCherry marker on seed coat (red fluorescence on seed coat under the fluorescence microscope).

2.2.3.2 Genotyping analysis of T-DNA insertion lines

The T-DNA lines used in this study were analyzed for their genotypes. The T-DNA insertion lines used for experiments have to be confirmed as homozygous. To distinguish wild-type (WT), heterozygous insertion and homozygous insertion, we performed two sets of PCR reactions. In the WT-PCR, a pair of primers match two regions flanking the T-DNA insertion site and thus amplify the WT allele, while the large size of the T-DNA at the insertion site inhibits the amplification in the mutated allele. WT and heterozygous insertion plants containing WT allele would get an amplification product. In the second PCR (insertion PCR), a T-DNA specific primer (match the left border of T-DNA) and a gene-specific primer are used to amplify a product only in plants carrying a T-DNA insertion (heterozygous and homozygous insertion plants). Therefore, homozygous insertion plants should exhibit a product only in the insertion PCR, WT plants only show a PCR product in the WT-PCR, whereas heterozygous plants produce amplicons in both WT-PCR and insertion PCR. Primers used for genotyping analysis of T-DNA insertion lines can be found in Appendix Table 9.

2.2.3.3 Generation of tagging lines

The NUP1 and CRWN tagging lines used in this study were generated by stably expressing native *NUP1* or *CRWN* tagging constructs in their corresponding mutants. The resulting vectors were transformed into *Agrobacteria* by electroporation, respectively. The stable expression of the constructs in their corresponding *Arabidopsis* mutants were conducted by using the floral dip method. Offspring were screened based on Basta resistance or selection of red fluorescence on seed coat under the fluorescence microscope (mCherry on seed coat). The genetic background of the selected lines was further verified by two sets of PCR reactions. In the first round of PCR, one pair of primers bind two regions flanking the T-DNA, amplifying product from the targeted locus including that in the complementary plasmid but not

endogenous locus of the homozygous mutant due to the T-DNA insertion. In the second PCR, another pair of primers that can only amplify regions from endogenous locus were used to verify the homozygous T-DNA insertion at the endogenous loci. Only tagging lines with homozygous mutant background were used to further analyses. Primers used for genotyping can be found in Appendix Table 9.

2.2.3.4 Crossing of *Arabidopsis*

To get high-order mutants and analyze the inheritance of mutant phenotypes in the progeny, we performed crossing between different *Arabidopsis* mutants. *Arabidopsis* are mostly self-pollinating, and their pollens do not disperse through the air. Therefore, *Arabidopsis* crossing is mainly conducted through manual emasculation of flowers just prior to flower opening, followed by hand transfer of pollen from the desired male parent to the stigma of the emasculated flower according to the method described in (Weigel and Glazebrook 2006). The crossed siliques were harvested by cutting them with scissors and placed them into a 1.5 ml Eppendorf tube.

The seeds were air-dried, and stratified at 4 °C in the dark for 2 days. These plants of F1 generation were grown in the greenhouse as usual until the plants were big enough for genotyping (2.2.3.2). The resulting F2 individuals from self-pollinated F1 plants were used for genotyping to get high-order homozygous mutant plants. Seeds from these F2 plants were used to do further analysis.

2.2.4 Molecular biology

2.2.4.1 Isolation of plasmid from *E. coli*

Plasmid DNA was extracted from 2 ml of overnight *E. coli* culture using the GeneJET MiniPrep Kit (Thermo Scientific) according to manufacturer's instructions.

2.2.4.2 Isolation of genomic DNA from plant material

A small piece of leaf tissue was ground in a 1.5 ml Eppendorf tube with 150 µl extraction buffer (200 mM Tris-HCl, pH 9.0; 400 mM LiCl; 25 mM Ethylenediaminetetraacetic acid (EDTA); 1% (w/v) sodium dodecyl sulfate (SDS)) by hand or using a homogenizer machine. The samples were centrifuge at ≥ 10000 rpm for 5 min. 100 µl of supernatant was transferred into a new 1.5 ml tube and mix thoroughly with 100 µl of isopropanol. The mixture was centrifuged for 10 min at ≥ 10000 rpm to precipitate genomic DNA. The genomic DNA pellet

was washed with 200 μ l of 70% (v/v) ethanol and was air-dried at RT. Finally, the DNA pellet was dissolved in 30-50 μ l ddH₂O.

2.2.4.3 Standard PCR

In a 10 μ l reaction system, 0.5 μ l template was added into the mixture (1 μ l of 10x Taq reaction buffer, 0.2 μ l of 10 mM dNTPs, 0.2 μ l of 10 μ M forward and reverse primer, 0.05 μ l lab-made Taq polymerase). The reaction was performed in a PCR machine (DIVERS/DUTSCHER) with the following program: 94 °C for 4 min; 40 cycles of 94 °C for 30 sec, 57 °C to 61 °C (determined by primers) for 15 sec, 72 °C for 1 min/kb; followed by 72 °C for 5 min.

2.2.4.4 DNA agarose gel electrophoresis

DNA electrophoresis was performed on a 1% agarose gel in 1x TAE buffer (40 mM Tris-acetate, pH 8.0; 2 mM EDTA, pH 8.0) at 150-180 V. A 1 kb plus ladder (Thermo Scientific) was used as size ladder. Ethidium bromide (Roth) or GelRed (GENAXXON bioscience) present in the gel makes the DNA visualized by a UV-Transilluminator (Quantum, Vilber Lourmat).

2.2.4.5 Sequencing

The constructs and PCR products were sequenced by Eurofins Genomics. 500-750 ng plasmid or a certain amount of PCR product (determined by the size of the PCR product) was used as a template, and mixed with 2 μ l of 10 μ M sequencing primer. The results were analyzed using SnapGene Viewer software.

2.2.4.6 Quantitative fluorescent real time PCR

Quantitative real-time PCR (qPCR) amplifications and measurements were performed with the iQ5 Real-Time PCR detection system from Bio-Rad. 0.8 μ l of 2 fold diluted ChIP DNA was used as the template for qPCR. Amplifications of qPCR were monitored by using MESA GREEN qPCR MasterMix plus (Eurogentec) or qPCRBIO Sygreen Mix (PCRBIO SYSTEMS). The gene expression data was quantified using the $2^{-\Delta\Delta CT}$ method (Livak and Schmittgen 2001). The normalization of the expression levels was done using the CT values obtained for the *TUB2* locus. All quantifications were made in duplicates on ChIP DNA samples obtained from two independent experiments. The primers used for qPCR analysis are listed in Table 9 (Appendix).

2.2.4.7 Digestion of plasmid with restriction endonuclease

To cleavage the plasmid, which was used as the template for plasmid cloning, PCR products were digested with DpnI (New England BioLabs). PCR products were digested in 20 μ l reaction volume with 1U of DpnI at 37 °C for 1 hour according to manufacturers' suggestions.

2.2.4.8 Preparation and calibration of Serapure Beads

The magnetic SeraMag Speed Beads used to purify DNA fragments from PCR or digestion products were prepared in our lab. 1 ml of washed SeraMag Speed Beads were added into a sterile 50 ml falcon tube, then 9g of PEG-8000, 25 ml of 5 M NaCl, 500 μ l of 1M Tris-HCl (pH 8.0), 100 μ l of 0.5 M EDTA (pH 8.0) were added slowly into the tube and the solution was topped up to 50 mL with ddH₂O.

The prepared SeraMag Speed Beads (lab-made Serapure Beads) were calibrated every two months. 2 μ l of DNA ladder was mixed with 18 μ l of ddH₂O and a volume of Serapure Beads in a PCR tube and then incubated at RT for 10 min. PCR tubes were placed on a magnet stand until the beads were drawn to magnet, the supernatant was removed. The beads were washed with 150 μ l ethanol (80%, v/v) twice, and air-dried. DNA on the beads was dissolved with a volume of 10 mM Tris-HCl (pH 8.0). After removing the beads with magnet, the DNA ladder recovered from the beads was compared with the original DNA ladder.

2.2.4.9 Purification of DNA fragments

DNA fragments were purified *via* lab-made Serapure Beads. To collect the DNA fragment with expected size from the PCR or digestion products, the products were mixed with equal volume of 10 mM Tris-HCl pH 8.0, then a proper volume of the calibrated lab-made Serapure Beads was added and mixed thoroughly with a pipettor. The mixture in a PCR tube was incubated for 10 min at RT, and then was placed on a magnet stand for 2 min. The beads were washed with 150 μ l ethanol (80%, v/v) twice and air-dried. Finally, the DNA on the beads was dissolved with 10 mM Tris-HCl (pH 8.0).

2.2.4.10 Gibson Assembly[®]

The cloning of DNA fragments into a Gateway-compatible pGREEN-IIS binary destination vector was done by Gibson Assembly[®] (New England BioLabs) according to the manufacturer's instructions.

2.2.4.11 Construction of plasmid

All the constructs used in this study were constructed with an overlapping PCR strategy. For *pNUP1::NUP1:GFP* construct, three fragments of the construct were amplified, respectively. One *NUP1* genomic fragment, which spanning 600 bp upstream of *NUP1* to the *NUP1* stop codon, was amplified with primers 5'-GTTCGTTAGACTGGTTTAGGT-3' and 5'-TTTCTTCCTGGTGGATTTCTT-3'. Another *NUP1* genomic fragment spanning the *NUP1* stop codon to 150 bp downstream of *NUP1* was amplified with primers 5'-TTTGGAGAAGAAGGCTTCTCT-3' and 5'-TAAGAAAAACACATTGTTCAAG-3'. The GFP cDNA was amplified with primers 5'-AAGAAATCCACCAGGAAGAAAGCGGCCGCTGTGAGCAAGGG-3' and 5'-CTTGAACAATGTGTTTTTCTTAAGATCCACCAGTATCCTCAC-3'. These PCR products were cleaned with lab-made Serapure Beads. Subsequently, these three cleaned PCR products were assembled by conducting overlapping PCR and amplified with primers 5'-GTTCGTTAGACTGGTTTAGGT-3' and 5'-TTTGGAGAAGAAGGCTTCTCT-3'. After purifying with lab-made Serapure Beads, the final PCR product was cloned into a Gateway-compatible pGREEN-IIS binary destination vector (pFK206) by Gibson Assembly[®] (Karlsson et al., 2015). Similar like this, to get the mCherry:CENH3 fusion protein, cDNA of mCherry was amplified with primers 5'-GTAAAAATCAATGGCCATCATCAAGGAGTT-3' and 5'-ACGCGATGCTTGGTTCTCGCACCGCCACCCTTGTACAGCTCGTCCATGC-3', and the genomic fragment of *CENH3* (AT1G01370) was amplified with primers 5'-GCGAGAACCAAGCATCGCGT-3' and 5'-TCACCATGGTCTGCCTTTTC-3'. These two fragments were purified with lab-made Serapure Beads, and then were cloned into a Gateway-compatible pGREEN-IIS binary destination vector including a 35S promoter (pFK210) by Gibson Assembly[®] (Karlsson et al., 2015).

Three native *CRWN1* tagging constructs were used to generate functional complementary lines of *crwn1*. Each of the three *CRWN1* tagging constructs was constructed *via* performing overlapping PCR of two fragments. For *pCRWN1::CRWN1:2HA* construct, in which a tandem HA tag was inserted into *CRWN1* at its C terminal. One fragment of the construct spanning 1.7 kb upstream of *CRWN1* to the *CRWN1* stop codon was amplified with primers 5'-TTACGTTTTATTGTGGTCTTC-3' and 5'-AGGGTATCCAGCATAATCTGGTACGTCGTATGGGTATCCCGTCGTCAAGAAAGTCAAAA-3'. The other fragment spanning the *CRWN1* stop codon to 500 bp downstream of

CRWN1 was amplified with primers 5'-GATTATGCTGGATAACCCTTACGACGTACCAGATTACGCTTAGCCCAATCTTTGATCAGAGA -3' and 5'-ATAATACTGTCAAGAGTGATG -3'. For *pCRWN1::2HA:CRWN1* construct, in which the tandem HA tag was inserted into *CRWN1* at its N terminal. The two fragments of the construct were amplified by two pairs of primers: 5'-TTACGTTTTATTGTGGTCTTC -3' in combination with 5'-AGGGTATCCAGCATAATCTGGTACGTCGTATGGGTATCCCATCTCTCACAATTCGCACAG -3'; and 5'-GATTATGCTGGATAACCCTTACGACGTACCAGATTACGCTTCCACGCCGTTGAAGGTGTGG -3' in combination with 5'-ATAATACTGTCAAGAGTGATG -3', respectively. For *pCRWN1::CRWN1_780:2HA* construct, which the tandem HA tag was inserted at the 780th amino acid residue of *CRWN1*. The two fragments of this construct were amplified by two pairs of primers: 5'-TTACGTTTTATTGTGGTCTTC -3' coupling with 5'-

AGGGTATCCAGCATAATCTGGTACGTCGTATGGGTATCCAGCAGTTGGGGATATATCCC -3'; and 5'-GATTATGCTGGATAACCCTTACGACGTACCAGATTACGCTGCTGGCTTAGGATTGCAGTT -3' coupling with 5'-ATAATACTGTCAAGAGTGATG -3', respectively. The two fragments of each construct were first cleaned with lab-made Serapure Beads, following by assembly with overlapping PCR, and then amplified with primers 5'-TTACGTTTTATTGTGGTCTTC -3' and 5'-ATAATACTGTCAAGAGTGATG -3'. Then, the final PCR products of individual constructs were cloned into pFK206 vectors by Gibson Assembly[®], respectively.

The native *CRWN4* and *CRWN2* tagging constructs were also generated by overlapping PCR of two fragments. The two fragments of the *pCRWN4::CRWN4_850:2HA* construct were amplified with primers: 5'-ACTAATCTTTTCTACTAGCTTAAC -3' in combination with 5'-

AGGGTATCCAGCATAATCTGGTACGTCGTATGGGTATCCAGTACATCGTTTTATCCATGA -3'; and 5'-GATTATGCTGGATAACCCTTACGACGTACCAGATTACGCTAATCTGATTTTCAAGACTTCTCCA -3' in combination with 5'-GCTACGAGCTACTTCGATGATAC -3', respectively. These two fragments were assembled with overlapping PCR after purification with lab-made Serapure Beads and amplified with primers 5'-

ACTAATCTTTTCTACTAGCTTAAC -3' and 5'- GCTACGAGCTACTTCGATGATAC -3'. The subsequent PCR product was firstly cleaned by lab-made Serapure Beads and then was cloned into the pFK206 vector. For *pCRWN2::CRWN2_800:2HA*, one fragment of the construct was amplified with primers 5'- AAACCCAACCTTTGAACGACGA -3' and 5'- AGGGTATCCAGCATAATCTGGTACGTCGTATGGGTATCCTGGAAGGTCATTCAAA ACTCC -3'. The other fragment of the construct was amplified with primers 5'- GATTATGCTGGATACCCTTACGACGTACCAGATTACGCTGGAAGCTCTAATGCAT CTGACTCT -3' and 5'- CGAGAGGTCGTTGGGAATCAA -3'. The two fragments were purified with lab-made Serapure Beads, followed by assembly with overlapping PCR, and amplification with primers 5'- AAACCCAACCTTTGAACGACGA -3' and 5'- CGAGAGGTCGTTGGGAATCAA -3'. After cleaning with lab-made Serapure Beads, the final PCR product was cloned into the pFK206 vector by Gibson Assembly[®].

2.2.4.12 Preparation and transformation of chemically competent *E. coli* DH5 α cells

E. coli DH5 α was streaked out onto a LB plate and grown overnight in a 37 °C oven. A mono-colony of *E. coli* DH5 α was grown in 5 ml of LB medium overnight in a 37 °C shaker with 180 rpm shaking. 20 μ l of overnight culture was inoculated into 200 ml LB medium in a sterile 1-liter flask and grown in a 37 °C shaker with 180 rpm to the second day until an OD600 of ~0.60. The culture was divided into four pre-chilled falcon tubes (50 ml/each) and incubated for 10 min on ice. The *E. coli* DH5 α cells were collected at 3000 rpm for 5 min at 4 °C. Cell pellets in every falcon tube were suspended in 16 ml of buffer I (100 mM RbCl; 50 mM MnCl₂; 30 mM C₂H₃KO₂; 10 mM CaCl₂; 1.6 M glycerol) and incubated on ice for 15 min. Cells of each falcon were re-collected at 3000 rpm for 5 min at 4 °C and resuspended with 4 ml buffer II (10 mM MOPS, pH 6.8; 10 mM RbCl; 75 mM CaCl₂; 1.6 M glycerol). The resuspensions were aliquoted in 100 μ l into pre-chilled Eppendorf tubes and immediately frozen in liquid nitrogen and stored at -80 °C.

One aliquot of chemically competent cells was taken from -80 °C and thawed on ice. Plasmid or recombination product from Gibson Assembly reaction was added to the aliquot and kept on ice for ~5 min. The mixture was heat-shocked at 42 °C for 1 min and immediately put on ice for ~5 min. After adding 1 ml LB medium, the mixture was incubated at 37 °C for 1 hour on a shaker. Subsequently, the mixture was centrifuged at 3500 rpm for 5 min at RT. Followed by removing 1 ml supernatant, and the cell pellet was resuspended with the

remaining liquid. The transformed cell resuspension was spread onto a LB medium plate with appropriate antibiotics.

2.2.4.13 Preparation and transformation of electrical competent cells of *Agrobacteria*

The *agrobacteria* strains were spread onto a YEP plate with selective antibiotics and grown at 28 °C for 2 days. A single colony was picked to inoculate in 5 ml LB liquid medium with appropriate antibiotics. The culture was grown overnight at 28 °C and then enlarged with 200 ml and grown to an OD600 of ~1.0. Next, the culture was equally divided into four pre-cooled 50 ml falcon tubes and then centrifuged at 4 °C for 10 min at 4,000g. The cell pellet in each tube was resuspended with ice-cooled resuspension buffer (10% (v/v) Glycerol; 1 mM Hepes, pH 7.0; autoclaved) and centrifuged at 4 °C for 10 min at 4000 G to wash the cells. After repeating this washing step once again, the cells in every tube were resuspended in 1 ml of resuspension buffer. Next, the resuspensions were aliquoted into 50 µl aliquots. Finally, these aliquots were frozen in liquid nitrogen immediately and stored at -80 °C.

One aliquot of electrical competent *Agrobacteria* cells was thawed on ice, and then 100-200 ng target plasmid and 50-100 ng helper plasmid (pSaup) were added. After transferring the mixture into a pre-cooled electroporation cuvette, the cells were pulsed once with 2,2000 voltage for ~ 5 milliseconds (BioRad), the cuvette was put back on ice, and then 1000 µl of SOC medium (2% Tryptone; 0.5% Yeast extract; 10 mM NaCl; 2.5 mM KCl; 10 mM MgCl₂; 10 mM MgSO₄•7H₂O; 10 mM Glucose; adjust pH to 7.0) was added to the cuvette. Cells were quickly resuspended by gently pipetting up and down and then transferred into a 1.5 ml Eppendorf tube. After incubating the tube in a shaker at 28 °C for 1 hour, the mixture was centrifuged at 3000 rpm at RT for 5 min. 950 µl of supernatant was discarded and cell pellet was resuspended with the remaining SOC medium. The resuspension was plated onto a selective YEP plate and incubated in a 28 °C incubator for 2 days.

2.2.4.14 Western blot analysis

The total protein used for Western blot analysis was extracted from plant leaf tissue using a protein isolation buffer (50 mM Tris-HCl pH 7.5; 0.1% (v/v) Tween 20; 150 mM NaCl; 0.1% (v/v) β-mecaptoethanol was added freshly before use). The plant tissue was first homogenized in liquid nitrogen and mixed thoroughly with the isolation buffer. Afterwards, the soluble proteins were separated from cell debris using centrifugation at 4°C and the supernatant was used for western blot analysis.

10% sodium dodecyl sulfate polyacrylamide (SDS-PA) gels were used as separating gels (with 5% stacking gels) for the discontinuous sodium dodecyl sulfate polyacrylamide gel electrophoresis (SDS-PAGE) by using the Laemmli method (Laemmli 1970). The PageRuler Prestained Protein Ladder (Thermo Scientific) was used as a protein marker.

For the western blot analysis, the proteins were transferred after SDS-PAGE onto a Pre-cut polyvinylidene difluoride (PVDF) membrane (0.2 μm pore size, Invitrogen) by semi-dry blot using the “Standard” protocol for 45 min. The transfer buffer comprised 48 mM Tris-HCl (pH 7.2), 39 mM Glycine, 0.0375% (w/v) SDS and 20% (v/v) methanol. For immunoblotting, unspecific binding sites were blocked by incubating the membrane for 1 hour at RT with 5% (w/v) milk powder in 1 x TBST (150 mM NaCl; 10 mM Tris-HCl, pH 7.6; and 0.05% (v/v) Tween 20). After two times washing the membrane with 1 x TBST for 5 min, the membrane was incubated with the anti-HA tag antibody conjugated with 1:5000 horseradish Peroxidase (HRP) (Santa Cruz) for at least 1 hour at 4 °C. Following by three times washing the membrane for 5 min with 1 x TBST, the signals of the HRP were detected by using the Western BloT Chemiluminescence Hyper HRP Substrate (TaKaRa) according to the manufacturer’s instructions. Finally, the signals were captured and analyzed with AmershamTM Imager 600 system (GE Healthcare Life Science).

2.2.4.15 RE-ChIP sequence library preparation

Seedlings (10-day-old) were collected and fixed in MC buffer (10 mM Potassium Phosphate, pH 7.0; 50 mM Sodium Chloride; 0.1 M sucrose) supplemented with 1% (v/v) formaldehyde by performing vacuum infiltration for 15 min at RT two times. The remaining formaldehyde was quenched by 0.15 M glycine in MC buffer. After briefly rinse the fixed samples with water twice, the fixed tissues were gently dried by blotting them with tissue towels gently.

Nuclei extracted from 0.5 g fixed materials were used for one round of RE-ChIP sequence (RE-ChIP-seq) library preparation. The procedure for this is presented in Figure 2. Nuclei isolation was performed according to the protocol described in (Wang et al., 2015a). Nuclei were incubated with 150 μl of 0.5% (w/v) SDS at 62 °C for 5 min to permeabilize the nuclear membrane, and the remaining SDS was quenched with addition of 75 μl of 10% (v/v) Triton X-100. Subsequently, chromatin inside nuclei was digested overnight at 37 °C with 150 U DpnII, which was deactivated on the next day morning at 62 °C for 20 min. Next, the treated nuclei were collected by centrifuging at 1000 G for 3 min, and resuspended with 1 ml sonication buffer (10 mM Potassium Phosphate, pH 7.0; 0.1 Mm NaCl; 0.5% (w/v) Sarkosyl;

10 mM EDTA, pH 8.0), and sheared by sonication with a Covaris S220 instrument (set at 20 dc, 1 i, 200 cpb, 15 sec). The sonicated sample was centrifuged at 14000 rpm for 5 min at 4 °C, and the supernatant was mixed with 100 µl of 10% (v/v) Triton X-100. Subsequently, the sheared chromatin was mixed with equal volume of IP buffer (50 mM Hepes, pH 7.5; 150 mM NaCl; 5 mM MgCl₂; 10 µM ZnSO₄; 1% (v/v) Triton X-100; 0.05% (w/v) SDS), and then equally divided into two tubes, followed by incubation with anti-GFP antibody (Abcam, ab-290) and normal rabbit IgG (Santa Cruz, sc-2027), respectively. Following overnight incubation at 4 °C with inversion, 10 µl of Protein A/G magnetic beads (Pierce) were added and incubated with inversion at 4°C for 2 hours. The beads were collected and then washed at 4°C as followings: three times with IP buffer, one time with IP buffer containing 500 mM NaCl, one time with LiCl buffer (0.25 M LiCl; 1% (v/v) NP-40; 1% (w/v) deoxycholate; 1 mM EDTA, pH 8.0; 10 mM Tris-HCl, pH 8.0), for 5 min each. Chromatin retained on the beads were incubated in 200 µl of elution buffer (50 mM Tris-HCl, pH 8.0; 200 mM NaCl; 1% (w/v) SDS; 10 mM EDTA, pH 8.0) at 65 °C for at least 6 hours. After the addition of Proteinase K, the mixture was incubated at 37 °C for 1 hour. DNA was extracted with a standard phenol-chloroform method. To increase sequence diversity at the ends of DNA, the immunoprecipitated DNA was incubated with dsDNA Fragmentase[®] (NEW ENGLAND BIOLABS) at 37°C for 25 min, leading to that the DNA was randomly cut into 100~200 bp fragments. The digested DNA was purified with AMPure[®] XP beads (Beckman Coulter), and all the subsequent end repairing, A-tailing, adaptor ligation, library amplification steps were performed according to a standard protocol (Illumina). The subsequent libraries were sequenced on an Illumina HiSeq 3000 instrument with 2 x 150 bp reads.

For sequencing analysis, pair-end reads were aligned against the *Arabidopsis thaliana* reference genome (TAIR 10) using Bowtie 2 v2.2.4 (Langmead and Salzberg 2012) with a “very sensitive” mapping mode. For each replicate, the mapped reads were analyzed by SICER v1.1 (Zang et al., 2009) to call enriched regions (parameters: W = 1000; G = 3000; FDR < 0.01). For each type of tissue, regions shared between the two replicates were extracted, which were categorized as domains enriched at the NP (or NUP1-enriched domains). The annotation of *Arabidopsis* gene was retrieved from Ensembl Genomes (<ftp://ftp.ensemblgenomes.org/>) (release-24) (Kersey et al., 2016). A gene was claimed as an enriched gene if more than 80% of its transcribed region overlapped with NUP1-enriched domains.

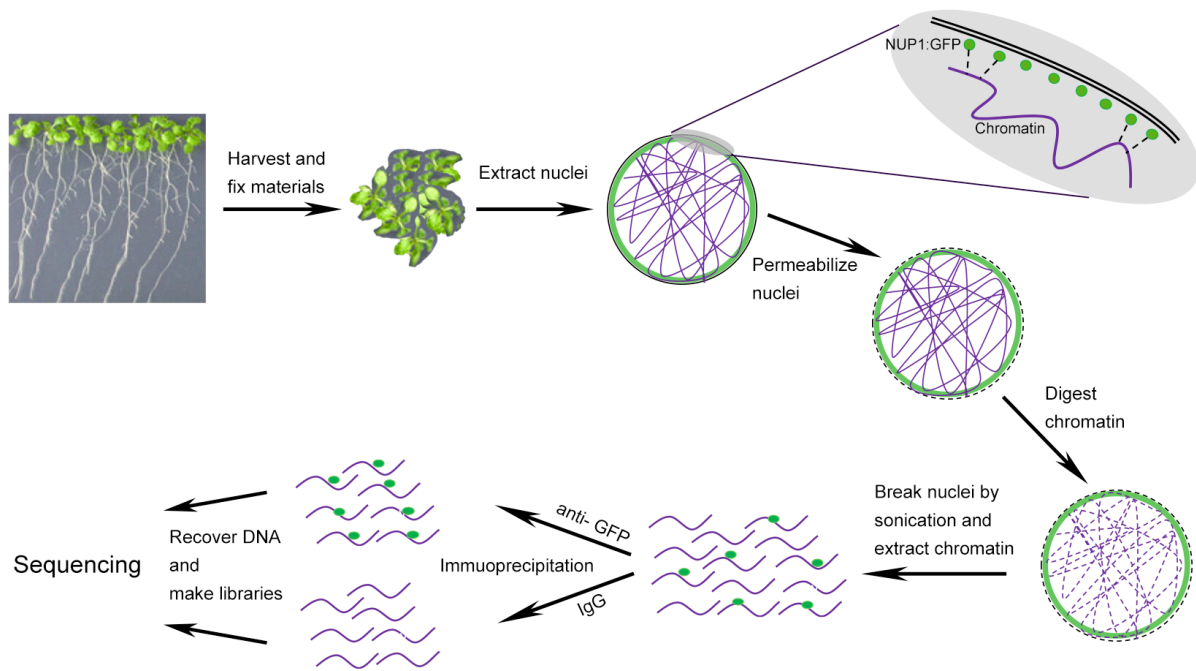


Figure 2. Experiment workflow of RE-ChIP-seq with transgenic *Arabidopsis* plants expressing NUP1:GFP.

In the zoomed-in sketch shown at the upper right corner, dash lines depict weak/indirect interactions between the bait proteins (NUP1:GFP) and chromatin located nearby.

2.2.4.16 FISH

The FISH experiment in this study was performed according to (Prieto et al., 2007; Wegel et al., 2009) with modifications. For labeling specific genomic regions, selected BACs were retrieved from the ABRC stock center. After DNA isolation by employing standard alkaline lysis protocol, the identities of BACs were confirmed by PCR. BACs selected for FISH in this study were labeled with either digoxigenin-11-dUTP (DIG) or Dintrophenyl-11-dUTP (DNP) by nick translation, which were detected with Alexa Fluor 488 (Green) or Alexa Fluor 546 (Red), respectively. The reactions were incubated for 90 min at 15 °C and subsequently stopped by the addition of 1 μ l of 0.5 M EDTA (pH 8.0) and heating up to 65 °C for 10 min. These individual FISH probes were detected in an electrophoresis gel and the size of every probe should be 200-500 bp. The labeled probes were then purified by using lab-made Serapure Beads and dissolved in 10 mM Tris-HCl (pH 8.0). Note that these labeled probes can be stored in -20 °C for months.

For each FISH experiment, one green FISH probe (DIG-labeled) and one red FISH probe (DNP-labeled) were used, allowing for performing dual color FISH. For probes targeting regions shown in Figure 12, the concentration of every labeled BAC was 1 ng/ μ l in working

hybridization solution. For probes used for chromosome painting shown in Figure 17, the concentration of each labeled BAC in the working hybridization solution was 0.05 ng/ μ l. To prepare the working hybridization solution of the green and red probes, a certain volume (the volume of every probe was determined by the number of the BACs in each probe and the probe concentration) of the green and red probe was mixed together and then dried by Speed Vacuum pump, followed by dissolving in 5 μ l of hybridization buffer (10 ml of hybridization buffer containing: 5 ml of deionized formamide; 2 ml of 50% dextran sulfate; 1 ml of 20x SSC (3M NaCl; 300 mM Sodium Citrate, pH 7.0), 125 μ l of 10 mg/ml salmon testes DNA, 125 μ l of 10% (w/v) SDS, 1750 μ l of sterile ddH₂O). After transferring the FISH probe work solution into a PCR tube, the FISH probe was denatured for 15 min at 95 °C and stored on ice until the hybridization.

Here is the procedure to collect 2C nuclei for FISH (Figure 3). *Arabidopsis* seedlings (10 days) grown on 1/2 MS medium supplied with 1% sucrose were fixed in 1% formaldehyde in PBS buffer (3.0 g/L NaCl; 0.24 g/L Potassium Phosphate; 1.42 g/L Disodium Phosphate; 0.2 g/L Potassium Chloride; adjust pH to 7.4) for 30 min under vacuum at RT. The seedlings were washed three times with sterilized water and then chopped in general purpose buffer (GPB) (0.5 mM Spermine •4HCl; 30 mM Sodium Citrate; 20 mM MOPS; 80 mM KCl; 20 mM NaCl; adjust pH to 7.0; sterilized by 0.2 μ m filter, store at 4 °C). To remove residual cellular debris, the nuclei were filtered through a 22~25 μ m Miracloth (Merck Millipore) and then filtered through a 40 μ m cell-stainer. The extracted nuclei were stained with 0.5 μ M DAPI to reveal their ploidy levels. Subsequently, the DAPI stained nuclei were flow sorted on a MoFlo (Modular Flow) XDP model (Beckman Coulter) flow-sorting platform. Around 5000 sorted 2C nuclei were collected for one hybridization spot (~1 cm²).

After nuclei sorting, the nuclei were centrifuged for 1000 G at 4 °C for 5 min, and the pellet was resuspended with 10 μ l of PBS buffer (pH 7.4). Then the nuclei were incubated at 65 °C for 30 min, and mixed with 5 μ l of 0.1 mg/ml RNase A. The mixture was transferred onto a Superfrost Ultra Plus Adhesion Slide (ThermoFisher Scientific) and incubated for 1 hour at 37 °C in a Thermocycler in humidity chamber (PBS buffer, pH 7.4). At the end of RNase A treatment, the nuclei became attached to the glass slide. The slide was washed with PBS buffer (pH 7.4) for 5 min at RT and with 0.75% (w/v) NaCl for 3 min at RT. Next, the nuclei on the slide were dehydrated in an ethanol gradient, stepping from 30% (containing 0.75%

NaCl), to 60% (containing 0.75% (w/v) NaCl), to 80%, to 90%, to 95%, to 100% (two times) ethanol (v/v). Then the slide was air-dried at RT for 30 min to 60 min.

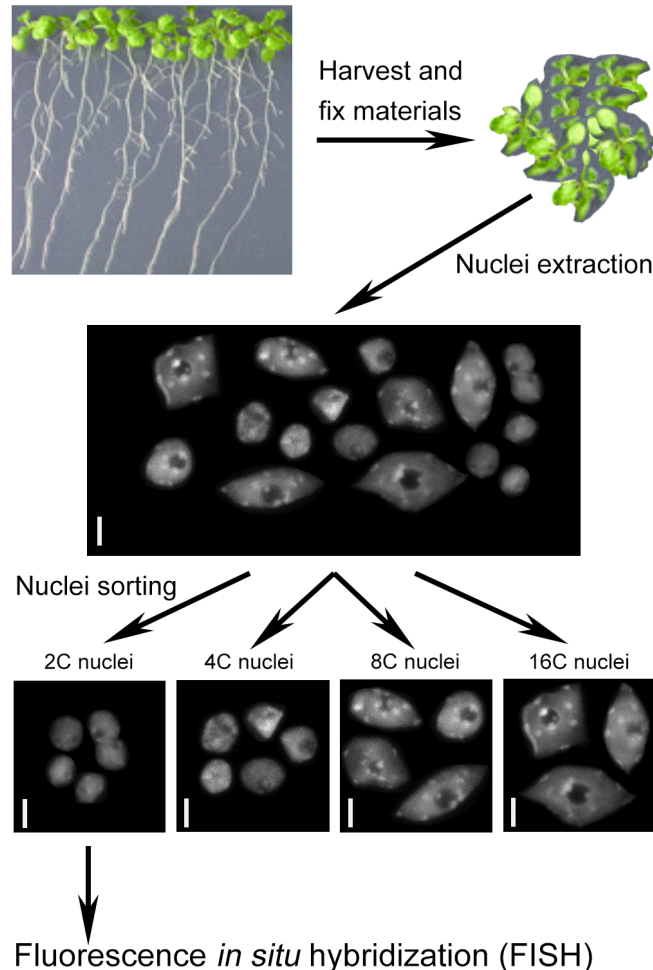


Figure 3. Procedure of 2C nuclei collection for FISH.

Scale bars: 5 μm .

The denatured probes were transferred onto the FISH spot of the slide, and then the spot was covered with a plastic coverslip to prevent evaporation. The chromatin regions within nuclei on the slide were hybridized with corresponding FISH probes in a Thermocycler in humidity chamber (soaking buffer (2x SSC buffer; 50% formamide)) with the programs: 75 °C for 8 min, 50 °C for 1 min, 37 °C for 16~20 hours.

After hybridization, the slide was washed at 42 °C as follows: once with soaking buffer, twice with 2x SSC buffer, twice with 20% (v/v) formamide in 0.1x SSC buffer, twice with 2x SSC buffer, for 5 min each. Then the slide was washed at RT twice with 2x SSC for 5 min, once with 4x SSC-Tween (0.2% (v/v) Tween 20 in 4x SSC buffer) for 10 min. Subsequently, the

nuclei on the slide were incubated for 10 min at RT in 100 μ l of blocking solution (5% bovine serum albumin (BSA); 4x SSC-Tween). Then the binding of antibody was performed for probe detection. To do this, 100 μ l of the working solution of first antibodies (1 μ l of monoclonal anti-digoxin mouse antibody (Sigma) and 1 μ l of rabbit anti-dinitrophenyl antibody (Sigma) stock solution were diluted in 500 μ l of blocking solution and mixed by pipetting) was added onto the slide and then incubated for 1 hour at RT. The slide was washed twice with 4x SSC-Tween for 5 min at RT. Next, 50-100 μ l of working solution of second antibodies (1 μ l of Alexa Fluor 488 goat anti-mouse antibody (Invitrogen) and 1 μ l of Alexa Fluor 546 goat anti-rabbit antibody (Invitrogen) were diluted in 150 μ l of blocking solution and mixed by pipetting). To remove the excess unbound antibodies, the slide was washed in 4x SSC-Tween for 5 min at RT. Finally, the slide was mounted with 5 μ l of SlowFade[®] Diamond Antifade Mountant with DAPI (ThermoFisher Scientific) to stain the DNA and protect the FISH signals from the laser.

2.2.5 Immunohistostaining

Seedlings of *CRWN1:2HA crwn1* were fixed and then embedded in paraffin as described in (Liu et al., 2013). Slides with paraffin sections of leaf tissue were dewaxed and rehydrated with PBS buffer (pH 7.4). Next, an antigen retrieval step was conducted with Universal HIER antigen retrieval reagent (Abcam) according to manufacturers' instructions. The slides were incubated with 1:500 diluted HA Tag Alexa Fluor 647 conjugate (ThermoFisher Scientific). After washing, SlowFade[®] Diamond Antifade Mountant with DAPI (ThermoFisher Scientific) was used to mount the slides.

2.2.6 Microscopy and image processing

Confocal images of fluorescent proteins (GFP and mCherry) in nuclei were acquired with the Leica SP8 AOBS system (Leica, Germany). These images were processed with ImageJ software and finally assembled in Photoshop.

Confocal images of the FISH treated nuclei were acquired with a Zeiss LSM 880 Airyscan system (Zeiss, Germany). To measure the distance of selected genomic regions to the NP, a single image of a nucleus was captured if it had at least one distinct green and red signal spots at the same focal plane. The distance between its estimated barycenter and the edge of DAPI signal was recorded as the distance of a signal spot to the NP. For example, see Figure 13. For chromosome painting, the data was acquired as z-stack. For each image, ImageJ (Schneider et

al., 2012) was used to determine the nuclear boundary according to DAPI signal; while signals in green and red channels were extracted from the corresponding image files (Figure 23). The nuclear part closed to the glass slide was found to become flattened, probably because of capillary forces. To reduce possible errors in the distance calculation of this area, two images at the bottom of each nucleus were excluded so that our data analyses were only applied to a subset of the nuclear space (Figure 23). Because nuclei were landed on slide randomly, the distribution of FISH signals along the z-axis is not dependent on distance to the nuclear boundary. Therefore, in principle, such data exclusion should have no effect on the conclusion concerning signal distribution in the remaining nuclear part.

Confocal images of immunohistostained tissue sections were acquired with a Zeiss LSM 880 Airyscan system (Zeiss, Germany). Image processing was done with the ImageJ software.

2.2.7 Statistical analysis

Statistical analysis was performed with R software using Mann-Wilcox U test (one-side) for data of distance distribution, Wilcoxon signed-ranked tests for data of $P_{0.5}$ (Figure 23 and Figure 24) and Mann-Whitney U test (two-side) for data of nuclear morphology and root length. The p values were listed in the corresponding figures.

3. Results

3.1 Identification and characterization of chromatin anchoring at the NP in *Arabidopsis*

3.1.1 Non-random chromatin distribution at the NP revealed by RE-ChIP

The nucleoporin NUP1 (also known as NUP136) has been shown to be localized specifically at the NP in *Arabidopsis* (Tamura et al., 2010). In this study, the NUP1 protein, fused with GFP was used to identify chromatin regions interacted with NPC, which might be involved in the “gene gating” events that have been reported in yeast and animals (Blobel 1985; Strambio-De-Castillia et al., 2010). In line with previously published results, the NUP1:GFP fusion protein shows specific localization at the NE (Figure 4A). However, we could not identify any chromatin regions enriched by NUP1:GFP when we conducted regular ChIP experiment (Figure 4B), although our ChIP-seq libraries had been sequenced more deeply than typically needed for *Arabidopsis* (Appendix Table 10). By comparison, a parallel ChIP experiment using an antibody against Pol II was performed on the same materials, exhibited expected enrichment of the transcribed genes, excluding possible technical failures in our ChIP experiments. This negative result implied that NUP1:GFP did not interact directly with chromatin, or did not show such interactions, if they existed, the interactions preserved by crosslinking treatment were not effectively preserved in our regular ChIP experiment. To enhance the sensitivity of enriching chromatin loosely dangling around NUP1:GFP, a modified ChIP protocol was developed in our lab, in which a RE is used to digest chromatin and then only mild sonication is applied to break the nuclei and fragmentize chromatin further (Figure 2) (see details in Methods). As a RE was used in the protocol, this protocol was called RE-mediated ChIP. Compared with a regular ChIP protocol, in which chromatin is sheared into small chromatin segments by much stronger sonic waves, higher-order structures are disrupted less slightly in the RE-mediated ChIP. In terms of NUP1:GFP ChIP, enrichment of the chromatin positioned around the NPC, or the NP would be achieved by the RE-mediated ChIP method.

Two RE-mediated ChIP-seq experiments with different sonication intensities were conducted, and the sequence coverage with a 50-kb window setting was used to gain an overview of the distribution of sequencing reads. Intriguingly, the RE-mediated ChIP with NUP1:GFP (from here termed as NUP1:GFP RE-ChIP-seq) revealed that pericentromeric chromatin regions were commonly enriched, whereas chromatin on the distal chromosome arms tended to be

depleted (Figure 4C). Furthermore, many interstitial regions on the chromosome arms were found to have stronger interact with NUP1:GFP, for example, an interval corresponding to 2.0-3.0 Mb on chromosome 5 (Figure 4C). In contrast, some chromatin regions closed to PRs were not enriched by NUP1:GFP ChIP (e.g., an interval corresponding to 9.8-10.2 on chromosome 3) (Figure 4C). It was found that the patterns revealed by NUP1:GFP RE-ChIP-seq were clearly correlated with sonication strength (Figure 4B). To verify our RE-ChIP method, a RE-ChIP-seq experiment with anti-H3K9me2 was carried out, and compared the results with those came from a regular ChIP-seq (Stroud et al., 2014). The RE-ChIP with anti-H3K9me2 clearly captured the heterochromatin in PRs, which were in accordance with the previously reported results that the *Arabidopsis* PRs exhibited heavy H3K9me2 mark (Figure 5). Notably, enriched chromatin regions captured by the RE-mediated ChIP method were found to be overlapped 70%-80% of the regions captured by a regular ChIP method (Figure 5C), indicating the feasibility of our RE-ChIP method in capturing chromatin regions in plants. Consistently, the results of FISH did by our collaborators (Ying-juan Cheng and Jia-Wei Wang, University of Chinese Academy of Sciences, Shanghai 200032, People's Republic of China) demonstrated that selected regions showing higher NUP1:GFP RE-ChIP signals were localized closer to the NP than those showing depleted contacts with NUP1:GFP. Taken together, the NUP1:GFP RE-ChIP experiments suggest that certain chromatin regions on the *Arabidopsis* chromosome arms are preferentially found close to the NP.

Chromocenters, which consist of the centromeric and pericentromeric regions, have been reported to be localized preferentially at the NP (Fransz et al., 2002; Fang and Spector 2005). Interestingly, it was found that chromatin in centromeric regions was not enriched in the NUP1:GFP RE-ChIP-seq experiments (Figure 4C). One possible speculation accounting for this observation was that NPCs (or at least NPCs that contain NUP1) were not equally distributed at the NE, such that the density of NPC was lower at places where chromocenters are localized. For instance, it has been demonstrated that kinetochore proteins interact with *Arabidopsis* centromeres (Lermontova et al., 2006), suggesting that centromeres might be sequestered away from NPCs by these kinetochore proteins. To verify this scenario, a transgenic line co-expressing NUP1:GFP and mCherry:CENH3 (It has been demonstrated that CENH3 was solely loaded to centromeres (Lermontova et al., 2006)) was generated, and the patterns of these two fusion proteins in the nucleus were examined. These two fusion proteins showed complementary patterns at the NP, which provided an explanation for the observation that centromeric chromatin was not captured by NUP1:GFP RE-ChIP (Figure 4C

and Figure 6). Except for centromeric regions, PRs on each individual chromosomes exhibited the highest NUP1:GFP RE-ChIP-seq signals (Figure 6B-6F), which was in line with the fact that *Arabidopsis* chromocenters showed preferential localization at the NP (Fransz et al., 2002).

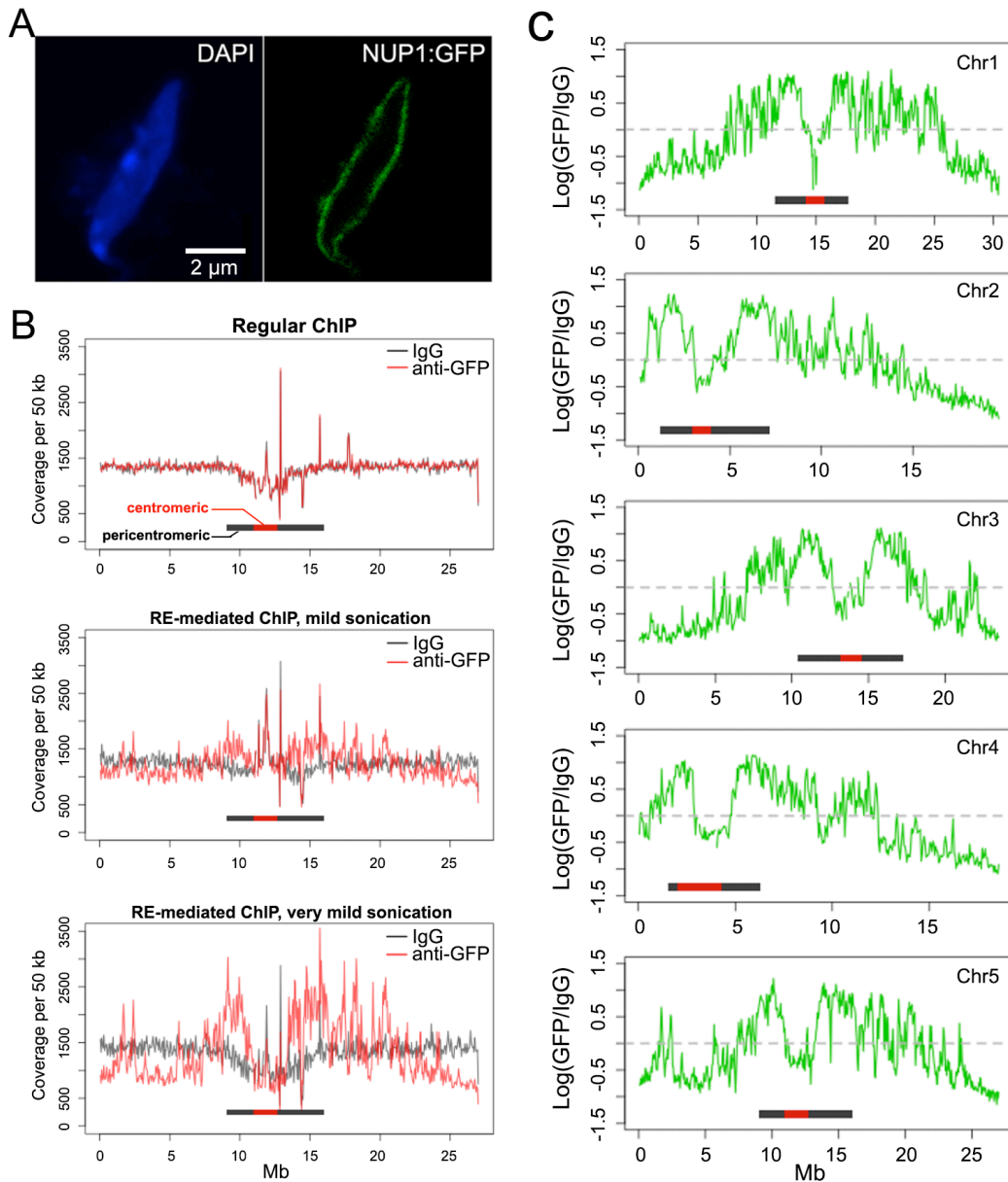


Figure 4. Identification of chromatin regions localized at the NP by NUP1:GFP RE-ChIP.

(A) Localization of the NUP1:GFP protein in a nucleus of *Arabidopsis*. Scale bar: 2 μ m. (B) Normalized sequence coverage (50-kb window size) on chromosome 5 from different ChIP experiments. The horizontal bar in each plot depicts pericentromeric region, within which centromeric region is highlighted in red. (C) NUP1:GFP RE-mediated ChIP-seq signal (50-kb window size), represented as the \log_2 value of the ratio between normalized anti-GFP and IgG coverage, over all five chromosomes. Horizontal bars indicate the centromeric/pericentromeric regions, as in (B). RE-ChIP data was analyzed by Dr. Chang Liu.

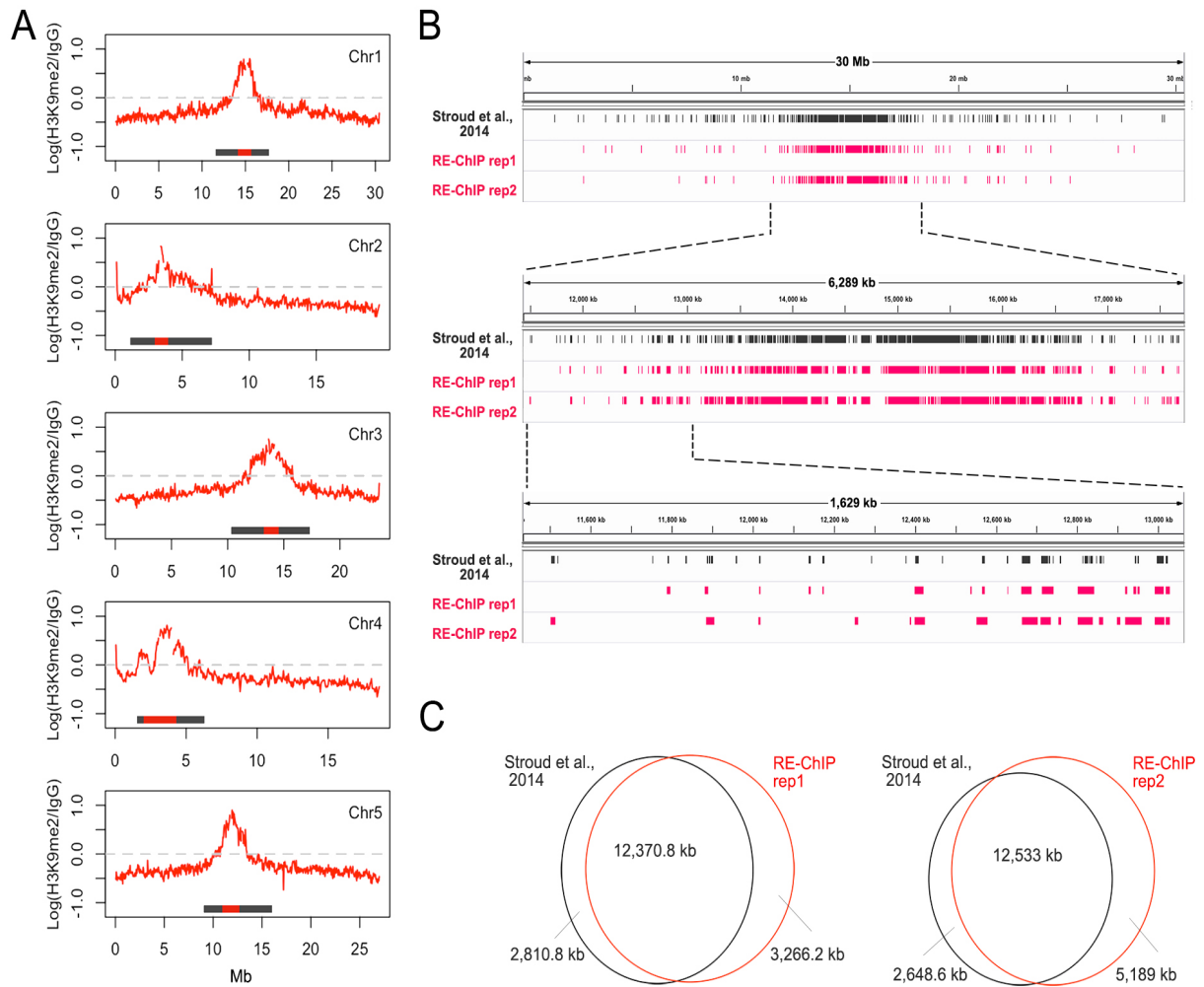


Figure 5. Comparison between RE-ChIP and regular ChIP.

(A) RE-ChIP-seq signals with anti-H3K9me2 antibodies (Abcam ab1220). The materials used for this experiment were 7-day-old WT seedlings. Labels in this figure are the same as in Figure 4C. (B) Distribution of enriched chromatin regions on chromosome 1, viewed with the Integrative Genomic Viewer browser (Robinson et al., 2011). For the regular ChIP-seq data (Stroud et al., 2014), the enriched regions were identified based on the SICER v1.1 program with window size and gap size set as 200 and 400, respectively (Zang et al., 2009). For the RE-ChIP, the enriched regions were revealed as described in Methods. The middle and the lower panels show zoomed-in areas of enriched pericentromeric heterochromatin. (C) Venn diagram of chromatin regions enriched with different ChIP methods. Data of these two kinds of ChIP experiments was analyzed by Dr. Liu.

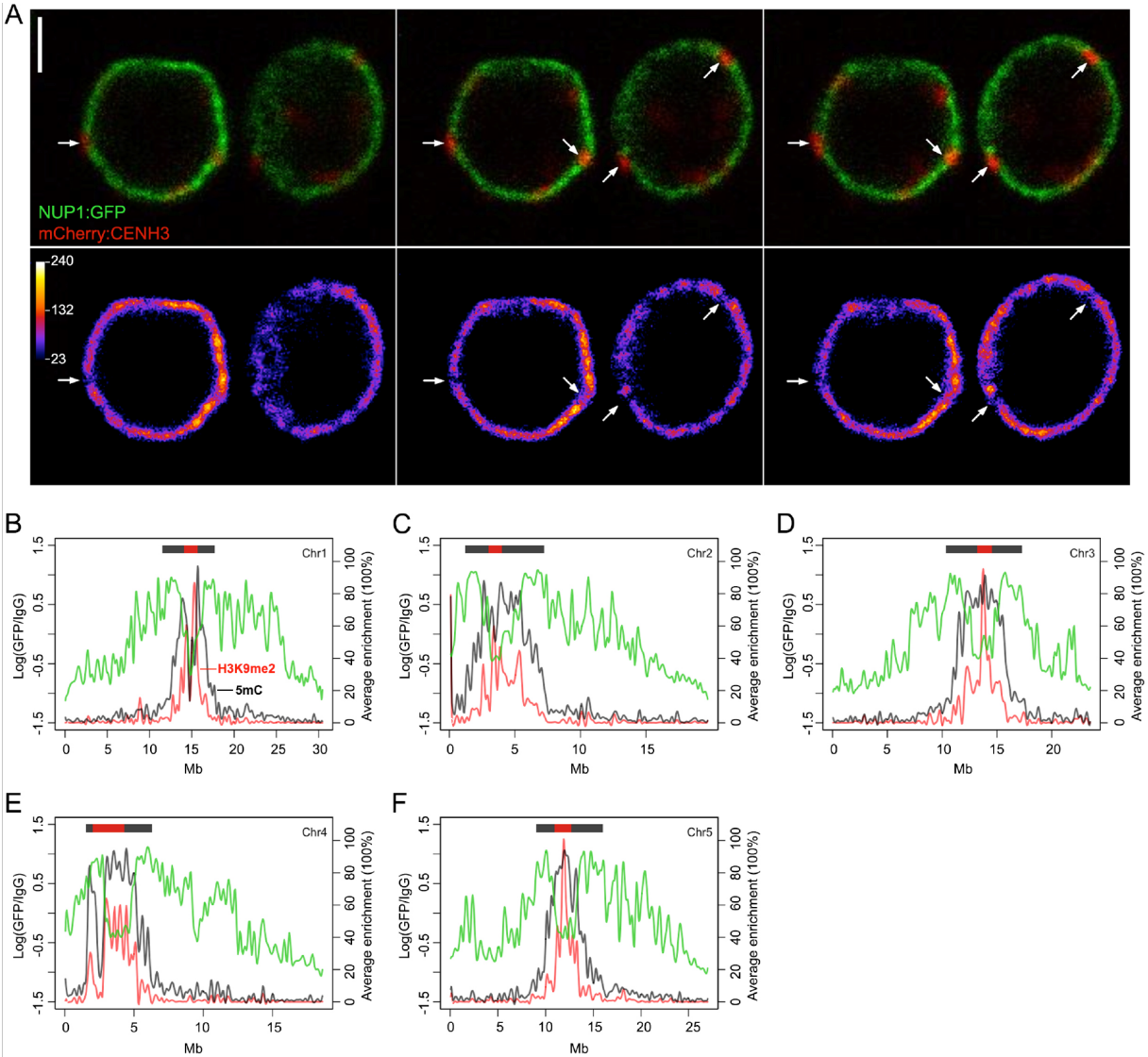


Figure 6. NUP1 and CENH3 display complementary patterns at the NP.

(A) Three consecutive z-stack confocal images of root cell nuclei showing NUP1:GFP and mCherry:CENH3 patterns. The top row shows NUP1:GFP (green) and mCherry:CENH3 (red) signals. The bottom row shows pixel intensities of the green fluorescence image. Arrows depict centromeres. Scale bar, 2 μm. (B to F) Distributions of NUP1:GFP RE-ChIP-seq signals (green line) and heterochromatic marks in five *Arabidopsis thaliana* chromosomes. Plots are according to a 50-kb bin setting. For the H3K9me2 (red line) and DNA methylation (black line) marks, the average enrichment (y-axis on right) means the percentage of regions enriched for the respective epigenetic mark. For all panels, the horizontal bars depict heterochromatic regions, within which centromeric regions are highlighted in red. Epigenetic data is from an integrated *Arabidopsis* epigenome (Wang et al., 2015a). Note that the data of DNA methylation and H3K9me2 was analyzed by Dr. Liu.

3.1.2 Chromatin positioning at the NP shows similar patterns in various tissues

As it was found that chromatin from the whole-plant seedlings positioning at the NP was not random, we next asked to which extent these profiles varied among different plant tissues. To investigate this, we explored NUP1:GFP RE-ChIP-seq data generated from four different tissues (root, 7-day-leaf, 30-day-leaf and inflorescence) (see Appendix Table 11). It was

found that patterns of NUP1:GFP RE-ChIP-seq signal in these tissues were highly reproducible between the two biological replicates (Figure 7-9). Interestingly, from the chromosomal scale, NUP1:GFP RE-ChIP-seq data acquired from various tissues displayed similar patterns (Figure 7-8). A common feature across these four *Arabidopsis* tissues was that the majority of enriched chromatin regions were located close to centromeres (Figure 7-8). These results imply that even though both the linear genome structure and the tissue identity make contributions to how the chromatin is tethered at the NP, the former is the main contributor. The difference in NUP1:GFP RE-ChIP-seq signal amplitudes between PRs and distal chromosome arms in inflorescence was found to be smaller than that in other tissues (Figure 7-8). It should be noted that all kinds of cell types presented in the harvested tissues were used to conduct RE-ChIP experiments; therefore, an average of the RE-ChIP-seq signals from the mixed cell types was generated. Compared with root and leaf tissues, the lower NUP1:GFP RE-ChIP signals near PRs in inflorescence tissue might be due to a dilution effect that different chromatin positioning profiles exist in various cells.

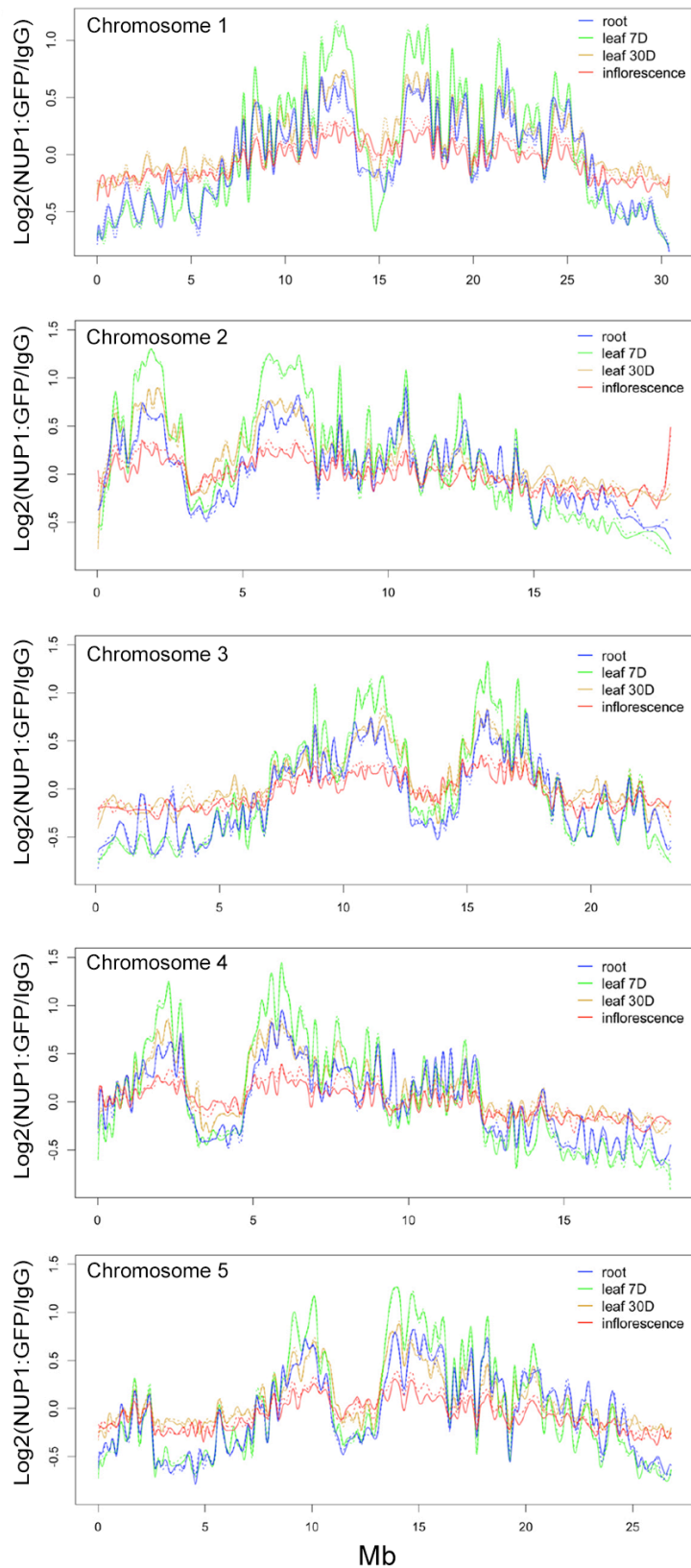


Figure 7. NUP1:GFP RE-ChIP-seq signals in various tissues.

Signals of NUP1:GFP RE-ChIP-seq (20-kb window size), represented as the \log_2 value of the ratio between normalized anti-GFP and IgG sequence coverage over all five chromosomes. For each tissue, the solid and dotted lines depict two replicates. The data was analyzed by Dr. Chang.

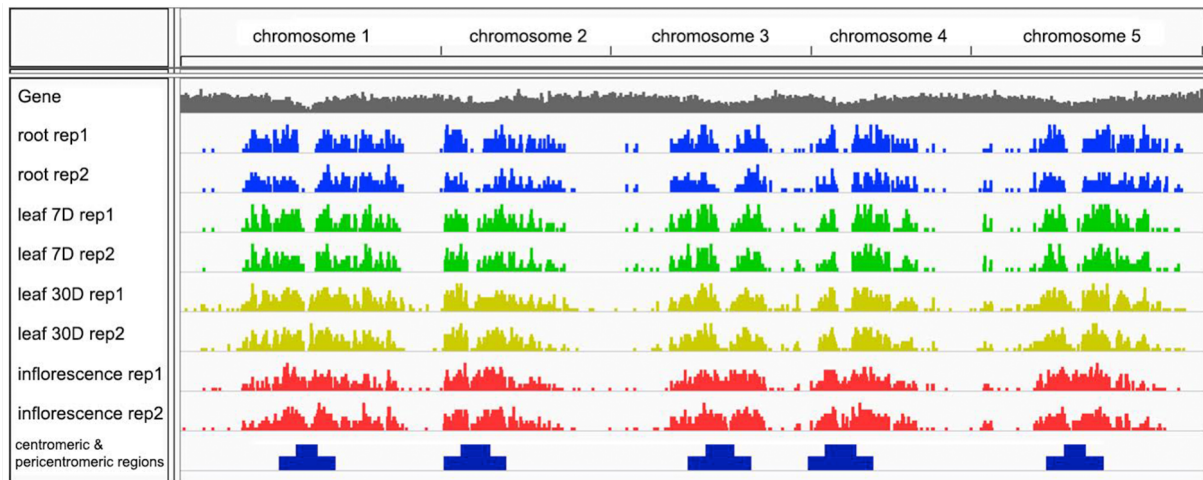


Figure 8. Comparison of NUP1-enriched chromatin segments in different tissues.

Distribution of NUP1-enriched domains across the genome viewed with the Integrative Genomic Viewer browser (Robinson et al., 2011).

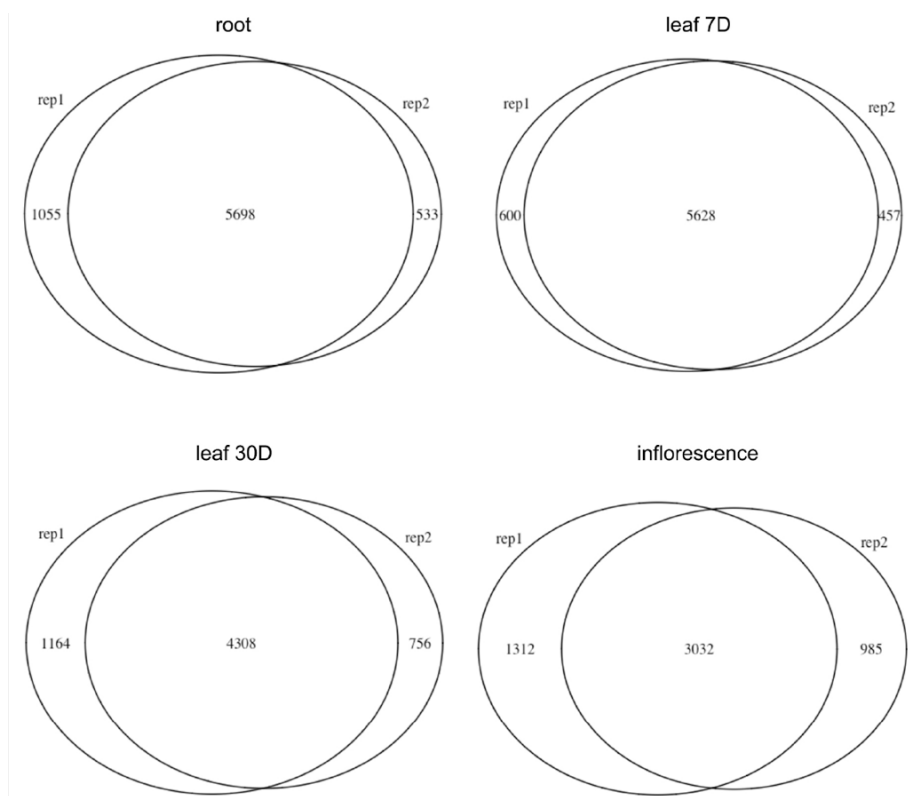


Figure 9. Comparison of NUP1-enriched genes in the two replicates.

Venn diagram of enriched genes. For each tissue, the number in middle means shared genes in two replicates. The data was analyzed by Dr. Chang Liu.

3.1.3 Chromatin positioned at the NP was enriched with repressed domains

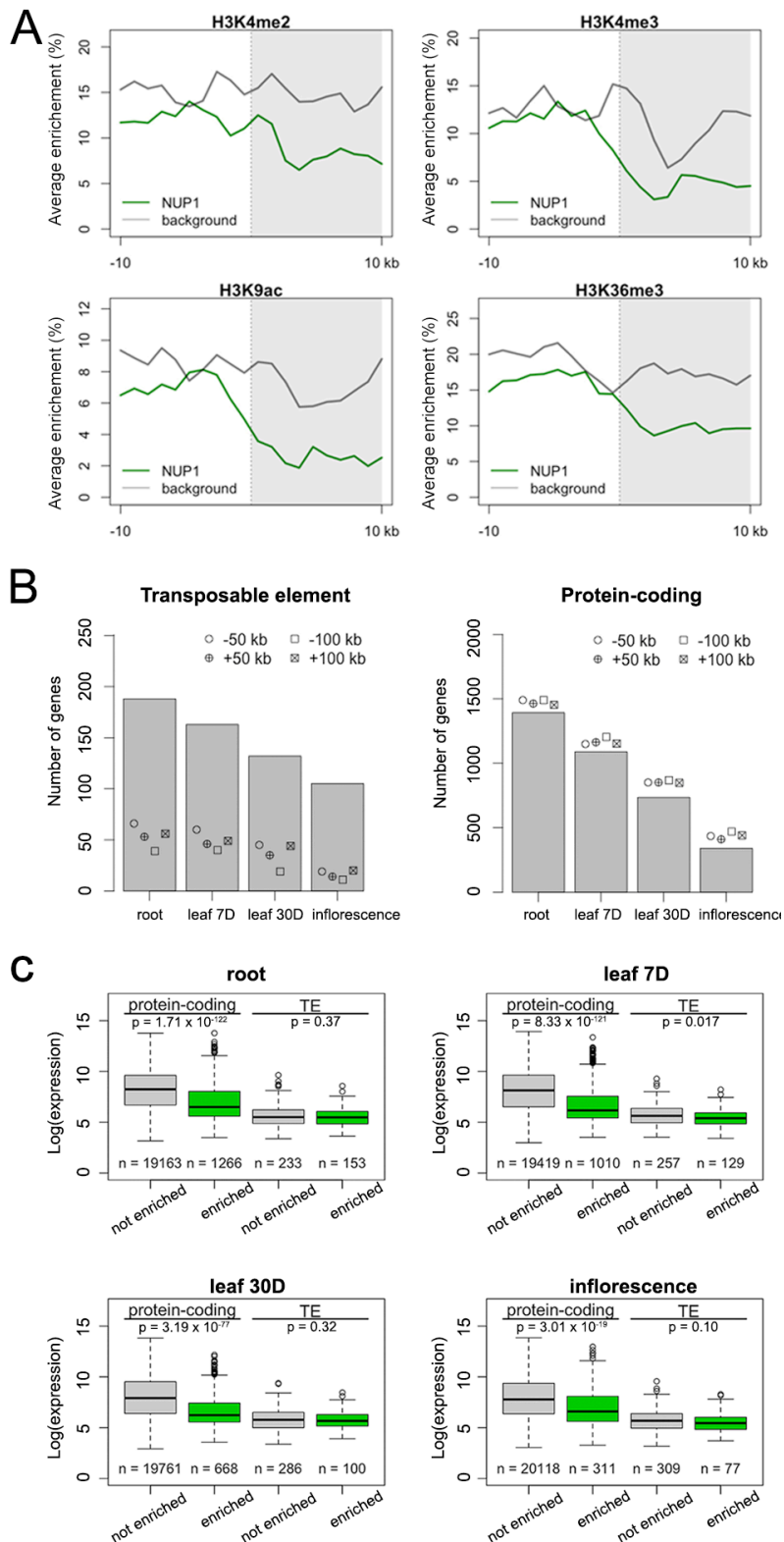


Figure 10. Enrichment of heterochromatin and silenced genes at the NP.

(A) Heterochromatin marks around NUP1-enriched domain borders, shown as a vertical line separating the white and gray blocks. For each plot, the area on the right indicates NUP1-enriched domains (although not all are larger than 10 kb). Average enrichment means the percentage of regions (calculated from 100-bp windows)

enriched for the respective heterochromatin mark. As enrichment of gene bodies is found inward from NUP1-enriched domain boundaries, for the background, 3000 genes with the same expression distribution profile as that of NUP1-enriched genes were picked randomly. For these control genes, we extracted the 20-kb regions flanking either their transcription start sites (TST) or their TTS, which were selected randomly. (B) Number of TE genes (left panel) and protein-coding genes (right panel) enriched in different tissues. For each column, the observed number of genes is significantly different ($p < 0.001$) relative to the permutation-based null distribution of the background (generated as described in A). (C) Comparison of gene expression levels, which are from a normalized tiling array dataset (Laubinger et al., 2008). The p-values indicate Mann-Whitney U test results. This analysis was done by Dr. Chang Liu.

Next, Dr. Liu helped with the characterization of the NUP1-enriched chromatin domains positioned at the NP. Because chromatin in centromeric and pericentromeric regions was preferentially captured by NUP1:GFP RE-ChIP, the features associated with centromeric and pericentromeric heterochromatin were expected to be enriched. To reduce such positional effects, only chromatin located at least 1 Mb from PRs was used for association analyses. In summary, in all tissues, heterochromatin marks and TE genes were found to be enriched in NUP1-enriched domains compared to the control sets, which were simulated by shifting the coordinates of the enriched regions a certain distance upstream or downstream (Figure 10A-10B). In addition, it was found that the enriched protein-coding genes showed significantly lower expression levels, while TE genes enriched at the NP did not exhibit lower expression levels than those that were not enriched (Figure 10C). Altogether, these results indicate that chromatin domains localized at the NP are generally repressed.

3.1.4 Positioning of TEs at the NP correlates with different silencing pathways

The finding of the enrichment of repressed chromatin domains at the NP prompted us to further investigate whether it was associated with TE silencing. DNA methylation in the CG, CHG, and CHH (H represents any nucleotide except G) sequence contexts has critical functions on regulating expression and transposition of TEs. Unlike LADs in animals which are not enriched with cytosine methylation (Berman et al., 2011), TEs enriched at the NP exhibited higher DNA methylation level in all the three sequence contexts (Figure 11). Next, how the corresponding methylation types in these two types of TEs would be affected in several DNA methylation mutants was explored. For TEs located either in the nuclear interior or at the NP, mutations impairing CG or CHG methylation had similar effects (Figure 11). Intriguingly, when comparing patterns of DNA methylation in CHH sequence context, we observed that TEs located at the NP lost more DNA methylation in the *cmt2* mutant; by contrast, TEs not localized at the NP lost more DNA methylation in the *drm1/2* double mutant (Figure 11). RNA-directed DNA methylation (RdDM) and RdDM-independent are two

partially overlapped pathways that are responsible for CHH DNA methylation over TE bodies (Zemach et al., 2013; Stroud et al., 2014), but how these two pathways branch to target different TEs is still not fully understood (reviewed by (Sigman and Slotkin 2016)). In the RdDM pathway, DOMAINS REARRANGED METHYLASE 1 (DRM1) and DRM2 are methyltransferases which are required to mediate CHH DNA methylation; whereas in RdDM-independent pathway, CHROMOMETHYLASE 2 (CMT2) is another methyltransferase which is required to catalyze CHH DNA methylation (Zemach et al., 2013; Sigman and Slotkin 2016). Our results imply that the spatial localizations of TE are associated with the demand on different CHH DNA methylation pathways, in which RdDM-independent pathway contributes more to the CHH DNA methylation of TEs positioned at the NP, while RdDM-dependent pathway contributes more to the CHH methylation of TEs not localized at the NP.

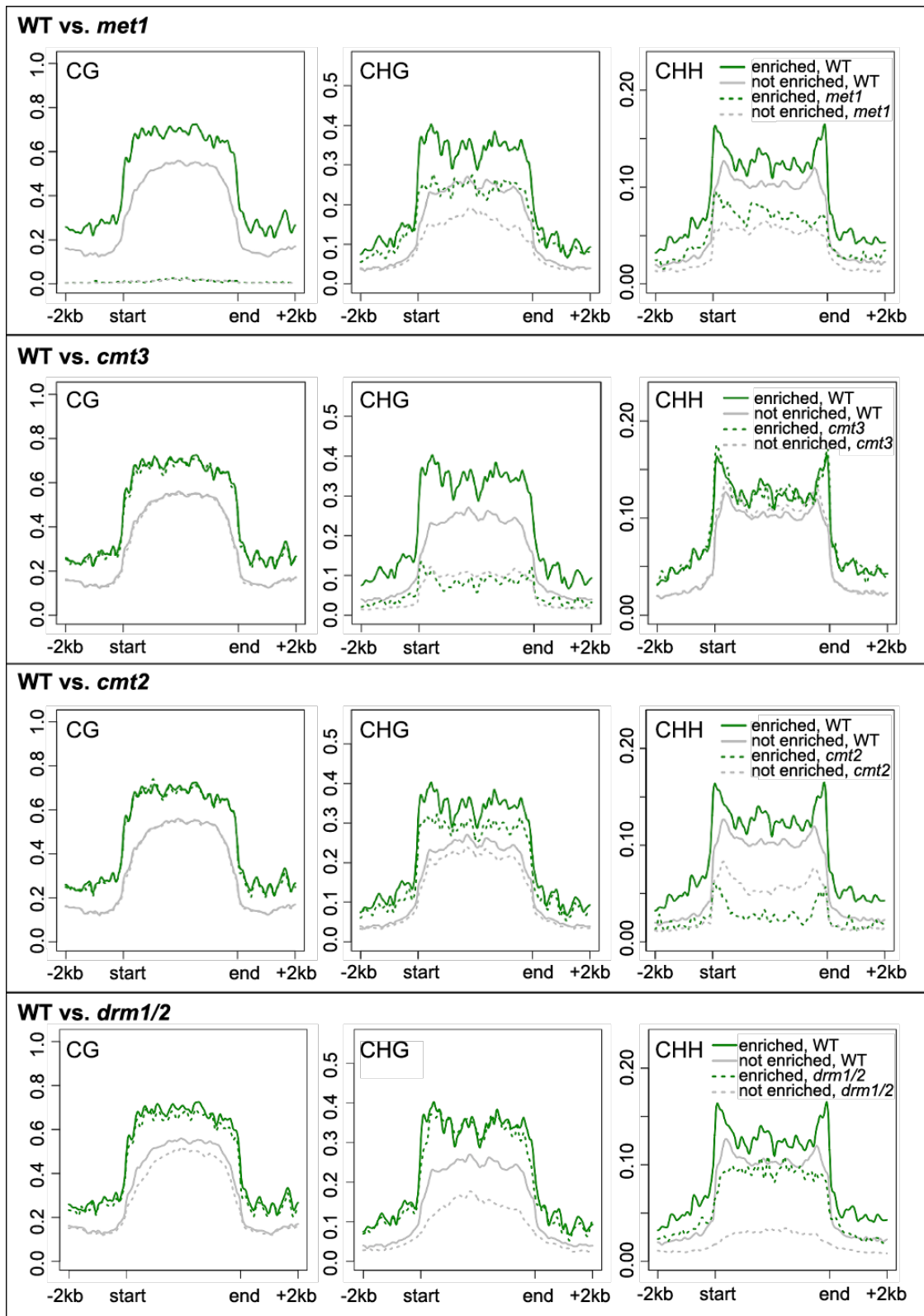


Figure 11. Comparison of DNA methylation over TEs.

Patterns of TE DNA methylation (CG, CHG, CHH) in WT plants and different methylation mutants. The grouping of TEs is according to the enrichment results of NUP1:GFP RE-ChIP-seq from 30-day-old leaf tissues. The methylation ratio is calculated in 100-bp windows. The signal over every TE is linearly transformed so that the boundaries of all TEs are aligned. Note: This data was analyzed by Xiaoli Ma.

3.2 Plant lamin-like proteins are required for specific chromatin positioning at the NP

3.2.1 Compare genomic loci positioning at the NP with FISH

The non-random chromatin organization at the NP in *Arabidopsis* has been revealed by our NUP1:GFP RE-ChIP experiments. Next, we asked how such spatial chromatin positioning at the NP is achieved in plants. To unveil the mechanism, we started from identifying mutant(s), which might no more exhibit specific perinuclear chromatin localization patterns in the nucleus. In this regard, we sought to compare localizations of chosen genomic loci to the NP by conducting comparative FISH analyses.

The two following criteria were applied to choose genomic regions for FISH experiments and the design of the FISH probes: firstly, the signal specificity of all the selected BACs had been validated (Pecinka et al., 2004). Secondly, the probed genomic regions must be several Mb away from PRs, as chromocenters have been shown localized at the NP (Fransz et al., 2002). Totally, five pairs of FISH probes were designed according to our NUP1:GFP RE-ChIP signals (Figure 12A, Appendix Table 12). Three pools of FISH probes targeting chromatin regions located on chromosome 1 (green 1, green 2, and red1/2), were used as two pairs (green 1 vs red1, green 2 vs red2). The other three pairs of FISH probes were targeted to chromatin regions located on chromosome 3, 4 and 5, respectively. Probes of each pair were labeled differently: those hybridized to genomic loci preferentially enriched by NUP1:GFP RE-ChIP were termed “green”, which were detected as green fluorescent signals. On the other hand, probes hybridized to genomic regions that were not enriched at the NP were referred as “red”, which were detected as red fluorescent signals. Each pool of probes was produced by nick translation labeling, and their size was distributed in a size range of 700- 200 bp (Figure 12B).

There has been no evidence showed that chromatin positioning at the NP would be affected by endoreduplication, although a preferential NP localization of PRs is still observed in nuclei with high endopolyploidy levels (Schubert et al., 2012). A comparison study of chromatin organization in the *Arabidopsis* nuclei with lower or higher endopolyploidy levels (4C vs 16C) suggested that chromatin would de-condense to a certain extent along with endoreduplication (Schubert et al., 2012). Therefore, to eliminate possible misleading or inconsistent FISH patterns associated with nuclei with different endopolyploidy levels, only 2C nuclei were collected for FISH analyses (see methods).

Generally, four FISH signals with two green FISH signals and two red FISH signals were detected in every 2C nucleus (Figure 13A). Distance from the estimated barycenter of each FISH signal to the NP was measured, and then the distance distributions of green and red FISH signals were analyzed and compared. In WT *Arabidopsis* plants cell nuclei, for all the five pairs of probes, the FISH comparison results were in agreement with our NUP1:GFP RE-ChIP data: the green FISH signals showed shorter distance to the NP than did those red FISH signals (Figure 13B). It should be noted that the green signals were not always localized closer to the NP. In some nuclei, genomic regions hybridized with the red probes were localized closer to the NP than were those chromatin regions targeted by the green probes. Such reversed patterns suggest a cell-to-cell variation scenario, which has been shown in mammals that LADs were not identical across a cell population (Kind et al., 2013; Kind et al., 2015).

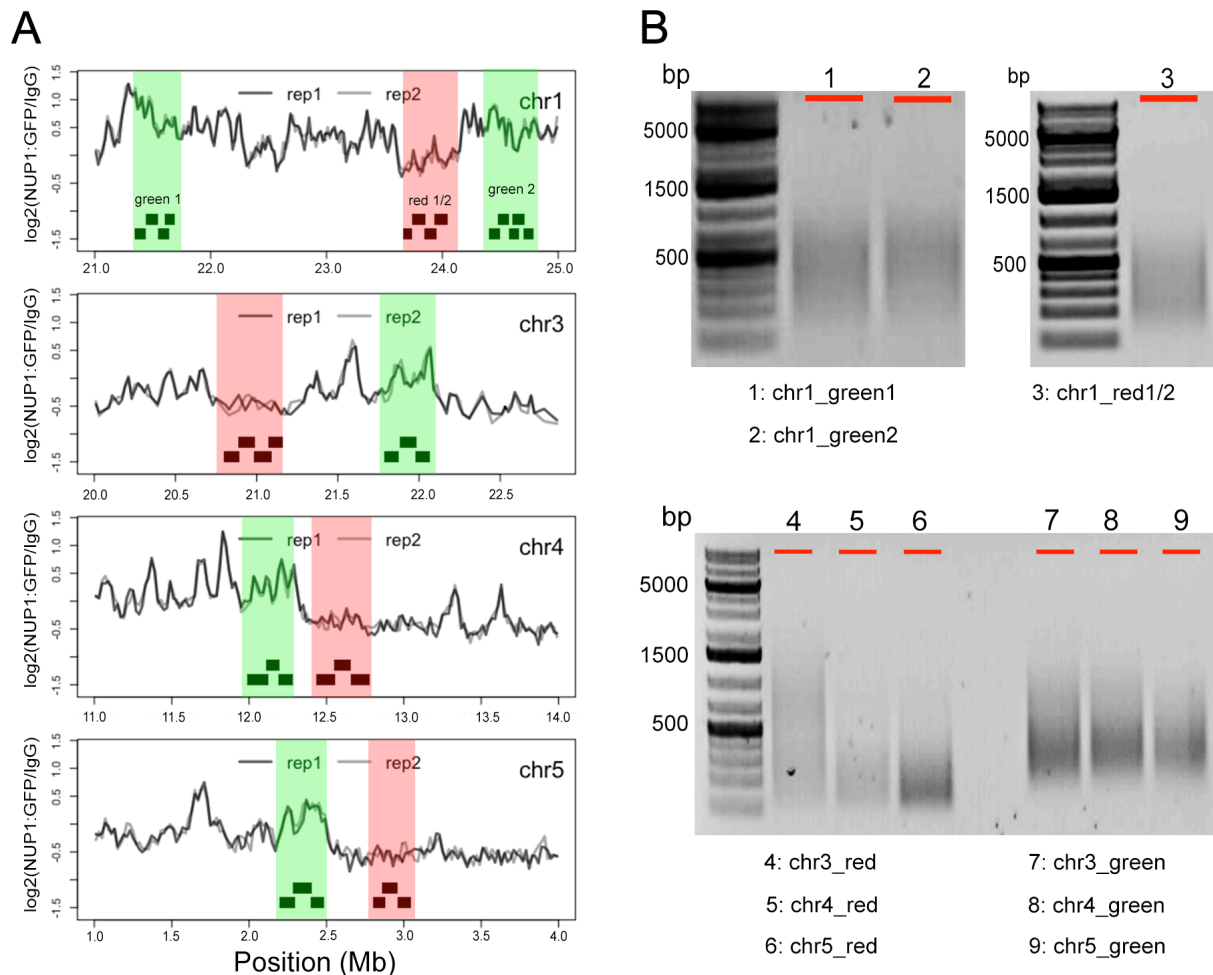


Figure 12. Design of probes targeting chromatin regions.

(A) Nine pools of tiling BAC probes (black segments) designed according to the NUP1:GFP RE-ChIP-seq signals, which are located on chromosome 1 (chr1), 3, 4 and 5, respectively. Each pool of probes targets a ~300 kb genomic region. (B) Size distribution of each pool of probes generated by nick translation labeling.

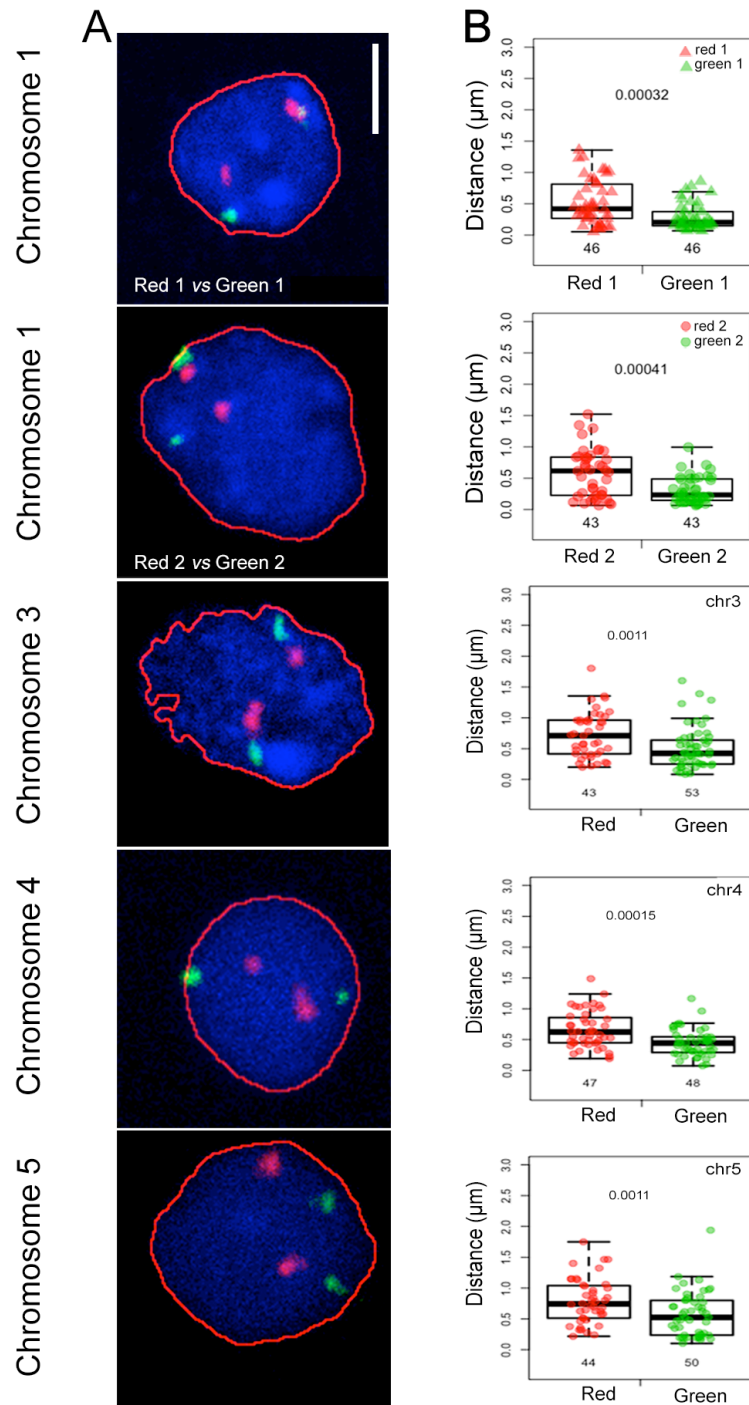


Figure 13. Probing chromatin localization with FISH.

(A) Representative confocal images showing nuclei with the FISH signals. The red contour shows the estimated edge of the nucleus. The estimated nuclear edge was defined in ImageJ with the ROI (regions of interest) manager according to DAPI signal. Scale bar: 2 μm . (B) Boxplots showing distribution patterns of the distance of FISH signals from the NP in 2C nuclei. Green and red dots in boxplots denote the distance data of green and red FISH signals, respectively. The number under each boxplot shows the number of the corresponding FISH signals. The p value on top in each panel indicates result of one-sided Mann-Whitney U test.

The situation, in which most WT cell nuclei showed chromatin regions targeted by green FISH probes were closer to the NP, was referred as “differential localization”. The differential localization of genomic regions targeted by green and red FISH probes at the NP in WT nuclei indicated that these FISH probes could be used to conduct comparative FISH analyses on mutants, which potentially lost specific perinuclear chromatin anchoring. Even though all the five pairs of FISH probes showed differential localization in WT 2C nuclei, three of them were chosen to do further analyses, which targeted chromatin regions located on chromosome 1 (green 2 vs red2), 3 and 5, respectively (Figure 12A). These three pairs of probes were chosen because for each pair of probes, the one hybridized to chromatin regions preferentially positioned at the NP was further away from PR compared to the other (Figure 12A). The reason that we paid attention to PRs in choosing FISH probes was due to possible position effects that passively brought chromatin to the NP. It has been shown that at a chromosomal scale, the closer a locus is to the PR the stronger it tends to be localized to the NP (Figure 4C). Because PRs have been shown to be localized preferentially at the NP, chromatin regions closer to PRs might passively exhibit NP-favored positioning patterns (Armstrong et al., 2001; Fransz et al., 2002). Therefore, these three pairs of probes were used to unveil whether or not there were changes in perinuclear chromatin anchoring in *Arabidopsis* mutants, except for *crwns* and *kaku4*, in which green 1 vs red1 probe pair was also used.

3.2.2 Plant lamin-like proteins are required for selectively tethering chromatin at the NP

In various metazoan species, such as *C. elegans*, *Drosophila* and mouse, it has been shown that lamin proteins are involved in anchoring heterochromatin to the NP (Solovei et al., 2013; Mattout et al., 2011; Shevelyov et al., 2009). Thus, we sought to examine whether specific chromatin positioning at the NP was influenced when plants lost plant lamin proteins. As CRWN proteins are one group of plant lamin candidates, among which CRWN1 and CRWN4 are localized at the NP (Sakamoto and Takagi 2013; Dittmer et al., 2007; Wang et al., 2013). We first tested the FISH signal distribution of the four pairs of FISH probes in *crwn1* and *crwn4* mutants. For all the examined pairs of FISH probes, we found that the differential localization patterns of the green and red FISH signals at the NP in WT nuclei were lost in the tested *crwn* mutants (Figure 14). This result implies that CRWN1 and CRWN4 are both required for positioning chromatin at the NP.

As knockout of *CRWN1* or *CRWN4* locus affected the specific positioning of chromatin targeted by the FISH probes, we explored whether knockout *CRWN1* and *CRWN4* loci

simultaneously gave rise to more extensive effect. However, except for FISH probes of green 1 vs red 1, the distance distribution patterns of other three pairs of FISH probes to the NP in *crwn1/4* mutant were similar like those in *crwn1* and *crwn4* mutants (Figure 14).

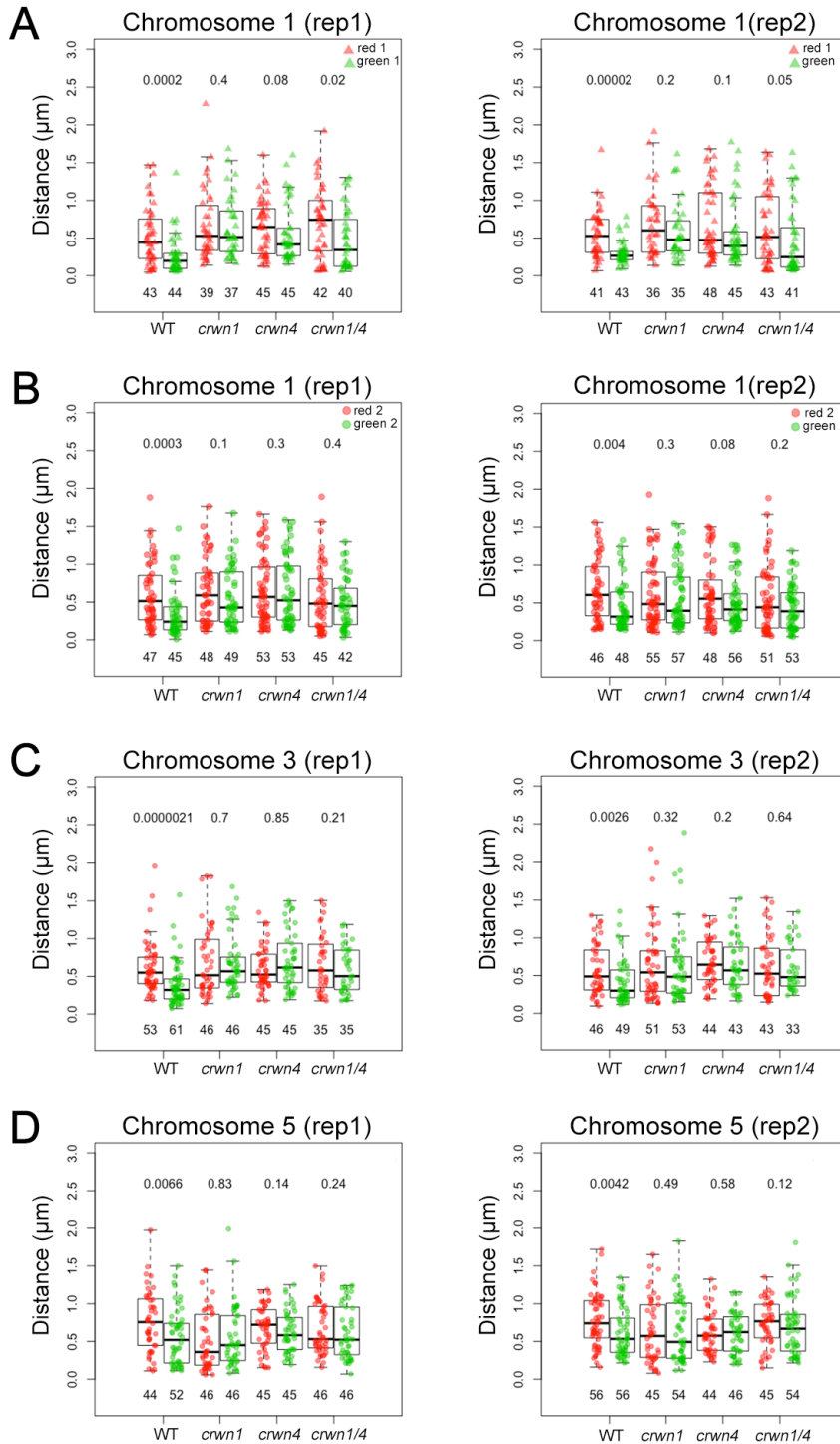


Figure 14. Analyses of FISH signals in *Arabidopsis* mutants of lamin-like gene.

Comparison of the distance of probed genomic regions in chromosome 1 (green 1 vs red 1 (A) and green 2 vs red 2 (B)), 3 (C), and 5 (D) to the NP in 2C nuclei of *crwn* mutants. The number under each boxplot shows the number of the corresponding FISH signals. Green and red dots in boxplots denote the distance data of green and

red FISH signals, respectively. For each pair of comparison (boxplots of the same genotype), the p value on top indicates result of one-sided Mann-Whitney U test.

As it has reported that *Arabidopsis* mutants with loss-of-function of *CRWN1* and/or *CRWN4* genes had smaller and spherical nuclei compared with WT plants (Sakamoto and Takagi 2013; Dittmer et al., 2007; Wang et al., 2013), the altered chromatin positioning at the NP in *crwn1*, *crwn4* or *crwn1/4* mutants might be attributed to changes of nuclear morphology.

3.2.3 Knocking out of *KAKU4* has no influence on specific chromatin positioning at the NP

KAKU4, as the only member of another group of plant lamin candidates in *Arabidopsis*, is localized at the NP, and *kaku4* mutant showed smaller and spherical nuclei (Goto et al., 2014). In 2C nuclei of *kaku4* mutants, we examined the signal distribution patterns of the four pairs of FISH probes, which located on chromosome 1, 3 and 5, respectively. For all the tested pairs of FISH probes, the differential localizations of green and red FISH signals are similar to that in 2C WT nuclei (Figure 15), suggesting that loss-of-function of *KAKU4* has no influence on specific chromatin positioning at the NP.

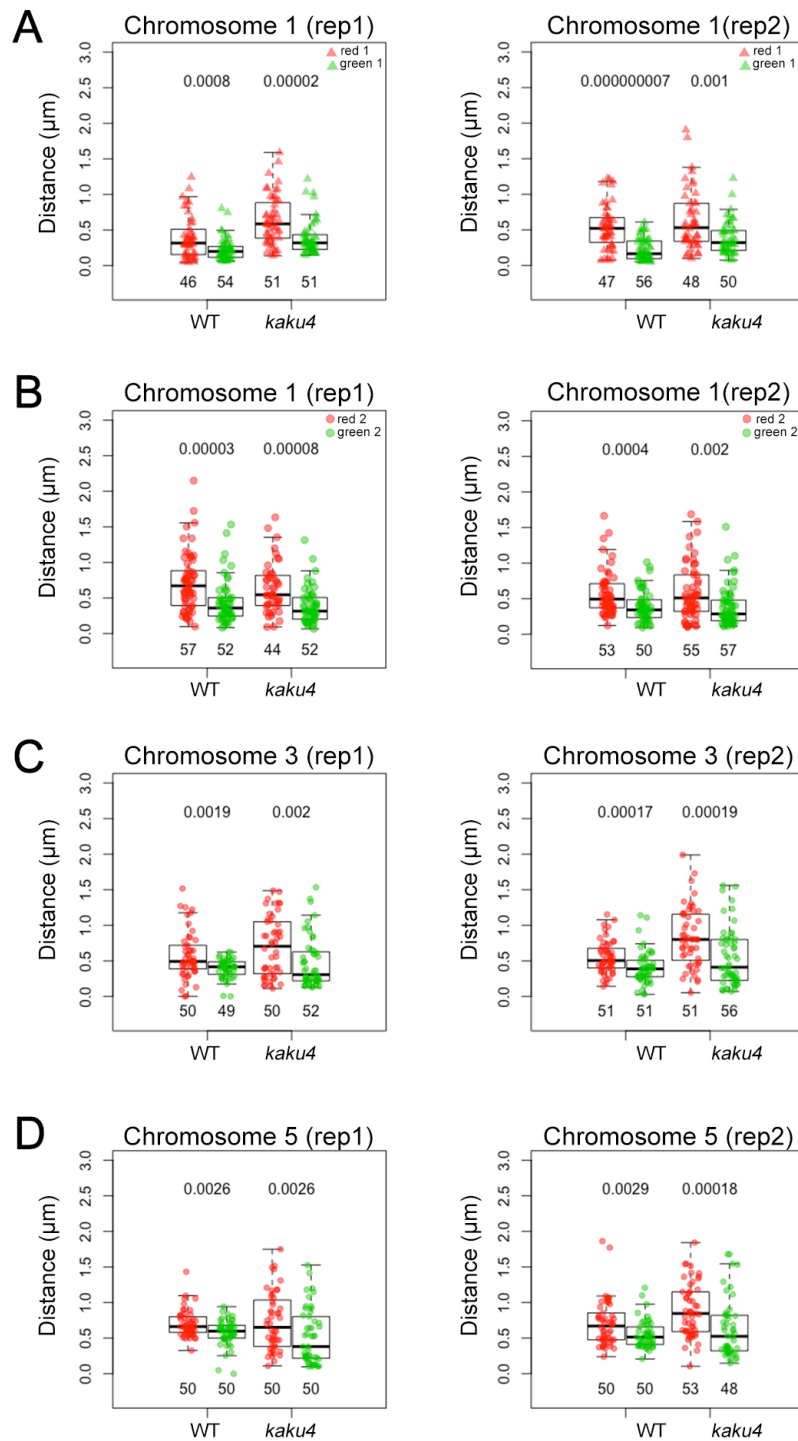


Figure 15. Analyses of FISH signals in *kaku4* mutant.

Comparison of the distance of probed genomic regions in chromosome 1 (green 1 vs red 1 (A) and green 2 vs red 2 (B)), 3 (C), and 5 (D) to the NP in 2C nuclei of *kaku4* mutants. The number under each boxplot shows the number of the corresponding FISH signals. Green and red dots in boxplots denote the distance data of green and red FISH signals, respectively. For each pair of comparison (boxplots of the same genotype), the p value on top indicates result of one-sided Mann-Whitney U test.

3.2.4 Specific chromatin positioning at the NP is not affected in *neap* mutants

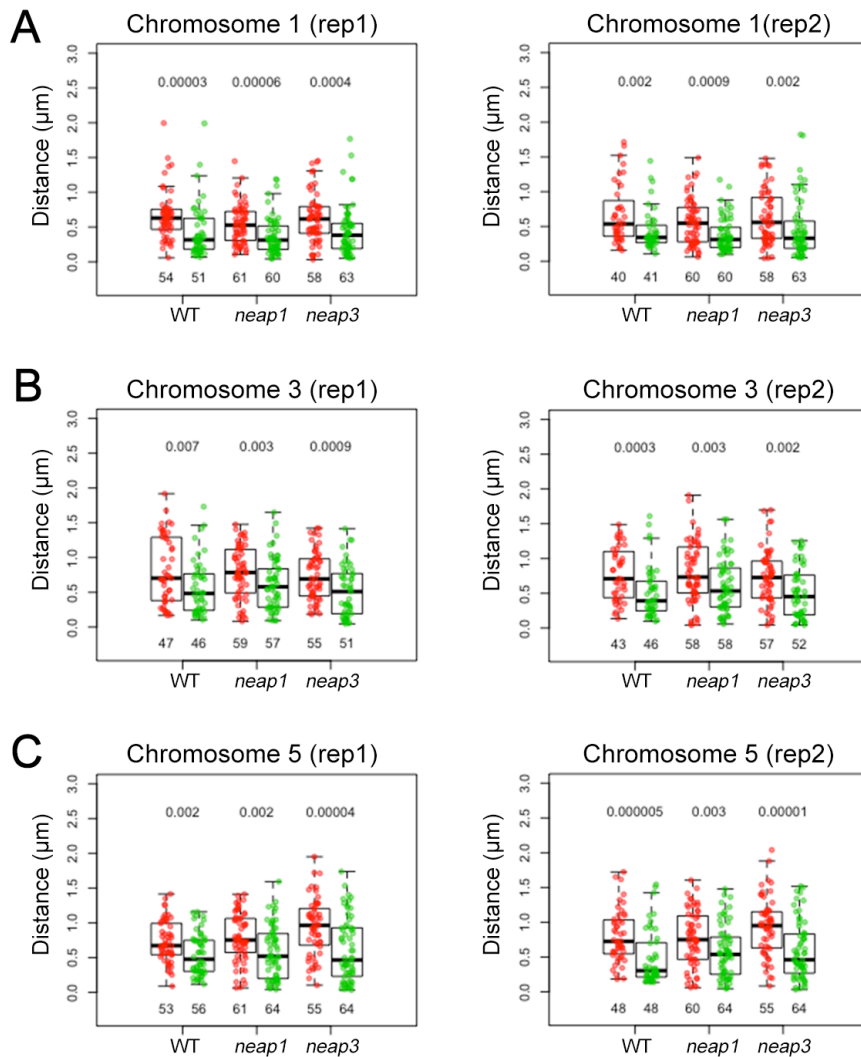


Figure 16. Analyses of FISH signals in *neap* mutants.

Comparison of the distance of probed genomic regions in chromosome 1 (green 1 vs red 1 (A) and green 2 vs red 2 (B)), 3 (C), and 5 (D) to the NP in 2C nuclei of *neap* mutants. Green and red dots in boxplots denote the distance data of green and red FISH signals, respectively. The number under each boxplot shows the number of the corresponding FISH signals. For each pair of comparison (boxplots of the same genotype), the p value on top indicates result of one-sided Mann-Whitney U test.

NEAPs are another group of plant candidate lamin proteins in *Arabidopsis*, among which NEAP1, NEAP2 and NEAP3 are located at the INM (Pawar et al., 2016). In addition, the alteration in nuclear morphology in *neap1*, *neap3* and *neap1/3* mutants suggests that they are involved in maintaining nuclear architecture (Pawar et al., 2016). We sought to verify whether the specific chromatin positioning in at the NP was impaired in *neap1* and *neap3* mutants. To this end, we inspected the signals of the selected three pairs of FISH probes (located on chromosome 1, 3, and 5, respectively) in 2C nuclei of *neap1* and *neap3* mutants. For all the examined genomic loci, we observed differential locations of the red and green probes in the

2C nuclei of *neap1* and *neap3* mutants (Figure 16), suggesting that the specific chromatin positioning at the NP is not affected in these two single *neap* mutants.

Altogether, our comparative FISH results in plant lamin mutants indicate that the differential localization of FISH signals is lost in *crwn1*, *crwn4* single mutant and *crwn1/4* double mutants, while it is not affected in *kaku4*, *neap1*, or *neap3* single mutants.

3.2.5 Knockout *CRWN1*, *CRWN4* or *KAKU4* locus decreases the size of nuclei

Although changes in nuclear morphology in several *Arabidopsis* lamin protein mutants (e.g., *crwn1*, *crwn4* and *kaku4*) have been characterized, there has been no report showing comparisons of nuclear size and shape in the context of having specific endopolyploidy levels. As only 2C nuclei were used to do FISH comparative analyses, the morphology of the 2C nuclei isolated from WT, *crwn1*, *crwn4*, *crwn1/4* and *kaku4* plants was characterized firstly.

As expected, size of the 2C nuclei was found to be significantly reduced in all the four plant lamin mutants compared with WT 2C nuclei (Figure 17B). This result was in accordance with the published data showing reduced nuclei size in *crwns* and *kaku4* mutants (Sakamoto and Takagi 2013; Dittmer et al., 2007; Goto et al., 2014; Wang et al., 2013). Surprisingly, we found that the differences of 2C nuclei shape among WT, *crwn1*, *crwn4*, *crwn1/4* and *kaku4* mutants were not significant (Figure 17A and 17C). This result was not consistent with previous studies that indicated nuclear shape in *crwns* and *kaku4* mutants was significantly altered (Sakamoto and Takagi 2013; Dittmer et al., 2007; Goto et al., 2014; Wang et al., 2013). A possible reason for such discrepancy could be attributed to the selection of nuclei of different cell types. In this study, most 2C nuclei were those in mesophyll cells (see methods and Figure 3). On the contrary, previous reports were mainly based on nuclear morphological analyses of nuclei in leaf epidermal cells and trichome cells (Sakamoto and Takagi 2013; Goto et al., 2014). Therefore, in 2C nuclei of *crwn1*, *crwn4* and *crwn1/4* mutants, the loss of differential localization of FISH signals with respect to the NP was unlikely attributed to the alterations of their nuclear morphology.

Similar to 2C nuclei, 8C nuclei in *crwns* and *kaku4* mutants were also found to become smaller (Figure 18B). Moreover, the circularity index of the 8C nuclei of these mutants was increased compared with that of WT (Figure 18A and 18C). These results are consistent with the former published results that nuclei in *crwns* and *kaku4* became more spherical and

smaller (Sakamoto and Takagi 2013; Dittmer et al., 2007; Goto et al., 2014; Wang et al., 2013).

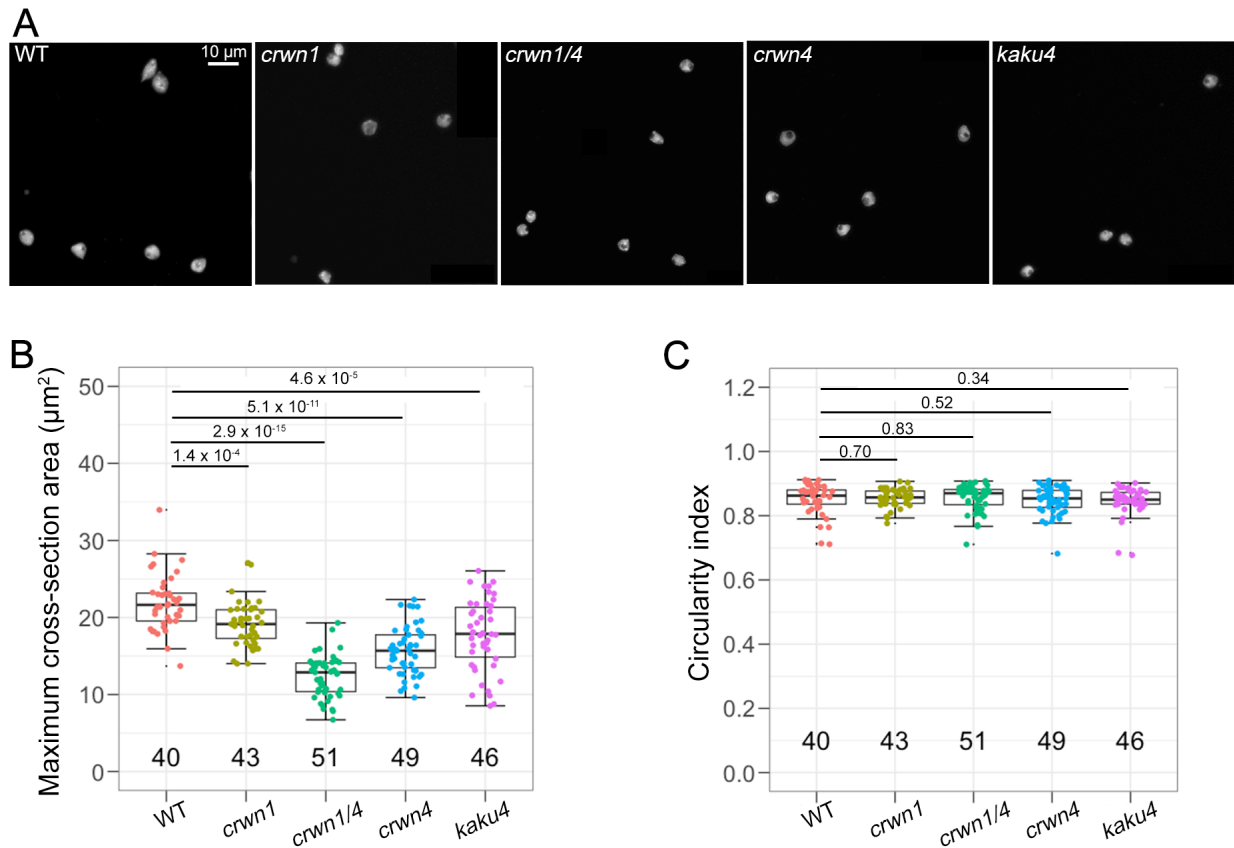


Figure 17. Characterization of nuclear morphology of *Arabidopsis* 2C nuclei.

(A) Images (z-projection) of representative DAPI-stained 2C leaf cell nuclei isolated from WT, *crwn1*, *crwn1/4*, *crwn4* and *kaku4* mutants. Cell nuclei were imaged using confocal microscopy with z-stack scanning. Scale bar: $10\ \mu\text{m}$. (B) Maximum cross-section area of 2C leaf cell nuclei isolated from WT, *crwn1*, *crwn1/4*, *crwn4* and *kaku4* mutants. (C) Circularity index of 2C leaf cell nuclei isolated from WT, *crwn1*, *crwn1/4*, *crwn4* and *kaku4* mutants. The circularity index was calculated as $4\pi A/P^2$, where A and P were the area and perimeter of the maximum cross-section of a nucleus retrieved from confocal images, respectively. The number under each boxplot shows the number of the examined nuclei. p values indicate Mann-Whitney U test results.

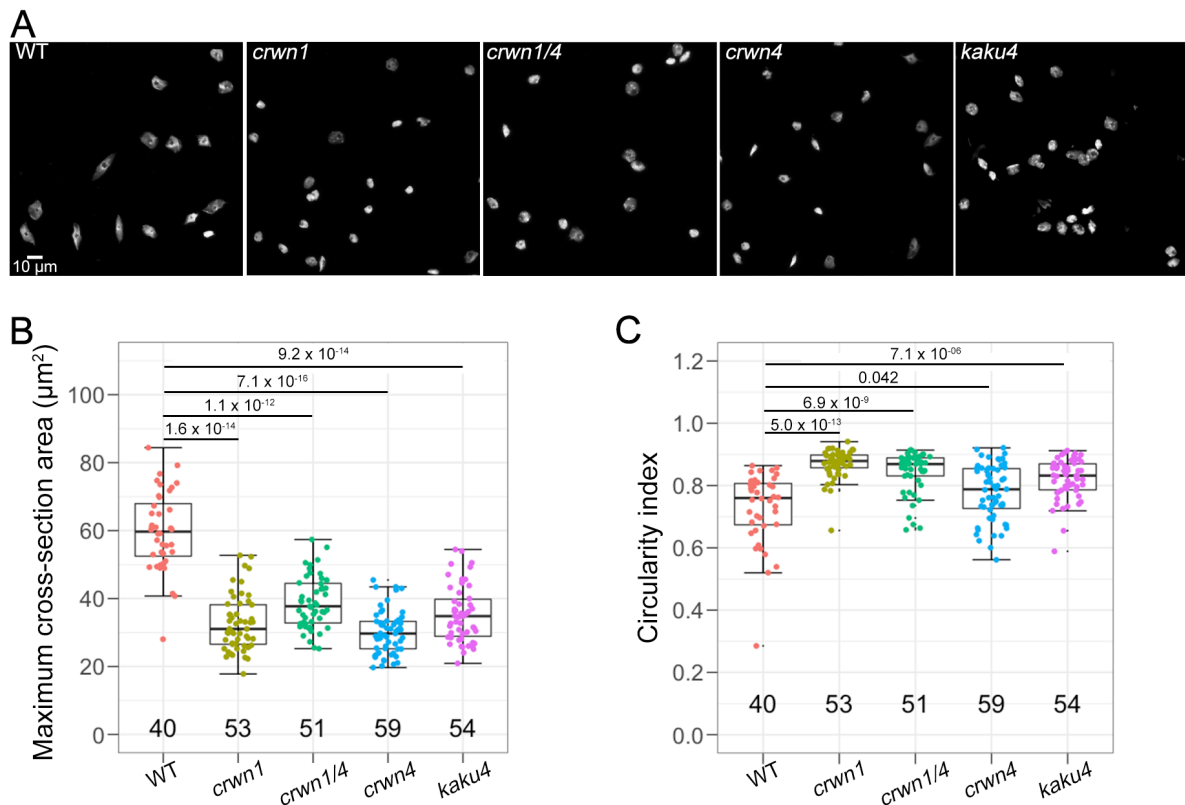


Figure 18. Characterization of nuclear morphology of *Arabidopsis* 8C nuclei.

(A) Images (z-projection) of representative DAPI-stained 8C leaf cell nuclei isolated from WT, *crwn1*, *crwn1/4*, *crwn4* and *kaku4* mutants. Cell nuclei were imaged using confocal microscopy with z-stack scanning. Scale bar: 10 µm. (B) Maximum cross-section area of 8C leaf cell nuclei isolated from WT, *crwn1*, *crwn1/4*, *crwn4* and *kaku4* mutants. (C) Circularity index of 8C leaf cell nuclei isolated from WT, *crwn1*, *crwn1/4*, *crwn4* and *kaku4* mutants. The circularity index was calculated as $4\pi A/P^2$, where A and P were the area and perimeter of the maximum cross-section of a nucleus retrieved from confocal images, respectively. The number under each boxplot shows the number of the examined nuclei. p values indicate Mann-Whitney U test results.

3.3 Role of H3K9me in specific chromatin positioning at the NP

In metazoans, the heterochromatic mark H3K9me is enriched in LADs at the NP (van Steensel and Belmont 2017). In nuclei of human and *C. elegans*, H3K9me is required for tethering chromatin at the NP (Towbin et al., 2012; Kind et al., 2013; Bian et al., 2013). In *Arabidopsis*, H3K9me was also found to be enriched in chromatin regions localized at the NP (Figure 10A). In *Arabidopsis*, SU(VAR)3-9 HOMOLOG 4 (SUVH4), SUVH5 and SUVH6 methyltransferases are responsible for histone H3 lysine di-methylation (H3K9me₂) (Ebbs and Bender 2006; Jackson et al., 2002), and the *suvh4/5/6* triple mutants exhibited extensive depletion of H3K9me₂ (Stroud et al., 2014). Therefore, FISH comparative analyses were applied to the nuclei of *suvh4/5/6* triple mutant to explore whether H3K9me₂ was involved in perinuclear chromatin anchoring. Surprisingly, for all the three pairs of FISH probes, the differential distribution of the red and green probes at the NP was detected as that in WT

nuclei (Figure 19), suggesting that H3K9me2 was dispensable for chromatin anchoring at the NP in plants.

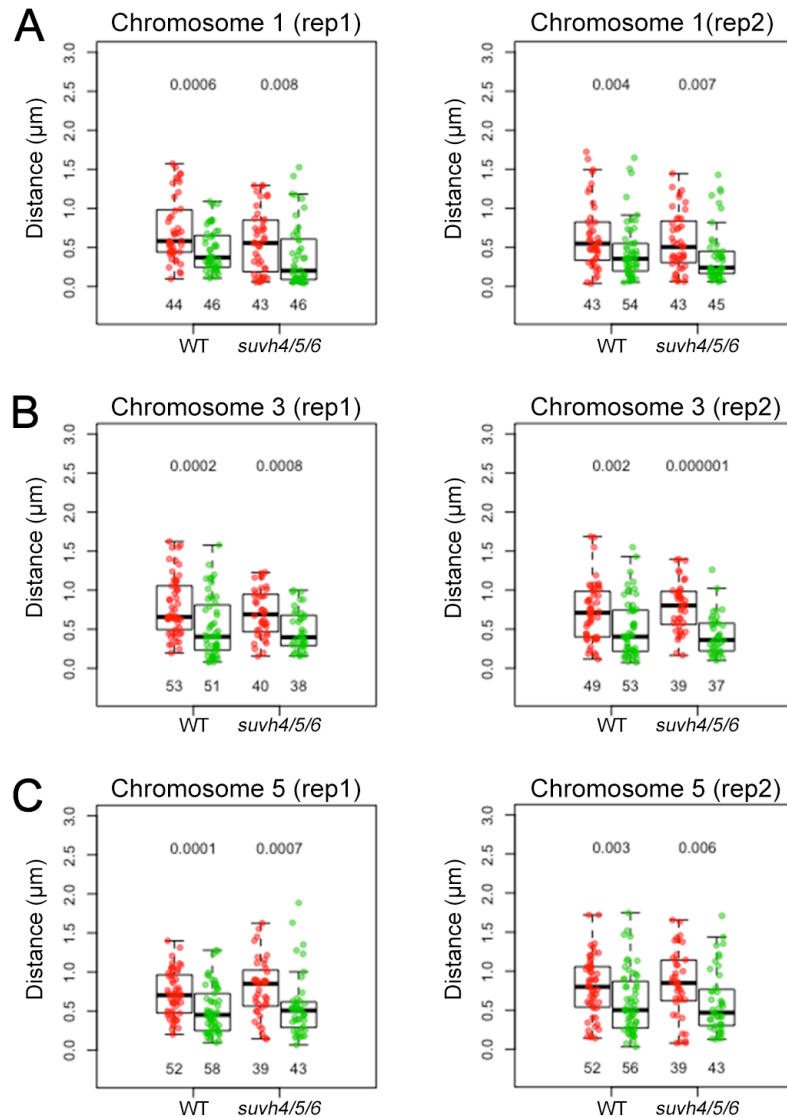


Figure 19. Analyses of FISH signals at in *suvh4/5/6*.

Comparison of the distance of probed genomic regions in chromosome 1 (green 2 vs red 2) (A), 3 (B), and 5 (C) to the NP in 2C nuclei of *suvh4/5/6* mutants. Green and red dots in boxplots denote the distance data of green and red FISH signals, respectively. The number under each boxplot shows the number of the corresponding FISH signals. For each pair of comparison (boxplots of the same genotype), the p value on top indicates result of one-sided Mann-Whitney U test.

3.4 Role of non-CG methylation in specific chromatin positioning at the NP

3.4.1 Non-CG methylation contributes to specific chromatin positioning at the NP

Our NUP1:GFP RE-ChIP results demonstrated that TEs enriched at the NP showed higher levels of cytosine methylation compared with TEs not enriched at the NP (Figure 11). Moreover, in several methylation mutants, analyses of the corresponding methylation types in

the two groups of TEs suggest that CHH DNA methylation of TEs located at the NP tends to be more dependent on RdDM-independent pathway, while TEs located in the nuclear interior rely more on RdDM (Figure 11). This finding motivated us to evaluate whether CHH DNA methylation contributed to positioning chromatin at the NP in plants. In *Arabidopsis*, DRM1 and DRM2 are methyltransferases required for CHH DNA methylation in the RdDM pathway; in contrast, CMT2 is required in RdDM-independent pathway (Zemach et al., 2013; Stroud et al., 2014). Thus, the localization of signals for the selected FISH probes in *cmt2* and *drm1/2* mutants was probed. Intriguingly, it was found that the distance distribution profiles of different probe pairs were variously affected in the *cmt2* mutant (Figure 20). For the FISH probe pairs targeting chromatin in chromosome 1 and chromosome 5, the distance distributions of green and red probes to the NP were significantly different; but for the FISH probe pair targeting chromatin in chromosome 3, the distance distributions of green and red probes toward the NP could not be differentiated (Figure 20). On the contrary, for all the three selected pairs of probes, the distance of green probes to the NP was shorter than that of green probes in *drm1/2* mutants (Figure 20), which is same as that in WT plants.

Next, we asked what would happen to the chromatin localization at the NP if plants lost all CHH DNA methylation. For this purpose, genetic crossing was performed to combine mutations of *CMT2*, *DRM1* and *DRM2*. After generating the triple homozygous of *cmt2 drm1/2*, we performed FISH comparison experiments using the three chosen probe pairs. It turned out that for all the tested FISH probe pairs, the localization distributions of green and red probes could not be differentiated in the triple mutant losing all the CHH DNA methylation (Figure 20).

In parallel, the effect of CHG DNA methylation on specific chromatin positioning at the NP was also evaluated. It has been reported that the CHG DNA methylation is mainly catalyzed through CMT3 methyltransferase in *Arabidopsis* (Stroud et al., 2014). In the nuclei of *cmt3* mutant, the differential location patterns of green and red probes of all the three selected probe pairs were similar to that in WT nuclei (Figure 20). This FISH comparison results indicated that the specific positioning chromatin at the NP was not influenced when plants lost CHG DNA methylation.

At last, we sought to test whether combining CHH and CHG DNA methylation mutations would result in alteration in nuclear localization of FISH signals. Accordingly, *cmt2 cmt3* double mutants and *cmt3 drm1/2* triple mutants were generated. Intriguingly, in the nuclei of

higher-order CHH and CHG DNA methylation mutants (*cmt2 cmt3* and *cmt3 drm1/2*), the different localization patterns of green and red probes of all the three chosen FISH probe pairs at the NP were lost (Figure 20). Altogether, these results suggest that non-CG DNA methylation (CHH and CHG DNA methylation) pathways play redundant roles in tethering chromatin at the NP.

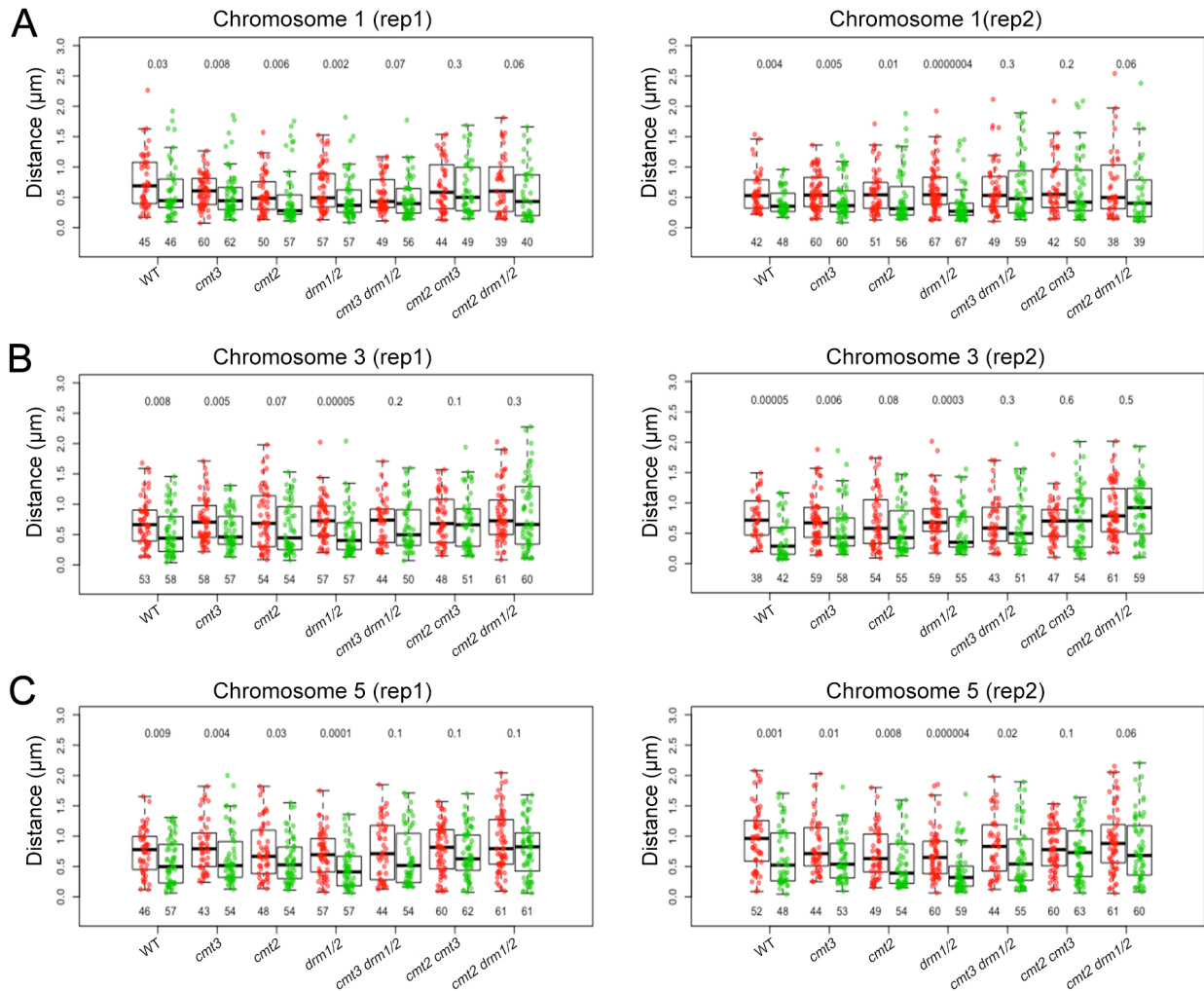


Figure 20. Analyses of FISH signals in *Arabidopsis* mutants losing non-CG methylation.

Comparison of the distance of probed genomic regions in chromosome 1 (green 2 vs red 2) (A), 3 (B), and 5 (C) to the NP in 2C nuclei of mutants losing non-CG methylation. Green and red dots in boxplots denote the distance data of green and red FISH signals, respectively. The number under each boxplot shows the number of the corresponding FISH signals. For each pair of comparison (boxplots of the same genotype), the p value on top indicates result of one-sided Mann-Whitney U test.

3.4.2 CG methylation has no effect on chromatin positioning at the NP

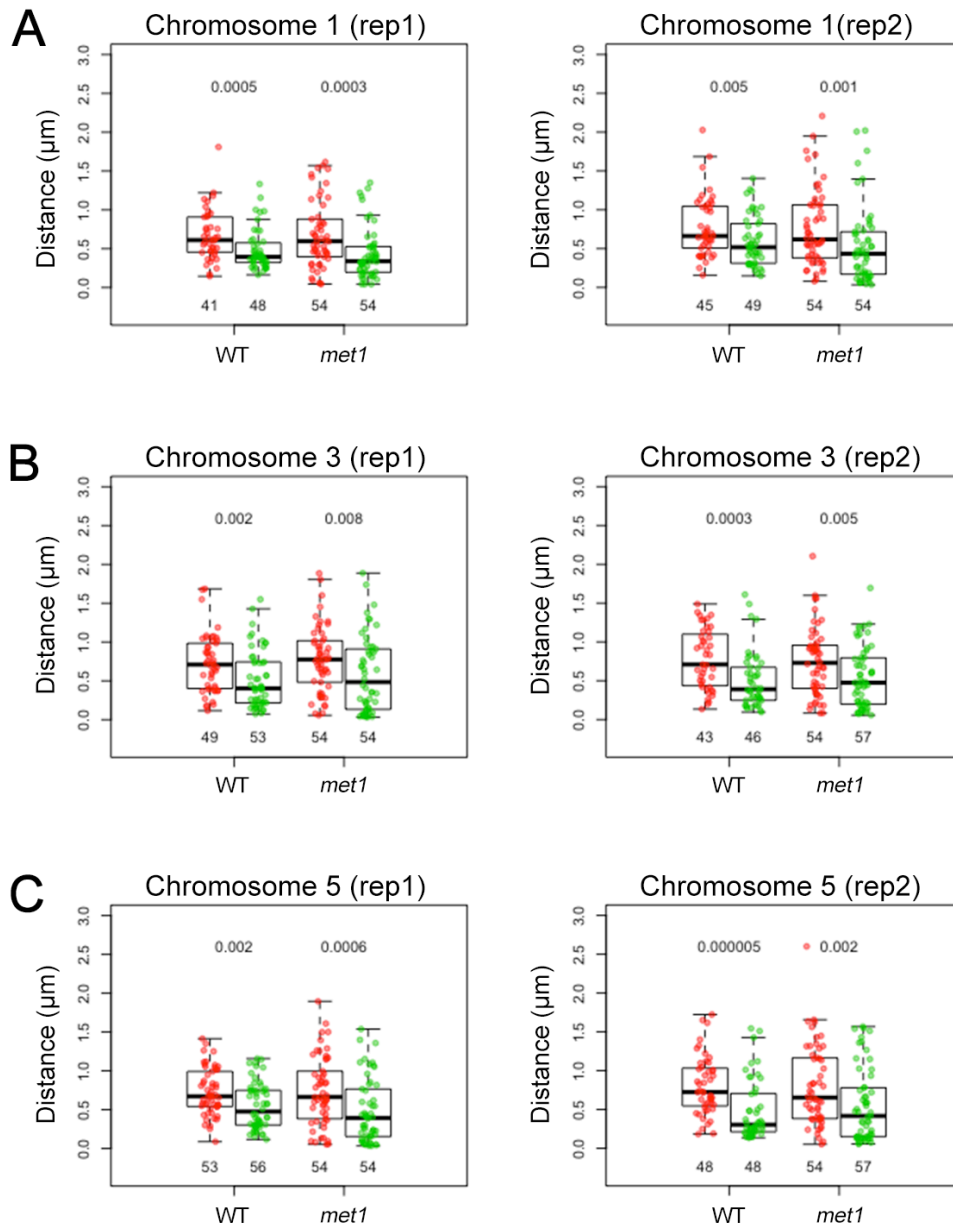


Figure 21. Analyses of FISH signals in *Arabidopsis* mutants losing CG methylation.

Comparison of the distance of probed genomic regions in chromosome 1 (green 2 vs red 2) (A), 3 (B), and 5 (C) to the NP in 2C nuclei of *met1* mutant. Green and red dots in boxplots denote the distance data of green and red FISH signals, respectively. The number under each boxplot shows the number of the corresponding FISH signals. For each pair of comparison (boxplots of the same genotype), the p value on top indicates result of one-sided Mann-Whitney U test.

Next, we questioned whether CG DNA methylation is involved in regulating perinuclear chromatin anchoring. In mammals, DNA methylation mostly occurs at CG sequence context, which is maintained by DNA (cytosine-5) methyltransferase 1 (DNMT1); while CG DNA methylation in plants is maintained *via* methyltransferase 1 (MET1), a homolog of DNMT1 (Stroud et al., 2013). Thus, the distribution of FISH signals at the NP with the

chosen FISH probe pairs were surveyed. Like in WT nuclei, the differential localization patterns of green/red FISH probes at the NP in 2C nuclei of *met1* mutant were found (Figure 21). This result suggests that losing CG DNA methylation has no effect on chromatin positioning at the NP.

3.5 *crwn* mutants lose specific chromatin positioning at a chromosomal scale

It has been suggested by our FISH experiments with FISH probe pairs located on three different chromosomes (chromosome 1, 3, and 5) that CRWN proteins play roles in mediating chromatin anchoring at the NP (Figure 14). A chromosome painting (an extended FISH approach) experiment with probes targeting almost the entire right arm of chromosome 1 was performed to explore how CRWNs regulate chromatin positioning at a chromosomal scale. For this purpose, a 10 Mb genomic region was labeled with tiling BACs (Appendix Table 13), among which the NUP1-enriched chromatin segments were assigned as green probes and the remaining regions as red probes (Figure 22A). As there were so many BACs for each color (green or red) of FISH probes, the green probes were produced in two pools, as well the red probes (Figure 22B).

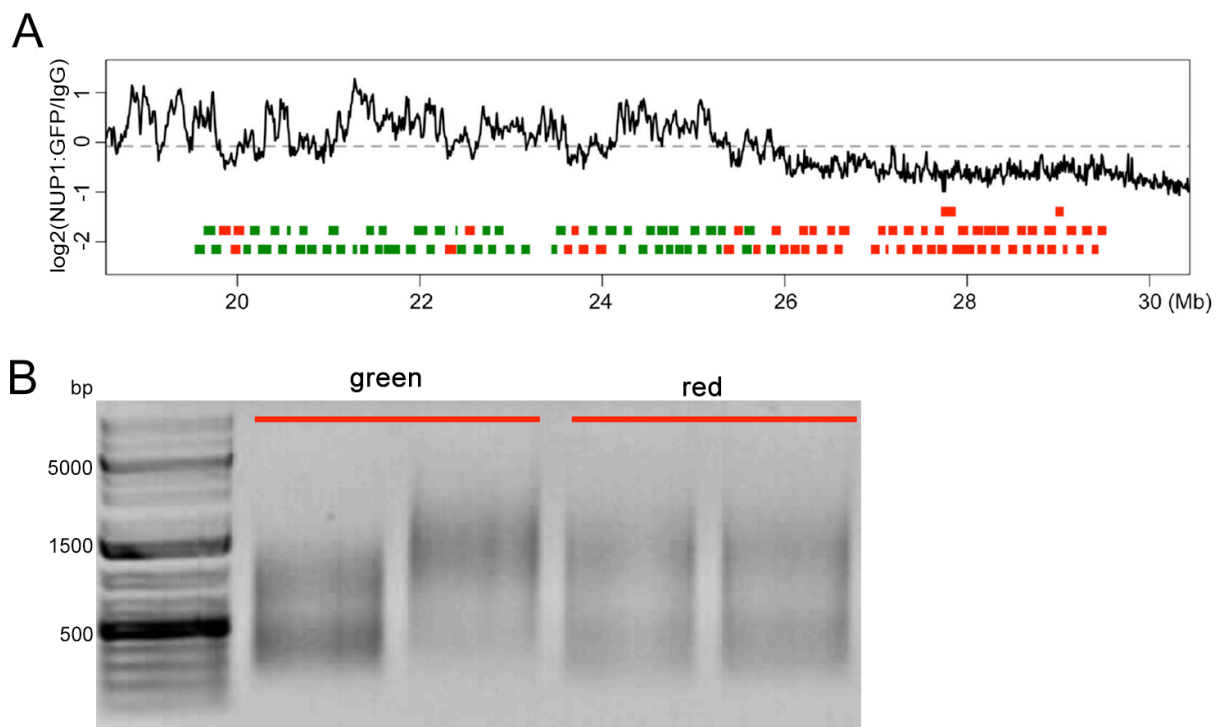


Figure 22. Design and labeling of dual-color FISH probes covering a 10 Mb region in chromosome 1 according to NUP1 RE-ChIP-seq signals.

(A) Green and red rectangles depict BACs. Green probes label chromatin regions exhibiting preferential localization close to the NP (having higher RE-ChIP signals), by contrast, red probes label chromatin regions

showing depleted contacts with NUP1:GFP. (B) Green probes were produced in two pools, as well as red probes. The FISH probes were designed by Dr. Chang Liu and labeled by Bo Hu.

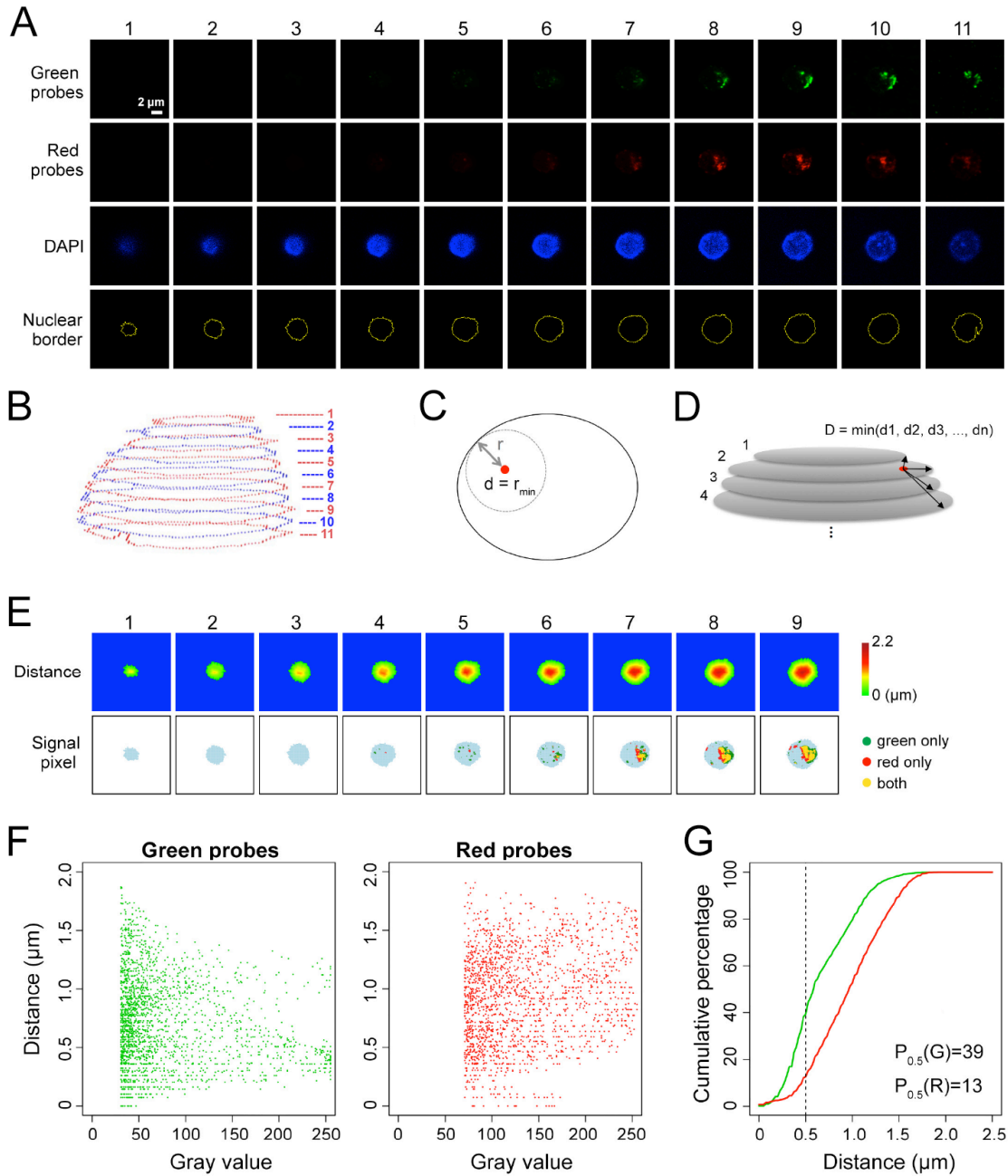


Figure 23. Approximation of chromosome painting data.

(A) Z-stack confocal image files of a WT 2C nucleus (its z-projection image is shown in Figure 24). The bottom row indicates nuclear border of each slice identified from the corresponding DAPI image. (B) Reconstructed nucleus. The bottom two slices (slice no. 10 and 11), which are close to the glass slide, are not included for further analyses. (C, D) Computing the distance to the NP. (C) Within an optical slice, the distance of a given point (red) to the nuclear border. (D) The distances of this point to the nuclear borders in other optical slices are calculated as well. At the end, the minimum value is defined as the distance of this point to the NP. (E) Processed confocal images showing the distance of each pixel to the NP (top row) and pixels with FISH signal (bottom row). (F) Relationship between FISH signal strength and distance to the NP. (G) Comparison of cumulative green and red FISH signals as a function of distance to the NP. With a distance cutoff of 0.5 μm , for

the analyzed optical slides in this nucleus, 39% and 13% of green and red signal is located at the NP, respectively. Bo Hu contributed to the design of the chromosome painting and image processing pipeline.

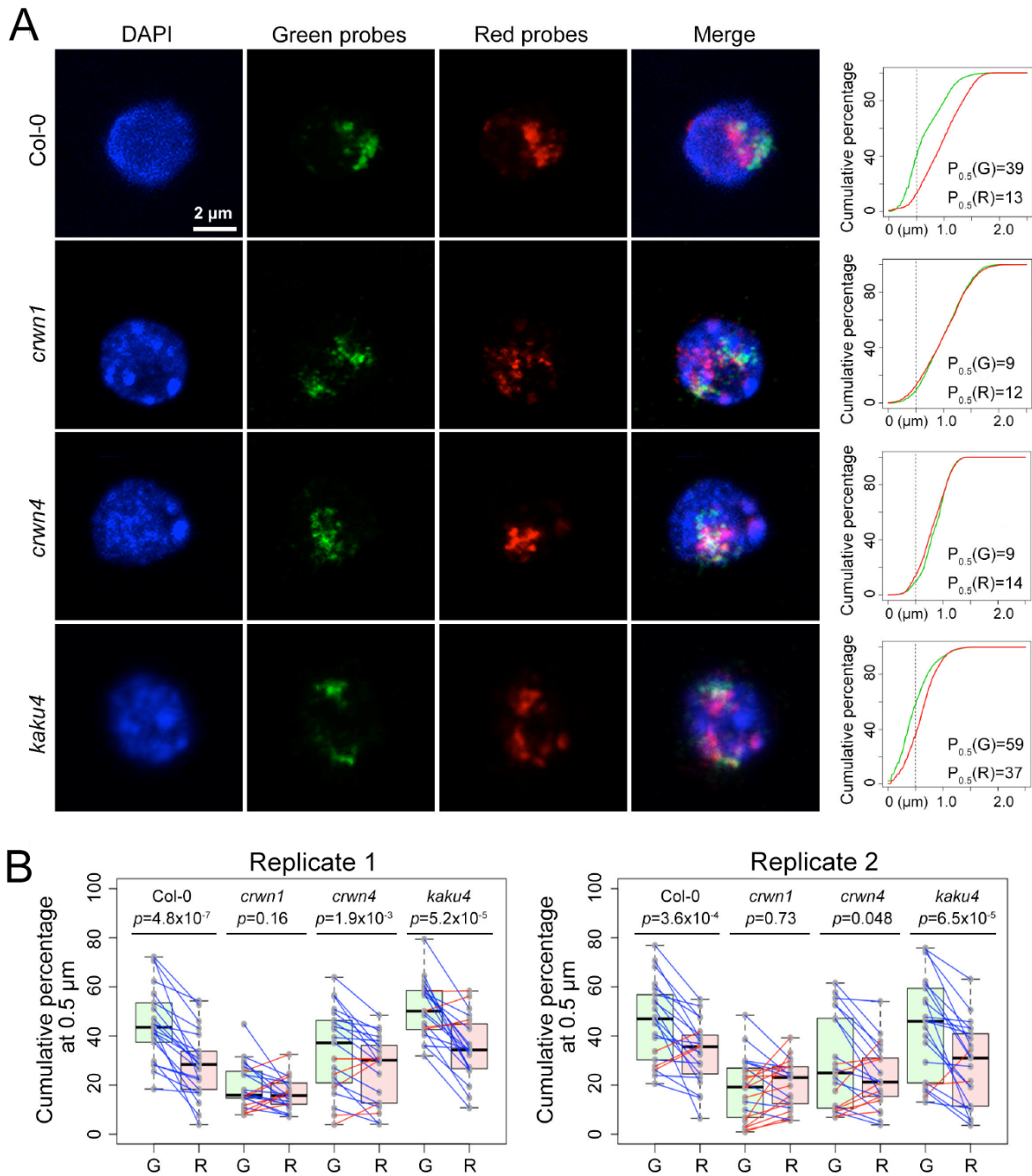


Figure 24. Deficiency of *crwn* mutants in specific chromatin positioning at the NP revealed by chromosome painting.

(A) Representative confocal images of 2C nuclei from WT and mutants. The plots on the right side show cumulative chromosome painting signal to indicate the distance to the NP. $P_{0.5}$ denotes the percentage of FISH signals detected within 0.5 μm from the NP. (B) Comparison of chromosome painting signals ($P_{0.5}$) in different plants. The $P_{0.5}$ values of green and red probes of every individual nucleus are connected by a blue or red line, indicating whether $P_{0.5}$ (green) is significantly higher or not, respectively. G or R, green and red probes as donated in (Figure 22A), respectively. p values indicate results of Wilcoxon signed-rank tests. Bo Hu contributed to the design of the chromosome painting and the pipeline of image processing.

For every individual nucleus, distance of probe signals to the NP was calculated (Figure 23 and Figure 24A). We arbitrarily chose $P_{0.5}$, which was defined as the percentage of FISH signals localized within 0.5 μm from the NP, as a cutoff to compare how green and red probes might be differentially positioned in each nucleus. In 2C nuclei of WT plants, the $P_{0.5}$ values of the green probes were significantly higher than those of the red probes (Figure 24B). It was interesting that a few WT nuclei exhibited an opposite pattern (Figure 24B, right panel). This cell-to-cell variation is in line with our former FISH comparative results which implies a scenario similar to that in mammals in which LADs are not identical throughout a cell population as they are reshuffled upon mitosis (Kind et al., 2013; Kind et al., 2015). Both *crwn1* and *crwn4* nuclei lost differential probe localization patterns to certain extents; while in *crwn1* nuclei, the localization of green and red probes could be no longer differentiated (Figure 24B), implying that these CRWN1 protein is the major CRWN proteins required for tethering chromatin at the NP. By contrast, in the *kaku4* nuclei, which show similar nuclear size and morphology alterations to those of the *crwns*, the differential localization of green and red probes at the NP was not affected, implying that different plant lamin proteins play diverse roles in mediating chromatin localization (Figure 24B).

3.6 Exploration of CRWN1-chromatin interactions

3.6.1 A native *CRWN1* tagging construct can fully rescue *crwn1* phenotypes

Having shown that the functional association of CRWN1 in nuclear peripheral chromatin anchoring, we would like to know if CRWN1 interacts with chromatin directly. Thus, we sought to generate native *CRWN1* tagging lines. To minimize the impact of the fusion of a tandem HA tag (2HA) on CRWN1, structural motifs from the amino acid sequence of CRWN1 were predicted. As CRWN1 is localized at the INM (Sakamoto and Takagi 2013; Dittmer et al., 2007), we analyzed the presence of nuclear import regions in the CRWN1 protein by a bioinformatics tool (open source software cNLS Mapper). The cNLS Mapper result showed that CRWN1 possessed two putative nuclear localization signals (NLSs), EMRKRKLESD and NGRKRGRVGSL, starting from positions 612 and 957, respectively (Figure 25A). Until now, all the identified plant lamin candidates including CRWNs have multiple coiled-coil domains, which can form filamentous dimers and play roles in controlling nuclear size, shape, and heterochromatin organization (Pawar et al., 2016; Sakamoto and Takagi 2013; Dittmer et al., 2007; Goto et al., 2014; Wang et al., 2013). The positions of coiled-coil domains of CRWN1 were predicted using COILS server (with window width 14,

21, and 28), which suggested that the coiled-coil regions were located between amino acid 70-612, and 621-750 (Figure 25B). According to results of cNLS Mapper and sequence predication of coiled-coils, a schematic representation of the full-length CRWN1 was depicted, with the red color and yellow color labeled the regions where coiled-coil domains and NLS were presented, respectively (Figure 25C). Thus, we planned to add the tandem HA tag to the unannotated regions (labeled in blue in Figure 25C), by which it was proposed to cause minimum structural perturbations to CRWN1 protein. In total, three versions of CRWN1:2HA fusion proteins were designed, in which the 2HA was added to the N-terminal, the C-terminal, and the 780th amino acid of CRWN1, respectively (Figure 25). A 1.7 kb upstream of the *CRWN1* locus was defined as the promoter of native *CRWN1:2HA* constructs. In addition, a 0.6 kb fragment of the *CRWN1*'s downstream was included in these constructs. In total, we designed three native *CRWN1:2HA* constructs: *pCRWN1::2HA_CRWN1*, *pCRWN1::CRWN1_2HA*, and *pCRWN1::CRWN1_780_2HA*, which were driven by the same promoter region with different HA tag insertion locations (Figure 26A). These three constructs were transformed into *crwn1* mutants by floral dip.

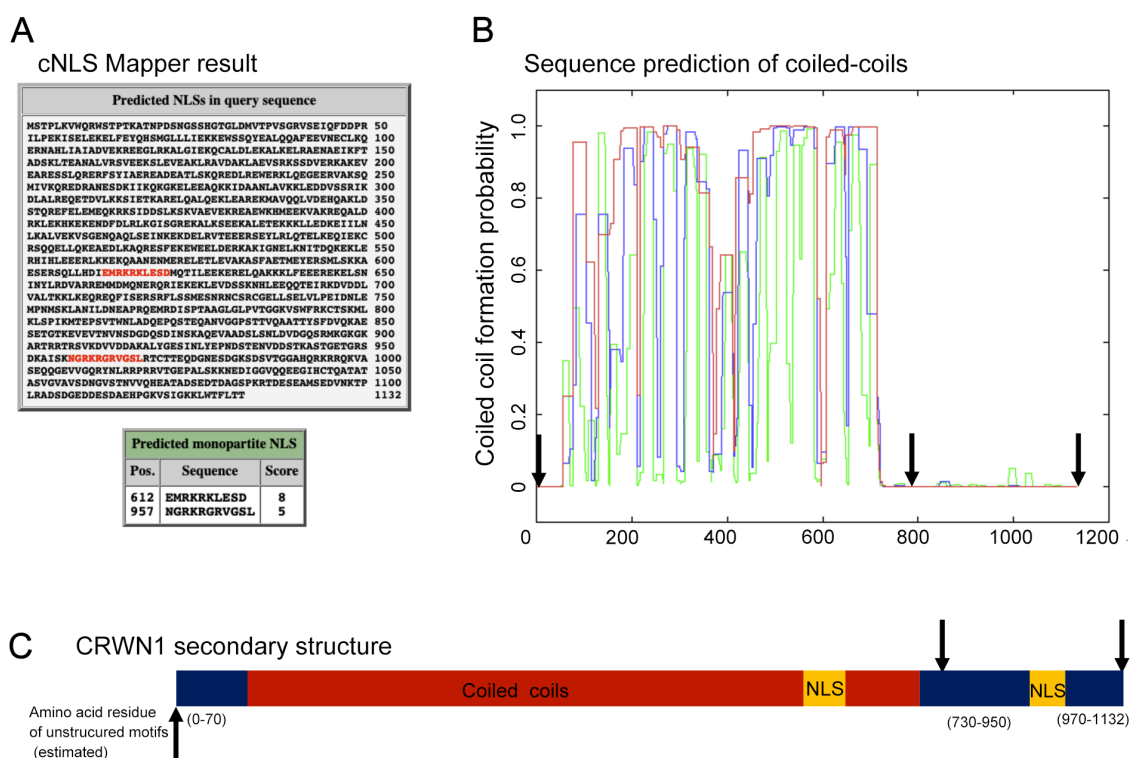


Figure 25. Prediction of structural motifs from the CRWN1 sequence.

(A) cNLS Mapper result of CRWN1 showing putative NLS sequences with a score equal or more than the selected cutoff score 5. Higher scores indicate stronger NLS activities. cNLS Mapper result was predicated by the cNLS Mapper server (http://nls-mapper.iab.keio.ac.jp/cgi-bin/NLS_Mapper_form.cgi). (B) Prediction of coiled-coil domains from the amino acid sequence of CRWN1 with the COILS server (<https://embnet.vital->

it.ch/software/COILS_form.html). Coiled-coil formation probability is plotted versus the residue number of CRWN1. Predictions using window width of 14 (green), 21 (blue) and 28 (red) are shown. Note that no coiled-coils are predicted in the N-terminal region, the C-terminal region, or the region around 800th amino acid. (C) Schematic representation of full-length CRWN1. The predicted coiled-coil regions are in red, NLS regions are in yellow, whereas the predicted unstructured regions are in blue. Black arrowheads (in B and C) point to sites where the HA tag can be inserted.

Even though *crwn1* nuclei with different endopolyploidy levels showed significant differences in nuclear morphology (Figure 17 and Figure 18), only those with higher endopolyploidy levels display conspicuous changes in nuclear size and shape. Thus, for the ease of comparison, morphology of 8C nuclei from WT, *crwn1* and *CRWN1* tagging lines was examined. The morphology comparison of 8C nuclei between WT, *crwn1*, and two lines of each type of *CRWN1* tagging lines indicated that the phenotype of small and spherical nuclei in *crwn1* could not be rescued at all by *pCRWN1::CRWN1:2HA* (Figure 26B), but it could be partially rescued by *pCRWN1::2HA_CRWN1* (Figure 26C). On the other hand, the nuclear morphology phenotypes could be fully rescued by *pCRWN1::CRWN1_780_2HA* (Figure 26D). Therefore, the *pCRWN1::CRWN1_780_2HA crwn1* lines were used to do further analyses.

To ensure that our tagging lines were in the *crwn1* homozygous background, genotyping was performed with primers CRWN1-seq-F3 and CRWN1-R1, confirming that these tagging lines were homozygous background of *crwn1* (Figure 27).

As described in the previous part, FISH comparative experiments indicated that specific chromatin positioning at the NP was lost in *crwn1* 2C nuclei, we asked whether this phenotype could be rescued in the *pCRWN1::CRWN1_780_2HA crwn1* tagging line, which showed full rescue of nuclear morphology phenotypes of *crwn1*. Thus, FISH comparative experiments were subsequently performed to examine the perinuclear distribution of green/red probes in this tagging line. The results indicated that the differential distribution patterns of green and red probes of the three selected pairs were detected in the 2C nuclei of *CRWN1:2HA* tagging line (Figure 28), suggesting that the loss of specific chromatin positioning at the NP in *crwn1* could be rescued by the construct *pCRWN1::CRWN1_780_2HA*. In short, the native *pCRWN1::CRWN1_780_2HA* tagging construct can fully rescue *crwn1* phenotypes (Figure 26 and Figure 28).

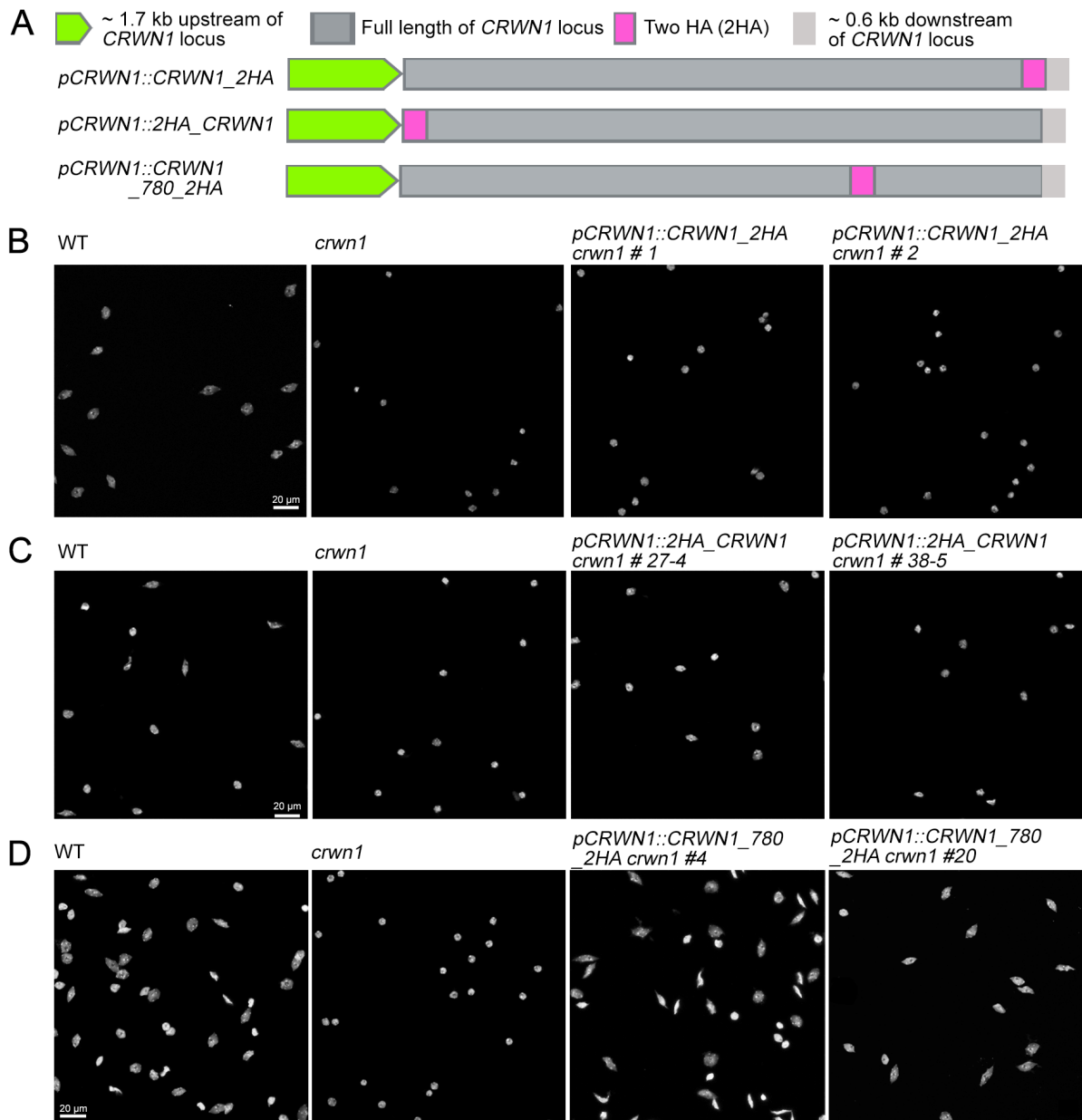


Figure 26. A native *CRWN1* tagging construct can rescue the nuclear phenotype of *crwn1*.

(A) Design of native *CRWN1* tagging constructs. The green pentagon represents the 1.7 kb upstream of *CRWN1*, which is used as the promoter of the constructs. In addition, a 0.6 kb downstream (the light grey rectangle) of *CRWN1* was included in these constructs. The dark grey rectangle represents the full length of *CRWN1* locus, the light purple rectangle represents the 2HA. In the construct of *pCRWN1::CRWN1_2HA*, the 2HA is inserted at the C-terminal region of *CRWN1*. In the middle, the 2HA is inserted at the N-terminal of *CRWN1* in the *pCRWN1::2HA_CRWN1* expression construct. For the *pCRWN1::CRWN1_780_2HA* construct, which is displayed at the bottom, the 2HA is placed after the 780th amino residue of the *CRWN1* protein. (B) Morphology comparison of 8C nuclei of WT, *crwn1*, two lines of *pCRWN1::CRWN1_2HA crwn1* plants. (C) Morphology comparison of 8C nuclei of WT, *crwn1*, two lines of *pCRWN1::2HA_CRWN1 crwn1* plants. (D) Morphology comparison of 8C nuclei of WT, *crwn1*, two lines of *pCRWN1::CRWN1_780_2HA crwn1* plants. The nuclei in (B), (C), and (D) were isolated from the first true leaf of 2-week old seedlings. Scale bars: 20 μ m.

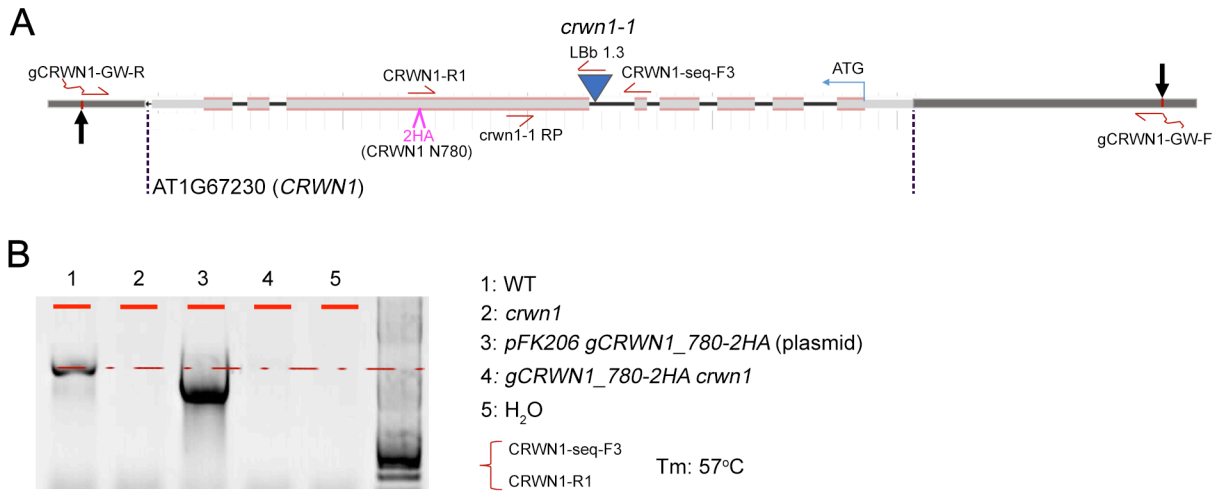


Figure 27. CRWN1 gene model and genotyping of CRWN1 tagging line.

(A) Gene model of *CRWN1* including the position of the T-DNA insertion, and the definition of *pCRWN1::CRWN1_780_2HA* construct. Exons and introns are indicated by light grey bars wrapped with light red lines and black lines, respectively. 5'- and 3'-UTR regions are represented by light grey bars. The T-DNA insertion is demonstrated by blue triangle. The grey bars depict the upstream and downstream regions of *CRWN1* locus. The light blue bent-up arrow indicates the ATG of *CRWN1*. The light purple check mark points to the site where the HA tag is inserted. The black arrows point to the start and end points of the *pCRWN1::CRWN1_780_2HA* construct. (B) Genotyping of the *CRWN1* tagging line was done with primer pair CRWN1-seq-F3 and CRWN1-R1. CRWN1-R1 matches the genomic region where the 2HA is inserted, leading to that this primer pair can only amplify the region of the endogenous *CRWN1* locus without T-DNA insertion.

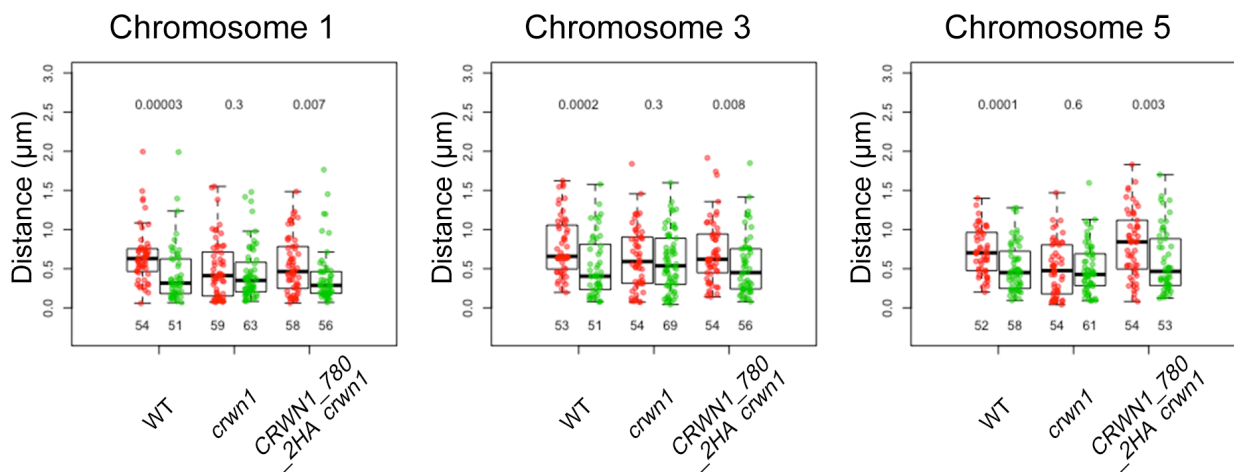


Figure 28. Distance distribution of probed genomic regions to the NP in the 2C nuclei of CRWN1 tagging lines.

Probes used here are located on chromosome 1 (green2 vs red2), 3, and 5, respectively. Green and red dots in boxplots denote the distance data of green and red FISH signals, respectively. *pCRWN1::CRWN1:2HA crwn1* tagging line #21 was used to conduct this FISH comparative analyses. The number under each boxplot shows the number of the corresponding FISH signals. For each pair of comparison (boxplots of the same genotype), the p value on top indicates result of one-sided Mann-Whitney U test.

3.6.2 CRWN1 directly interacts with chromatin at the NP

Having generated *CRWN1:2HA* tagging line successfully, the distribution of CRWN1:2HA proteins within nuclei was detected. As expected, immunohistostaining result demonstrated that CRWN1:2HA proteins were dominantly found at the periphery of nuclei (Figure 29). Subsequently, regular ChIP experiment using anti-HA antibody was performed to verify direct CRWN1-chromatin interactions. Before conventional ChIP experiment, a western blot assay was conducted to probe whether or not the expressed CRWN1:2HA fusion proteins could be captured by the anti-HA antibody. The western blot with anti-HA antibody successfully detected the CRWN1:2HA protein (Figure 30), indicating that the 2HA in the CRWN1:2HA fusion protein is specific to the anti-HA antibody.

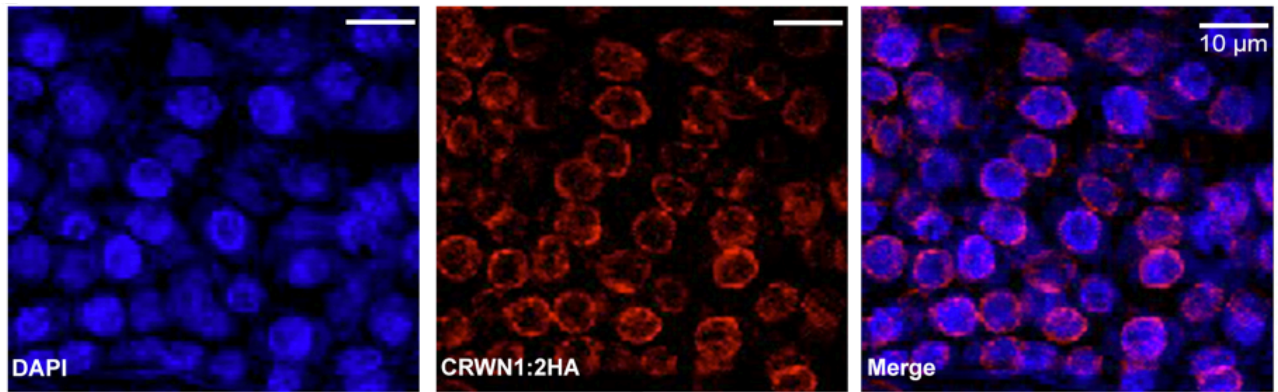


Figure 29. Distribution of CRWN1:2HA at the NP.

Immunohistostaining of a leaf section of *pCRWN1::CRWN1_780_2HA crwn1* plant with the anti-HA antibody. The immunohistostaining was done by the Dr. Nan Wang in our group.

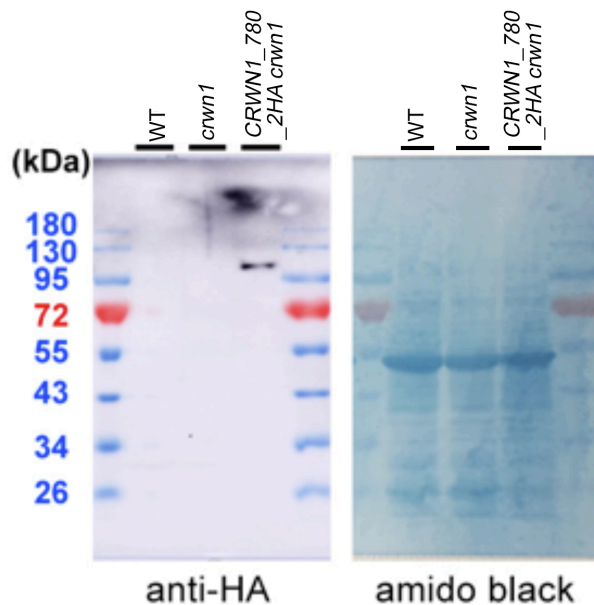


Figure 30. Expression of CRWN1:2HA in *crwn1* leaves.

The CRWN1:2HA protein in leaf crude extract was detected by anti-HA antibody. This western blot was done by Ezgi Süheyla Karaaslan in our group.

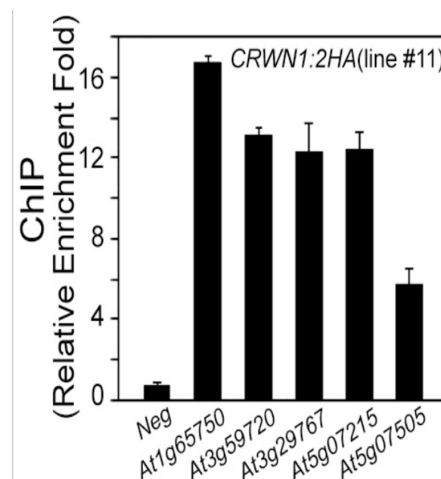


Figure 31. Chromatin regions targeting green FISH probes are enriched by CRWN1:2HA ChIP. Three independent qPCRs of DNA captured by CRWN1:2HA ChIP. The ChIP was done by Dr. Nan Wang in our group.

A ChIP experiment using the anti-HA antibody was performed on our *CRWN1:2HA* tagging lines. Before preparing the sequencing library, qPCRs were done to explore whether chromatin regions targeted by green FISH probes were enriched in DNA captured by CRWN1:2HA ChIP. The results of CRWN1:2HA ChIP qPCR showed enrichment of chromatin regions covered by green FISH probes (Figure 31), suggesting that CRWN1 directly associates with these chromatin regions at the NP. Next, genome-wide patterns of CRWN1-chromatin contacts at the NP were analyzed by ChIP-seq, which led to the identification of many chromatin domains showing direct contacts with CRWN1 at the NP (Figure 32). These regions were named plant lamin-associated domains (PLADs). These PLADs largely overlapped with NUP1-enriched chromatin domains that were identified previously (Figure 32).

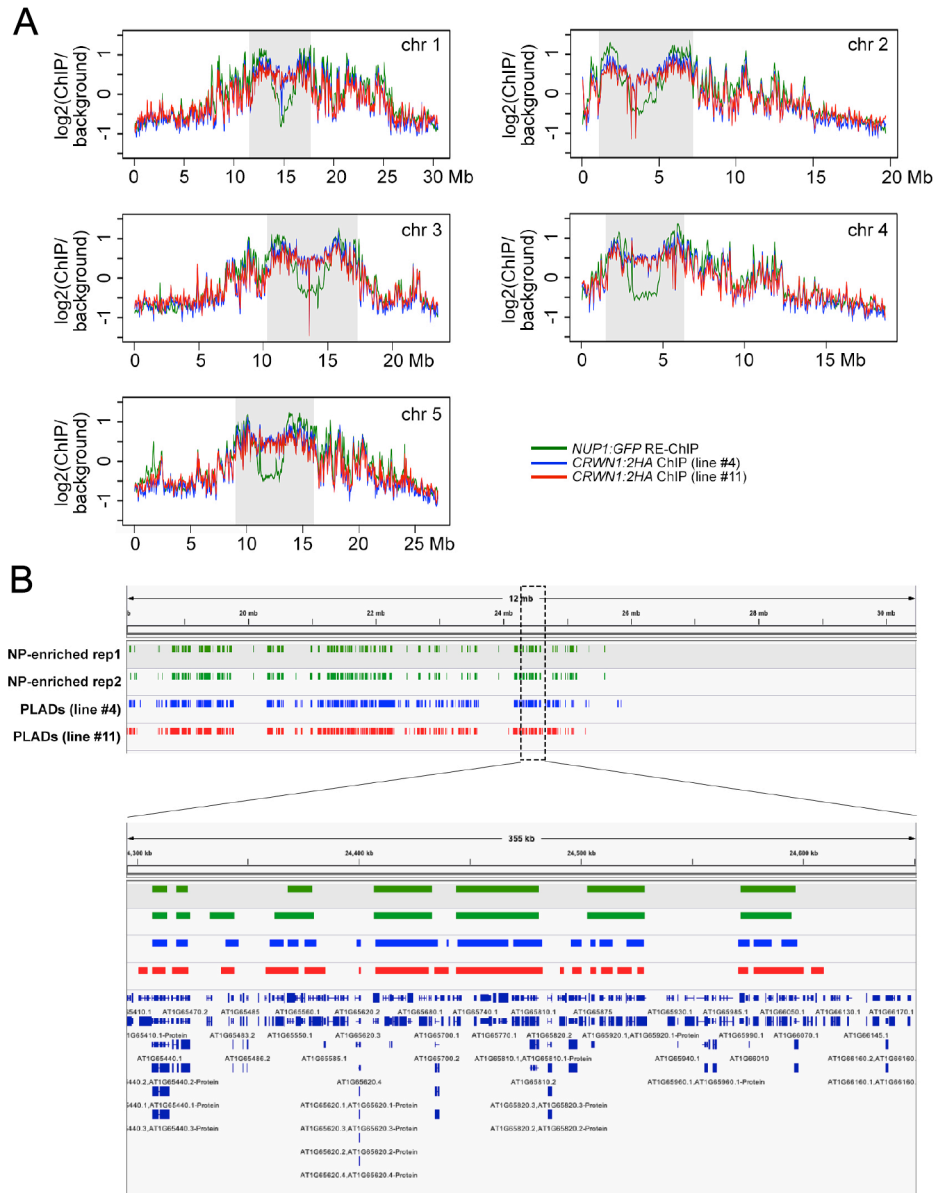


Figure 32. Comparison of NP-chromatin interaction patterns revealed from different ChIP methods.

(A) Genome-wide view of NUP1:GFP RE-ChIP and CRWN1:2HA ChIP signals. The plots are in 50-kb windows. Grey blocks depict the heterochromatin located at centromeric and pericentromeric regions. (B) A representative genomic region from chromosome 1. ChIP-seq and analyses were done by Dr. Liu.

3.7 Characterization of *crwn1* mutants under different treatments

It has been shown that plant lamin-like proteins (CRWN1 and/or CRWN4) have function on regulating chromatin anchoring at the NP, in which CRWN1 is the major determinant (Figure 14 and Figure 24) and CRWN1 interacts directly with chromatin at the NP (Figure 31 and Figure 32). We sought to examine the morphological response of *crwn1* mutant under stresses to question the possible physiological functions of the CRWN1-chromatin interactions in plants. As KAKU4, another plant lamin candidate, is required for maintaining nuclear size

and shape but not involving in specific chromatin organization at the NP. *kaku4* mutant was selected as a control to test whether changes in nuclear morphology played roles in plant physiological response to various stress conditions.

Cells in plants and animals are constantly exposed to a spectrum of mechanical cues, such as shear stress, compression, differential tissue rigidity, and strain. Cells adapt to these mechanical forces by engaging mechanisms of mechanotransduction (Miroshnikova et al., 2017). However, the mechanical cues reach far beyond the plasma membrane and the cytoskeleton, and are transmitted directly to the nucleus (Miroshnikova et al., 2017). Thus, the nucleus needs to have the capacity to sense and respond rapidly to changes in mechanical forces. It has been reported that the mechanical stress responses happen at the nuclear lamina-chromatin interface in animals (summarized in (Miroshnikova et al., 2017)). Therefore, we sought to test the morphological response of *crwn1* mutant to salt stress, which leads to not only ion toxicity but also mechanical stress to the plant root cells (then the mechanical stress could be transduced to the nuclei of root cells).

All cells, whether post-mitotic or proliferating, are frequently challenged by DNA damage events, and damage commonly happens irrespective of the underlying sequence. Damage can be induced by exogenous agents (e.g., radiation, radiomimetic cancer drugs, or toxins) as well as endogenous activities (e.g., free radicals arising from cell metabolism or replication errors) (Hauer and Gasser 2017). A recent study has implied that CRWN-family proteins are involved in quenching ROS accumulation and show a protective role in DNA from oxidative damage (Wang et al., 2018b).

3.7.1 Morphological response of *crwn1* to hydrogen oxide

Recently, a report showed that *crwn* double mutants (i.e. *crwn1/3*, *crwn2/3*, *crwn2/4*) over-accumulated reactive oxygen species (ROS) under normal growth conditions and 0.01% genotoxic agent methyl methanesulfonate treatment with more severe DNA damage compared with WT plants, suggesting that the CRWN-family proteins have function on consuming ROS accumulation and protecting genomic DNA against extreme oxidative damage (Wang et al., 2018b). Therefore, the growth of *crwn1* mutants in response to various concentrations of hydrogen oxide (H₂O₂) treatments was examined. It was found that for all tested genotypes (WT, *crwn1*, and *kaku4*), high concentrations of H₂O₂ (1.0 mM and 5.0 mM H₂O₂) reduced the global growth of all the three genotypes of *Arabidopsis* plants to a similar extent (Figure 33A). In contrast, a slight increase in the global growth was observed when all

the three genotypes were grown in plates supplied with a low concentration of H_2O_2 (0.5 mM H_2O_2), with a little higher increase in vegetative growth of *crwn1* compared with WT plants (Figure 33). When we compared the root length of WT, *crwn1* and *kaku4* plants, we observed that high concentrations of H_2O_2 (1.0 mM and 5.0 mM H_2O_2) suppressed root growth in these plants (Figure 33B). Specially, plants exhibited almost no growth after transferring to the medium containing 5.0 mM H_2O_2 (Figure 33). Only under 0.5 mM H_2O_2 treatment, a slightly higher increase in root growth of *crwn1* plants was found compared with that of WT plants (Figure 33B). Altogether, these results indicate that the loss of CRWN1 almost has no additive negative impact on the vegetative growth under high H_2O_2 treatments, implying that CRWN1 does not play a role in inhibiting the consumption of H_2O_2 .

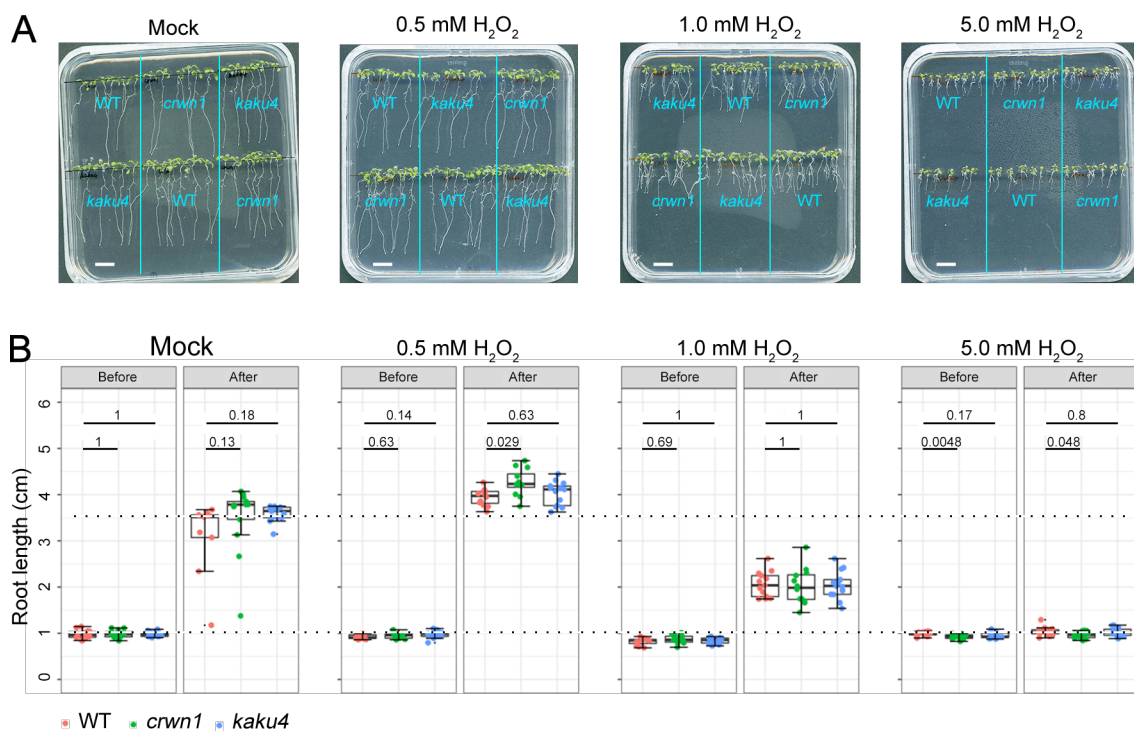


Figure 33. Phenotypes of WT, *crwn1* and *kaku4* seedlings under H_2O_2 stress.

(A) Seedlings of WT, *crwn1* and *kaku4* under H_2O_2 stress. WT, *crwn1* and *kaku4* plants were grown in 1/2 MS media plates vertically for 5 days, then were transferred to 1/2 MS medium supplied with or without H_2O_2 (mock) to further grow for another 5 days. The seedlings were photographed after treatments. Scale bars: 1cm. (B) Comparison of root length of WT, *crwn1* and *kaku4* under H_2O_2 stress. The root length was measured before and after the treatment. The bottom and upper dot lines marked the root length of the WT plants under normal conditions on the fifth and tenth day. Significant analyses were done by Mann-Whitney U test.

3.7.2 Morphological response of *crwn1* to salt stress

Salinity has a critical effect on crop growth in many parts of arid and semi-arid regions in the world. It also has a negative impact on the growth and development of many plant species. Plant growth is adversely affected by salinity, which results from ion toxicity because of high

concentrations of certain ions, reducing plant's capacity of water uptake (Park et al., 2016). In agriculture, sodium ions are accumulated in the soil during water supplying from irrigation systems, even though the low concentration in irrigation water (Park et al., 2016). Therefore, we characterized the phenotypes of WT, *crwn1* and *kaku4* plants under NaCl treatments. As expected, high concentrations of NaCl (100 mM and 150 mM NaCl) adversely suppressed the growth of whole seedlings including root elongation, while the effects in WT, *crwn1* and *kaku4* plants were at the same level (Figure 34). Thus, knockout of *CRWN1* has no additive effect on vegetative growth under NaCl treatments compared with WT plants, suggesting that *CRWN1* has no function on plants' adaptation to salinity stress caused by NaCl.

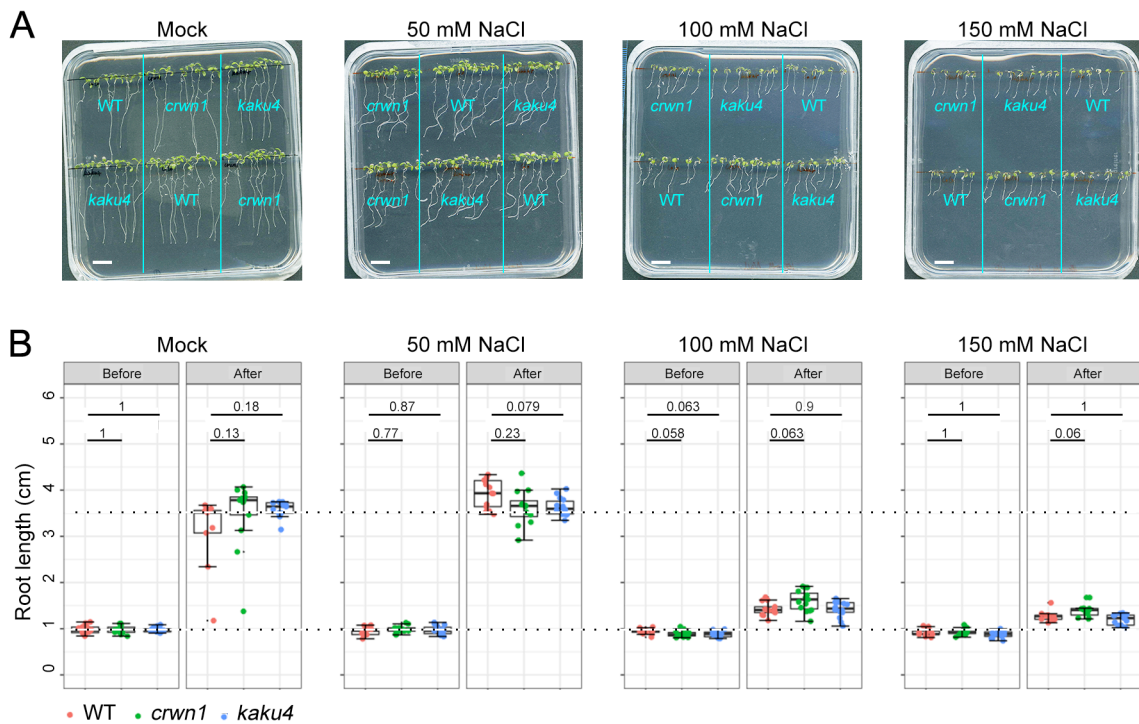


Figure 34. Sensitivity of WT, *crwn1* and *kaku4* seedlings to NaCl.

(A) Seedlings of WT, *crwn1* and *kaku4* under NaCl treatments. The growth of plants and the application of different concentrations of NaCl to plants were as the same as plants in Figure 33A. Scale bars: 1 cm. (B) Comparison of root length of WT, *crwn1* and *kaku4* under NaCl treatments. The root length was measured before and after treatment. The bottom and upper dot lines marked the root length of the WT plants under normal conditions on the fifth and tenth day. Significant analyses were done by Mann-Whitney U test.

3.7.3 Morphological response of *crwn1* to inorganic nitrogen

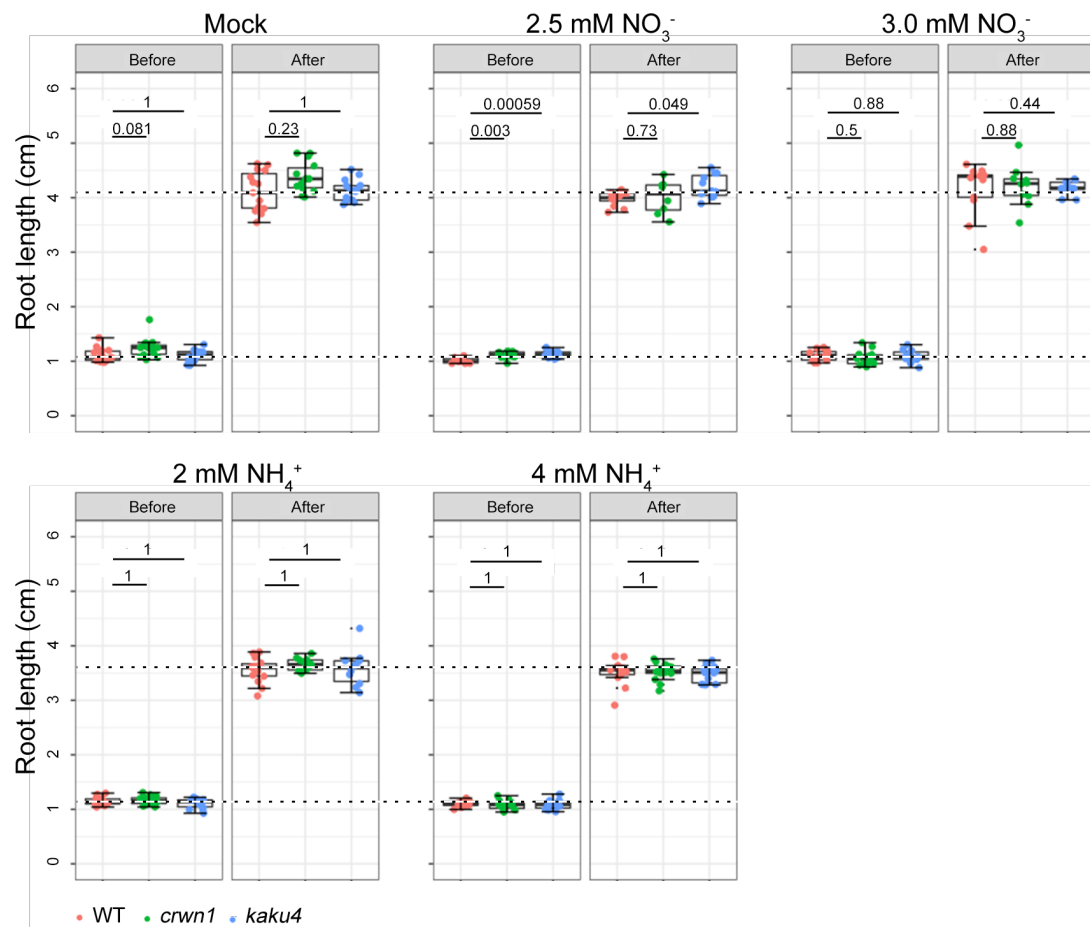


Figure 35. Sensitivity of WT, *crwn1* and *kaku4* seedlings to NO_3^- or NH_4^+ .

Comparison of root length of WT, *crwn1* and *kaku4* under treatments of NO_3^- or NH_4^+ . The growth of plants and the application of different concentrations of NO_3^- or NH_4^+ to plants were as the same as plants in Figure 33A. Scale bars: 1 cm. The root length was measured before and after treatment. The bottom and upper dot lines marked the root length of the WT plants under normal conditions on the fifth and tenth day. Significant analyses were done by Mann-Whitney U test.

Plant growth is fundamentally dependent on exogenous inorganic nitrogen (N), and intensive agriculture is required the usage of N compounds to replenish the natural supply from the soil. NH_4^+ , together with NO_3^- , are the two main forms of N available for plants (Sarasketa et al., 2014). Even though plants have different N source preferences, they depend not only on their genetic background but also on various environmental factors, including soil pH, temperature, ect. It has been concluded that non-bred plants preferentially take up NH_4^+ (Sarasketa et al., 2014). Additionally, crop species have a preference for absorbing NO_3^- nutrition, but in conditions of NO_3^- deficiency in the soil, plants take up N as NH_4^+ (M'rah Helali et al., 2010; Sarasketa et al., 2014). However, when only N source was used, NH_4^+ toxicity might be induced (M'rah Helali et al., 2010). *Arabidopsis thaliana* is one kind of species which is

sensitive to NH_4^+ (M'rah Helali et al., 2010; Sarasketa et al., 2014). In most of the studies with regard to NH_4^+ toxicity in *Arabidopsis*, plants fed with NO_3^- versus plants fed with a combined nutrition of NO_3^- supplemented with different concentrations of NH_4^+ were compared (Sarasketa et al., 2014). While studies focusing on only a sole N source in *Arabidopsis* are scarce (Sarasketa et al., 2014). Based on these studies, concentrations of NH_4^+ and NO_3^- were decided for our nitrogen treatments. Then treatments with different concentrations of NH_4^+ or NO_3^- were applied to WT, *crwn1* and *kaku4* *Arabidopsis* plants, and the performance of these plants was examined. Interestingly, we did not observe any difference between *crwn1*, *kaku4* and WT plants grown in the medium supplied with NH_4^+ or NO_3^- (Figure 35). The concentrations of NH_4^+ and NO_3^- used in this study were higher than the highest sole nitrogen source used in Helali's study, in which the growth of *Arabidopsis* plants was not affected by 2.5 mM NO_3^- treatment but was negatively affected by 2.5 mM NH_4^+ treatment (M'rah Helali et al., 2010). Nevertheless, these results suggest that CRWN1 does not function on plant's response to the NH_4^+ or NO_3^- .

3.7.4 Morphological response of *crwn1* to zeocin treatment

As a radiomimetic chemical, zeocin has been widely used as an inducer of DNA double-strand breaks (DSB) in many studies (Chankova et al., 2007; Adachi et al., 2011; Jia et al., 2016; Sakamoto et al., 2011). It has been known that the DSB caused by zeocin could lead to cell death or result in structural chromosome aberrations and micronuclei (Chankova et al., 2007). Furthermore, the genome integrity would be threatened by such DSB (Adachi et al., 2011). Therefore, we attempted to explore whether CRWN1 plays roles in defense mechanisms to the DSB caused by zeocin. To this end, the *crwn1*, *kaku4* and WT plants were transferred to 1/2 MS medium plates supplied with different concentrations of zeocin after growing on normal 1/2 MS medium for five days. When seedlings were transferred to 10 μM zeocin plates, the vegetative growth of the whole seedlings was found to be severely arrested (Figure 36). To a less extent, exposing to 2 μM of zeocin also adversely affected the growth of the WT, *crwn1* and *kaku4* seedlings (Figure 36). Nonetheless, no difference was observed between *crwn1*, *kaku4* and WT plants (Figure 36), indicating that CRWN1 is not involved in the defense mechanisms of the stress caused by zeocin.

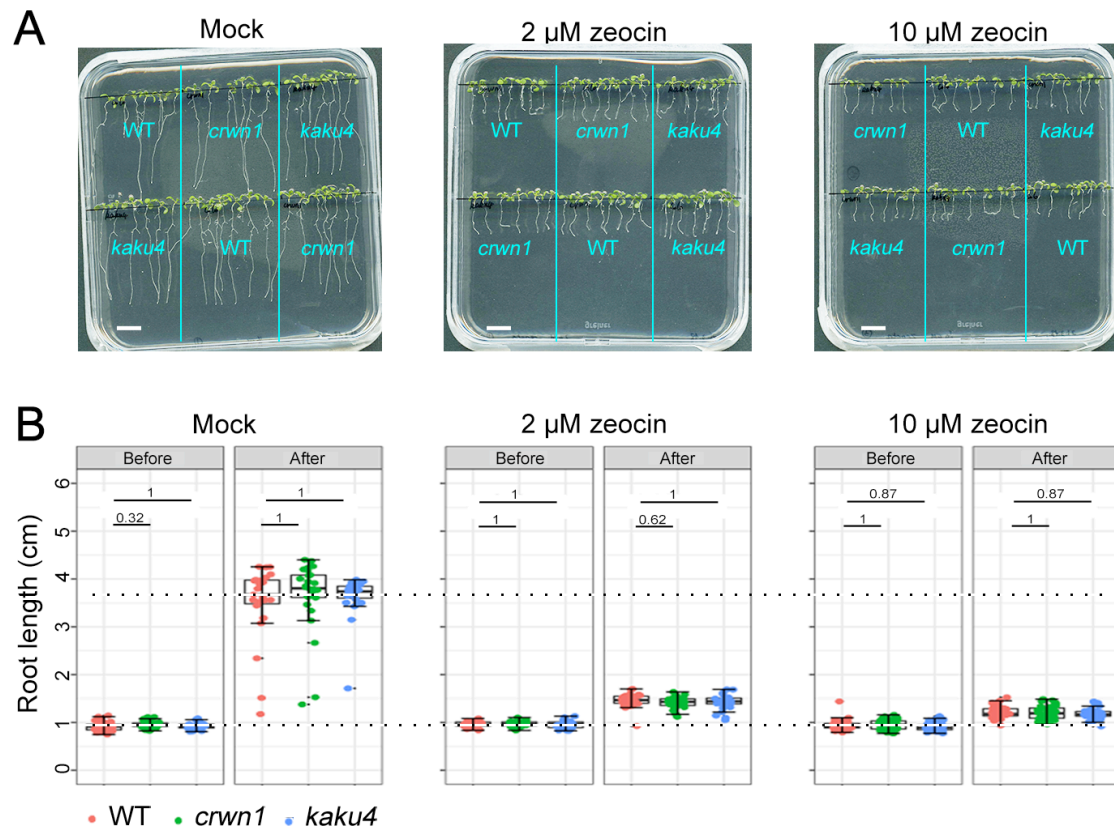


Figure 36. Phenotypes of WT, *crwn1* and *kaku4* seedlings under zeocin treatments.

(A) Seedlings of WT, *crwn1* and *kaku4* under zeocin treatments. The growth of plants and the application of different concentrations of zeocin to plants were as the same as plants in Figure 33A. Scale bars: 1 cm. (B) Comparison of root length of WT, *crwn1* and *kaku4* under zeocin treatments. The root length was measured before and after treatment. The bottom and upper dot lines marked the root length of the WT plants under normal conditions on the fifth and tenth day. Significant analyses were done by Mann-Whitney U test.

3.8 Generating functional *CRWN2* and *CRWN4* tagging lines

As our ChIP results of *CRWN1:2HA* show that *CRWN1* directly binds to chromatin at the NP, we asked whether there were direct interactions between chromatin and other *CRWN*s. Apart from *CRWN1*, there are three other *CRWN* proteins (*CRWN2*, *CRWN3* and *CRWN4*) (Sakamoto and Takagi 2013; Wang et al., 2013). Among these three *CRWN*s, similar like *CRWN1*, *CRWN4* is located at the NP (Sakamoto and Takagi 2013; Wang et al., 2013). And *CRWN2* has the highest sequence similarity with *CRWN1* protein (Figure 37). For this purpose, a native *CRWN4:2HA* tagging line and a *CRWN2:2HA* tagging line were planned to generate. Similar to the strategy used for generating *CRWN1:2HA* fusion proteins, insertion sites of the 2HA in the *CRWN4* and *CRWN2* tagging constructs were based on the prediction of structural motifs from their protein sequences (Figure 38 and Figure 42).

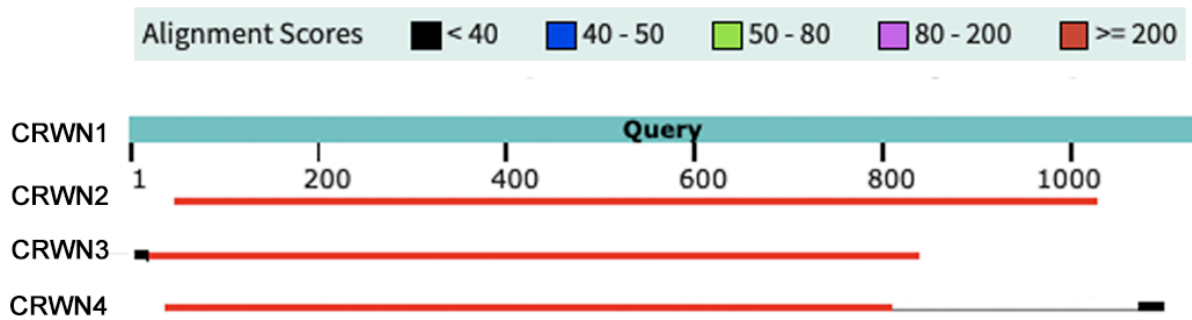


Figure 37. Blast Hits on CRWN1 protein sequence with the other three CRWN proteins.

Global alignment of CRWN2, CRWN3 and CRWN4 sequences with CRWN1 sequence. The alignment was generated with BLAST (<https://blast.ncbi.nlm.nih.gov/Blast.cgi>).

According to the complementation efficiency of different native *CRWN1:2HA* constructs, we first tried to insert the 2HA at the site of 850th amino acids from the N-terminal of CRWN4 and at the site of 800th amino acids from the N-terminal of CRWN2, respectively (Figure 38 and Figure 42). After getting the *pCRWN4::CRWN4_850_2HA crwn4* tagging line by floral dip, the morphology comparison of 8C nuclei from WT, *crwn4*, and *pCRWN4::CRWN4_850_2HA crwn4* plants was done. The nuclear phenotype of small and spherical nuclei of *crwn4* was fully rescued by the *pCRWN4::CRWN4_850_2HA* construct (Figure 39). Moreover, I observed that the *pCRWN2::CRWN2_800_2HA* construct rescued the whole-plant phenotype of *crwn1/2* plants (Figure 43). The genotyping PCR result confirmed that *pCRWN4::CRWN4_850_2HA crwn4* tagging lines were in homozygous *crwn4* background (Figure 40), and *pCRWN2::CRWN2_800_2HA crwn1/2* tagging lines were in homozygous *crwn1/2* background (Figure 44).

The presence of 2HA in *pCRWN4::CRWN4_850_2HA crwn4* and *pCRWN2::CRWN2_800_2HA crwn1/2* tagging lines was confirmed by western blot with the anti-HA antibody (Figure 41 and Figure 45). These rescue lines can be used for analyzing the function of CRWN4 and CRWN2 on chromatin binding.

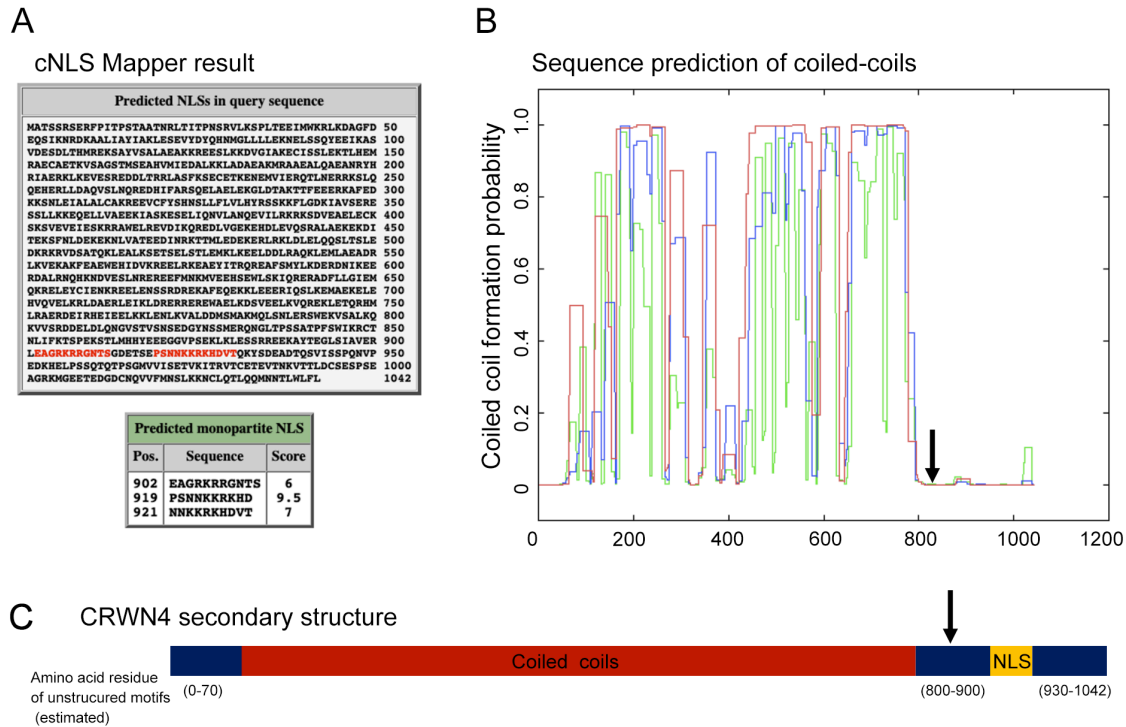


Figure 38. Prediction of structural motifs from the CRWN4 sequence.

(A) cNLS Mapper results of CRWN4 (Settings in this Figure were as the same as that in Figure 25A). (B) Prediction of coiled-coils from the sequence of CRWN4 with the COILS server (Settings and plotting are as the same as that in Figure 25B). Note that no coiled-coil is predicted in the N-terminal region and the region between 800th-900th amino acid of CRWN4. (C) Schematic representation of full-length CRWN4. The description of the representation of CRWN2 is as the same as that in Figure 25C.

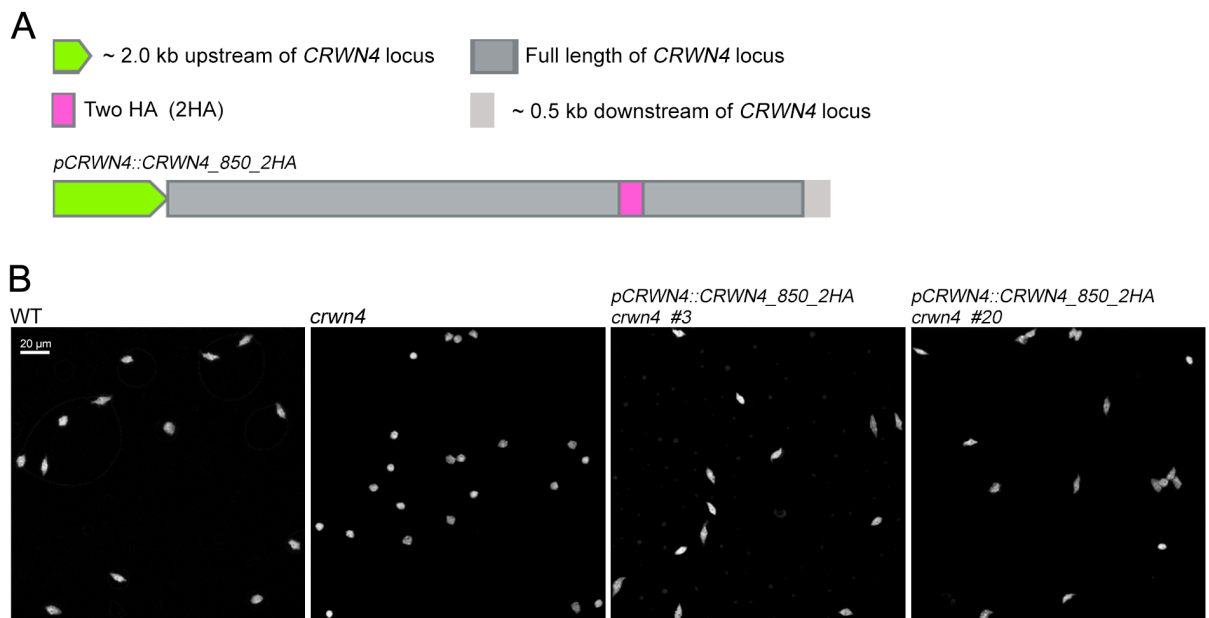


Figure 39. A native CRWN4 tagging construct can rescue the nuclear phenotype of crwn4.

(A) Design of a native CRWN4 expression construct. The green pentagon represents the 2.0 kb upstream of CRWN4 locus which is defined as promoter of the construct. A 0.5 kb downstream (the light grey rectangle) of CRWN4 was included in this construct. The dark grey rectangle represents the full length of the genomic

CRWN4 locus. The light purple rectangle represents the 2HA tag. In this construct, the 2HA is inserted at the 850th amino residue of the CRWN4 protein. (B) Morphology comparison of 8C nuclei of WT, *crwn4*, and two lines of *pCRWN4::CRWN4_850_2HA crwn4* plants. The nuclei were isolated from a rosette leaf of 4-week old plants.

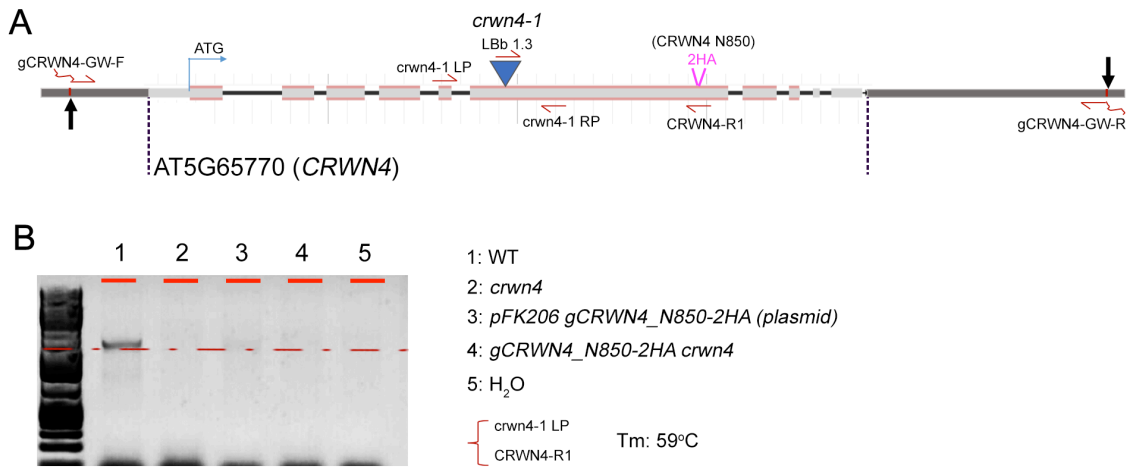


Figure 40. *CRWN4* gene model and genotyping of *CRWN4* tagging lines.

(A) Gene model of *CRWN4* including the positions of the T-DNA insertion, and the definition of the *pCRWN4::CRWN4_850_2HA* construct. Depictions of the gene model are as the same as described in Figure 27. (B) Genotyping of the *CRWN4* tagging line was done with primer pair *crwn4-1 LP* and *CRWN4-R1*. *CRWN4-R1* matches the endogenous genomic region where the 2HA are inserted.

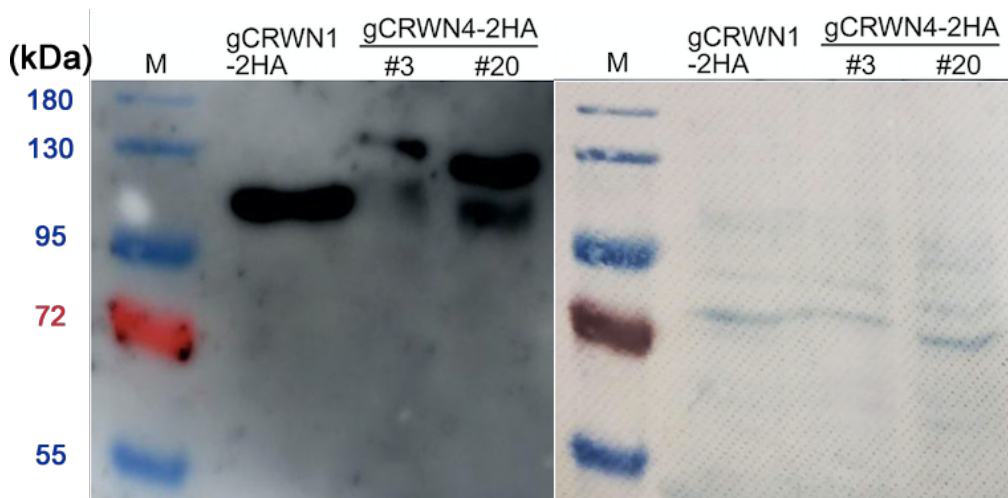


Figure 41. Expression of *CRWN4:2HA* in *crwn4* leaves.

The *CRWN4:2HA* protein in leaf crude extract was detected by the anti-HA antibody. This western blot was done by Dr. Nan Wang in our group.

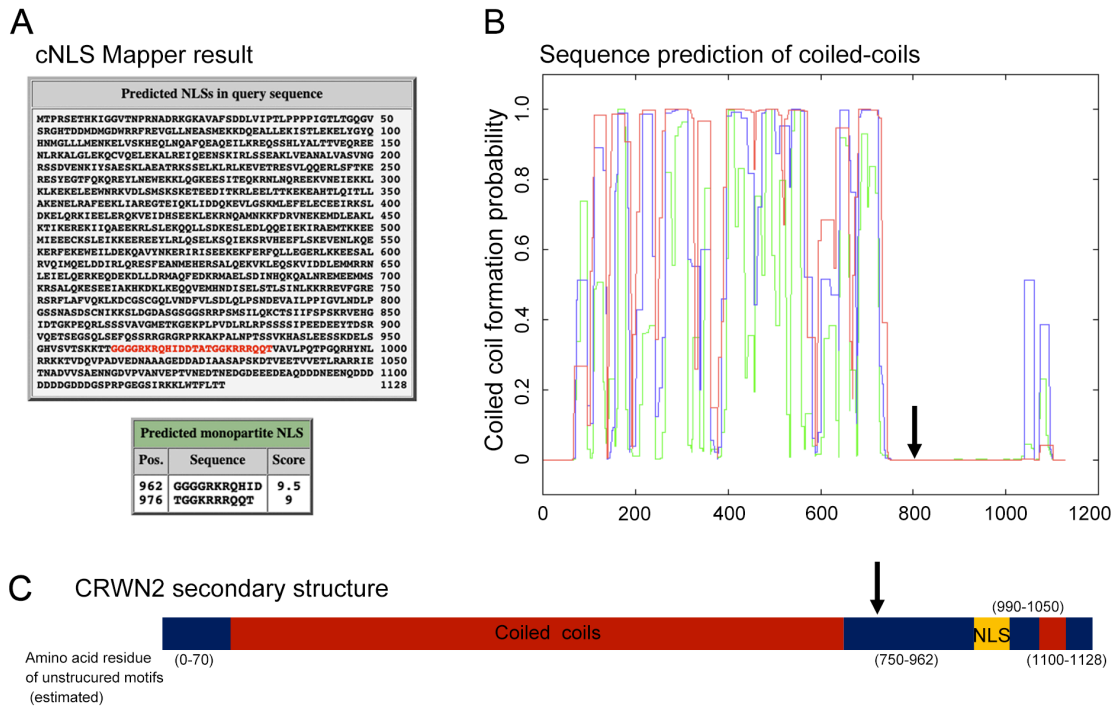


Figure 42. Prediction of structural motifs from the CRWN2 sequence.

(A) cNLS Mapper results of CRWN2 (Settings in this Figure were as the same as that in Figure 25A). (B) Prediction of coiled-coils from the sequence of CRWN2 with the COILS server (Settings and plotting are as the same as that in Figure 25B). Note that no coiled-coil is predicted in the N-terminal region and regions between 750th-962th and 990th-1050th amino acid of CRWN2. (C) Schematic representation of full-length CRWN2. The description of the representation of CRWN2 is as the same as that in Figure 25C.

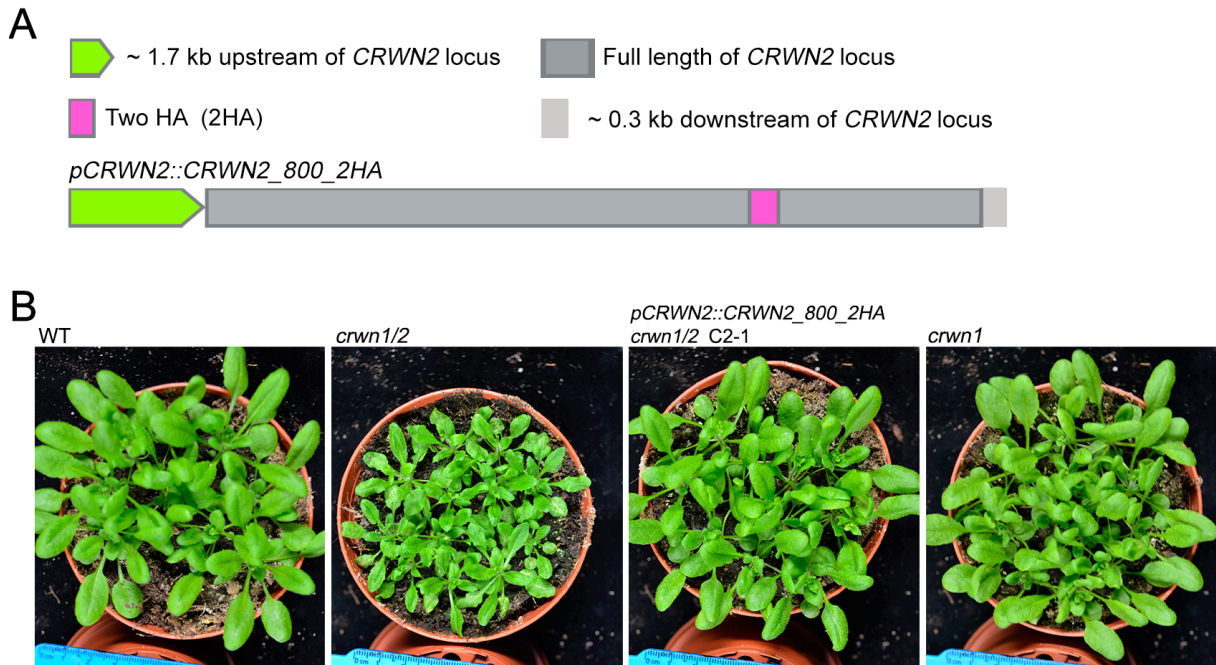


Figure 43. A native CRWN2 tagging construct can rescue the whole-plant phenotype of crwn1/2. (A) Design of a native CRWN2 expression construct with a 2HA tag. The green pentagon represents the 1.7 kb upstream of CRWN2 which is defined as the promoter of the construct. A 0.3 kb downstream (the light rectangle) of CRWN2 was included in this construct. The dark gray rectangle represents the full length of the genomic

CRWN2 locus, the light purple rectangle represents the 2HA tag. In the construct, the 2HA is inserted at the region of the 800th amino residue of *CRWN2* protein. (B) Phenotype of WT, *crwn4*, two lines of *pCRWN2::CRWN2_800_2HA crwn1/2* plants. Plants are grown in greenhouse for three weeks and then photographed.

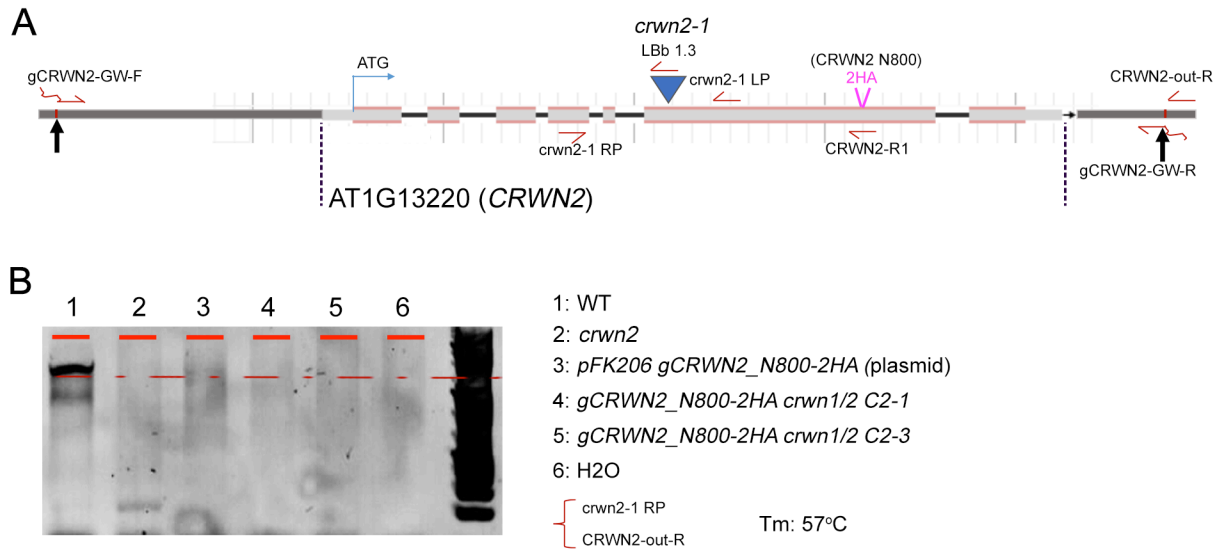


Figure 44. *CRWN2* gene model and genotyping of *CRWN2* tagging lines.

(A) Gene model of *CRWN2* including the positions of the T-DNA insertion, and the definition the *pCRWN2::CRWN2_800_2HA* construct. Depictions of the gene model are as the same as described in Figure 27. (B) Genotyping of the *CRWN2* tagging lines was done with primer pair *crwn2-1 RP* and *CRWN2-out-R*. *CRWN2-out-R* can only amplify the endogenous *CRWN2* allele as it matches the genomic region not included in the construct.

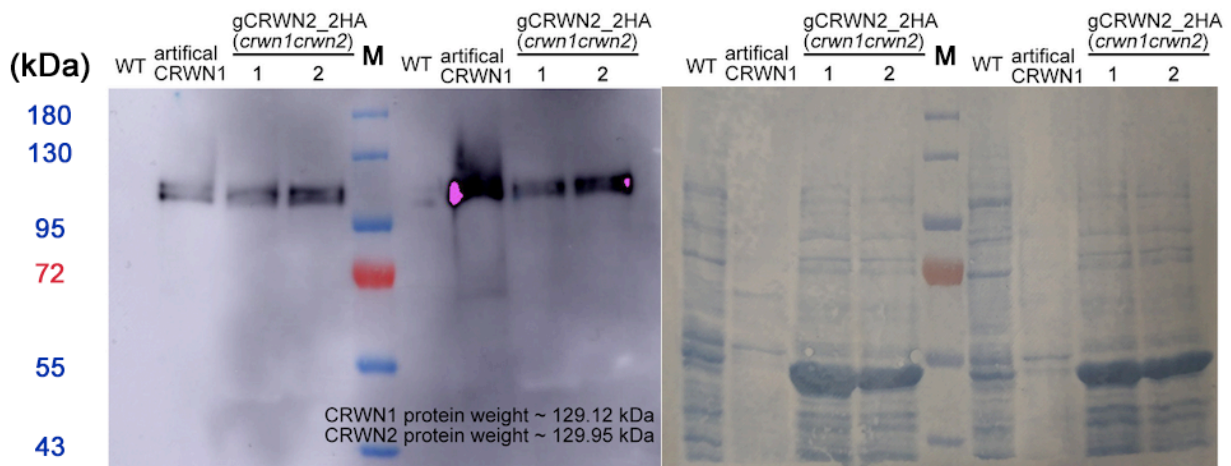


Figure 45. Expression of *CRWN2:2HA* in *crwn1/2* leaves.

The *CRWN2:2HA* protein in leaf crude extract was detected by the anti-HA antibody. This western blot was done by Dr. Nan Wang in our group.

3.9 Loss of *CRWNs* increased root hair density in *Arabidopsis thaliana*

Single and double *crwn* mutants have been reported to show changes in whole-plant phenotypes, nuclear morphology and chromatin organization (Wang et al., 2018b; Zhou et al.,

2015; Sakamoto and Takagi 2013; Choi et al., 2019; Dittmer et al., 2007; Wang et al., 2013; Poulet et al., 2017a). Nevertheless, there is no report in regard to plant root phenotype of plant lamin mutants. Even though both CRWN2 and CRWN3 belong to the same clade as CRWN1 (Wang et al., 2013), CRWN2 shows the highest sequence similarity with CRWN1 protein (Figure 37). Thus, more attention was paid to CRWN2 than CRWN3. In addition, *crwn1/2* double mutant shows more severe growth retardation than *crwn1/3* does (Wang et al., 2013). Moreover, CRWN4 has been shown to play a role in regulating chromatin organization and nuclear architecture (Sakamoto and Takagi 2013; Dittmer et al., 2007; Poulet et al., 2017a). Therefore, growth and root phenotype of mutants (single, double and triple) of *CRWN1*, *CRWN2* and *CRWN4* locus have been examined in this study.

As expected, no difference in length of plant root was observed between WT, *crwn1*, *crwn2* and *crwn4* plants (Figure 46 A), which was in accordance with the observation of the whole-plant phenotype (Wang et al., 2013). Changes in the length of root phenotype were differentially influenced in different double *crwn* mutants: *crwn1/4* and *crwn2/4* plants shows similar plant root length as WT plants, while root of *crwn1/2* became shorter compared with that of WT plants (Figure 46 A). And similar like change in the whole plant, plant root in triple *crwn* mutant — *crwn1/2/4* became even more shorter compared to WT plants (Figure 46 A) (Wang et al., 2013). In addition, I also found higher density of root hairs in *crwn1/2* and *crwn1/2/4* compared with WT plants and other *crwn* mutants (Figure 46 B). Root hairs in *crwn1/2/4* were longer than those in other *crwn* mutants and it seems that in *crwn1/2/4*, some root cells have two root hairs (Figure 46 B).

Even though I observed higher density of root hairs on *crwn1/2* and *crwn1/2/4* roots, roots in these mutants became shorter than those in WT plants and other *crwn* mutants (Figure 46). Therefore, the increased density of root hairs might be attributed to the shorter or smaller root cells in *crwn1/2* and *crwn1/2/4* mutants. To verify this point, I examined the cell length of root cells from different *crwn* mutants. However, except in *crwn1/2/4*, root cell length of *crwn1/2* was similar to that of WT plants and other *crwn* mutants (Figure 47). Thus, the increased root hair density in *crwn1/2* and *crwn1/2/4* was not due to changes in size of root cells in these *crwn* mutants.

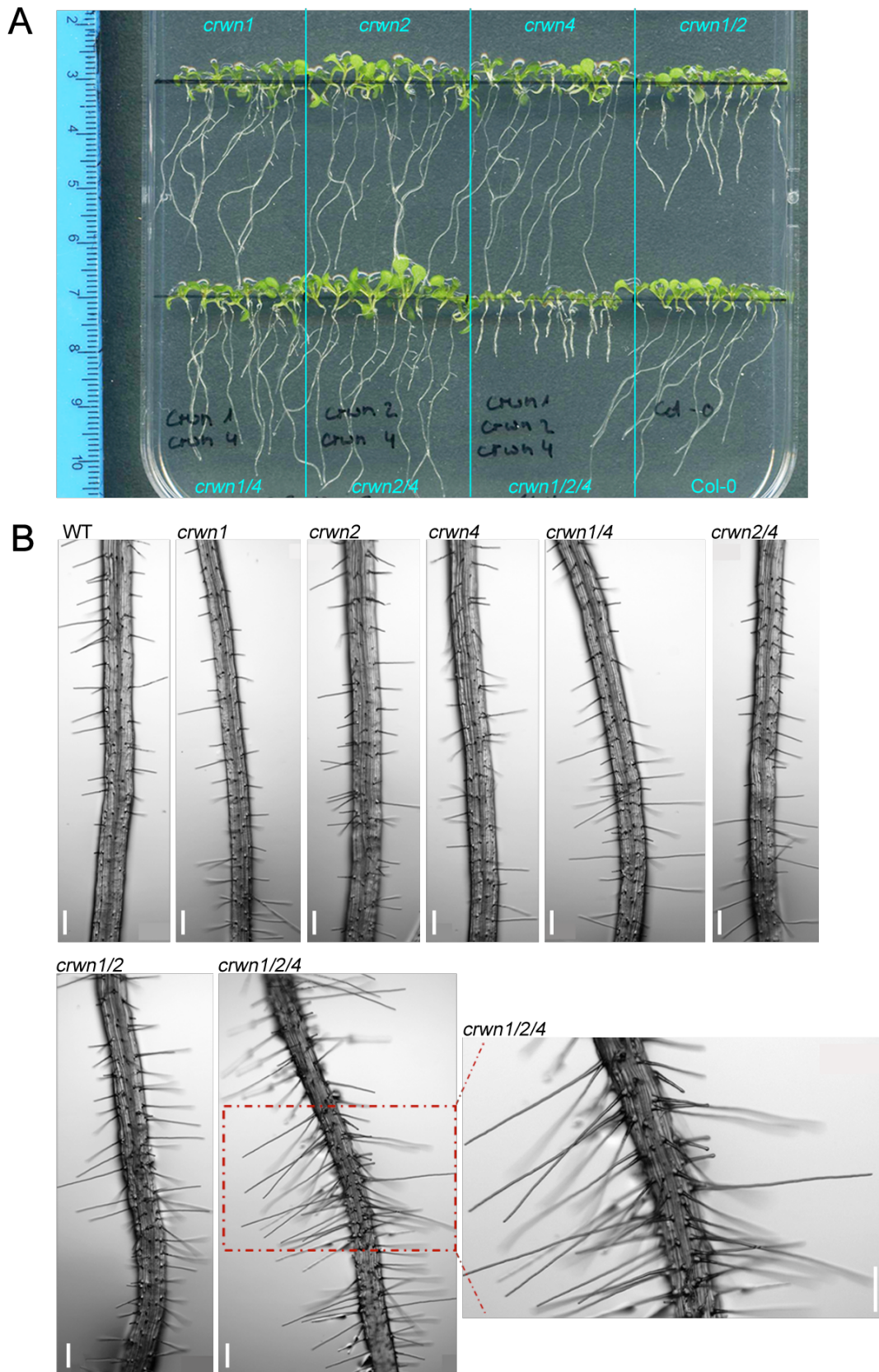


Figure 46. Morphology of root hairs of *crwn* mutants.

(A) Global view of roots of *crwn* mutants. Plants were grown vertically on 1/2 MS medium for 10 days and then imaged. (B) Representative images of root hairs from 10-day-old plants grown on 1/2 MS medium. Images were captured from the elongation zone of each root. Scale bars: 200 μ m.

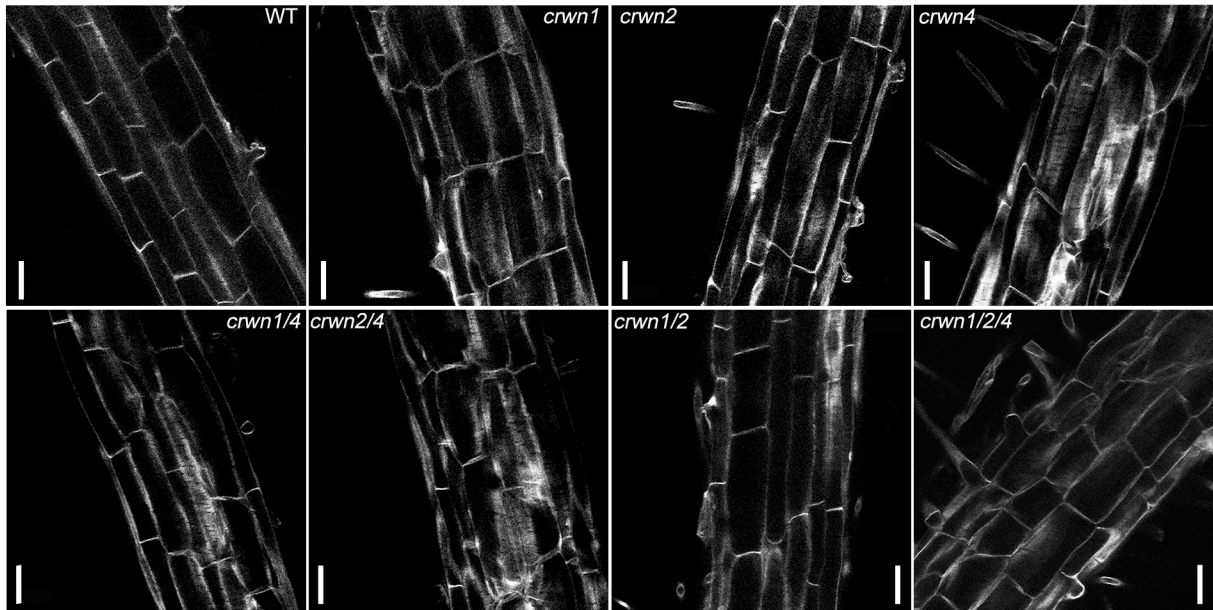


Figure 47. Comparison of cell length of root cells in *crwn* mutants.

Roots of 10-day-old plants were incubated with Calcofluor White to stain cell wall and photographed. Scale bars: 50 μ m.

4. Discussion

Chromatin positioning within the 3D nuclear space, especially at the NP, is non-random and crucial for many cellular processes including gene transcription and silencing (Gibcus and Dekker 2013; Sigman and Slotkin 2016; Van Bortle and Corces 2012). The discovery of LADs, which are featured with transcriptionally repressed chromatin regions, gives rise to the extensive studies on the non-random positioning of chromatin at the NP and its biological relevance (reviewed in (van Steensel and Belmont 2017)). In animals, it has shown that repressive histone mark H3K9 methylation, the lamina network, and many bridging proteins that connect chromatin to the lamina are required for positioning chromatin specially at the NP (van Steensel and Belmont 2017; Mattout et al., 2015; Harr et al., 2016). Whether or not the specific chromatin organization exists in plant is still unclear. If so, how plants achieve such comparable chromatin organization at the NP remains largely a mystery. Therefore, this thesis focused on these topics and aimed at answering these important questions.

It is generally little understood chromatin positioning at the NP in plants, except for a preferential association of chromocenters with the NE evidenced by cytological studies. The main reason for this is plants do not encode proteins sharing sequence similarity with nuclear lamin proteins in animals, although a similar meshwork like the animal NL underneath the NE has been observed in several plant species (Ciska and Moreno Diaz de la Espina 2014). Nevertheless, three types of plant-specific proteins, localized preferentially or exclusively at the INM have been listed as candidates of plant lamins over the past few years. In *Arabidopsis*, they are CRWN1-4, which belong to the NMCP family; KAKU4, which interacts physically with CRWNs at the NP; and plant NEAPs (reviewed in (Meier et al., 2017)). Moreover, the role in anchoring chromatin at the NP of the NPC which located at NE has also been shown, and components of plant NPC have been systematically identified and investigated (Strambio-De-Castillia et al., 2010; Tamura and Hara-Nishimura 2013; Tamura et al., 2010). These advances offer opportunities for in-depth studies on whether and how chromatin organize specifically at the plant NP.

4.1 Specific perinuclear positioning of repressed chromatin regions revealed by RE-ChIP

As a functional compartment, the NP plays crucial roles in regulating chromatin organization within the 3D nuclear space and gene expression (reviewed in (Lemaitre and Bickmore 2015;

Arib and Akhtar 2011; Buchwalter et al., 2019)). In general, the NP in animals is a transcriptionally repressed compartment enriched for silenced chromatin regions (reviewed in (Buchwalter et al., 2019)). Chromatin regions showing preferential localization at the NP can be identified by the conventional ChIP method, offered by the protein of interest, which is positioned at the NP, interacts directly with chromatin. For example, conventional ChIP approach has been applied to animal nuclear lamin A and lamin B, leading to the discovery of LADs (Kubben et al., 2012; Pascual-Reguant et al., 2018). Additionally, the DamID approach, which utilizes a fusion protein of lamin B1 and a methyltransferase (Dam), has been used to identify and characterize chromatin regions interacting with nuclear lamins in individual cells (Kind et al., 2013). In this approach, the Dam enzyme produces tracks on chromatin-lamina interactions by methylating DNA on the N⁶-adenine residue. A potential limitation of these two methods is that the protein of interest must be in close contact with chromatin.

Although three types of plant-specific proteins have been identified as plant lamin candidates, it remains unknown whether these plant-specific lamin candidate proteins and nuclear associated proteins are engaged in direct contacts with chromatin (Parry 2015; Ciska and Moreno Diaz de la Espina 2014). Because of such uncertainty, applying the formerly mentioned approaches on plants to explore chromatin positioning at the NP might cause misleading results. In this study, a RE-ChIP method was developed to identify *Arabidopsis thaliana* chromatin specifically positioned at the NP. By combining RE digestion and a mild sonication to fragmentize chromatin, our RE-ChIP alleviates the requirement that proteins of interest must have direct contacts with chromatin. In this method, high-order structures in nuclei can be largely preserved compared to those in conventional ChIP approach. Therefore, even the protein of interest indirectly interacts with chromatin to a certain extent, the RE-ChIP still permits recovery of chromatin in the proximity of the protein. It should be noted that chromatin fragmentation pattern in a RE-ChIP experiment is not random and is relied on both the density of restriction-cutting sites and the efficiency of digestion (Wang et al., 2015a). Therefore, the RE-ChIP cannot achieve resolution at a nucleosomal scale and is not suitable for genome-wide identification of narrow peaks, but it is suitable for studying indirect protein-DNA interactions.

In the RE-ChIP method conducted in this study, a fusion protein, NUP1:GFP, which was specialized localized at the NE, was used as a bait in RE-ChIP experiments to capture chromatin regions at its proximity. Our NUP1 RE-ChIP-seq results indicate that the

peripheral zone of the *Arabidopsis* nucleus is enriched with intermittent chromatin regions at chromosome arms (Figure 4). Chromatin segments adjacent to centromere (located at the PRs) from these tissues were more frequently to be found at the NP than those on the distal chromosome arms (Figure 4, Figure 7 and Figure 8), supporting the previous finding that chromocenters are located at the NP in *Arabidopsis* (Fransz et al., 2002). Intriguingly, the NUP1 RE-ChIP-seq signals from the root tissue, which composed of non-mesophyll cells, showed the highest similarity to those from leaves, in which the majority cell type being mesophyll cell (Figure 7 and Figure 8). Compared to other tissues, NUP1 RE-ChIP-seq signals from inflorescence tissue exhibited a much lower degree of enrichment of chromatin at the NP (Figure 7 and Figure 8), which might be caused by a dilution effect due to cell-type heterogeneity. In total, the chromatin regions localized at the NP in plants tend to be conserved among various tissues. Therefore, the tissue specificity makes a little contribution to the distribution of plant genome with respect to the nuclear peripheral zone on the chromosomal scale, the substantial contributor is linear genome per se.

Findings in this study suggest that the plant NP is a functional compartment for docking repressed heterochromatin. This is reflected by the finding that these regions show higher percentages of TE genes and silenced protein-coding genes (Figure 10). Thus, the biological functions of the NP in eukaryotes are highly conserved. An intriguing question is how plants achieve such spatial chromatin positioning which could not be revealed by the RE-ChIP approach with this engineered bait protein.

In this study, not all the genes enriched at the NP were found at lower expression levels (Figure 10C), which partially could be ascribed to the following reasons. Firstly, both the preparation of NUP1 RE-ChIP-seq libraries and analyses of gene expression were performed on plant tissues with different cell types; thus, if active transcription and positioning at the NP are mutually exclusive, both events might be pulled down finally at a gene locus in a mixed cell population. Secondly, the NP is not a zone that absolutely inhibits transcription. This idea is proved by one study, in which only a subset of a pool of genes were found to be down-regulated after artificially anchoring the pool of genes to the NP in human cells (Finlan et al., 2008). Specifically, in *Arabidopsis*, it has been documented that the repositioning of the *CHLOROPHYLL A/B BINDING (CAB) PROTEIN* locus from the nuclear interior to the NP together with its transcriptional activation can be triggered by light stimuli (Feng et al., 2014a). Thirdly, in the “gene gating” mechanism, positioning a gene at the NP leads to its

transcriptional activation because of interactions with nucleoporins (Blobel 1985). One report has discussed several potential interactions between transcription regulators (e.g., the TREX2 complex and SUMO proteases) and NPC (Parry 2015). Although no direct interactions between NUP1 and chromatin were detected with a conventional CHIP approach, such potential interactions could not be excluded.

Furthermore, the results presented in this study demonstrate that TEs are selectively tethered at the NP, suggesting additional features of this spatial compartment. The different loss of CHH DNA methylation on TEs in the RdDM and RdDM-independent mutants implies a spatial preference of these two TE-silencing pathways, in which RdDM is under more demand in nuclear interior while RdDM-independent is under more demand at the NP (Figure 11). This finding correlates to observations that many components in small RNA pathways are localized around *Arabidopsis* nucleoli, which are localized in nuclear interior (Li et al., 2008; Pontes et al., 2013). From a spatial view, results in this study offer insights into how these two silencing pathways work together in regulating TE methylation (Zemach et al., 2013), as well as how certain components of one pathway cooperate with each other (such as one study found a positive feedback loop between Pol IV-dependent small RNA biogenesis and DRM2 –dependent CHH DNA methylation (Li et al., 2015)). The possible dynamic locations of TEs in mutants of TE-silencing pathways are also an interesting topic for further investigations.

4.2 Specific chromatin positioning at the NP requires plant lamin proteins

Combining the previous part of the study and extensive studies on LADs in animals, the opinion that the NP is a functional compartment enriched with repressed chromatin domains and is highly conserved in eukaryotes. The next highly demand question is how these chromatin regions are selectively tethering to the plant NP. In animals, lamins and lamin-associated proteins play critical roles both in regulating nuclear architecture by offering mechanical support, and in modulating high-order genome organization and a wide range of chromatin activities, which based on selectively tethering chromatin to the NP (reviewed in (van Steensel and Belmont 2017)). Unfortunately, to identify counterparts in plants, lacking orthologs of lamins and most lamin-associated proteins leads to the strategy ground on a protein-sequence similarity search might be of little use compared with forward genetics methods (Ciska and Moreno Diaz de la Espina 2014). With intensive efforts in identifying and characterizing components of the plant NE, the plant lamina has been established by a set

of plant-specific proteins (Tamura et al., 2015). In *Arabidopsis*, CRWNs, KAKU4 and NEAPs have been considered as plant lamina constituents according to their structures of protein domain, displayed patterns of sub-nuclear distribution, and phenotypes of nuclear architecture showing in their loss-of-function mutants (Pawar et al., 2016; Sakamoto and Takagi 2013; Dittmer et al., 2007; Goto et al., 2014). However, it is still unclear whether or not they take part in selectively tethering chromatin regions at the NP. It is also a mystery whether they have involvement in mediating chromatin activities at the NP.

To answer these questions (at least partially), dual-color FISH experiments on 2C *Arabidopsis* nuclei were conducted to compare how chromatin-NP interactions differ in various mutants of plant lamina. The results imply that plant lamina candidates CRWN1 and CRWN4 show involvement in regulating selective chromatin positioning at the NP (Figure 14, Figure 24, Figure 48 and Figure 50), which is one of the important functions that metazoan lamins have (van Steensel and Belmont 2017). The documented function of CRWNs on regulating chromatin organization in previous studies was mainly focused on heterochromatic chromocenters (Wang et al., 2013; Poulet et al., 2017a). In this study, it is generalized to the genome-wide scale by presenting that CRWN1 and CRWN4 are required to selectively anchor genomic regions located on different chromosomes to the NP (Figure 14). Notably, like metazoan lamin proteins, CRWN1 shows direct interactions with chromatin regions localized at the NP (Figure 29, Figure 31 and Figure 32). Moreover, our chromosome painting experiments with probes covering the whole right arm of chromosome 1 (a 10-Mb genomic region) demonstrate that this large chromatin region shows increased dispersion in *crwn* mutants, especially in *crwn1*, compared to WT plants (Figure 24 and Figure 48). This finding implies that CRWN proteins might be involved in global genome organization, which can be determined by checking genome-wide chromatin interaction patterns with an *in situ* Hi-C approach. Furthermore, whether or not CRWNs are associated with changes in local chromatin structure, one can conduct the assay for the transposase-accessible chromatin using sequencing. Altogether, although CRWN1 has no sequence similarity with metazoan lamins, it could be concluded as a functional equivalent to them. CRWN proteins are found in all plant species, and most of the characterized CRWN proteins show localization preference at the NP (Ciska et al., 2018; Sakamoto and Takagi 2013; Kimura et al., 2014). We speculate that CRWN proteins have evolved across all the plant species to serve as the key factors in mediating interactions between chromatin and the plant nuclear lamina.

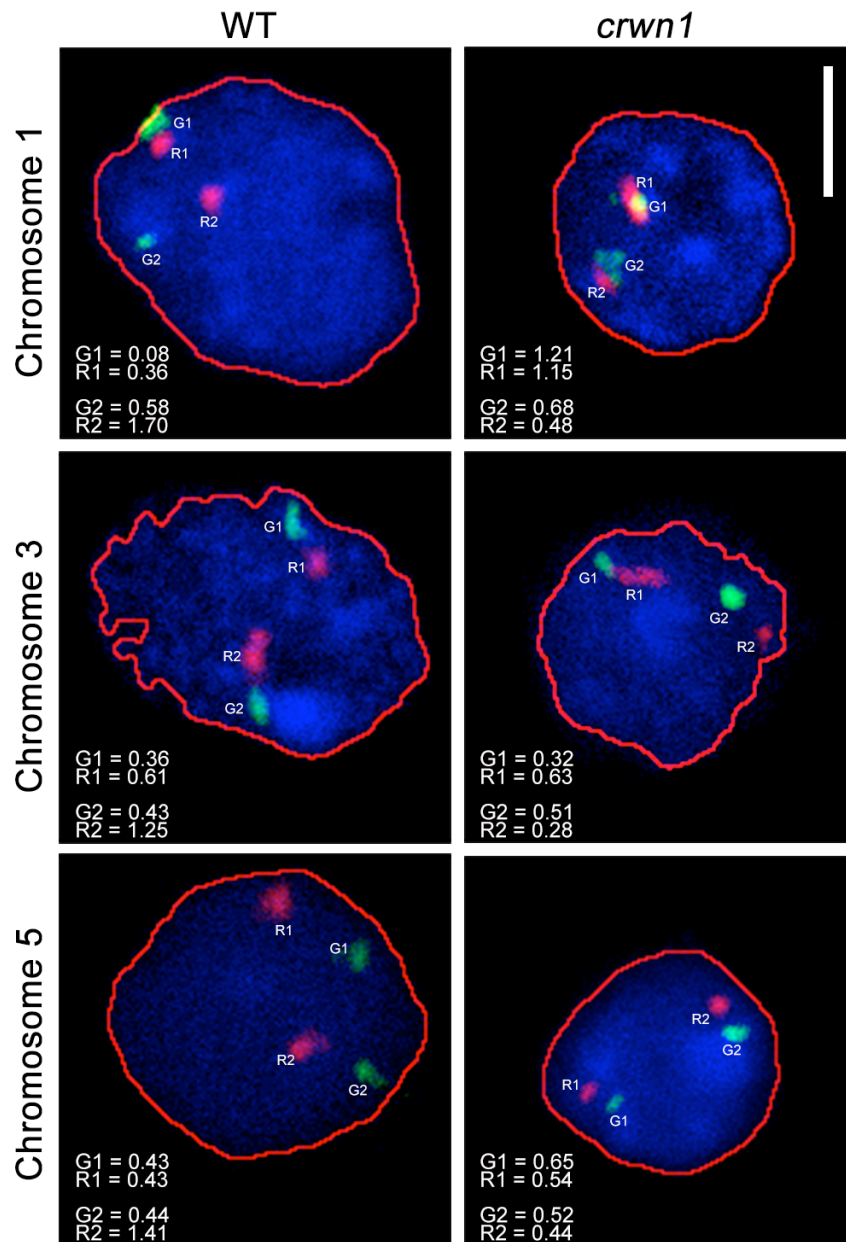


Figure 48. Representative confocal images showing localizations of FISH signal in 2C nuclei of WT and *crwn1* plants.

Three pairs of FISH probes are located on chromosome 1 (green 2 vs red 2), 3 and 5 respectively. The red contour of every nucleus shows the estimated edge of the nucleus. The estimated nuclear edge was defined in ImageJ with the ROI (regions of interest) manager according to DAPI signals. The value of G1 and G2 in every image represents the distance of the two green FISH signals to the NP, the value of R1 and R2 represents that of the red FISH signals. Scale bar: 2 μ m.

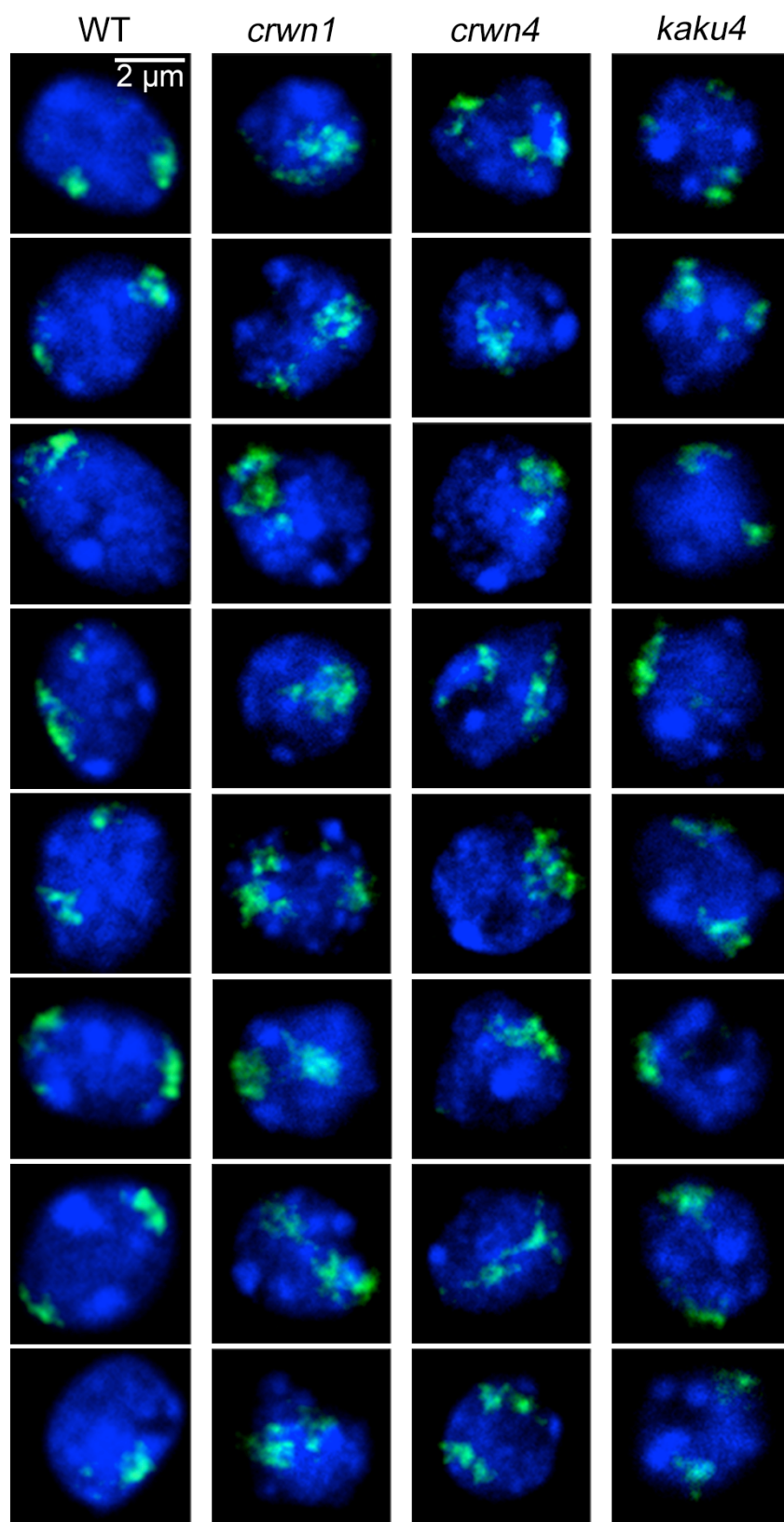


Figure 49. Representative confocal images of chromosome painting.

The signal distribution of FISH probes covering all the NUP1-enriched regions in the entire right arm of chromosome 1 in 2C nuclei of WT, *crwn1*, *crwn4*, and *kaku4* plants. Scale bar: 2 μm.

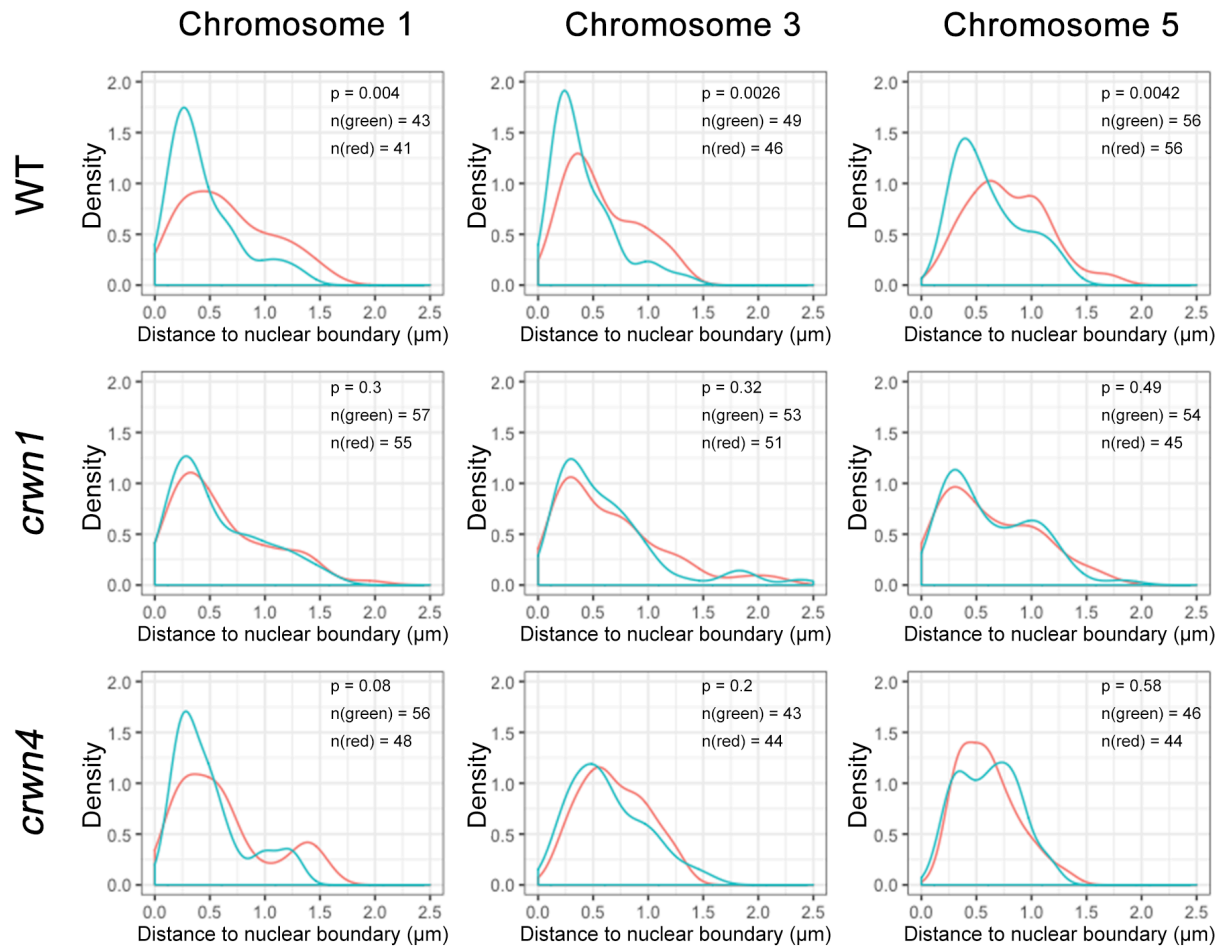


Figure 50. Distribution of distances of probed genomic regions to the NP in *crwn* mutants.

The genomic regions targeted by FISH probes in chromosome 1 (green 2 vs red 2). The figure is generated from distance data of replicate 2 in Figure 14. The p values indicate one-sided Mann-Whitney U test results.

It should be noted that not all the selected chromatin regions targeted by green FISH probes were found to be localized at the NP in WT *Arabidopsis* nuclei (Figure 50). This is due to cell-to-cell variations, which were caused by the following reasons. First, the 2C nuclei used in this study were collected from various types of cells, in which the major type of cells are mesophyll cells, and guard and phloem cells are also included in. Second, chromatin undergoing different processes or at different stages is dynamic, leading to the dynamics of the chromatin localizations.

Interestingly, KAKU4 and NEAPs, which are another two types of plant lamina constituents, do not show any function on modulating specific chromatin positioning at the NP (Figure 15 and Figure 16). This notion is not in agreement with what is found in metazoans. As all the three tested animal lamins, lamin B1, B2 and A, show interactions with chromatin at the NP, although they belong to two different lamin types (reviewed in (van Steensel and Belmont

2017)). In *Arabidopsis*, loss-of-function mutants of NEAP1 and NEAP3 show decreased number of chromocenters and fraction of heterochromatin in guard cells, implying their function on chromatin organization (Pawar et al., 2016). Moreover, the association of NEAP1 with chromatin has been suggested *via* a transcription factor, bZIP18 (Pawar et al., 2016). There might be two explanations for not detecting interactions of chromatin-NEAPs in this study. First, the majority of cells used in this study are mesophyll cells, the possible chromatin-NEAPs interactions existed in guard cells might be masked by results from mesophyll cells. Second, plants showing only a single mutation in *NEAP1* or *NEAP3* is used in this study, these two NEAPs might play redundant roles in mediating chromatin positioning at the NP.

In this study, the alterations in morphology of nuclei with the same endopolyploidy level in plant lamin mutants suggest a role of plant lamins in regulating nuclear shape (Figure 17 and Figure 18). This finding is in agreement with one of the key functions of animal lamin proteins in maintaining the nuclear architecture (van Steensel and Belmont 2017). As only nuclei with the same endopolyploidy level were compared among different plants, more accurate results were achieved. Intriguingly, the shape of 8C nuclei from WT *Arabidopsis* varies considerably (Figure 18A and Figure 18C). This is due to that the examined 8C nuclei were isolated from a mixture of different cell types (such as guard cells, mesophyll cells, and phloem cells). In general, the nuclei of mesophyll cells are longer than those of guard cells but shorter than those of phloem cells. For 2C nuclei, almost all the 2C WT nuclei exhibit spherical nuclear shape (Figure 17A and Figure 17C), even though they are from different cell types.

It would be interesting to further clarify how CRWN1 and CRWN4 would interact to modulate specific chromatin tethering at the NP in *Arabidopsis*. The relationship between CRWN1 and CRWN4 seems confusing. From the view of the physiological level, the two CRWN proteins should be functional redundancy as a result of the growth retardation phenotype of *crwn1/4* double mutants (Wang et al., 2013). However, from the view of the molecular level, the relationship of these two genes seems partially antagonizing. On the basis of a recent transcriptomic report of *crwn* mutants, the number of up-/down-regulated genes in *crwn1*, *crwn4* and *crwn1/4* mutants was 455/271, 1539/1151, and 395/329, respectively (Choi et al., 2019). Therefore, the knockout of *CRWN1* can largely suppress global alteration in expression of genes in the *crwn4* background. Moreover, the relationship becomes even more

puzzling because of the discrepancy in nuclear morphological alterations in *crwn1*, *crwn4* and *crwn1/4* plants (Figure 17 and Figure 18). A range of experiments to compare the difference of chromatin-NP interactions from one another among single and high-order *crwn* mutants need to be performed, to elucidate the potential redundant, cooperative, or antagonistic nature of these two CRWNs in modulating selective chromatin positioning at the NP. In animals, the genome-wide DamID patterns of three different lamin proteins, which belong to two lamin types, are similar (reviewed in (van Steensel and Belmont 2017)). Therefore, it would be intriguing to evaluate whether or not CRWN4 also interacts with the chromatin at the NP as CRWN1 does, if yes, is there any difference between the chromatin regions interacted by these two CRWN proteins. As we all know, with the same nuclear localization at the NP, CRWN1 and CRWN4 are categorized into two different clades of *Arabidopsis* CRWN proteins (Sakamoto and Takagi 2013; Dittmer et al., 2007; Wang et al., 2013).

In *Arabidopsis*, CRWN2 and CRWN3 are categorized into the same clade of CRWN protein as CRWN1 (Wang et al., 2013). However, they are distributed in the nuclear interior, not at the NP (Sakamoto and Takagi 2013; Dittmer et al., 2007). In addition, knockout of *CRWN2* in *crwn1* contributes to plant growth retardation phenotype, which is not found in *crwn1* single mutant plants (Wang et al., 2013). It has been reported recently that the number of mis-regulated genes in *crwn1*, *crwn2* and *crwn1/2* is 726, 149 and 3028, respectively (Choi et al., 2019). Therefore, loss-of-function of CRWN2 can lead to extensive transcriptomic mis-regulation in the *crwn1* background. All these findings suggest that CRWN1 and CRWN2 have at least overlapping functions. Questions that we are interested are whether these overlapping functions are linked to nuclear chromatin organization. In addition, whether or not CRWN2 interacts directly with chromatin, and where these interactions occur (in the nuclear plasma or at the NP)?

4.3 Roles of heterochromatin marks on specific chromatin positioning at the NP

The understanding of the molecular mechanisms by which LADs are brought to the NP in animals is still on the way (van Steensel and Belmont 2017). During the process of *C. elegans* embryogenesis, this relies on the repressive mark, H3K9me (Towbin et al., 2012; Gonzalez-Sandoval et al., 2015; Chen et al., 2014). Nevertheless, in differentiated *C. elegans* cells, regulation of perinuclear chromatin positioning at different developmental stages might be mediated by different mechanisms, because tethering LADs at the NP is partially maintained in the absence of H3K9me (Towbin et al., 2012). The finding in this study implies that

interactions between chromatin and the NP in *Arabidopsis* seedlings are not influenced when plants lose the H3K9me mark (Figure 19). In accordance with this concept, PRs were found to be retained at the NP in *svh4/5/6* triple plants that lost H3K9me (Jacob et al., 2009). Definitely, the requirement of H3K9me for chromatin-NP interaction might exist in other plant tissues and species.

Even though no further characterization of plant PLADs was conducted, PLADs should be enriched with transposons and protein-coding genes with lower expression levels comparing to non-PLADs, due to the high overlap between PLADs and NUP1-enriched chromatin domains (Figure 10 and Figure 32). Therefore, an enrichment of a variety of heterochromatic marks can be expected in PLADs. Moreover, in this study, it has been revealed that the positioning of TEs at the NP correlated with different CHH DNA methylation pathways (Figure 11). Thus, it would be necessary to perform comparative FISH analyses in mutants losing each of these heterochromatic marks to clarify whether or not they are required for specific chromatin positioning at the NP. Intriguingly, in high-order *Arabidopsis* mutants combining mutations in CHG and CHH DNA methylation pathways, the chromatin-NP interactions were found to be much attenuated (Figure 20). Mutation in the RdDM pathway alone, which is part of the CHH DNA methylation mechanisms, appears to be not enough to destroy chromatin-NP interactions, because the loss-of-function mutations in *DRM1* and *DRM2* have no influence on the specific perinuclear chromatin localization (Figure 20). Whereas, the loss-of-function mutation in *CMT2* affects the specific perinuclear positioning of chromatin regions located on chromosome 3 (Figure 20), suggesting that RdDM-independent pathway contributes more than RdDM in perinuclear chromatin anchoring in plants. Although it has been documented that CG DNA methylation is the most abundant type of DNA methylation, and is present over heterochromatic regions enriched with TEs and genic regions (Lister et al., 2008; Cokus et al., 2008), our findings suggest that CG DNA methylation is not involved in tethering chromatin at the NP (Figure 21). Based all these results, we speculate a mechanism that might involve in *Arabidopsis* perinuclear chromatin localization patterns: the non-CG methylated chromatin regions might be easily read by certain factor(s) which need to be identified (perhaps a protein complex containing plant lamin proteins, such as CRWN1), which triggers the initial contacts between chromatin and the NP. After that, the pre-formed chromatin-NP contacts can be further spread to their adjacent genomic loci.

4.4 Do CRWN1-chromatin interactions have any biological relevance?

It is interesting to know whether the loss of specific chromatin-NP interactions can cause any biological changes in *crwn1* plants. The impacts of global loss of chromatin-NP interactions in different metazoan species have been evaluated, showing that it results in a varying extent of gene derepression, depending on species and cell types (van Steensel and Belmont 2017). In our opinion, attention should be paid to the effects of CRWN1-mediated chromatin-NP interactions on transcriptional regulation. Homologs of CRWN1, namely CRWN2 and CRWN3, might be important in this regard, because of the throughout localization in the nucleoplasm (Bajic et al., 2018; Sakamoto and Takagi 2013; Dittmer et al., 2007). These CRWNs might act as backups to maintain chromatin structure and gene expression when an originally perinuclear tethered chromatin region detaches from the NP. Our newly prepared *CRWN2* tagging line might be useful for this purpose (Figure 43). Although phenotypic and expression analyses of single and high-order *crwn* mutants indicate that CRWN proteins play redundant roles in regulating heterochromatin organization, the protection of genomic DNA against excess oxidation, and salicylic acid (SA) synthesis (Wang et al., 2018b; Guo et al., 2017; Choi et al., 2019; Wang et al., 2013), in this study, *crwn1* does not show any phenotypic alterations comparing to WT plants under different stresses (Figure 33, Figure 34, Figure 35 and Figure 36). Switching to other model plant species with less CRWN genes, such as *Marchantia polymorpha*, might be useful to answer this question.

It should be noted that although *Arabidopsis CRWN1* or other *CRWN* locus appear to show stable transcriptional activities under biotic and abiotic stress conditions (expression data integrated by (Winter et al., 2007)), they might have intensive post-translational modifications (PTMs). It has been reported recently that CRWN1 proteins would be degraded quickly *via* a SA signaling mediated pathway upon *Pseudomonas syringae pathovar maculicola* infection (Guo et al., 2017). For the function of CRWN1 on regulating chromatin tethering and CT, it can be assumed that when SA signaling pathway becomes highly activated under stress, the down-regulation of CRWN1 proteins is also one way to give rise to alterations in chromatin organization as part of stress responses. In this study, the SA signaling or other related pathways might be activated by stress stimuli, leading to the plants *crwn1* single mutant appears like WT *Arabidopsis* plants under stresses.

Lamin proteins in metazoans tend to be phosphorylated at various sites, which would affect how they interact with themselves and other molecules (reviewed in (Machowska et al.,

2015)). According to a database of plant protein phosphorylation (<http://dbppt.biocuckoo.org>) (Cheng et al., 2014), CRWN1 has over 30 identified phosphorylation sites, the majority of them are located outside of its coiled-coil rod domain, and CRWN1 has more phosphorylation sites than other three *Arabidopsis* CRWNs. This information suggests that CRWN1 is easier to be phosphorylated, which can, in turn, act as a critical way to mediate CRWN1's activities. In addition, many other types of PTMs, such as sumoylation, acetylation, glycosylation, and farnesylation, have been described in metazoan lamins (Snider and Omary 2014). Although these PTMs have not been documented, they are likely present in CRWNs. The state and/or crosslinks of phosphorylation and other PTMs of CRWN1 might be changed in response to stresses, which might be another reason that *crwn1* mutants do not show phenotypes under artificial stresses.

5. Summary

The biochemical environment within the 3D nuclear space is not homogeneous. It has been demonstrated in many studies that the transcriptional activity of a gene is linked to its positioning inside the nuclear space. The NE not only serves as a physical barrier separating the nuclear content from the cytoplasm but also plays crucial roles in mediating the 3D organization of genomic DNA. Following the discovery of LADs, which are transcriptionally repressed chromatin regions, the non-random chromatin positioning at the NP and its biological relevance have been studied intensively in animals. However, it still remains unknown in plants that whether comparable chromatin organizations exist or not.

In this study, RE-ChIP was used to reveal the genome-wide identification of non-random organization of chromatin domains positioned at the peripheral zone of *Arabidopsis thaliana* nuclei. The patterns of chromatin regions positioned at NP were similar across different tissues. These chromatin domains are enriched with silenced protein-coding genes, TE genes and heterochromatic marks, which collectively define a repressed environment at the NP. Furthermore, our results suggest a spatial compartment of different DNA methylation pathways that regulate TE silencing, where the CHH DNA methylation of TEs localized at the NP and in the nuclear interior is preferentially mediated by CMT2 and DRM methyltransferases, respectively.

To elucidate how such chromatin positioning patterns at the NP was achieved in plants, dual-color FISH experiments were conducted to compare the difference of chromatin-NP interactions among various mutants. Our results show that in *Arabidopsis thaliana*, specific chromatin positioning at the NP requires plant lamin proteins CRWN1, CRWN4 and non-CG DNA methylation, which are all plant-specific. The result of chromosome painting indicates global attenuation of chromatin positioning patterns at the NP in both the *crwn1* and *crwn4* mutants. Moreover, ChIP-seq shows that CRWN1 directly interacts with chromatin regions localized at the NP.

In summary, the NP is a functional sub-compartment enriched with heterochromatic domains. In addition, CRWN1 is a key component of lamin-chromatin network in plants. It is functionally equivalent to animals lamins, which play crucial roles in regulating chromatin positioning at the NP.

6. Zusammenfassung

Die biochemische Umgebung innerhalb des 3D Kernraums ist nicht homogen. In vielen Studien wurde gezeigt, dass die Transkriptionsaktivität eines Gens mit seiner Positionierung im Kernraum zusammenhängt. Das NE nicht nur als physikalische Barriere, die den Kerninhalt vom Zytoplasma trennt, sondern spielt auch eine entscheidende Rolle bei der Vermittlung der 3D-Organisation genomischer DNA-Regionen. Nach der Entdeckung von LADs, die transkriptionell unterdrückte Chromatinregionen darstellen, wurden die nicht zufällige Chromatinpositionierung im NP und ihre biologische Relevanz bei Tieren intensiv untersucht. In Pflanzen ist jedoch noch nicht bekannt, ob vergleichbare Chromatin-Organisationen existieren oder nicht.

In dieser Studie wird unter Verwendung einer Strategie des RE-ChIP, die genomweite Identifizierung der nicht zufälligen Domänenorganisation von Chromatin in der peripheren Zone von *Arabidopsis thaliana*-Kernen untersucht. Die Muster der am NP positionierten Chromatinregionen waren in verschiedenen Geweben ähnlich. Diese Chromatindomänen sind mit stummgeschaltete proteinkodierende Genen, transposable Element-Genen (TEs) und heterochromatische Markierungen angereichert, die zusammen eine verdrängte Umgebung definieren. Darüber hinaus deuten unsere Ergebnisse auf ein Kompartiment verschiedener DNA-Methylierungswege hin, welche die Stummschaltung von TEs regeln, wobei die CHH-DNA-Methylierung von am NP und im Kerninneren lokalisierten TEs bevorzugt durch CMT2- bzw. DRM-Methyltransferasen vermittelt wird.

Zur Aufklärung, wie Pflanzen eine solche Chromatinpositionierung am NP erreichen, wurden In-situ-Hybridisierungsexperimente mit zweifarbiger Fluoreszenz durchgeführt, um den Unterschied der Chromatin-NP-Wechselwirkungen zwischen verschiedenen Mutanten zu vergleichen. Unsere Ergebnisse zeigen, dass in *Arabidopsis thaliana*, die spezifische Chromatinpositionierung am NP erfordert pflanzenlaminatartige Proteine CROWDED NUCLEI 1 (CRWN1), CRWN4 und nicht-CG DNA Methylierung, die alle pflanzenspezifisch sind. Das Chromatin-Malergebnis zeigt eine globale Dämpfung der Chromatin-Positionierungsmuster am NP bei beiden, sowohl *crwn1* als auch *crwn4* Mutanten. Darüber hinaus zeigt ChIP-seq, dass CRWN1 direkt mit am NP lokalisierten Chromatinregionen interagiert.

Zusammenfassend ist der NP ein funktionelles Subkompartiment, das mit heterochromatischen Domänen angereichert ist. Darüber hinaus ist CRWN1 eine Schlüsselkomponente des Lamin-Chromatin-Netzwerks in Pflanzen. Es ist funktionell äquivalent zu Tier-Laminen, die eine entscheidende Rolle bei der Regulierung der Chromatin-Positionierung im NP spielen.

7. References

- Adachi S, Minamisawa K, Okushima Y, Inagaki S, Yoshiyama K, Kondou Y, Kaminuma E, Kawashima M, Toyoda T, Matsui M et al. 2011. Programmed induction of endoreduplication by DNA double-strand breaks in Arabidopsis. *Proceedings of the National Academy of Sciences of the United States of America* **108**: 10004-10009.
- Akhtar W, de Jong J, Pindyurin AV, Pagie L, Meuleman W, de Ridder J, Berns A, Wessels LF, van Lohuizen M, van Steensel B. 2013. Chromatin position effects assayed by thousands of reporters integrated in parallel. *Cell* **154**: 914-927.
- Alonso JM, Stepanova AN, Leisse TJ, Kim CJ, Chen H, Shinn P, Stevenson DK, Zimmerman J, Barajas P, Cheuk R et al. 2003. Genome-wide insertional mutagenesis of Arabidopsis thaliana. *Science* **301**: 653-657.
- Amendola M, van Steensel B. 2015. Nuclear lamins are not required for lamina-associated domain organization in mouse embryonic stem cells. *EMBO reports* **16**: 610-617.
- Antonin W, Neumann H. 2016. Chromosome condensation and decondensation during mitosis. *Current opinion in cell biology* **40**: 15-22.
- Arib G, Akhtar A. 2011. Multiple facets of nuclear periphery in gene expression control. *Current opinion in cell biology* **23**: 346-353.
- Ariel F, Jegu T, Latrasse D, Romero-Barrios N, Christ A, Benhamed M, Crespi M. 2014. Noncoding transcription by alternative RNA polymerases dynamically regulates an auxin-driven chromatin loop. *Molecular cell* **55**: 383-396.
- Armstrong SJ, Franklin FC, Jones GH. 2001. Nucleolus-associated telomere clustering and pairing precede meiotic chromosome synapsis in Arabidopsis thaliana. *J Cell Sci* **114**: 4207-4217.
- Bajic M, Maher KA, Deal RB. 2018. Identification of Open Chromatin Regions in Plant Genomes Using ATAC-Seq. *Methods in molecular biology* **1675**: 183-201.
- Beagrie RA, Scialdone A, Schueler M, Kraemer DC, Chotalia M, Xie SQ, Barbieri M, de Santiago I, Lavitas LM, Branco MR et al. 2017. Complex multi-enhancer contacts captured by genome architecture mapping. *Nature* **543**: 519-524.
- Belton JM, McCord RP, Gibcus JH, Naumova N, Zhan Y, Dekker J. 2012. Hi-C: a comprehensive technique to capture the conformation of genomes. *Methods* **58**: 268-276.
- Benham CJ, Mielke SP. 2005. DNA mechanics. *Annu Rev Biomed Eng* **7**: 21-53.
- Berman BP, Weisenberger DJ, Aman JF, Hinoue T, Ramjan Z, Liu Y, Noushmehr H, Lange CP, van Dijk CM, Tollenaar RA et al. 2011. Regions of focal DNA hypermethylation and long-range hypomethylation in colorectal cancer coincide with nuclear lamina-associated domains. *Nature genetics* **44**: 40-46.

- Bian Q, Khanna N, Alvikas J, Belmont AS. 2013. beta-Globin cis-elements determine differential nuclear targeting through epigenetic modifications. *Journal of Cell Biology* **203**: 767-783.
- Blobel G. 1985. Gene gating: a hypothesis. *Proceedings of the National Academy of Sciences of the United States of America* **82**: 8527-8529.
- Bonev B, Cavalli G. 2016. Organization and function of the 3D genome. *Nature reviews Genetics* **17**: 661-678.
- Bourbousse C, Mestiri I, Zabulon G, Bourge M, Formiggini F, Koini MA, Brown SC, Fransz P, Bowler C, Barneche F. 2015. Light signaling controls nuclear architecture reorganization during seedling establishment. *Proceedings of the National Academy of Sciences of the United States of America* **112**: E2836-2844.
- Brickner JH, Walter P. 2004. Gene recruitment of the activated INO1 locus to the nuclear membrane. *Plos Biology* **2**: 1843-1853.
- Brown CR, Kennedy CJ, Delmar VA, Forbes DJ, Silver PA. 2008. Global histone acetylation induces functional genomic reorganization at mammalian nuclear pore complexes. *Genes & development* **22**: 627-639.
- Buchwalter A, Kaneshiro JM, Hetzer MW. 2019. Coaching from the sidelines: the nuclear periphery in genome regulation. *Nature reviews Genetics* **20**: 39-50.
- Burke B, Roux KJ. 2009. Nuclei take a position: managing nuclear location. *Developmental cell* **17**: 587-597.
- Carter D, Chakalova L, Osborne CS, Dai YF, Fraser P. 2002. Long-range chromatin regulatory interactions in vivo. *Nature genetics* **32**: 623-626.
- Casolari JM, Brown CR, Komili S, West J, Hieronymus H, Silver PA. 2004. Genome-wide localization of the nuclear transport machinery couples transcriptional status and nuclear organization. *Cell* **117**: 427-439.
- Chang W, Worman HJ, Gundersen GG. 2015. Accessorizing and anchoring the LINC complex for multifunctionality. *The Journal of cell biology* **208**: 11-22.
- Chankova SG, Dimova E, Dimitrova M, Bryant PE. 2007. Induction of DNA double-strand breaks by zeocin in *Chlamydomonas reinhardtii* and the role of increased DNA double-strand breaks rejoining in the formation of an adaptive response. *Radiat Environ Biophys* **46**: 409-416.
- Chen X, Yammine S, Shi C, Tark-Dame M, Gondor A, Ohlsson R. 2014. The visualization of large organized chromatin domains enriched in the H3K9me2 mark within a single chromosome in a single cell. *Epigenetics* **9**: 1439-1445.
- Cheng H, Deng W, Wang Y, Ren J, Liu Z, Xue Y. 2014. dbPPT: a comprehensive database of protein phosphorylation in plants. *Database (Oxford)* **2014**: bau121.
- Choi J, Strickler SR, Richards EJ. 2019. Loss of CRWN nuclear proteins induces cell death and salicylic acid defense signaling. *Plant Physiology* doi:10.1104/pp.18.01020.

- Ciska M, Masuda K, de la Espina SMD. 2018. Characterization of the lamin analogue NMCP2 in the monocot *Allium cepa*. *Chromosoma* **127**: 103-113.
- Ciska M, Moreno Diaz de la Espina S. 2014. The intriguing plant nuclear lamina. *Frontiers in plant science* **5**: 166.
- Clough SJ, Bent AF. 1998. Floral dip: a simplified method for *Agrobacterium*-mediated transformation of *Arabidopsis thaliana*. *Plant Journal* **16**: 735-743.
- Cokus SJ, Feng S, Zhang X, Chen Z, Merriman B, Haudenschild CD, Pradhan S, Nelson SF, Pellegrini M, Jacobsen SE. 2008. Shotgun bisulphite sequencing of the *Arabidopsis* genome reveals DNA methylation patterning. *Nature* **452**: 215-219.
- Concia L, Brooks AM, Wheeler E, Zynda GJ, Wear EE, LeBlanc C, Song J, Lee TJ, Pascuzzi PE, Martienssen RA et al. 2018. Genome-Wide Analysis of the *Arabidopsis* Replication Timing Program. *Plant Physiology* **176**: 2166-2185.
- Cowan CR, Carlton PM, Cande WZ. 2001. The polar arrangement of telomeres in interphase and meiosis. Rabl organization and the bouquet. *Plant Physiol* **125**: 532-538.
- Cremer T, Cremer C. 2006a. Rise, fall and resurrection of chromosome territories: a historical perspective. . *Eur J Histochem* **50**: 161-176.
- Cremer T, Cremer C. 2006b. Rise, fall and resurrection of chromosome territories: a historical perspective. Part II. Fall and resurrection of chromosome territories during the 1950s to 1980s. Part III. Chromosome territories and the functional nuclear architecture: experiments and models from the 1990s to the present. *Eur J Histochem* **50**: 223-272.
- Dechat T, Pfliegerhaer K, Sengupta K, Shimi T, Shumaker DK, Solimando L, Goldman RD. 2008. Nuclear lamins: major factors in the structural organization and function of the nucleus and chromatin. *Genes & development* **22**: 832-853.
- Dekker J, Belmont AS, Guttman M, Leshyk VO, Lis JT, Lomvardas S, Mirny LA, O'Shea CC, Park PJ, Ren B et al. 2017. The 4D nucleome project. *Nature* **549**: 219-226.
- Dekker J, Marti-Renom MA, Mirny LA. 2013. Exploring the three-dimensional organization of genomes: interpreting chromatin interaction data. *Nature reviews Genetics* **14**: 390-403.
- Dekker J, Rippe K, Dekker M, Kleckner N. 2002. Capturing chromosome conformation. *Science* **295**: 1306-1311.
- Dittmer TA, Stacey NJ, Sugimoto-Shirasu K, Richards EJ. 2007. LITTLE NUCLEI genes affecting nuclear morphology in *Arabidopsis thaliana*. *The Plant cell* **19**: 2793-2803.
- Dixon JR, Selvaraj S, Yue F, Kim A, Li Y, Shen Y, Hu M, Liu JS, Ren B. 2012. Topological domains in mammalian genomes identified by analysis of chromatin interactions. *Nature* **485**: 376-380.
- Doğan ES, Liu C. 2018. Three-dimensional chromatin packing and positioning of plant genomes. *Nat Plants* **4**: 521-529.

- Dong P, Tu X, Chu PY, Lu P, Zhu N, Grierson D, Du B, Li P, Zhong S. 2017. 3D Chromatin Architecture of Large Plant Genomes Determined by Local A/B Compartments. *Molecular plant* **10**: 1497-1509.
- Dong Q, Li N, Li X, Yuan Z, Xie D, Wang X, Li J, Yu Y, Wang J, Ding B et al. 2018. Genome-wide Hi-C analysis reveals extensive hierarchical chromatin interactions in rice. *The Plant journal : for cell and molecular biology* **94**: 1141-1156.
- Dostie J, Richmond TA, Arnaout RA, Selzer RR, Lee WL, Honan TA, Rubio ED, Krumm A, Lamb J, Nusbaum C et al. 2006. Chromosome Conformation Capture Carbon Copy (5C): a massively parallel solution for mapping interactions between genomic elements. *Genome research* **16**: 1299-1309.
- Dryden NH, Broome LR, Dudbridge F, Johnson N, Orr N, Schoenfelder S, Nagano T, Andrews S, Wingett S, Kozarewa I et al. 2014. Unbiased analysis of potential targets of breast cancer susceptibility loci by Capture Hi-C. *Genome research* **24**: 1854-1868.
- Du Z, Zheng H, Huang B, Ma R, Wu J, Zhang X, He J, Xiang Y, Wang Q, Li Y et al. 2017. Allelic reprogramming of 3D chromatin architecture during early mammalian development. *Nature* **547**: 232-235.
- Durut N, Abou-Ellail M, Pontvianne F, Das S, Kojima H, Ukai S, de Bures A, Comella P, Nidelet S, Rialle S et al. 2014. A duplicated NUCLEOLIN gene with antagonistic activity is required for chromatin organization of silent 45S rDNA in Arabidopsis. *The Plant cell* **26**: 1330-1344.
- Ebbs ML, Bender J. 2006. Locus-specific control of DNA methylation by the Arabidopsis SUVH5 histone methyltransferase. *The Plant cell* **18**: 1166-1176.
- Fang R, Yu M, Li G, Chee S, Liu T, Schmitt AD, Ren B. 2016. Mapping of long-range chromatin interactions by proximity ligation-assisted ChIP-seq. *Cell research* **26**: 1345-1348.
- Fang Y, Spector DL. 2005. Centromere positioning and dynamics in living Arabidopsis plants. *Molecular biology of the cell* **16**: 5710-5718.
- Feng CM, Qiu Y, Van Buskirk EK, Yang EJ, Chen M. 2014a. Light-regulated gene repositioning in Arabidopsis. *Nature communications* **5**: 3027.
- Feng S, Cokus SJ, Schubert V, Zhai J, Pellegrini M, Jacobsen SE. 2014b. Genome-wide Hi-C analyses in WT and mutants reveal high-resolution chromatin interactions in Arabidopsis. *Molecular cell* **55**: 694-707.
- Ferraiuolo MA, Sanyal A, Naumova N, Dekker J, Dostie J. 2012. From cells to chromatin: capturing snapshots of genome organization with 5C technology. *Methods* **58**: 255-267.
- Finlan LE, Sproul D, Thomson I, Boyle S, Kerr E, Perry P, Ylstra B, Chubb JR, Bickmore WA. 2008. Recruitment to the nuclear periphery can alter expression of genes in human cells. *PLoS genetics* **4**.

- Finn EH, Misteli T. 2017. Genome Architecture from a Different Angle. *Developmental cell* **41**: 3-4.
- Flemming W. 1965. Contributions to the Knowledge of the Cell and Its Vital Processes. *The Journal of cell biology* **25**: 3-69.
- Fransz P, de Jong JH, Lysak M, Castiglione MR, Schubert I. 2002. Interphase chromosomes in Arabidopsis are organized as well defined Chromocenters from which euchromatin loops emanate. *Proceedings of the National Academy of Sciences of the United States of America* **99**: 14584-14589.
- Fraser J, Williamson I, Bickmore WA, Dostie J. 2015. An Overview of Genome Organization and How We Got There: from FISH to Hi-C. *Microbiol Mol Biol R* **79**: 347-372.
- Fujimoto S, Sugano SS, Kuwata K, Osakabe K, Matsunaga S. 2016. Visualization of specific repetitive genomic sequences with fluorescent TALEs in Arabidopsis thaliana. *Journal of experimental botany* **67**: 6101-6110.
- Fullwood MJ, Han Y, Wei CL, Ruan X, Ruan Y. 2010. Chromatin interaction analysis using paired-end tag sequencing. *Curr Protoc Mol Biol* **Chapter 21**: Unit 21 15 21-25.
- Fullwood MJ, Liu MH, Pan YF, Liu J, Xu H, Mohamed YB, Orlov YL, Velkov S, Ho A, Mei PH et al. 2009. An oestrogen-receptor-alpha-bound human chromatin interactome. *Nature* **462**: 58-64.
- Gibcus JH, Dekker J. 2013. The hierarchy of the 3D genome. *Molecular cell* **49**: 773-782.
- Giorgetti L, Heard E. 2016. Closing the loop: 3C versus DNA FISH. *Genome biology* **17**: 215.
- Gonzalez-Sandoval A, Towbin BD, Kalck V, Cabianna DS, Gaidatzis D, Hauer MH, Geng L, Wang L, Yang T, Wang X et al. 2015. Perinuclear Anchoring of H3K9-Methylated Chromatin Stabilizes Induced Cell Fate in C. elegans Embryos. *Cell* **163**: 1333-1347.
- Goto C, Tamura K, Fukao Y, Shimada T, Hara-Nishimura I. 2014. The Novel Nuclear Envelope Protein KAKU4 Modulates Nuclear Morphology in Arabidopsis. *The Plant cell* **26**: 2143-2155.
- Grob S, Grossniklaus U. 2018. Invasive DNA elements modify nuclear architecture by KNOT-Linked silencing in plants. doi:10.1101/500496.
- Grob S, Schmid MW, Grossniklaus U. 2014. Hi-C analysis in Arabidopsis identifies the KNOT, a structure with similarities to the flamenco locus of Drosophila. *Molecular cell* **55**: 678-693.
- Grob S, Schmid MW, Luedtke NW, Wicker T, Grossniklaus U. 2013. Characterization of chromosomal architecture in Arabidopsis by chromosome conformation capture. *Genome biology* **14**: R129.
- Groves NR, Biel AM, Newman-Griffis AH, Meier I. 2018. Dynamic Changes in Plant Nuclear Organization in Response to Environmental and Developmental Signals. *Plant Physiol* **176**: 230-241.

- Gruenbaum Y, Foisner R. 2015. Lamins: nuclear intermediate filament proteins with fundamental functions in nuclear mechanics and genome regulation. *Annu Rev Biochem* **84**: 131-164.
- Guo TT, Mao XG, Zhang H, Zhang Y, Fu MD, Sun ZF, Kuai P, Lou YG, Fang YD. 2017. Lamin-like Proteins Negatively Regulate Plant Immunity through NAC WITH TRANSMEMBRANE MOTIF1-LIKE9 and NONEXPRESSOR OF PR GENES1 in *Arabidopsis thaliana*. *Molecular plant* **10**: 1334-1348.
- Han J, Zhang Z, Wang K. 2018. 3C and 3C-based techniques: the powerful tools for spatial genome organization deciphering. *Mol Cytogenet* **11**: 21.
- Happel N, Doenecke D. 2009. Histone H1 and its isoforms: contribution to chromatin structure and function. *Gene* **431**: 1-12.
- Harr JC, Gonzalez-Sandoval A, Gasser SM. 2016. Histones and histone modifications in perinuclear chromatin anchoring: from yeast to man. *EMBO reports* **17**: 139-155.
- Harr JC, Luperchio TR, Wong XR, Cohen E, Wheelan SJ, Reddy KL. 2015. Directed targeting of chromatin to the nuclear lamina is mediated by chromatin state and A-type lamins. *Journal of Cell Biology* **208**: 33-52.
- Hauer MH, Gasser SM. 2017. Chromatin and nucleosome dynamics in DNA damage and repair. *Genes & development* **31**: 2204-2221.
- Heslop-Harrison JS, Schwarzacher T. 2011. Organisation of the plant genome in chromosomes. *The Plant journal : for cell and molecular biology* **66**: 18-33.
- Hong Y, Lu G, Duan J, Liu W, Zhang Y. 2018. Comparison and optimization of CRISPR/dCas9/gRNA genome-labeling systems for live cell imaging. *Genome biology* **19**: 39.
- Hou C, Corces VG. 2010. Nups take leave of the nuclear envelope to regulate transcription. *Cell* **140**: 306-308.
- Hsieh THS, Weiner A, Lajoie B, Dekker J, Friedman N, Rando OJ. 2015. Mapping Nucleosome Resolution Chromosome Folding in Yeast by Micro-C. *Cell* **162**: 108-119.
- Hsu PD, Lander ES, Zhang F. 2014. Development and applications of CRISPR-Cas9 for genome engineering. *Cell* **157**: 1262-1278.
- Huber D, Voith von Voithenberg L, Kaigala GV. 2018. Fluorescence in situ hybridization (FISH): History, limitations and what to expect from micro-scale FISH? *Micro and Nano Engineering* **1**: 15-24.
- Hughes JR, Roberts N, McGowan S, Hay D, Giannoulatou E, Lynch M, De Gobbi M, Taylor S, Gibbons R, Higgs DR. 2014. Analysis of hundreds of cis-regulatory landscapes at high resolution in a single, high-throughput experiment. *Nature genetics* **46**: 205-212.
- Jackson JP, Lindroth AM, Cao XF, Jacobsen SE. 2002. Control of CpNpG DNA methylation by the KRYPTONITE histone H3 methyltransferase. *Nature* **416**: 556-560.

- Jacob Y, Feng SH, LeBlanc CA, Bernatavichute YV, Stroud H, Cokus S, Johnson LM, Pellegrini M, Jacobsen SE, Michaels SD. 2009. ATXR5 and ATXR6 are H3K27 monomethyltransferases required for chromatin structure and gene silencing. *Nature structural & molecular biology* **16**: 763-U796.
- Jia N, Liu XM, Gao HB. 2016. A DNA2 Homolog Is Required for DNA Damage Repair, Cell Cycle Regulation, and Meristem Maintenance in Plants. *Plant Physiology* **171**: 318-333.
- Kadauke S, Blobel GA. 2009. Chromatin loops in gene regulation. *Biochimica et biophysica acta* **1789**: 17-25.
- Karlsson P, Christie MD, Seymour DK, Wang H, Wang X, Hagmann J, Kulcheski F, Manavella PA. 2015. KH domain protein RCF3 is a tissue-biased regulator of the plant miRNA biogenesis cofactor HYL1. *Proceedings of the National Academy of Sciences of the United States of America* **112**: 14096-14101.
- Kersey PJ, Allen JE, Armean I, Boddu S, Bolt BJ, Carvalho-Silva D, Christensen M, Davis P, Falin LJ, Grabmueller C et al. 2016. Ensembl Genomes 2016: more genomes, more complexity. *Nucleic acids research* **44**: D574-D580.
- Kimura Y, Fujino K, Ogawa K, Masuda K. 2014. Localization of *Daucus carota* NMCP1 to the nuclear periphery: the role of the N-terminal region and an NLS-linked sequence motif, RYNLRR, in the tail domain. *Frontiers in plant science* **5**.
- Kind J, Pagie L, de Vries SS, Nahidiazar L, Dey SS, Bienko M, Zhan Y, Lajoie B, de Graaf CA, Amendola M et al. 2015. Genome-wide maps of nuclear lamina interactions in single human cells. *Cell* **163**: 134-147.
- Kind J, Pagie L, Ortazokoyun H, Boyle S, de Vries SS, Janssen H, Amendola M, Nolen LD, Bickmore WA, van Steensel B. 2013. Single-cell dynamics of genome-nuclear lamina interactions. *Cell* **153**: 178-192.
- Kind J, van Steensel B. 2014. Stochastic genome-nuclear lamina interactions: modulating roles of Lamin A and BAF. *Nucleus* **5**: 124-130.
- Koch L. 2018. Chromosome interaction hubs around nuclear bodies. *Nature reviews Genetics* **19**: 470-471.
- Kubben N, Adriaens M, Meuleman W, Voncken JW, van Steensel B, Misteli T. 2012. Mapping of lamin A- and progerin-interacting genome regions. *Chromosoma* **121**: 447-464.
- Laemmli UK. 1970. Cleavage of Structural Proteins during the Assembly of the Head of Bacteriophage T4. *Nature* **227**: 680-685.
- Lakadamyali M, Cosma MP. 2015. Advanced microscopy methods for visualizing chromatin structure. *FEBS Lett* **589**: 3023-3030.
- Langmead B, Salzberg SL. 2012. Fast gapped-read alignment with Bowtie 2. *Nature methods* **9**: 357-U354.
- Laubinger S, Zeller G, Henz SR, Sachsenberg T, Widmer CK, Naouar N, Vuylsteke M, Scholkopf B, Ratsch G, Weigel D. 2008. At-TAX: a whole genome tiling array resource for

- developmental expression analysis and transcript identification in *Arabidopsis thaliana*. *Genome biology* **9**: R112.
- Lemaitre C, Bickmore WA. 2015. Chromatin at the nuclear periphery and the regulation of genome functions. *Histochem Cell Biol* **144**: 111-122.
- Lermontova I, Schubert V, Fuchs J, Klatt S, Macas J, Schubert I. 2006. Loading of *Arabidopsis* centromeric histone CENH3 occurs mainly during G2 and requires the presence of the histone fold domain. *The Plant cell* **18**: 2443-2451.
- Li CF, Henderson IR, Song L, Fedoroff N, Lagrange T, Jacobsen SE. 2008. Dynamic regulation of ARGONAUTE4 within multiple nuclear bodies in *Arabidopsis thaliana*. *PLoS genetics* **4**: e27.
- Li S, Vandivier LE, Tu B, Gao L, Won SY, Li S, Zheng B, Gregory BD, Chen X. 2015. Detection of Pol IV/RDR2-dependent transcripts at the genomic scale in *Arabidopsis* reveals features and regulation of siRNA biogenesis. *Genome research* **25**: 235-245.
- Lieberman-Aiden E, van Berkum NL, Williams L, Imakaev M, Ragoczy T, Telling A, Amit I, Lajoie BR, Sabo PJ, Dorschner MO et al. 2009. Comprehensive mapping of long-range interactions reveals folding principles of the human genome. *Science* **326**: 289-293.
- Lister R, O'Malley RC, Tonti-Filippini J, Gregory BD, Berry CC, Millar AH, Ecker JR. 2008. Highly integrated single-base resolution maps of the epigenome in *Arabidopsis*. *Cell* **133**: 523-536.
- Liu C, Cheng YJ, Wang JW, Weigel D. 2017. Prominent topologically associated domains differentiate global chromatin packing in rice from *Arabidopsis*. *Nat Plants* doi:10.1038/s41477-017-0005-9.
- Liu C, Teo ZW, Bi Y, Song S, Xi W, Yang X, Yin Z, Yu H. 2013. A conserved genetic pathway determines inflorescence architecture in *Arabidopsis* and rice. *Developmental cell* **24**: 612-622.
- Liu C, Wang CM, Wang G, Becker C, Zaidem M, Weigel D. 2016. Genome-wide analysis of chromatin packing in *Arabidopsis thaliana* at single-gene resolution. *Genome research* **26**: 1057-1068.
- Liu C, Weigel D. 2015. Chromatin in 3D: progress and prospects for plants. *Genome biology* **16**: 170.
- Livak KJ, Schmittgen TD. 2001. Analysis of relative gene expression data using real-time quantitative PCR and the 2(T)(-Delta Delta C) method. *Methods* **25**: 402-408.
- Lysak MA, Fransz PF, Ali HBM, Schubert I. 2001. Chromosome painting in *Arabidopsis thaliana*. *Plant Journal* **28**: 689-697.
- M'rah Helali S, Nebli H, Kaddour R, Mahmoudi H, Lachaâl M, Ouerghi Z. 2010. Influence of nitrate—ammonium ratio on growth and nutrition of *Arabidopsis thaliana*. *Plant and Soil* **336**: 65-74.

- Ma H, Tu LC, Naseri A, Huisman M, Zhang S, Grunwald D, Pederson T. 2016. Multiplexed labeling of genomic loci with dCas9 and engineered sgRNAs using CRISPRainbow. *Nature biotechnology* **34**: 528-530.
- Ma W, Ay F, Lee C, Gulsoy G, Deng X, Cook S, Hesson J, Cavanaugh C, Ware CB, Krumm A et al. 2015. Fine-scale chromatin interaction maps reveal the cis-regulatory landscape of human lincRNA genes. *Nature methods* **12**: 71-78.
- Maass PG, Barutcu AR, Rinn JL. 2019. Interchromosomal interactions: A genomic love story of kissing chromosomes. *The Journal of cell biology* **218**: 27-38.
- Machowska M, Piekarowicz K, Rzepecki R. 2015. Regulation of lamin properties and functions: does phosphorylation do it all? *Open Biol* **5**.
- Manuelidis L, Borden J. 1988. Reproducible compartmentalization of individual chromosome domains in human CNS cells revealed by in situ hybridization and three-dimensional reconstruction. *Chromosoma* **96**: 397-410.
- Mattout A, Cabianca DS, Gasser SM. 2015. Chromatin states and nuclear organization in development--a view from the nuclear lamina. *Genome biology* **16**: 174.
- Mattout A, Pike BL, Towbin BD, Bank EM, Gonzalez-Sandoval A, Stadler MB, Meister P, Gruenbaum Y, Gasser SM. 2011. An EDMD mutation in *C. elegans* lamin blocks muscle-specific gene relocation and compromises muscle integrity. *Current biology : CB* **21**: 1603-1614.
- Meier I. 2016. LINCing the eukaryotic tree of life - towards a broad evolutionary comparison of nucleocytoplasmic bridging complexes. *J Cell Sci* **129**: 3523-3531.
- Meier I, Griffis AH, Groves NR, Wagner A. 2016. Regulation of nuclear shape and size in plants. *Current opinion in cell biology* **40**: 114-123.
- Meier I, Richards EJ, Evans DE. 2017. Cell Biology of the Plant Nucleus. *Annual review of plant biology* **68**: 139-172.
- Meuleman W, Peric-Hupkes D, Kind J, Beaudry JB, Pagie L, Kellis M, Reinders M, Wessels L, van Steensel B. 2013. Constitutive nuclear lamina-genome interactions are highly conserved and associated with A/T-rich sequence. *Genome research* **23**: 270-280.
- Mikulski P, Hohenstatt ML, Farrona S, Smaczniak C, Stahl Y, Kalyanikrishna K, Kaufmann K, Angenent GC, Schubert D. 2019. The chromatin-associated protein PWO1 interacts with plant nuclear lamin-like components to regulate nuclear size. *The Plant cell* doi:10.1105/tpc.18.00663.
- Miroshnikova YA, Nava MM, Wickstrom SA. 2017. Emerging roles of mechanical forces in chromatin regulation. *J Cell Sci* **130**: 2243-2250.
- Mumbach MR, Rubin AJ, Flynn RA, Dai C, Khavari PA, Greenleaf WJ, Chang HY. 2016. HiChIP: efficient and sensitive analysis of protein-directed genome architecture. *Nature methods* **13**: 919-922.

- Nagano T, Lubling Y, Stevens TJ, Schoenfelder S, Yaffe E, Dean W, Laue ED, Tanay A, Fraser P. 2013. Single-cell Hi-C reveals cell-to-cell variability in chromosome structure. *Nature* **502**: 59-64.
- Nagano T, Lubling Y, Vaarnai C, Dudley C, Leung W, Baran Y, Cohen NM, Wingett S, Fraser P, Tanay A. 2017. Cell-cycle dynamics of chromosomal organization at single-cell resolution. *Nature* **547**: 61-+.
- Nagano T, Varnai C, Schoenfelder S, Javierre BM, Wingett SW, Fraser P. 2015. Comparison of Hi-C results using in-solution versus in-nucleus ligation. *Genome biology* **16**.
- Németh A, Conesa A, Santoyo-Lopez J, Medina I, Montaner D, Peterfia B, Solovei I, Cremer T, Dopazo J, Langst G. 2010. Initial genomics of the human nucleolus. *PLoS genetics* **6**: e1000889.
- Németh A, Langst G. 2011. Genome organization in and around the nucleolus. *Trends Genet* **27**: 149-156.
- Park HJ, Kim WY, Yun DJ. 2016. A New Insight of Salt Stress Signaling in Plant. *Mol Cells* **39**: 447-459.
- Parry G. 2015. The plant nuclear envelope and regulation of gene expression. *Journal of experimental botany* **66**: 1673-1685.
- Pascual-Reguant L, Blanco E, Galan S, Le Dily F, Cuartero Y, Serra-Bardenys G, Di Carlo V, Iturbide A, Cebria-Costa JP, Nonell L et al. 2018. Lamin B1 mapping reveals the existence of dynamic and functional euchromatin lamin B1 domains. *Nature communications* **9**: 3420.
- Pawar V, Poulet A, Detourne G, Tatout C, Vanrobays E, Evans DE, Graumann K. 2016. A novel family of plant nuclear envelope-associated proteins. *Journal of experimental botany* doi:10.1093/jxb/erw332.
- Pecinka A, Dinh HQ, Baubec T, Rosa M, Lettner N, Scheid OM. 2010. Epigenetic Regulation of Repetitive Elements Is Attenuated by Prolonged Heat Stress in Arabidopsis. *The Plant cell* **22**: 3118-3129.
- Pecinka A, Schubert V, Meister A, Kreth G, Klatter M, Lysak MA, Fuchs J, Schubert I. 2004. Chromosome territory arrangement and homologous pairing in nuclei of Arabidopsis thaliana are predominantly random except for NOR-bearing chromosomes. *Chromosoma* **113**: 258-269.
- Pederson T. 2011. The nucleus introduced. *Cold Spring Harb Perspect Biol* **3**.
- Poleshko A, Mansfield KM, Burlingame CC, Andrade MD, Shah NR, Katz RA. 2013. The Human Protein PRR14 Tethers Heterochromatin to the Nuclear Lamina during Interphase and Mitotic Exit. *Cell reports* **5**: 292-301.
- Pombo A, Dillon N. 2015. Three-dimensional genome architecture: players and mechanisms. *Nat Rev Mol Cell Bio* **16**: 245-257.

- Pontes O, Vitins A, Ream TS, Hong E, Pikaard CS, Costa-Nunes P. 2013. Intersection of small RNA pathways in *Arabidopsis thaliana* sub-nuclear domains. *PLoS one* **8**: e65652.
- Pontvianne F, Blevins T, Chandrasekhara C, Mozgova I, Hassel C, Pontes OM, Tucker S, Mokros P, Muchova V, Fajkus J et al. 2013. Subnuclear partitioning of rRNA genes between the nucleolus and nucleoplasm reflects alternative epiallelic states. *Genes & development* **27**: 1545-1550.
- Pontvianne F, Carpentier MC, Durut N, Pavlistova V, Jaske K, Schorova S, Parrinello H, Rohmer M, Pikaard CS, Fojtova M et al. 2016. Identification of Nucleolus-Associated Chromatin Domains Reveals a Role for the Nucleolus in 3D Organization of the *A. thaliana* Genome. *Cell reports* doi:10.1016/j.celrep.2016.07.016.
- Poulet A, Duc C, Voisin M, Desset S, Tutois S, Vanrobays E, Benoit M, Evans DE, Probst AV, Tatout C. 2017a. The LINC complex contributes to heterochromatin organisation and transcriptional gene silencing in plants. *J Cell Sci* **130**: 590-601.
- Poulet A, Probst AV, Graumann K, Tatout C, Evans D. 2017b. Exploring the evolution of the proteins of the plant nuclear envelope. *Nucleus* **8**: 46-59.
- Prendergast L, Muller S, Liu Y, Huang H, Dingli F, Loew D, Vassias I, Patel DJ, Sullivan KF, Almouzni G. 2016. The CENP-T/-W complex is a binding partner of the histone chaperone FACT. *Genes & development* **30**: 1313-1326.
- Prieto P, Moore G, Shaw P. 2007. Fluorescence in situ hybridization on vibratome sections of plant tissues. *Nature Protocols* **2**: 1831-+.
- Prieto P, Santos AP, Moore G, Shaw P. 2004. Chromosomes associate premeiotically and in xylem vessel cells via their telomeres and centromeres in diploid rice (*Oryza sativa*). *Chromosoma* **112**: 300-307.
- Quinodoz SA, Ollikainen N, Tabak B, Palla A, Schmidt JM, Detmar E, Lai MM, Shishkin AA, Bhat P, Takei Y et al. 2018. Higher-Order Inter-chromosomal Hubs Shape 3D Genome Organization in the Nucleus. *Cell* doi:10.1016/j.cell.2018.05.024.
- Ramani V, Shendure J, Duan Z. 2016. Understanding Spatial Genome Organization: Methods and Insights. *Genomics Proteomics Bioinformatics* **14**: 7-20.
- Rao SSP, Huntley MH, Durand NC, Stamenova EK, Bochkov ID, Robinson JT, Sanborn AL, Machol I, Omer AD, Lander ES et al. 2014. A 3D Map of the Human Genome at Kilobase Resolution Reveals Principles of Chromatin Looping. *Cell* **159**: 1665-1680.
- Rao SSP, Huntley MH, Durand NC, Stamenova EK, Bochkov ID, Robinson JT, Sanborn AL, Machol I, Omer AD, Lander ES et al. 2015. A 3D Map of the Human Genome at Kilobase Resolution Reveals Principles of Chromatin Looping (vol 159, pg 1665, 2014). *Cell* **162**: 687-688.
- Reddy KL, Zullo JM, Bertolino E, Singh H. 2008. Transcriptional repression mediated by repositioning of genes to the nuclear lamina. *Nature* **452**: 243-247.

- Ren R, Deng L, Xue Y, Suzuki K, Zhang W, Yu Y, Wu J, Sun L, Gong X, Luan H et al. 2017. Visualization of aging-associated chromatin alterations with an engineered TALE system. *Cell research* **27**: 483-504.
- Robinson JT, Thorvaldsdottir H, Winckler W, Guttman M, Lander ES, Getz G, Mesirov JP. 2011. Integrative genomics viewer. *Nature biotechnology* **29**: 24-26.
- Rodriguez-Granados NY, Ramirez-Prado JS, Veluchamy A, Latrasse D, Raynaud C, Crespi M, Ariel F, Benhamed M. 2016. Put your 3D glasses on: plant chromatin is on show. *Journal of experimental botany* **67**: 3205-3221.
- Rosa S, Shaw P. 2013. Insights into chromatin structure and dynamics in plants. *Biology (Basel)* **2**: 1378-1410.
- Rudan MV, Barrington C, Henderson S, Ernst C, Odom DT, Tanay A, Hadjur S. 2015. Comparative Hi-C Reveals that CTCF Underlies Evolution of Chromosomal Domain Architecture. *Cell reports* **10**: 1297-1309.
- Ryba T, Hiratani I, Lu J, Itoh M, Kulik M, Zhang J, Schulz TC, Robins AJ, Dalton S, Gilbert DM. 2010. Evolutionarily conserved replication timing profiles predict long-range chromatin interactions and distinguish closely related cell types. *Genome research* **20**: 761-770.
- Sakamoto T, Inui YT, Uruguchi S, Yoshizumi T, Matsunaga S, Mastui M, Umeda M, Fukui K, Fujiwara T. 2011. Condensin II Alleviates DNA Damage and Is Essential for Tolerance of Boron Overload Stress in Arabidopsis. *The Plant cell* **23**: 3533-3546.
- Sakamoto Y, Takagi S. 2013. LITTLE NUCLEI 1 and 4 regulate nuclear morphology in Arabidopsis thaliana. *Plant & cell physiology* **54**: 622-633.
- Santos AP, Ferreira L, Maroco J, Oliveira MM. 2011. Abiotic stress and induced DNA hypomethylation cause interphase chromatin structural changes in rice rDNA loci. *Cytogenetic and genome research* **132**: 297-303.
- Santos AP, Shaw P. 2004. Interphase chromosomes and the Rab1 configuration: does genome size matter? *J Microsc-Oxford* **214**: 201-206.
- Sarasketa A, Gonzalez-Moro MB, Gonzalez-Murua C, Marino D. 2014. Exploring ammonium tolerance in a large panel of Arabidopsis thaliana natural accessions. *Journal of experimental botany* **65**: 6023-6033.
- Saze H, Scheid OM, Paszkowski J. 2003. Maintenance of CpG methylation is essential for epigenetic inheritance during plant gametogenesis. *Nature genetics* **34**: 65-69.
- Schneider CA, Rasband WS, Eliceiri KW. 2012. NIH Image to ImageJ: 25 years of image analysis. *Nature methods* **9**: 671-675.
- Schubert I, Shaw P. 2011. Organization and dynamics of plant interphase chromosomes. *Trends in Plant Science* **16**: 273-281.
- Schubert V, Berr A, Meister A. 2012. Interphase chromatin organisation in Arabidopsis nuclei: constraints versus randomness. *Chromosoma* **121**: 369-387.

- Schwarzacher TL, A.R. , Bennett MD, Heslop-Harrison JS. 1989. In Situ Localization of Parental Genomes in a Wide Hybrid. *Annals of botany* **64**: 315-324.
- Schwarzer W, Abdennur N, Goloborodko A, Pekowska A, Fudenberg G, Loe-Mie Y, Fonseca NA, Huber W, C HH, Mirny L et al. 2017. Two independent modes of chromatin organization revealed by cohesin removal. *Nature* **551**: 51-56.
- Sexton T, Cavalli G. 2015. The role of chromosome domains in shaping the functional genome. *Cell* **160**: 1049-1059.
- Shachar S, Voss Ty C, Pegoraro G, Sciascia N, Misteli T. 2015. Identification of Gene Positioning Factors Using High-Throughput Imaging Mapping. *Cell* **162**: 911-923.
- Shevelyov YY, Lavrov SA, Mikhaylova LM, Nurminsky ID, Kulathinal RJ, Egorova KS, Rozovsky YM, Nurminsky DI. 2009. The B-type lamin is required for somatic repression of testis-specific gene clusters. *Proceedings of the National Academy of Sciences of the United States of America* **106**: 3282-3287.
- Sigman MJ, Slotkin RK. 2016. The First Rule of Plant Transposable Element Silencing: Location, Location, Location. *The Plant cell* doi:10.1105/tpc.15.00869: TPC2015-00869-REV.
- Simonis M, Klous P, Homminga I, Galjaard RJ, Rijkers EJ, Grosveld F, Meijerink JPP, de Laat W. 2009. High-resolution identification of balanced and complex chromosomal rearrangements by 4C technology. *Nature methods* **6**: 837-U879.
- Smith S, Galinha C, Desset S, Tolmie F, Evans D, Tatout C, Graumann K. 2015. Marker gene tethering by nucleoporins affects gene expression in plants. *Nucleus* **6**: 471-478.
- Snider NT, Omary MB. 2014. Post-translational modifications of intermediate filament proteins: mechanisms and functions. *Nature reviews Molecular cell biology* **15**: 163-177.
- Solovei I, Wang AS, Thanisch K, Schmidt CS, Krebs S, Zwerger M, Cohen TV, Devys D, Foisner R, Peichl L et al. 2013. LBR and Lamin A/C Sequentially Tether Peripheral Heterochromatin and Inversely Regulate Differentiation. *Cell* **152**: 584-598.
- Speicher MR, Carter NP. 2005. The new cytogenetics: blurring the boundaries with molecular biology. *Nature reviews Genetics* **6**: 782-792.
- Splinter E, de Wit E, van de Werken HJG, Klous P, de Laat W. 2012. Determining long-range chromatin interactions for selected genomic sites using 4C-seq technology: From fixation to computation. *Methods* **58**: 221-230.
- Starr DA, Fridolfsson HN. 2010. Interactions between nuclei and the cytoskeleton are mediated by SUN-KASH nuclear-envelope bridges. *Annu Rev Cell Dev Biol* **26**: 421-444.
- Stevens TJ, Lando D, Basu S, Atkinson LP, Cao Y, Lee SF, Leeb M, Wohlfahrt KJ, Boucher W, O'Shaughnessy-Kirwan A et al. 2017. 3D structures of individual mammalian genomes studied by single-cell Hi-C. *Nature* **544**: 59-64.

- Strambio-De-Castillia C, Niepel M, Rout MP. 2010. The nuclear pore complex: bridging nuclear transport and gene regulation. *Nature reviews Molecular cell biology* **11**: 490-501.
- Stroud H, Do T, Du J, Zhong X, Feng S, Johnson L, Patel DJ, Jacobsen SE. 2014. Non-CG methylation patterns shape the epigenetic landscape in Arabidopsis. *Nature structural & molecular biology* **21**: 64-72.
- Stroud H, Greenberg MVC, Feng SH, Bernatavichute YV, Jacobsen SE. 2013. Comprehensive Analysis of Silencing Mutants Reveals Complex Regulation of the Arabidopsis Methylome. *Cell* **152**: 352-364.
- Szabo Q, Jost D, Chang JM, Cattoni DI, Papadopoulos GL, Bonev B, Sexton T, Gurgo J, Jacquier C, Nollmann M et al. 2018. TADs are 3D structural units of higher-order chromosome organization in Drosophila. *Sci Adv* **4**: eaar8082.
- Taddei A, Van Houwe G, Hediger F, Kalck V, Cubizolles F, Schober H, Gasser SM. 2006. Nuclear pore association confers optimal expression levels for an inducible yeast gene. *Nature* **441**: 774-778.
- Talwar S, Kumar A, Rao M, Menon GI, Shivashankar GV. 2013. Correlated spatio-temporal fluctuations in chromatin compaction states characterize stem cells. *Biophys J* **104**: 553-564.
- Tamura K, Fukao Y, Iwamoto M, Haraguchi T, Hara-Nishimura I. 2010. Identification and characterization of nuclear pore complex components in Arabidopsis thaliana. *The Plant cell* **22**: 4084-4097.
- Tamura K, Goto C, Hara-Nishimura I. 2015. Recent advances in understanding plant nuclear envelope proteins involved in nuclear morphology. *Journal of experimental botany* **66**: 1641-1647.
- Tamura K, Hara-Nishimura I. 2011. Involvement of the nuclear pore complex in morphology of the plant nucleus. *Nucleus* **2**: 168-172.
- Tamura K, Hara-Nishimura I. 2013. The molecular architecture of the plant nuclear pore complex. *Journal of experimental botany* **64**: 823-832.
- Tiang CL, He Y, Pawlowski WP. 2012. Chromosome organization and dynamics during interphase, mitosis, and meiosis in plants. *Plant Physiol* **158**: 26-34.
- Tolhuis B, Palstra RJ, Splinter E, Grosveld F, de Laat W. 2002. Looping and interaction between hypersensitive sites in the active beta-globin locus. *Molecular cell* **10**: 1453-1465.
- Tomita K, Cooper JP. 2006. The meiotic chromosomal bouquet: SUN collects flowers. *Cell* **125**: 19-21.
- Towbin BD, Gonzalez-Aguilera C, Sack R, Gaidatzis D, Kalck V, Meister P, Askjaer P, Gasser SM. 2012. Step-Wise Methylation of Histone H3K9 Positions Heterochromatin at the Nuclear Periphery. *Cell* **150**: 934-947.

- Van Bortle K, Corces VG. 2012. Nuclear organization and genome function. *Annu Rev Cell Dev Biol* **28**: 163-187.
- Van de Vosse DW, Wan YK, Lapetina DL, Chen WM, Chiang JH, Aitchison JD, Wozniak RW. 2013. A Role for the Nucleoporin Nup170p in Chromatin Structure and Gene Silencing. *Cell* **152**: 969-983.
- van Holde K, Zlatanova J. 1995. Chromatin higher order structure: chasing a mirage? *The Journal of biological chemistry* **270**: 8373-8376.
- van Koningsbruggen S, Gierlinski M, Schofield P, Martin D, Barton GJ, Ariyurek Y, den Dunnen JT, Lamond AI. 2010. High-Resolution Whole-Genome Sequencing Reveals That Specific Chromatin Domains from Most Human Chromosomes Associate with Nucleoli. *Molecular biology of the cell* **21**: 3735-3748.
- van Steensel B, Belmont AS. 2017. Lamina-Associated Domains: Links with Chromosome Architecture, Heterochromatin, and Gene Repression. *Cell* **169**: 780-791.
- Walter J, Joffe B, Bolzer A, Albiez H, Benedetti PA, Muller S, Speicher MR, Cremer T, Cremer M, Solovei I. 2006. Towards many colors in FISH on 3D-preserved interphase nuclei. *Cytogenetic and genome research* **114**: 367-378.
- Wang C, Liu C, Roqueiro D, Grimm D, Schwab R, Becker C, Lanz C, Weigel D. 2015a. Genome-wide analysis of local chromatin packing in *Arabidopsis thaliana*. *Genome research* **25**: 246-256.
- Wang H, Dittmer TA, Richards EJ. 2013. *Arabidopsis* CROWDED NUCLEI (CRWN) proteins are required for nuclear size control and heterochromatin organization. *BMC plant biology* **13**: 200.
- Wang LC, Wu JR, Hsu YJ, Wu SJ. 2015b. *Arabidopsis* HIT4, a regulator involved in heat-triggered reorganization of chromatin and release of transcriptional gene silencing, relocates from Chromocenters to the nucleolus in response to heat stress. *New Phytol* **205**: 544-554.
- Wang M, Wang P, Lin M, Ye Z, Li G, Tu L, Shen C, Li J, Yang Q, Zhang X. 2018a. Evolutionary dynamics of 3D genome architecture following polyploidization in cotton. *Nat Plants* **4**: 90-97.
- Wang MJ, Tu LL, Lin M, Lin ZX, Wang PC, Yang QY, Ye ZX, Shen C, Li JY, Zhang L et al. 2017. Asymmetric subgenome selection and cis-regulatory divergence during cotton domestication. *Nature genetics* **49**: 579-+.
- Wang Q, Liu S, Lu C, La Y, Dai J, Ma H, Zhou S, Tan F, Wang X, Wu Y et al. 2018b. Roles of CRWN-family proteins in protecting genomic DNA against oxidative damage. *Journal of plant physiology* **233**: 20-30.
- Wang SY, Su JH, Beliveau BJ, Bintu B, Moffitt JR, Wu CT, Zhuang XW. 2016. Spatial organization of chromatin domains and compartments in single chromosomes. *Science* **353**: 598-602.

- Wegel E, Koumproglou R, Shaw P, Osbourn A. 2009. Cell Type-Specific Chromatin Decondensation of a Metabolic Gene Cluster in Oats. *The Plant cell* **21**: 3926-3936.
- Weigel D, Glazebrook J. 2006. Setting up Arabidopsis crosses. *CSH Protoc* **2006**.
- Williamson I, Berlivet S, Eskeland R, Boyle S, Illingworth RS, Paquette D, Dostie J, Bickmore WA. 2014. Spatial genome organization: contrasting views from chromosome conformation capture and fluorescence in situ hybridization. *Genes & development* **28**: 2778-2791.
- Wilson KL, Foisner R. 2010. Lamin-binding Proteins. *Csh Perspect Biol* **2**.
- Winter D, Vinegar B, Nahal H, Ammar R, Wilson GV, Provart NJ. 2007. An "Electronic Fluorescent Pictograph" browser for exploring and analyzing large-scale biological data sets. *PloS one* **2**: e718.
- Yu M, Ren B. 2017. The Three-Dimensional Organization of Mammalian Genomes. *Annu Rev Cell Dev Biol* doi:10.1146/annurev-cellbio-100616-060531.
- Zang C, Schones DE, Zeng C, Cui K, Zhao K, Peng W. 2009. A clustering approach for identification of enriched domains from histone modification ChIP-Seq data. *Bioinformatics* **25**: 1952-1958.
- Zemach A, Kim MY, Hsieh PH, Coleman-Derr D, Eshed-Williams L, Thao K, Harmer SL, Zilberman D. 2013. The Arabidopsis nucleosome remodeler DDM1 allows DNA methyltransferases to access H1-containing heterochromatin. *Cell* **153**: 193-205.
- Zhou X, Groves NR, Meier I. 2015. Plant nuclear shape is independently determined by the SUN-WIP-WIT2-myosin XI-i complex and CRWN1. *Nucleus* **6**: 144-153.
- Zhu W, Hu B, Becker C, Dogan ES, Berendzen KW, Weigel D, Liu C. 2017. Altered chromatin compaction and histone methylation drive non-additive gene expression in an interspecific Arabidopsis hybrid. *Genome biology* **18**: 157.

8. Appendix

Table 9. Oligonucleotides used in this study

Name	Sequence	Note
crwn1-1_LP	GCAACTTTGTCAAAGCAGAGG	SALK_025347, genotyping
crwn1-1_RP	AGTTTCCAATGCCTTCTCCTC	
crwn2-1_LP	CTCGAACTGAGCCATTCTGTC	SALK_076653, genotyping
crwn2-1_RP	AGCTCATTGCTAGAGAAGGGG	
crwn3-1_LP	TTGCCTCTGAAATCCATGTC	SALK_099283, genotyping
crwn3-1_RP	CAGTGACGCATATACGCATTC	
crwn4-1_LP	GCAAAGACCACATTTGAGGAG	SALK_079296, genotyping
crwn4-1_RP	ATCAATGTGTTCCCACTCAGC	
nup136-1_LP	GGCATCTAGCATGAAGCTCAG	SALK_104728 genotyping
nup136-1_RP	TGGTGAGACGCCTTTACAATC	
cmt3-11_LP	CCCTCAACAATTAAGTACGCGC	SALK_148381, genotyping
cmt3-11_RP	ATAAGAGAAGGAGCTGCTGCC	
drm1-2 LP	CCTGTGTTGATTGGGATTACAG	SALK_031705, genotyping
drm1-2 RP	GTCGATGGAGTGCAACTTCTC	
drm2-2 LP	AGATCGCTTCCAGAGTTAGCC	SALK_150863, AT5G14620
drm2-2 RP	TTGTCGCAAAAAGCAAAGAG	
neap4_LP	TTGAACGAATAGATTTTGCCG	SALK_082247, genotyping
neap4_RP	ACGCTAGGTGATGTCACCAAG	
neap3_LP	ATCCCTACCTCGATAATGGC	GABI_221C05, genotyping
neap3_RP	ACTGATACAGCCCGATAATG	
neap2_LP	ACACAACGATCTTGAACCTG	GABI_365F02, genotyping
neap2_RP	TGGTTTTGGAATGCTAACTGG	
neap1_LP	CTCTGCAGCTTTCTGTCTGG	SAIL_846_B07, genotyping
neap1_RP	AGCTTGAAGCTTCTGCATCTG	
suvh4-LP	ACTGGTGAACCACTGGTATG	SALK_041474, genotyping
suvh4-RP	TGAGGGGTACCTGTTCAATTG	
suvh5-LP	CTCTTTTATCCAGGGCAACC	GABI_263C05, genotyping
suvh5-RP	TCATGGGTTTTGAAGATCTGC	
suvh6-LP	TGCATATTTGGGAGAAGTGC	SAIL_1244_F04, genotyping
suvh6-RP	GTCGTTCCCGATTCTTCTTC	

NP_posi_F1	TAGGGAAATCGAAAGAATCG	For the NP ChIP
NP_posi_R1	AACTCAGTCTTAAGCCTTC	
NP_posi_F2	AATGAGCTATTCAAGTGTAGC	
NP_posi_R2	TCGAATTGGTTTCCTGATAC	
NP_posi_F3	CCAAATATCGGTTATACTCC	
NP_posi_R3	GTACGAGCTGATGCCAGGTG	
NP_neg_F1	TAGGATTGTCATAGTTGTAA	
NP_neg_R1	AGTCTTAGTAATATGTGACG	
NP_neg_F2	AAGGCCATACTAGATGTTT	
NP_neg_R2	TGCCAAAGGTGGCTCACTAC	
TUB_F	AAGAACCATGCACCTCATCAGC	for ChIP normalization
TUB_R	ATCCGTGAAGAGTACCCAGAT	
RBCS_R	ACTGATGCATTGAACTTGACG	specific primers for pFK206 or pFK210 vectors
M13 F	CGTTGTAAAACGACGGCCAGT	
M13 R	GCCAGGAAACAGCTATGACC	
gNUP1-GW-F	TGTACAAAAAGCAGGCTTT GTTCGTTAGACTGGTTTAGGT	500 bp 5'
gNUP1-GW-R	CTTTGTACAAGAAAGCTGGGT TTTGGAGAAGAAGGCTTCTCT	300 bp 3'
NUP1-GFP_StrpII-F	AAGAAATCCACCAGGAAGAAA GCGGCCGCTGTGAGCAAGGG	GFP followed by StrepII
NUP1-GFP_StrpII-R	CTTGAACAATGTGTTTTTCTTA AGATCCACCAGTATCCTCAC	
NUP1-R1	TTTCTTCTGGTGGATTTCTT	to make three fragments for overlapping PCR: gNUP1-GW-F/NUP1-R1; NUP1-GFP-StrpII-F/NUP1-GFP-StrpII-R; NUP1-F1/NUP1-GW-R
NUP1-F1	TAAGAAAAACACATTGTTCAAG	
NUP1-seq-F1	TTGTTTGCTCTTTGTCTCGAT	NUP1 sequence primers
NUP1-seq-F2	ACAAGGAGGACGTCTCTAATG	
NUP1-seq-F3	TTCAGAAGTTACTCCTTCTAT	
NUP1-seq-F4	CACCATCCATGCTACGGGGTC	
NUP1-seq-F5	CCAACCTCAGAAGAGAAACGT	
NUP1-seq-F6	AAAAGCAGACCTGGTTTTGTG	
NUP1-seq-F7	CCAACAACACCCCGTCACTT	
gCRWN1-GW-F	TGTACAAAAAGCAGGCTTT TTACGTTTTATTGTGGTCTTC	1.5 kb upstream,
gCRWN1-GW-R	CTTTGTACAAGAAAGCTGGGT ATAATACTGTCAAGAGTGATG	0.5kb downstream
CRWN1-2HA-F	GATTATGCTGGATACCCTTACGACGTACCAGATTACGCT TAGCCCAATCTTTGATCAGAGA	add 2HA to C-terminal of CRWN1
CRWN1-2HA-R	AGGGTATCCAGCATAATCTGGTACGTCGTATGGGTATCC CGTCGTCAAGAAAGTCCAAA	

CRWN1-seq-F1	ATTTCAAGTGTTCATTTCCG	CRWN1 sequence primers
CRWN1-seq-F2	TTCTGTTGCAGCTGGAGAAGG	
CRWN1-seq-F3	AGAGAAACTGGAAGCCAGAGA	
CRWN1-seq-F4	AATTAAGGAGCAAATAGAAAAG	
CRWN1-seq-F5	AACATTCTTGATAACGAAGCAC	
CRWN1-seq-F6	TGCTTTCAAACACAGTCACTG	
2HA_CRWN1_F	GATTATGCTGGATACCCTTACGACGTACCAGATTACGCT TCCACGCCGTTGAAGGTGTGG	add 2HA to N-terminal of CRWN1
2HA_CRWN1_R	AGGGTATCCAGCATAATCTGGTACGTCGTATGGGTATCC CATCTCTACAATTGCGACAG	
CRWN1_N780_2HA_F	GATTATGCTGGATACCCTTACGACGTACCAGATTACGCT GCTGGCTTAGGATTGCCAGTT	insert 2HA at 780 amino acid from N-terminal of CRWN1
CRWN1_N780_2HA_R	AGGGTATCCAGCATAATCTGGTACGTCGTATGGGTATCC AGCAGTTGGGGATATATCCC	
gCRWN4-GW-F	TGTACAAAAAAGCAGGCTTT ACTAATCTTTTCTACTAGCTTAAC	0.5kb upstream
gCRWN4-GW-R	CTTTGTACAAGAAAGCTGGGT GCTACGAGCTACTTCGATGATAC	2kb downstream
CRWN4-2HA-F	GATTATGCTGGATACCCTTACGACGTACCAGATTACGCT TAGACTGGGATAAACGCGTCTGA	add 2HA to c-terminal of CRWN4
CRWN4-2HA-R	AGGGTATCCAGCATAATCTGGTACGTCGTATGGGTATCC CAGAAATAGCCAAAGGGTATTAT	
CRWN4-seq-F1	AAGTGAAGAGACAAGCACCGT	CRWN4 sequence primers
CRWN4-seq-F2	CACATATGCGAGAGAAATCAG	
CRWN4-seq-F3	TTTCTGGGAGACAAGATAGTA	
CRWN4-seq-F4	GAGTGGGAACACATTGATGTGA	
CRWN4-seq-F5	ATAAAACGATGTACTAATCTGAT	
CRWN4_seq-F6	TGCCGATATTAGAAATCCGAAG	
CRWN4_seq-F7	ACATTGACATTAACCCAGCAG	
CRWN4_N850_2HA-F	GATTATGCTGGATACCCTTACGACGTACCAGATTACGCTAATCT GATTTTCAAGACTTCTCCA	insert the 2HA at 850 amino acid from N-terminal of CRWN4
CRWN4_N850_2HA-R	AGGGTATCCAGCATAATCTGGTACGTCGTATGGGTATCCAGTA CATCGTTTTATCCATGA	
gCRWN2_GW_F	TGTACAAAAAAGCAGGCTTTAAACCCAACTTTGAACGACGA	around 1.7 kb upstream of CRWN2
gCRWN2_GW_R	TGTACAAAAAAGCAGGCTTTAAACCCAACTTTGAACGACGA	
gCRWN2_N800_2HA-F	GATTATGCTGGATACCCTTACGACGTACCAGATTACGCTGGAA GCTCTAATGCATCTGACTCT	insert the 2HA at 800 amino acid from N-terminal of CRWN2
gCRWN2_N800_2HA-R	AGGGTATCCAGCATAATCTGGTACGTCGTATGGGTATCCTGGA AGGTCATTCAAAACCTCC	

CRWN2_seq-F1	TTGATTTCCAGTGATCTCCGC	CRWN2 sequence primers
CRWN2_seq-F2	ATGTTCACTTTACATCAGCG	
CRWN2_seq-F3	GATGCAATTGGTAACCTTTAGC	
CRWN2_seq-F4	AAAGCAAGCTCGCAGAGGCAAC	
CRWN2_seq-F5	TTGTTATGCAGTGGATATCG	
CRWN2_seq-F6	TAAGATATGTTGAGGTAGAGAGGG	
CRWN2_seq-R4	GTTGCCTCTGCGAGCTTGCTTT	for the genotyping of CRWN constructs
CRWN2_seq-R6	AATGGAGCTACTAGATGGTCGC	
CRWN1_R1	CTAAGCCAGCAGCAGTTGGGGATA	
CRWN4_R1	GAAAATCAGATTAGTACATCGTTTTATCC	
CRWN2_out_R	GAACAAGAACAGGAGAAACAGA	

Table 10. Reads of ChIP-seq and NUP1:GFP RE-ChIP

	Sample	Raw reads	Mapped reads
Regular ChIP	Leaf_7D_GFP	29,112,043	26,269,989
	Leaf_7D_IgG	22,505,801	19,903,273
RE-mediated ChIP	Leaf_7D_GFP_mild	4,356,381	3,774,643
	Leaf_7D_IgG_mild	4,051,577	3,534,263
	Leaf_7D_GFP_very mild	4,150,919	3,585,992
	Leaf_7D_IgG_very mild	4,243,746	3,591,349
RE-mediated ChIP	Col-0_H3K9me2_rep1	11,311,406	10,468,807
	Col-0_H3K9me2_rep2	13,895,221	12,985,863
	Col-0_IgG_rep1	8,619,667	7,386,643
	Col-0_IgG_rep2	9,085,510	7,679,964

Table 11. Reads of NUP1:GFP RE-ChIP in various tissues

Sample	Raw reads	Mapped reads
Root_GFP_rep1	18,271,323	14,635,135
Root_GFP_rep2	14,788,390	10,736,901
Root_IgG_rep1	13,182,145	11,146,699
Root_IgG_rep2	14,724,600	11,723,771
Leaf_7D_GFP_rep1	15,330,888	12,859,124
Leaf_7D_GFP_rep2	17,395,095	15,648,196
Leaf_7D_IgG_rep1	16,492,325	14,335,355
Leaf_7D_IgG_rep2	15,633,267	13,063,288
Leaf_30D_GFP_rep1	15,191,514	13,694,876
Leaf_30D_GFP_rep2	11,597,466	9,670,522
Leaf_30D_IgG_rep1	10,866,188	9,517,570
Leaf_30D_IgG_rep2	10,817,251	9,048,152
Inflorescence_GFP_rep1	16,815,632	14,518,475
Inflorescence_GFP_rep2	19,482,233	17,890,959
Inflorescence_IgG_rep1	12,663,466	10,962,140
Inflorescence_IgG_rep2	11,605,240	9,991,679

Table 12. FISH BACs paired loci to compare ~300 kb genomic regions

BAC_name	chromosome	from	to	type
T12P18	1	23661243	23740711	red1/2
F22C12	1	23739672	23850893	
F15H21	1	23846788	23947940	
F1N19	1	23931714	24044865	
F12K22	1	21343213	21436355	green1
F16M22	1	21547302	21638248	
F19C14	1	21603875	21689863	
T15M6	1	21438151	21541775	
F1E22	1	24402490	24494832	green 2
F12P19	1	24481718	24576124	
F15E12	1	24574440	24664687	
T6J19	1	24600752	24714167	
T27F4	1	24698381	24784055	
F18O21	3	20797061	20896552	red
T5P19	3	20889207	20990745	
T8M16	3	20984085	21091343	
F24I3	3	21071991	21163293	
F17J16	3	21786770	21876286	green
F25L23	3	21879703	21986845	
T16L24	3	21977058	22068881	
F22K18	4	12655405	12781187	red
T19F6	4	12437071	12553155	
T22A6	4	12548958	12657399	
F16G20	4	12187957	12284931	green
F21P8	4	12112093	12197846	
F7H19	4	11986966	12126272	
T28J14	5	2195755	2300355	green
T2I1	5	2284839	2401589	
MIBK20	5	2399513	2487684	
T2K12	5	2798547	2881442	red
T5E8	5	2859328	2962753	
F17I14	5	2956230	3048720	

Table 13. FISH BACs for chromatin painting

BAC_name	chromosome	from	to	type
F6D8	1	19528072	19645809	green
F14G24	1	19630929	19757181	green
F8L10	1	19715330	19825940	green
F12M16	1	19801096	19931330	red
T3F20	1	19931131	20031090	red
F22G10	1	19960251	20072148	red
T18A20	1	20064778	20150177	green
F15I1	1	20139673	20244996	green
F20D21	1	20228503	20371688	green
T22H22	1	20364882	20459233	green
F14C21	1	20442994	20545128	green
T7N22	1	20540063	20584602	green
T18I3	1	20643073	20743878	green
T5A14	1	20682970	20770932	green
F20N2	1	20761870	20871029	green
T6H22	1	20933306	21029772	green
F14G9	1	20996737	21108217	green
F13N6	1	21089988	21180685	green
F12K22	1	21343213	21436355	green
F13D13	1	21410223	21497002	green
T18I24	1	21510714	21596483	green
F16M22	1	21547302	21638248	green
F19C14	1	21603875	21689863	green
F9K23	1	21267762	21316652	green
F20B16	1	21695457	21784716	green
T30E16	1	21850893	21950895	green
F23H11	1	21934168	22078557	green
T2K10	1	22072198	22162481	green
T13D8	1	22160034	22276210	green
F8A5	1	22276012	22396781	red
F23C21	1	22390486	22410749	green
T7P1	1	22404923	22507206	green
F11P17	1	22499257	22602586	red

T1F9	1	22594665	22692453	green
T25B24	1	22687213	22771634	green
T13M11	1	22748107	22835492	green
F8K4	1	22823067	22914219	green
F19K23	1	22938507	23035933	green
T3P18	1	23109020	23206059	green
F9N12	1	23441115	23508826	green
F2K11	1	23495971	23596827	green
F24D7	1	23581209	23668774	red
T12P18	1	23661243	23740711	red
F22C12	1	23739672	23850893	red
F15H21	1	23846788	23947940	green
F1N19	1	23931714	24044865	red
F13O11	1	24036587	24154913	green
T23K8	1	24181059	24265703	green
T8F5	1	24233947	24323592	green
F1E22	1	24402490	24494832	green
F12P19	1	24481718	24576124	green
F15E12	1	24574440	24664687	green
T6J19	1	24600752	24714167	green
T27F4	1	24698381	24784055	green
F28G11	1	24731528	24836010	green
T12I7	1	24795026	24896884	green
T4O24	1	24904437	24986219	green
F1O19	1	24970314	25060679	green
F5A8	1	25046400	25148342	green
F1N21	1	25137131	25251850	green
T1F15	1	25251667	25307387	green
F12B7	1	25267551	25359079	green
F12A21	1	25329174	25443363	red
T23K23	1	25442431	25544361	red
T22E19	1	25536056	25642907	green
T2E12	1	25558058	25675471	green
T26J14	1	25658662	25732284	red
F14K14	1	25800728	25897489	green

T6L1	1	25858361	25958868	red
F4N2	1	25948151	26047838	red
F10D13	1	26056685	26163879	red
F24J1	1	26156412	26253864	red
T6C23	1	26183757	26270902	red
T17F3	1	26268624	26353346	red
F20P5	1	26348186	26462675	red
F17O7	1	26462488	26554615	red
F24J13	1	26550088	26637487	red
F5A18	1	26596009	26704584	red
F14O23	1	26940740	27039210	red
F17M19	1	27027663	27108075	red
F28P5	1	27102781	27141409	red
T9N14	1	27136056	27234929	red
T10D10	1	27226190	27313229	red
F28P22	1	27309419	27410511	red
F3N23	1	27397435	27514338	red
T18K17	1	27496878	27567708	red
T9L24	1	27562521	27652966	red
F6D5	1	27647892	27745799	red
F25P22	1	27672065	27777994	red
F2P9	1	27716975	27873173	red
F9E11	1	27835380	27940264	red
F1O17	1	27902147	28014061	red
F1M20	1	27943688	28078075	red
F25A4	1	28059309	28175029	red
F9E10	1	28106104	28203366	red
F22H5	1	28186055	28313033	red
F1B16	1	28261127	28361802	red
F10A5	1	28329769	28459299	red
T4O12	1	28450937	28546899	red
T23E18	1	28543830	28641378	red
F15M4	1	28610978	28705455	red
F14G6	1	28663699	28764504	red
F28O16	1	28763229	28850912	red

F7O12	1	28846608	28977690	red
F22K20	1	28881050	28977691	red
T14N5	1	28971473	29055298	red
F2P24	1	29049586	29096440	red
T5M16	1	29089487	29192827	red
T32E8	1	29192644	29275099	red
F28K19	1	29256736	29367301	red
T11I11	1	29365244	29434737	red
F3F9	1	29430666	29526428	red

9. Acknowledgements

This study was carried out at the Center for Plant Molecular Biology (ZMBP) and could not be completed without encouragement, support, and inspiration from numerous people including my supervisors, colleagues, friends, and family. The completion of this thesis is almost the end of my journey in obtaining my Ph.D. degree. At the end of this beautiful journey, it is my great pleasure to express gratitude to all those who contributed to the success of the whole study and made it an incredible experience for me.

First and foremost, I would like to thank my supervisor Dr. Chang Liu, for giving me the opportunity to pursue this work in his laboratory, for all his guidance and advice during my studies, and for the continuous support. His efficient organization, exceptional expertise, and patience will help me a lot in my future career.

Thanks to Prof. Dr. Thomas Lahaye and Prof. Dr. Ulrike Zentgraf, who gave me insightful suggestions during my study, and have accepted to be examiners for my thesis and my defense. Thanks to Prof. Dr. Marja Timmermans and Prof. Dr. Sascha Laubinger for stimulating discussions and suggestions in my TAC meetings. Thanks to Professor Dr. Klaus Harter for being my supervisor and who would be an examiner for my defense. I would express my thanks to our collaborators from the Max Planck Institute for Developmental Biology (Genome Center and Department Weigel) and from National Key Laboratory of Plant Molecular Genetics (NKLPMG), Shanghai Institutes for Biological Sciences (SIBS) for giving help and intellectual suggestions to my study.

I also would like to thank the Chinese Scholarship Council and University Tuebingen, from which I received financial support for four years and ten months, respectively, for this precious opportunity to study in Germany.

I am deeply grateful to my colleagues in Dr. Liu's laboratory and other members of the General Genetics Department, who have given me a lot of help, ideas, and encouragement while doing my research and during the process of writing this thesis. I sincerely thank all people, who contributed their results presented in this thesis.

I am very grateful to ZMBP central facilities for its technical support in microscopy and plant cultivation. I would like to express my sincere appreciations to Dr. Kenneth W. Berendzen in the FACS unit for sorting nuclei used in this study.

Acknowledgements

Last but not least, many thanks to my family and friends, who have shared my frustrations, worries, and hopefully my ultimate happiness in eventually finishing this thesis.

10. Curriculum vitae

Personal Details

Name: Xiuli Bi

M/F: Female

Date of Birth: 02.12.1988

Marital status: Unmarried

e-mail: xiulibi89@gmail.com

Phone: (+86) 158 2924 0975

Address: Center for Plant Molecular Biology (ZMBP)

University of Tuebingen

Auf der Morgenstelle 32, 72076

Tuebingen Germany

Education

- 2015 - University of Tuebingen, Ph.D.
Major: General Genetics, Center for Plant Molecular Biology
Advisor: Dr. Chang Liu
- 2011 - 2014 Northwest A & F University, M.A.
Major: Pomology, College of Horticulture
Advisor: Prof. Dr. Pengmin Li
- 2007 - 2011 Northwest A & F University, B.A.
Major: Protected Agriculture Science and Engineering, College of
Horticulture